An Analysis of Axisymmetric Receding Contacts

Jhonatan Da Ponte Lopes

Christ Church

Department of Engineering Science

University of Oxford

A thesis submitted for the degree of

Doctor of Philosophy

Trinity 2020

Acknowledgements

First, I would like to thank Professor David Hills for all the guidance and advice that I was given during my DPhil. I feel very fortunate to have had an excellent supervisor, who made me feel welcomed from the beginning and always showed patience and kindness towards me on the many difficult moments that I faced throughout this work.

I would like to gratefully thank Sir John Aird (through Christ Church Oxford), Rolls Royce PLC, and Coordenação de Aperfeiçoamento de Pessoal de Nível Superior (CAPES) for the financial support throughout this thesis.

I also would like to thank my parents, who always invested in my education. Without them, this work would not be possible.

To my wife, Mariana, and my daughter, Luiza, thank you. You are the reason that I am always happy and glad to go to work.

Lastly, I would like to thank God for giving me the breath of life everyday.

Abstract

Bolted joints are one of the most used types of fixture in industry and when the contact area is small compared with the joint's thickness, they represent an example of receding contacts, which are characterised by the reduction of the contact area when a loading is applied. Despite their ubiquity, axisymmetric receding contacts are not fully understand, and the current literature on the problem is limited either to plane problems or to frictionless cases.

This thesis presents an analysis of the frictional behaviour of fundamental axisymmetric receding contacts. The geometry of the problem is represented in an idealised format, through the contact of a semi-infinite thin layer of material and an elastic half-space. This allows for a precise solution to be found.

The methodology consists of assuming that the bodies are fully adhered and applying circular dislocation densities as nuclei of strain to correct the stresses when conditions of partial slip and separation are violated. Singular integral equations with Cauchy kernels are posed and solved in order to recover Signorini and orthogonality conditions.

In Part I, the methodology is implemented and verified through the solution of ring cracks in a half-space and the frictional behaviour of a shaft/hub system under partial slip subjected to an extraction force and to a torque.

Part II presents the solution for the thin layer resting against an elastic half-space under three different normal loadings: uniform pressure outside a disk (stamping loading); concentrated force; and uniform pressure over a disk.

It was shown that the receding contacts modelled present the basic properties that the contact snaps upon the application of any load, the interfacial tractions are proportional to the applied load, the extent of the contact size and slip zone are independent of the load, and the tractions are independent of the material parameters (namely the Poisson's ratio).

Contents

List of Figures

List of Tables

1

Introduction

One of the main classifications of contacts is done by comparing the extent of the contact in the deformed configuration with the initial configuration in the unloaded state and observing whether or not new points come in contact as the bodies deform. In *advancing* contacts, such as when two spheres are pressed against each other, new surface points come in contact as the bodies deform and the extent of the contact is dependent on the magnitude of the applied pressure. Now, consider the case where a piece of cardboard is laid on a flat, soft cushion. Initially, contact is made throughout the surface of the cardboard. However, if a line of load is applied to the cardboard layer (say, by pressing the edge of your hand against it), the contact recedes. In *receding* contacts, the contact shrinks when a load is applied, resulting in the deformed contact being contained in the initial state.

In machines or structures with carefully fitted parts, receding contacts are more likely to appear than advancing contacts, because of the opening of gaps between the individual parts as they distort under application of loads. Examples of receding contacts are found throughout solid mechanics, including a plate on unilateral simple supports, a layer resting on a substrate, or a cylindrical shell fitted inside another shell.

A property of some receding contacts is that the change from the unloaded to the loaded state is discontinuous, i.e. the contact ‘snaps’ to the deformed configuration as

soon as any load is applied [1]. This presents a challenge in obtaining solutions through the Finite Element Method, as a large portion of the nodes change status from being in contact to being free with the application of any increment of load.

Notwithstanding the difficulties in obtaining converging solutions for receding contacts through the usage of Finite Element Analysis, Thaitirarot et al. [2] were able to develop a model for a lap joint formed using friction grip bolts. Even though it represents a case of a frictional receding contact, the geometry is still in a plane formulation. Nonetheless, the authors show that convergence is difficult and care must be taken to guarantee a properly refined mesh around the contact.

Despite its importance, the literature in receding contacts was often limited to cases where there is no friction between the bodies. Keer et al. [3] analysed the frictionless receding contact between a layer and a half space for both the plane and axisymmetric cases. The analysis results in a homogeneous Fredholm integral equation, which leads to the extent of the contact being viewed as a eigenvalue problem. These results were later expanded to a layer with a slightly curved bottom pressed against a half space [4]. Now the analysis leads to solving an inhomogeneous Fredholm integral equation, as the contact advances gradually with the level of loading when the bottom is slightly curved. Even recent studies were limited to investigating the properties of receding contacts with no friction for different materials and geometries [5–8].

Expanding the work into frictional contacts, Ciavarella et al. [9] showed that the extent of the contact remains independent of the load magnitude under Coulomb friction, as long as the loading increases monotonically in time. Ahn & Barber [10] showed that if the load changes non-monotonically, the size of the contact will vary during both loading and unloading periods until a steady periodic state is achieved. Other studies focused on including frictional contacts assuming slip throughout the contact area, characterizing fully sliding cases [11, 12].

The next step was to consider the fundamental quasi-static frictional behaviour of receding contacts when stick, slip and separation are present. Ahn & Barber [10] used

finite elements to solve a quasi-static receding problem when both stick and slip are present, applying a cyclic load. By using dislocation densities to correct stresses in the region of contact of a receding problem, Chaise et al. [13] were able to modify a fully stuck solution for a plane semi-infinite layer pressed against a half plane into a solution where both slip, stick and separation are present. Furthermore, Parel et al. [14] solved the problem of a semi-infinite elastic layer pressed against a half plane by a semi-infinite surface pressure, using dislocation densities.

One of the applications of receding contacts in industry is to the analysis of frictional contact in bolted joints, which are naturally axisymmetric, either for the whole joint or for its individual elements. However, the work currently present in the literature for frictional receding contacts is scarce, and generally focused on plane contacts. A thorough review of receding contacts is presented by Barber [1].

Regarding experimental data, the current literature in receding contacts is restricted to the analysis of fretting fatigue life in bolted joints [15, 16]. Even though the experiments consider frictional receding contacts as their objects of investigation, their aim is to probe ways of increasing fretting fatigue life, not to understand the fundamental properties of the contact, such as the interfacial stress distributions.

An extension of the method used by Parel et al. [14] and Chaise et al. [13] can be made to the solution of frictional axisymmetric contacts. Dislocation densities can be applied as arrays of strain nuclei to correct the stresses in the contact, to satisfy either the slip condition or contact opening. Ring dislocations have been used to solve axisymmetric cracks [17, 18] and general contact problems [19].

The choice of strain nucleus can be any point source of strain (or stress), such as a dislocation [17], a force-pair [20] or a dipole [21]. The consequence of the choice of strain nucleus is the presence of higher order Cauchy terms in the singular integral equations, which make the inversion more difficult. The dislocation is chosen as the strain nucleus in this work, since it only induces singular Cauchy terms in the interfacial stresses, which can be inverted using well known numerical quadrature schemes [22].

While the dipole is desirable for being path-cut independent, it induces hypersingular Cauchy terms in the stresses, which leads to a more difficult inversion. Besides, the geometries considered in this work have the path-cuts along straight lines (parallel to the r or z axes) and, therefore, can be solved using a path-cut dependent approach.

The objective of this thesis is to analyse frictional axisymmetric receding contacts, through the solution of models of an axisymmetric layer pressed against a half space under different loading regimes. This solution can then be applied to examples in industry, such as the study of bolted joints. The focus is to represent the geometry in an idealised way, so that a precise solution may be obtained, in contrast with methods such as the Finite Element Method, where the geometry is precise but the obtained solution is approximate.

1.1 Summary

This thesis is a collection of research performed by the author in the Department of Engineering Science under the supervision of Professor David Hills. This work is original and no part of it has been submitted for a degree at this university of elsewhere. The work in Parts I and II corresponds to the following published papers:

1. J. Lopes and D. Hills. “Ring cracks at the surface of a half-space”. In: *Engineering Fracture Mechanics* 194 (2018), pp. 105–116

2. J. Lopes, D. Hills, and R. Paynter. “The axisymmetric shrink fit problem subjected to axial force”. In: *European Journal of Mechanics-A/Solids* 70 (2018), pp. 172–180

3. J. Lopes and D. Hills. “The axisymmetric shrink fit problem subjected to torsion”. In: *International Journal of Engineering Science* 150 (2020), p. 103259

4. J. Lopes and D. Hills. “The axisymmetric frictional receding contact of a layer pressed against a half-space by pressure outside a disk”. In: *European Journal of Mechanics-A/Solids* 77 (2019), p. 103787

5. J. Lopes and D. Hills. "The axisymmetric frictional receding contact of a layer pressed against a half-space by a point force". In: *International Journal of Solids and Structures* 171 (2019), pp. 47–53

6. J. Lopes and D. Hills. "An idealised description of the frictional receding contact behaviour of a bolted joint". In: *European Journal of Mechanics-A/Solids* (2020), p. 104022

In Chapter 2, an overview of axisymmetric contact mechanics is presented in increasing levels of complexity. The chapter focuses on the loading of a half-space and interactions between axisymmetric elastic bodies. The conditions for partial slip are presented, as well as the basics of solving contact problems using dislocation densities. An overview of the properties of receding contacts is also shown.

One of the difficulties in obtaining numerical solutions to receding contacts using dislocation densities is that it usually involves solving singular integral equations which are posed over a semi-infinite region. In addition, because of the complexity of the kernel functions for the dislocation densities, the literature for the circular dislocation kernels and Lipschitz-Hankel integrals are replete with typos and errors. The manual transcription of the kernels and integrals when they are being implemented is also a considerable source of errors. To circumvent these difficulties, it was proposed that simpler problems were solved first in Part I, to guarantee that the kernel solutions were transcribed and implemented correctly, and that the frictional problems can be solved using circular dislocations.

Chapter 4 uses a distribution of ring dislocations to determine the crack tip stress intensity factors for a ring crack at the surface of a half-space subjected to a concentrated normal force P put at the axis of symmetry. This solution will show that the circular edge dislocations are suitable quantities to be used as stress correctors (nuclei of strain) and will provide a verification for the implementation of the kernels.

Next, two 'simpler' axisymmetric frictional problems are proposed, where no opening is expected. The first problem is presented in Chapter 5, where a shaft-hub system is

subjected to a concentrated normal force. This illustrates the use of circular dislocations to obtain the stress fields of a frictional contact in partial slip. In the second problem (presented in Chapter 6), the same shaft-hub system is subjected to a monotonically increasing torque after being shrink fitted in assembly. This shows the use of dislocation densities in frictional contacts that involve orthogonal components of shear stress, as the application of torque induces shear which is perpendicular to the one induced by the shrink fit assembly. Careful consideration must be taken to ensure that the solution satisfies the orthogonality condition at each time step, i.e. that the direction of the equivalent shear stress is collinear but opposed to the slip velocity.

Part II corresponds to the solution of receding contacts involving a thin sheet of material being pressed against an elastic substrate. In these problems, the sheet is modelled by a semi-infinite layer of thickness a, which rests against an elastically similar half-space (substrate). For each problem, a different loading is applied to the upper surface of the layer, which will result in different frictional behaviour.

In Chapter 7, a stamping receding contact is proposed, where uniform pressure is applied over the whole surface of the sheet, except for a disk of radius b. In this case, the contact may recede over the unloaded region, depending on the radius of the unloaded region and the coefficient of friction. Because this area is finite, this constitutes a receding contact where the singular integrals are finite, and corresponds to an intermediate case of complexity between the problems in Part I and the problems in Chapters 8 and 9.

The simplest axisymmetric frictional receding contact model is when the layer is subjected to a concentrated force applied at its axis of symmetry (Chapter 8). Because there are no intrinsic length dimensions associated with the loading, the only independent parameter of the problem is the interfacial coefficient of friction.

In order to construct a better model for a bolted joint, Chapter 9 considers the case where the layer is subjected to uniform pressure over a disk, which represents the washer pressure.

Finally, Chapter 10 presents the conclusions drawn from this thesis.

2

Fundamentals of Contact Mechanics

While it is possible to apply body forces at the interior points of engineering components through physical processes that act 'at a distance' (such as forces due to gravity and magnetic or electrostatic attraction), the majority of the forces applied to engineering components arise from contact with one or more parts. The scope of contact mechanics is the mathematical analysis of the transmission of forces between contacting surfaces, which is paramount for better describing the behaviour of assembled components.

As stated in Chapter 1, the aim of this thesis is to have an idealised geometry associated with a precise solution. Since the contact area is usually small and the exact geometry of the bodies away from the contact region is unimportant, a half-space approximation is often very adequate to model the characteristics of the contact. Therefore, an idealised geometry associated with a precise solution is preferred.

This chapter presents an overview of basic axisymmetric contact mechanics through a half-space formulation in increasing levels of complexity. First, a categorisation of contacts is presented, together with the properties of receding contacts and a mathematical formulation for defining the contact between bodies. Afterwards, a half-space formulation is presented, where a semi-infinite body is subjected to different loadings. This is followed by the indentation of two elastic bodies under frictionless conditions. Later, the conditions for partial slip are presented, as well as the problem of the indentation of two spheres

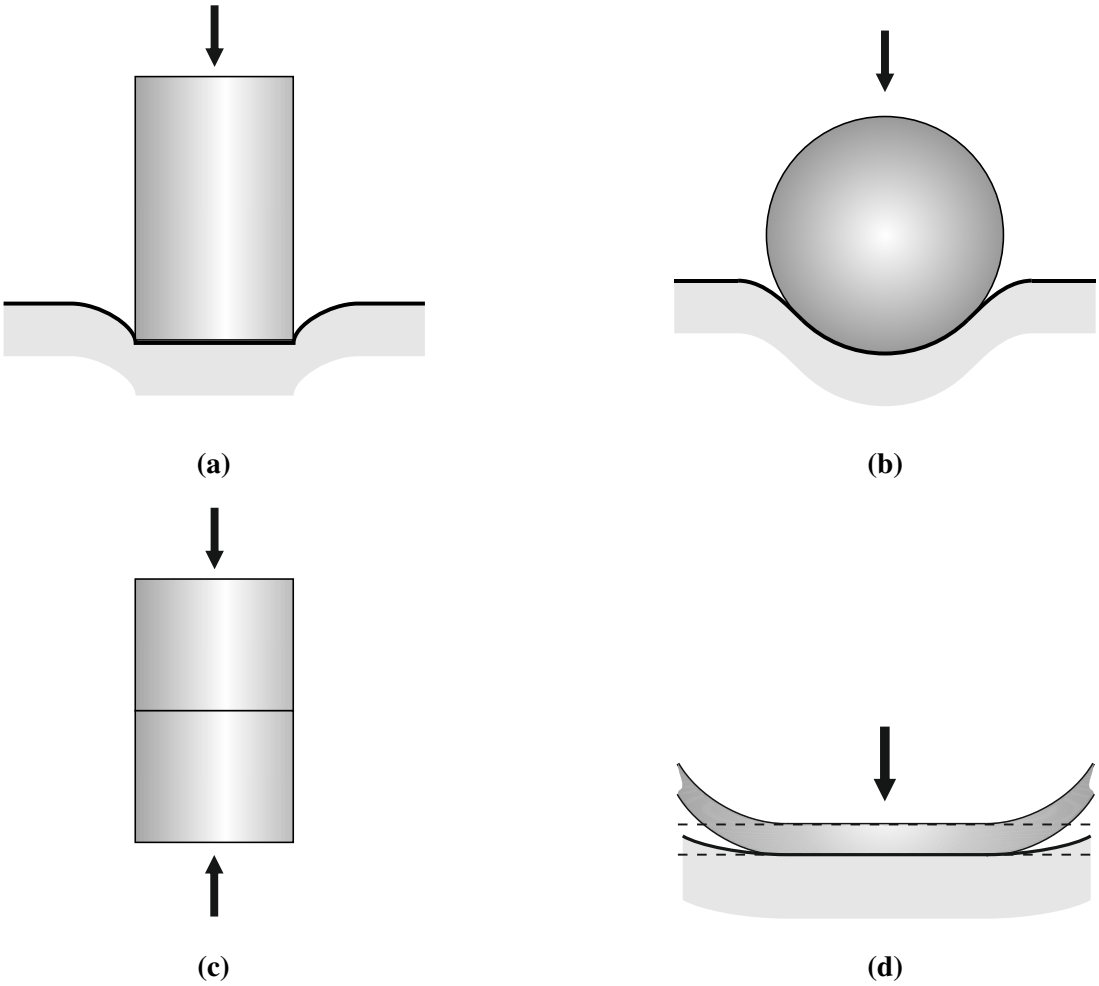

Figure 2.1: Characterisation of contacts. (a) Complete and conformal. (b) Incomplete and non-conformal. (c) Common edge. (d) Receding.

subjected to a shearing load. Finally, the usage of dislocations as a distribution of strain nuclei to correct the stresses is shown.

2.1 Contact Classification

In order to understand better the contacts between elastic bodies, it is advantageous to classify them, as similar contacts should have similar properties. Figure 2.1 shows four basic configurations in which contacts are generally classified, either as one type or some combination of them [29].

The first classification regards the contact's conformality (see [1, 29]). Figure 2.1a

represents a rigid, flat-ended punch pressed against an elastic space, an example of *conformal* or *complete* contacts, in which the contact is fixed geometrically and the undeformed bodies share a common tangent. The bodies can be placed over an extended region without requiring any material deformation.

Figure 2.1b shows a sphere pressed against an elastic space. Now, the contact is said to be *non-conformal* or *incomplete*, and the contact's extent is not fixed geometrically but is dependent on the applied load. Initially, contact is restricted to a line (one or more isolated points) and, as the load is increased, it is broaden to form a narrow strip. Therefore, while the contact area is known *a priori* in conformal contacts, it must be found as part of the solution for non-conformal contacts.

A *common edge* contact is formed when two components of the same size are clamped together (Figure 2.1c). Finally, Figure 2.1d shows *receding* contact, exemplified by a thin layer resting over an elastic substrate. A particularly interesting example of this is to think of the layer as a piece of cardboard resting over a flat cushion. Initially, contact is made throughout the layer's surface, resulting in a significant contact area. As soon as a normal load is applied, the contact area *recedes* to a deformed configuration.

The asymptotic behaviour of the contact pressure at the edges of the contact also varies accordingly to the type of contact, as shown by Hills et al. [30]. In conformal contacts, there is a common tangent for the bodies in contact at the edge of the contact, and the slope of the deformed surfaces is continuous there. As a consequence, the contact pressure falls continuously to zero at the contact edges. In non-conformal contacts, however, the bodies do not have a common tangent at the edge of the contact, which results in the contact pressure being singular there.

In common edge contacts, the pressure at the edges is not zero nor singular, but falls to a finite value, determined by the contact's characteristics. In receding contacts, since the two bodies share a common tangent at the point of contact opening, the pressure must also be zero at the edges.

The contact pressure singularity is relevant when considering the introduction of

defects in manufacturing. In incomplete contacts, minor imperfections in surface finish disturb the contact pressure only locally, but the same is not true for complete contacts, where a minor manufacturing flaw may grossly influence the contact pressure distribution [29].

2.1.1 Receding Contacts

Another characterization of contacts is done by comparing the extent C of the contact in the deformed configuration with the initial configuration C^0 in the unloaded state. While the initial state is the determined by the geometric features of the bodies and their fixtures, the deformed contact state C generally depends on the nature of the applied loads, the level of loading and the elastic constants of the materials.

The classification is done by observing whether or not new surface points come in contact as the bodies deform. In *advancing contacts*, new surface points come in contact as the load is applied and, as a consequence, the deformed contact C is not contained in the initial state C^0. However, in *receding contacts*, the contact shrinks everywhere resulting in C being contained in C^0.

Although it is not possible to determine whether the contact is advancing or receding for every case prior to the solution of the problem, in many cases this can be predicted by inspection.

Dundurs [31, 32] proved the following properties about receding contacts:

(i) The displacement, strain and stress are proportional to the level of loading.

(ii) The contact C is independent of the level of loading and remains stationary.

(iii) Except for the special case of $C = C^0$, the change from C^0 to C is discontinuous.

The first property allows us to normalise the stresses with respect to the applied loads. Thus, as the load changes the normalised stresses remain the same. However, it should be noted that the proportionality between the applied loads and the elastic fields do not

imply that the problem is linear in the sense of addition. Therefore, the application of two systems of loads cannot be superposed [33].

The third property makes the study of receding contacts difficult when using Finite Element Analysis. When any increment of load is applied from the unloaded configuration, the contact 'snaps' to the deformed condition. This sudden change might lead to convergence problems in FE codes.

Another property of receding contacts is that '*if the bodies in the assemblage are homogeneous and made of identical materials, neither the extent of contact nor the stresses depend on the elastic constants*' [31, 32]. Therefore, in theses conditions, the stresses and the contact extent are the same for all pairs of contacts between the same materials.

2.2 Contact Definition

Figure 2.2 shows a non-conformal contact between the bodies 1 and 2. When no load is applied, they make contact at the point O. As long as the bodies profiles are smooth, we can identify a common tangent plane and a common normal at the point of contact. In a Cartesian coordinate system, the undeformed profiles of the bodies can be defined by the functions $g_1(x, y)$ and $g_2(x, y)$, which represent the gap between the undeformed surface and the common tangent or the equivalent gap that would exist in the contact between the body in question and a plane surface. We can define a composite initial gap function as

$$g_0(x, y) = g_1(x, y) + g_2(x, y), \tag{2.1}$$

which is the resulting gap between the bodies in the undeformed configuration shown in Figure 2.2a.

Now, suppose we apply a normal force P that pushes the bodies together (Figure 2.2b),

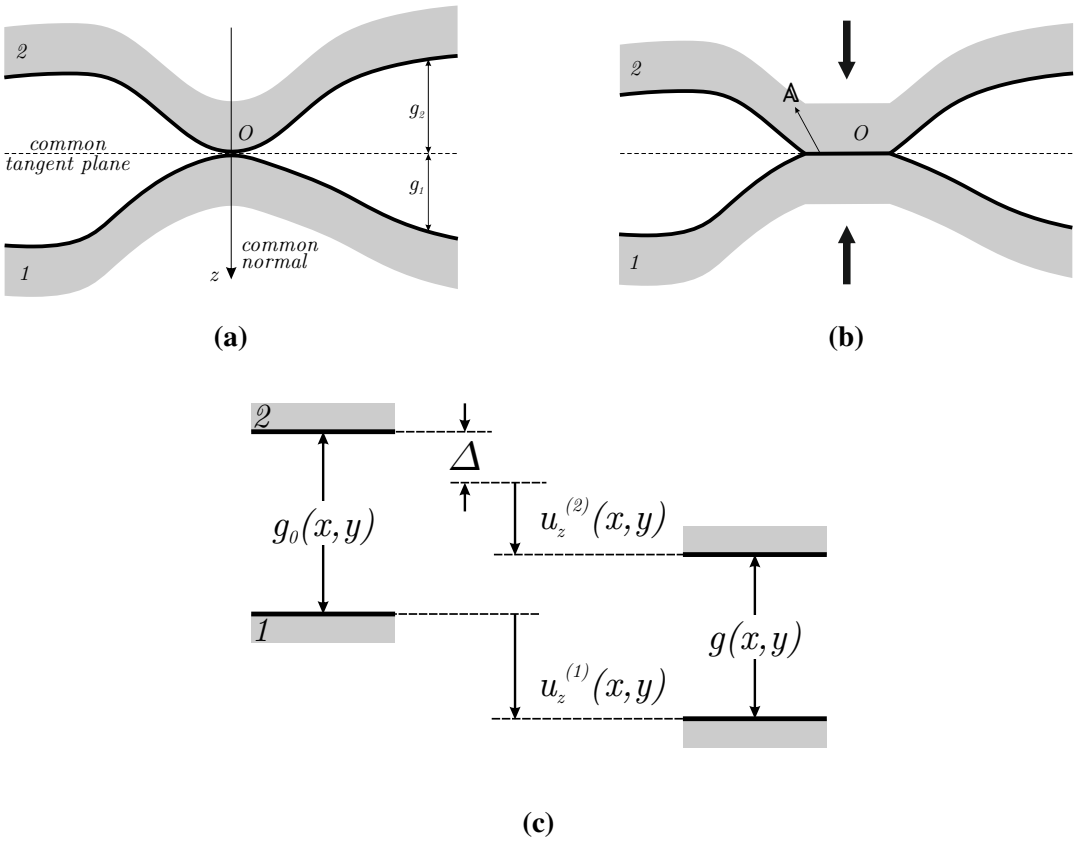

Figure 2.2: Description of the gap for a non-conformal contact. (a) Unloaded state. (b) Establishment of a contact region $\mathbb{A}$. (c) Diagram of final gap function as function of the rigid body displacement Δ and surface displacements $u_z^{(1)}(x,y)$ and $u_z^{(2)}(x,y)$.

which will deform the bodies and establish a finite contact region $\mathbb{A}$. Let Δ be the vertical rigid body motion caused by the application of the force. This is equivalent to moving the upper body downwards along the common normal by the same amount, which will simply reduce the gap $g_0(x,y)$ everywhere by Δ. We can superpose the rigid body motion to the deformation of the bodies, which are characterized through the surface displacements $\boldsymbol{u}^{(1)}(x,y)$, $\boldsymbol{u}^{(2)}(x,y)$. A vertically downward displacement $u_z^{(1)}(x,y)$ in the lower body will result in the gap widening, while a vertically downward displacement $u_z^{(2)}(x,y)$ in the upper body will decrease the gap.

Superposing these effects at a point on the surface of the undeformed bodies (Figure 2.2c), the final gap is given by

$$g(x,y) = g_0(x,y) - \Delta + u_z^{(1)}(x,y) + u_z^{(2)}(x,y). \tag{2.2}$$

Since the bodies are not physically allowed to penetrate each other, the gap function cannot be negative. In fact, the contact area $\mathbb{A}$ is *defined* as the region where the final gap is zero, i.e. $g(x,y) = 0$. The region $\bar{\mathbb{A}}$ not in contact, where $g(x,y) > 0$, defines the separation zone.

Assuming, for simplicity, that the contact is frictionless (only a normal traction in the form of the contact pressure $p(x,y)$ appears in the contact region), it stands to reason that outside the contact region the contact pressure $p(x,y)$ must be zero, since there is no contact between the material to induce tractions. Therefore, $p(x,y)$ is only non-zero inside the contact region $\mathbb{A}$. Also, we assume throughout this work that the pressure cannot be tensile. Thus, we can push against a frictionless surface, but we cannot 'pull' against it, i.e. $p(x,y) \leq 0$. At very small length scales (e.g. nanometer), van der Waals attractive forces can be significant and would require the relaxation of our assumptions regarding the contact pressure.

A formal statement of the frictionless contact problem can be established with these definitions, through the following conditions:

$$g(x,y) = 0 \qquad (x,y) \in \mathbb{A} \tag{2.3}$$

$$> 0 \qquad (x,y) \in \bar{\mathbb{A}} \tag{2.4}$$

$$p(x,y) < 0 \qquad (x,y) \in \mathbb{A} \tag{2.5}$$

$$= 0 \qquad (x,y) \in \bar{\mathbb{A}}. \tag{2.6}$$

Notice that each region contains one equality and one inequality. Also, the product $p(x,y)g(x,y) = 0$ for all x, y.

2.3 Half-Space Approximation

One property of contacts is that the contact area is generally small, which results in the strains due to contact forces being concentrated in a small region. Hence, regions away from the contact experience at most a rigid-body motion and, consequently, the exact geometry of the bodies away from the contact region is unimportant. Therefore, we can simplify our problem by assuming that the body extends to infinity and concentrate our analysis in the contact region.

In addition, as long as there are no sharp corners or rapidly varying slopes on the surface near the contact area, we can assume that the contact deformation is equivalent to one produced by a body with a plane surface subjected to the same loading. Thus, we can replace the contact problem by applying the same load to a half-space.

Green and Zerna [34] postulated a solution for the three-dimensional stress fields in a homogeneous and isotropic half-space $z \geq 0$, with Poisson's ratio ν and shear modulus μ, loaded purely by normal tractions. This solution can be expressed in terms of a single harmonic potential function $\varphi(r, \theta, z)$, where φ satisfies

$$\nabla^2 \varphi \equiv \frac{\partial^2 \varphi}{\partial r^2} + \frac{1}{r}\frac{\partial \varphi}{\partial r} + \frac{1}{r^2}\frac{\partial^2 \varphi}{\partial \theta^2} + \frac{\partial^2 \varphi}{\partial z^2} = 0. \tag{2.7}$$

The stress fields in a point (r, θ, z) are given by

$$\sigma_{r\theta}(r,\theta,z) = \frac{z}{r}\frac{\partial^3 \varphi}{\partial r \partial \theta \partial z} - \frac{z}{r^2}\frac{\partial^2 \varphi}{\partial \theta \partial z} + \frac{(1-2\nu)}{r}\left[\frac{\partial^2 \varphi}{\partial r \partial \theta} - \frac{1}{r}\frac{\partial \varphi}{\partial r}\right] \tag{2.8}$$

$$\sigma_{rr}(r,\theta,z) = z\frac{\partial^3 \varphi}{\partial r^2 \partial z} + (1-2\nu)\frac{\partial^2 \varphi}{\partial r^2} - 2\nu\frac{\partial^2 \varphi}{\partial z^2} \tag{2.9}$$

$$\sigma_{\theta\theta}(r,\theta,z) = -(1-2\nu)\frac{\partial^2 \varphi}{\partial r^2} - \frac{\partial^2 \varphi}{\partial z^2} - z\frac{\partial^3 \varphi}{\partial r^2 \partial z} - z\frac{\partial^3 \varphi}{\partial z^3} \tag{2.10}$$

$$\sigma_{zz}(r,\theta,z) = z\frac{\partial^3 \varphi}{\partial z^3} - \frac{\partial^2 \varphi}{\partial z^2} \tag{2.11}$$

$$\sigma_{rz}(r,\theta,z) = z\,\frac{\partial^3\varphi}{\partial r\partial z^2} \tag{2.12}$$

$$\sigma_{z\theta}(r,\theta,z) = \frac{z}{r}\,\frac{\partial^3\varphi}{\partial\theta\partial z^2}. \tag{2.13}$$

Notice that the component of shear stress parallel to the free surface, σ_{rz}, vanish when $z = 0$. Therefore, the stress function satisfies the boundary condition that there is no shear stress in the free surface.

The displacements of the surface can also be determined from the potential function, being given as:

$$2\mu\, u_r(r,\theta,z) = z\,\frac{\partial^2\varphi}{\partial r\partial z} + (1-2\nu)\frac{\partial\varphi}{\partial r} \tag{2.14}$$

$$2\mu\, u_\theta(r,\theta,z) = \frac{z}{r}\,\frac{\partial^2\varphi}{\partial\theta\partial z} + \frac{(1-2\nu)}{r}\,\frac{\partial\varphi}{\partial\theta} \tag{2.15}$$

$$2\mu\, u_z(r,\theta,z) = z\,\frac{\partial^2\varphi}{\partial z^2} - 2(1-\nu)\frac{\partial\varphi}{\partial z}. \tag{2.16}$$

This formulation can be used to find solutions to the stresses and displacements for different loadings in a half-space under axisymmetric conditions by taking the variations with respect to θ as zero, i.e. $\partial(\cdot)\,/\,\partial\theta = 0$.

2.3.1 The Boussinesq Solution

The fundamental problem for the frictionless half-space is the application of a normal force acting at the surface of the half-space. This problem was first solved by Boussinesq [35, 36], but a more modern approach is presented by Barber [37]. Consider the isotropic elastic half-space $z \geq 0$ of Poisson's ratio ν and shear modulus μ, shown in Figure 2.3a. A normal force P is applied at the origin of the cylindrical coordinate system shown, at the surface of the half-space.

Notice that the problem is self-similar, since there is no intrinsic length scale. An enlarged view of the body including the loaded portion would be identical to the

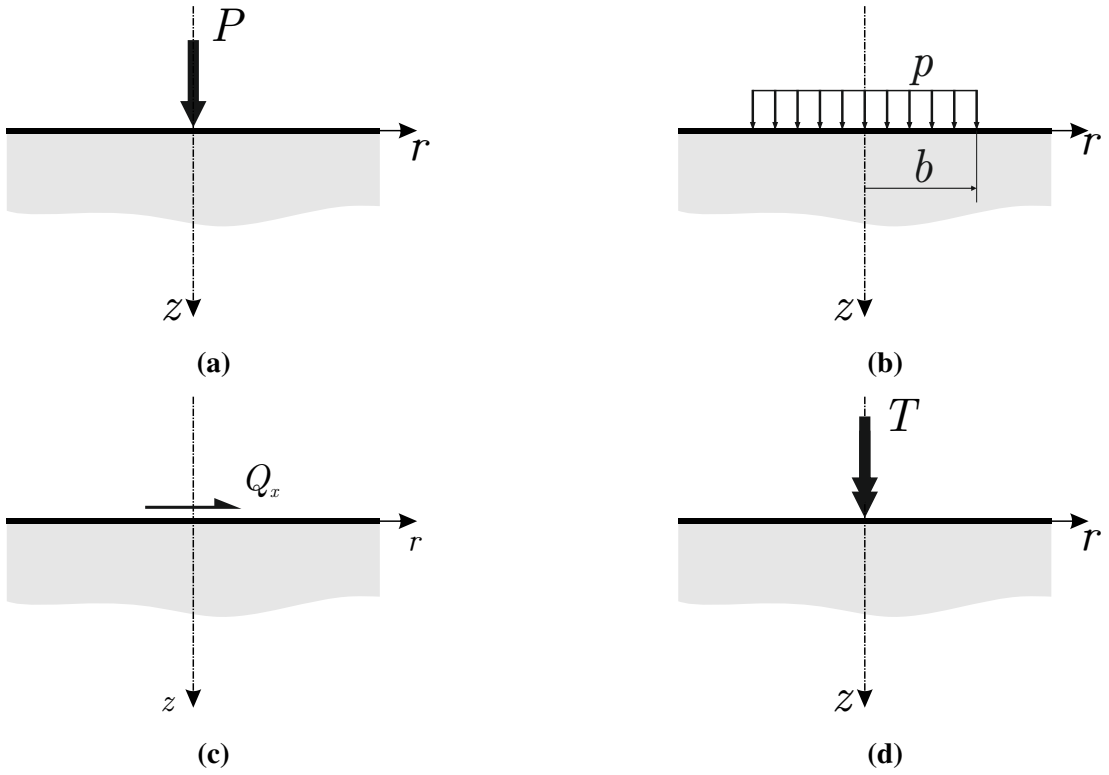

Figure 2.3: Half-space subjected to different loadings. (a) Concentrated normal force P. (b) Uniform pressure p over a disk of radius b. (c) Concentrated tangential force Q_x. (d) Concentrated torque T.

original figure. Therefore, the elastic fields must also be self similar, i.e. the stress and displacement contours must all have the same shape. Equilibrium considerations result in fields being proportional to R^{-2} ($R = \sqrt{r^2 + z^2}$), as the force P must be transmitted across a sequence of self-similar surfaces whose surface area is proportional to R^{-2}.

Barber [37] proposes the following potential function as a solution:

$$\varphi = A \ln (R + z), \tag{2.17}$$

where A is a constant to be determined by the boundary conditions of the problem.

Substituting eq. (2.17) into eq. (2.11), we find

$$\sigma_{zz} = z\,\frac{\partial^3\varphi}{\partial z^3} - \frac{\partial^2\varphi}{\partial z^2} = \frac{3\,A\,z^3}{R^5}, \tag{2.18}$$

resulting in the surface $z = 0$ being free of normal traction except at the origin, as required.

The remaining boundary condition is that the force at the origin must be P. Since the body is in equilibrium, the integral of the normal stress over a finite depth h gives the applied force over the origin:

$$\begin{aligned} P =& -\int_0^{2\pi}\int_0^{\infty} \sigma_{zz}(r,\theta,h)\,r dr d\theta \\ =& -6\pi A h^3 \int_0^{\infty} \frac{r}{(r^2+h^2)^{5/2}} dr \\ =& -2\pi A. \end{aligned} \tag{2.19}$$

Substituting eq. (2.19) into eq. (2.17), the solution for the problem is given by the following potential

$$\varphi = -\frac{P}{2\pi}\,\ln\,(R+z). \tag{2.20}$$

Finally, the non-zero stress fields arising on a point (r, z) are given by [36]:

$$\sigma_{rr}(r,z) = \frac{P}{2\,\pi}\left\{(1-2\,\nu)\left[\frac{1}{r^2} - \frac{z}{r^2\,(r^2+z^2)^{1/2}}\right] - \frac{3\,r^2\,z}{(r^2+z^2)^{5/2}}\right\} \tag{2.21}$$

$$\sigma_{\theta\theta}(r,z) = \frac{P}{2\,\pi}\left\{(1-2\,\nu)\left[-\frac{1}{r^2} + \frac{z}{r^2\,(r^2+z^2)^{1/2}} + \frac{z}{(r^2+z^2)^{3/2}}\right]\right\} \tag{2.22}$$

$$\sigma_{zz}(r,z) = -\frac{3\,P}{2\,\pi}\left\{\frac{z^3}{(r^2+z^2)^{5/2}}\right\} \tag{2.23}$$

$$\sigma_{rz}(r,z) = -\frac{3\,P}{2\,\pi}\left\{\frac{r\,z^2}{(r^2+z^2)^{5/2}}\right\}. \tag{2.24}$$

2.3.2 Circular Disk of Pressure

Since the elastic problem is linear, additional solutions can be obtained by superposition. The displacements corresponding to Boussinesq's solution can be integrated over a finite area to produce a solution for uniform pressure p applied over the circular region $0 \leq r \leq b$ (Figure 2.3b). This solution was obtained by Love [38] (see also [39, 40]).

In the cylindrical coordinate set shown in the figure, the tractions $\sigma_{ij}(r,z)$ arising at a point (r,z) of the half-space are given by:

$$\begin{aligned}\sigma_{rr}(r,z) = -\frac{p\,z}{\pi\,r^2\,l_2\,(1-k^2)}\Bigg\{&\left[-(k^2-3)\,(l_2^2-r^2)+2(k^2-1)\,(l_2^2+r^2)\right]\boldsymbol{K}(k)+\\ &\left[2r(bk-r)\,(1+k^2)+(1-k^2)\,(3-2\nu-k^2(1-2\nu))\right]\boldsymbol{E}(k)-\\ &(1-k^2)\left[b^2\,(1-2\nu)+r^2\,(2+2\nu)\right]\boldsymbol{\Pi}(n;k)\Bigg\}\end{aligned} \tag{2.25}$$

$$\begin{aligned}\sigma_{\theta\theta}(r,z) = \frac{p}{2\,\pi\,r^2\,l_2}\Bigg\{&-b^2\,l_2\,\pi\,(1-2\nu)+2\,z\left[\left(l_2^2\,(3-2\nu)+r^2\,(1+2\nu)\right)\boldsymbol{K}(k)+\right.\\ &\left.l_2^2\,(-3+2\nu)\,\boldsymbol{E}(k)-\left(-b^2(1-2\nu)+r^2(1+2\nu)\right)\boldsymbol{\Pi}(n;k)\right]\Bigg\}\end{aligned} \tag{2.26}$$

$$\sigma_{zz}(r,z) = -p\left\{\frac{2z}{\pi}\left[\frac{r^2+z^2-b^2}{(l_2)^3\,(1-k^2)^2}\boldsymbol{E}(k)+\frac{b^2-(l_1)^2}{(l_2)^3\,(1-k^2)}\boldsymbol{K}(k)-\frac{1}{l_2}\boldsymbol{\Pi}(n;k)\right]\right\} \tag{2.27}$$

$$\sigma_{rz}(r,z) = p\left\{\frac{2z^2}{\pi}\left[\frac{(1+k^2)\,\boldsymbol{E}(k)-(1-k^2)\,\boldsymbol{K}(k)}{(k^2-1)^2\,l_2\,r}\right]\right\}, \tag{2.28}$$

where

$$l_1 = \frac{1}{2}\left\{\sqrt{(r+b)^2+z^2} - \sqrt{(r-b)^2+z^2}\right\} \tag{2.29}$$

$$l_2 = \frac{1}{2}\left\{\sqrt{(r+b)^2+z^2} + \sqrt{(r-b)^2+z^2}\right\} \tag{2.30}$$

$$k = \frac{l_1}{l_2} \tag{2.31}$$

$$n = \left(\frac{l_1}{r}\right)^2 \tag{2.32}$$

and $\boldsymbol{K}(k^2)$, $\boldsymbol{E}(k^2)$, $\boldsymbol{\Pi}(h;k^2)$ are the complete elliptic integrals of the first, second and third kind respectively. These functions are continuous and bounded at every point inside the half-space, but $\boldsymbol{\Pi}(h;k^2)$ cannot be evaluated numerically along the z-axis, since $r = 0$ there. In this region, we take the limits as $r \to 0$, which gives:

$$\sigma_{rr}(0,z) = p\left\{\frac{z^3\ (2\,\nu+1) - (2\,\nu+1)\ (b^2+z^2)^{\frac{3}{2}} + 2\,b^2\,z\ (\nu+1)}{2\,(b^2+z^2)^{\frac{3}{2}}}\right\} \tag{2.33}$$

$$\sigma_{zz}(0,z) = -\,p\left\{\frac{z^3}{(b^2+z^2)^{3/2}}\right\} \tag{2.34}$$

$$\sigma_{\theta\theta}(0,z) = \sigma_{rr}(0,z) \tag{2.35}$$

$$\sigma_{rz}(0,z) = 0. \tag{2.36}$$

2.3.3 Concentrated Tangential Force

An analogous to the Boussinesq solution is presented in this section, where a tangential point force Q_x is applied to the origin of a half-space, acting along the x direction (Figure 2.3c). The solution is given by Johnson [41] and at a point (r,θ,z) of the half-space, the force will induce tractions $\sigma_{ij}(r,\theta,z)$ given by:

$$\sigma_{rr}(r,\theta,z) = \frac{Q_x}{2\,\pi}\,r\,\cos(\theta)\left\{\frac{3\,z^2}{R^5} - \frac{3}{R^3} + \quad (1-2\nu)\left(\frac{r^2+2\,z\,(z-R)}{r^4\,R}\right)\right\} \tag{2.37}$$

$$\sigma_{\theta\theta}(r,\theta,z) = \frac{Q_x}{2\,\pi}\, r\, \cos(\theta)\,(1-2\nu)\left\{\frac{z\,(z+2\,R)}{(z+R)^2\,R^3}\right\} \tag{2.38}$$

$$\sigma_{zz}(r,\theta,z) = -\frac{Q_x}{2\,\pi}\, r\, \cos(\theta)\left\{\frac{3\,z^2}{R^5}\right\} \tag{2.39}$$

$$\sigma_{r\theta}(r,\theta,z) = \frac{Q_x}{2\,\pi}\, r\, \sin(\theta)\,(1-2\nu)\left\{\frac{z^2}{(z+\,R)^2\,R}\right\} \tag{2.40}$$

$$\sigma_{rz}(r,\theta,z) = -\frac{Q_x}{2\,\pi}\, r^2\, \cos(\theta)\left\{\frac{3\,z}{R^5}\right\}, \tag{2.41}$$

where $R = \sqrt{r^2+z^2}$ is the spherical radius.

Note that, in an axial cut (z = constant surface) the application of a tangential force induces both shear (σ_{rz} and $\sigma_{r\theta}$) and normal (σ_{zz}) components, which have no axisymmetry because of the non-axisymmetric nature of Q_x.

2.3.4 Concentrated Torque

Another solution of interest is when a point torque T is applied normal to the free surface of the half-space, at its origin (Figure 2.3d). Chowdhury [42, 43] showed that this results in the following non-zero stress components:

$$\sigma_{z\theta}(r,z) = -\frac{3\,T}{4\,\pi}\left\{\frac{z\,r}{(r^2+z^2)^{5/2}}\right\} \tag{2.42}$$

$$\sigma_{r\theta}(r,z) = -\frac{3\,T}{4\,\pi}\left\{\frac{r^2}{(r^2+z^2)^{5/2}}\right\}. \tag{2.43}$$

2.4 Frictionless Indentation

In Section 2.3, the contact was represented by a known loading being exerted onto a half-space, which represented a single body. The next level of complexity is to consider the interaction between two axisymmetric deformable bodies being pushed against each other. It is assumed that either the bodies are elastically similar or the contact is perfectly

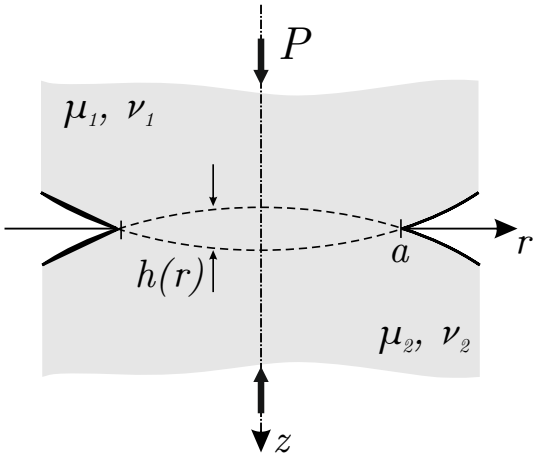

Figure 2.4: Frictionless indentation of two half-spaces.

lubricated, such that the indentation will produce no shear tractions.

Figure 2.4 depicts the indentation of the two axisymmetric bodies, represented by two half-spaces with Poisson's ratio ν_i, shear modulus μ_i, and Kolosov's constant κ_i ($\kappa_i = 3 - 4\nu_i$ under plane strain), $i = 1, 2$. The relationship between the contact pressure $p(r)$ and the degree of overlap of freely interpenetrating bodies $h(r)$ is given by Green and Zerna [34] as

$$h^*(r) = -A \int_r^a \frac{s\, p(s)\, ds}{\sqrt{s^2 + r^2}}, \tag{2.44}$$

where $h^*(r)$ is a transformed displacement, defined by

$$h^*(r) = \frac{d}{dr} \int_0^r \frac{s\, h(s)\, ds}{\sqrt{r^2 - s^2}}, \tag{2.45}$$

a is the contact radius and A is the composite compliance of the materials, given as

$$A = \frac{\kappa_1 + 1}{4\mu_1} + \frac{\kappa_2 + 1}{4\mu_2}. \tag{2.46}$$

The degree of overlap $h(r)$ is obtained from the geometry of the specific problem and substituted into eq. (2.45) to determine $h^*(r)$, which is then inserted into eq. (2.44) to obtain the contact pressure distribution, $p(r)$.

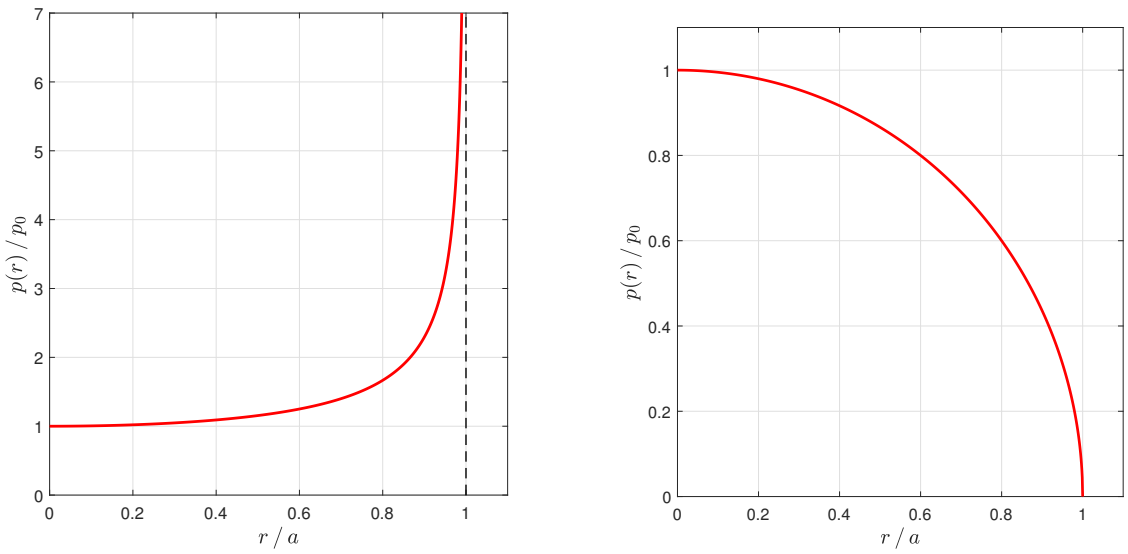

Figure 2.5: Normalised contact pressure $p(r)\,/\,p_0$ for frictionless indentation of: (a) cylindrical punch in a half-space; (b) two spheres.

2.4.1 Cylindrical Punch

In this example, we consider the case where one of the bodies is an elastic half-space and the other is a flat-ended rigid cylindrical punch of radius a. This indentation produces a complete contact. If the punch were to penetrate the half-space freely, the resultant deformation would be a constant amount Δ, since it has a square end. Hence,

$$h(r) = \Delta. \tag{2.47}$$

Substituting eq. (2.47) into eq. (2.45), we find that $h^*(r) = \Delta$, which results in the contact pressure being given as:

$$p(r) = -\frac{2\,\Delta}{A\,a}\,\frac{1}{\sqrt{1-(r/a)^2}}. \tag{2.48}$$

Equilibrium states that

$$P = \int_0^a p(r)\,2\,\pi\,r\,dr, \tag{2.49}$$

which results in

$$\Delta = \frac{P\,A}{4\,a} \tag{2.50}$$

and

$$p(r) = -\frac{P}{2\,\pi\,a^2}\,\frac{1}{\sqrt{1-(r/a)^2}}. \tag{2.51}$$

Figure 2.5a depicts the normalised contact pressure as a function of the radial distance r. As expected, since this is a complete contact, the pressure is finite inside the contact but singular at the edge, when $r = a$.

2.4.2 Hertzian Contact of Spheres

We now consider the case where two spheres of radii R_1 and R_2 are being pressed against each other. This represents an axisymmetric Hertzian contact [44] and produces an incomplete contact. Besides the assumption that no shear tractions arise in the contact, we also assume that the contact radius is small in comparison with the radii of the contacting bodies. This restriction ensures that each sphere may be replaced by a half-space, which results in the penetration function $h(r)$ being represented by a rotated parabola:

$$h(r) = \Delta - \frac{1}{2}k\,r^r, \tag{2.52}$$

where Δ is the approach of two remote points and k is the relative curvature, given by

$$k = \frac{1}{R_1} + \frac{1}{R_2}. \tag{2.53}$$

Substituting eq. (2.52) into eq. (2.45), we find that

$$h^*(r) = -\left(\Delta - k\,r^2\right), \tag{2.54}$$

which results in the contact pressure being given as

$$p(r) = \frac{2}{\pi\, A}\left[-\frac{\Delta - k\, r^2}{\sqrt{a^2 - r^2}} - k\,\sqrt{a^2 - r^2}\right]. \tag{2.55}$$

Equation (2.55) represents the most general solution to the indentation problem. Note that there are singular terms, varying with $(a^2 - r^2)^{-1}$, which represent either adhesion at the edges of the contact or indentation in a complete contact. Since this is an incomplete contact, the two bodies share a common tangent at $r = a$, and hence the contact pressure must fall continuously to zero at that point, i.e. $p(a) = 0$. This gives

$$\Delta = k\, a^2, \tag{2.56}$$

which results in

$$p(r) = -\frac{4\, k}{\pi\, A}\,\sqrt{a^2 - r^2}. \tag{2.57}$$

Because this is a complete contact, a is also an output of the problem and must change with the applied force P. Equilibrium states that

$$P = \int_0^a p(r)\, 2\,\pi\, r\, dr, \tag{2.58}$$

which results in

$$a^3 = \frac{3\, P\, A}{8\, k}. \tag{2.59}$$

We can rewrite the results as

$$p(r) = -p_0\,\sqrt{1 - (r/a)^2}, \tag{2.60}$$

where p_0 represents the peak pressure, given by

$$p_0 = \frac{3\, P}{2\,\pi\, a^2}. \tag{2.61}$$

Figure 2.5b depicts the normalised contact pressure as a function of the radial distance r. As expected, the pressure is maximum at the centre of the contact and falls to zero at the edge.

2.5 Partial Slip Formulation

The previous section focused on cases where the contact is either frictionless or the friction is high enough to prevent slip everywhere. We now turn our attention to the effects of shearing tractions on the contact surface.

First, it is necessary to introduce the commonly accepted laws of frictional contact. In this work, we make use of Coulomb's friction, formulated by Amontons [45] and Coulomb [46] based on experimental investigations of *sliding* contact between two *rigid* bodies, defined as macroscopic relative tangential motion between the two contacting bodies.

Consider two rigid bodies put in contact with a normal force P. If there is gross sliding between the bodies, Coulomb's law states that:

(i) The frictional force Q is proportional to the normal force P between the bodies through the relationship

$$|Q| = f\,P, \tag{2.62}$$

where f is the coefficient of friction between the bodies.

(ii) The direction of the slip velocity $\mathbf{V}_s$ must be such as to oppose the frictional force.

(iii) The frictional force is independent of the apparent area of contact.

(iv) The frictional force occurring during gross sliding is independent of the velocity of sliding.

If the bodies are not sliding, then the slip velocity is null and the frictional force is limited by friction:

$$\boldsymbol{V}_s = 0, \qquad |Q| \leq f\, P. \tag{2.63}$$

It must be emphasised that not all contacting bodies conform to this model. It is observed that tyres with larger width have better frictional performance, an apparent violation of the observation (iii).

Even though this frictional model is restricted to the sliding contact of rigid bodies, an extension can be made to enable the analysis of frictional elastic contacts by restating the frictional law in terms of contact tractions. Consider a three dimensional contact where $p(r,\theta)$ and $\boldsymbol{q}(r,\theta)$ are the normal and shear tractions at the contacting surface. We turn our attention now to the interaction between the surfaces at a particular point (r,θ). At this point, the surfaces will either be slipping relative to each other or stuck. If they are slipping, the tractions are related by the friction law:

$$|\boldsymbol{q}(r,\theta)| = f\, p(r,\theta). \tag{2.64}$$

Furthermore, the direction of the shear tractions is opposite the relative motion of the surfaces (orthogonality condition), i.e.

$$\frac{\boldsymbol{q}(r,\theta)}{|\boldsymbol{q}(r,\theta)|} = \frac{\dot{\boldsymbol{h}}(r,\theta)}{|\dot{\boldsymbol{h}}(r,\theta)|} \tag{2.65}$$

where $h(r,\theta,t) = u_r^{(1)}(r,\theta,t) - u_r^{(2)}(r,\theta,t)$ is the relative tangential displacement of the contacting surfaces as a function of the time t. The problem is quasi-static and the introduction of a time variable is necessary, as a truly static load would not cause changes

in surface displacements and the particles would not be slipping.

If the point (r, θ) is not in a slip condition (there is no relative tangential motion between surfaces), then it is in a stick condition and the shear tractions must be less or equal than the limiting frictional value:

$$|\boldsymbol{q}(r,\theta)| \leq f\, p(r,\theta) \quad and \quad \dot{\boldsymbol{h}}(r,\theta) = 0. \tag{2.66}$$

It is possible now to analyse contacts where a shear force is applied which is less than the limiting frictional value, by using the formulation in eqs. (2.64) to (2.66) at each individual point of the contact rather than to the elastic body as a whole. These contacts are generally said to be in *partial slip*, characterized by two distinct regions in the contact: the stick zone, where the shear tractions are less than the limiting frictional value, with no relative motion between particles; and the slip zone, where the shear tractions are limited by friction (eqs. (2.64) and (2.65)).

In two-dimensional problems, where the contact can be represented along a line, we can distinguish between *forward slip* ($\dot{h}(x) > 0$) and *backward slip* ($\dot{h}(x) < 0$). The frictional law can be stated as $p(x) \geq 0$ for all r and

$$\dot{h}(x) = 0 \qquad g(x) = 0 \qquad |q(x)| \leq f\, p(x) \qquad stick \tag{2.67}$$

$$\dot{h}(x) > 0 \qquad g(x) = 0 \qquad q(x) = f\, p(x) \qquad forward\, slip \tag{2.68}$$

$$\dot{h}(x) < 0 \qquad g(x) = 0 \qquad q(x) = -f\, p(x) \qquad backward\, slip \tag{2.69}$$

$$g(x) > 0 \qquad q(x) = 0,\ p(x) = 0 \qquad separation. \tag{2.70}$$

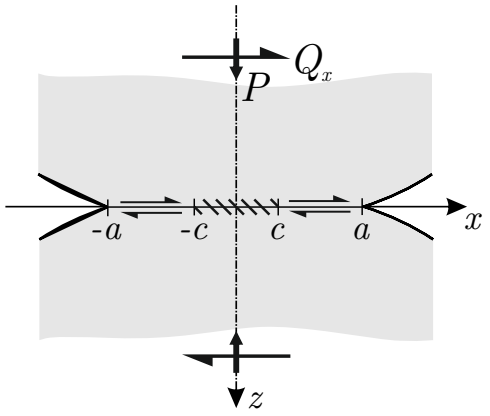

Figure 2.6: A contact between two spheres subjected to shear force Q_x.

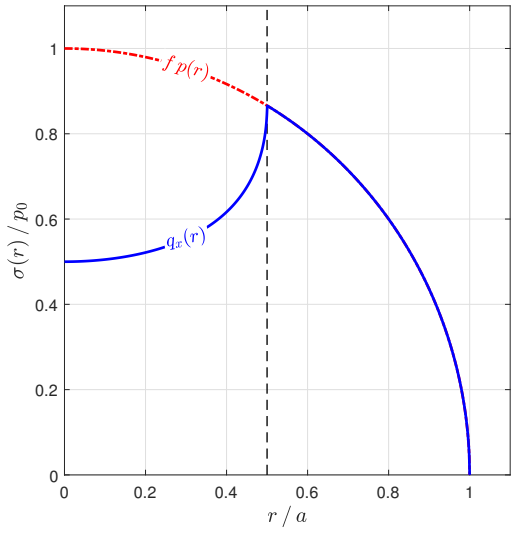

Figure 2.7: Normalised tractions for a contact between two spheres. $Q_x = 7/8$, $P = 1$ and $f = 1.0$.

2.5.1 Contact of Spheres under Partial Slip

Mindlin [47, 48] extended the solution presented in Section 2.4.2 to cases where a tangential force Q_x is applied to the spheres, resulting in the contact being in partial slip (Figure 2.6). A detailed exposition of the results is done by Hills et al. [29] and Johnson [41].

Assuming that the materials are elastically similar, the normal pressure in the contact remains the one obtained in the Hertzian case, i.e.

$$p(r) = -p_0 \sqrt{1 - (r/a)^2}, \tag{2.71}$$

where a is the radius of contact, given by eq. (2.59).

Because of the nature of tangential force Q_x, axisymmetry is lost as soon as the load is applied. If the contact was fully stuck, the shear traction required to cause a constant $x-$direction displacement over the contact area is given by [30]

$$q_x = \frac{q_0}{\sqrt{1 - (r/a)^2}}, \tag{2.72}$$

where

$$q_0 = \frac{Q_x}{2\,\pi\,a^2}. \tag{2.73}$$

In eq. (2.72), the magnitude of the distribution is radially symmetric, but the traction is applied only in the x direction. Note that an infinite coefficient of friction would be necessary to prevent slip at the edges of the contact, since $q_x(r) \to \infty$ when $r \to a$. Hence, we expect the contact to be stuck at a central disk of radius c, and to be in partial slip inside the annulus $c \leq r \leq a$.

Mindlin [47] states that the solution for the shear traction along the x axis, $q_x(r)$, can be obtained as the sum of a full sliding term ($f\,p(r)$) together with a corrective term $q_x^{'}(r)$:

$$q_x(r) = f\,p_0\,\sqrt{1-(r/a)^2} + q_x^{'}(r). \tag{2.74}$$

This corrective term is characterized by a geometrically similar distribution of opposed sign and reduced magnitude, distributed over the central stick disk $r < c$:

$$q_x^{'}(r) = -f\,p_0\,\left(\frac{c}{a}\right)\sqrt{1-(r/c)^2}. \tag{2.75}$$

The size of the stick disk c is obtained through overall equilibrium, i.e.

$$Q_x = \int_0^a 2\,\pi\,r\,q_x(r)\,dr, \tag{2.76}$$

which gives

$$\frac{c}{a} = \sqrt[3]{1-\frac{Q}{f\,P}}. \tag{2.77}$$

Figure 2.7 depicts the distributions of shear traction and pressure over the contact for a case where $P = 1$, $Q_x = 7/8$ and $f = 1.0$. From eq. (2.77), $c/a = 1/2$. Note that $q_x^{'}(c) = 0$, which results in $q_x(c) = f\,p(c)$, as required, since this point is in partial

slip. Also, in the partial slip annulus $q_x^{'}(r) = 0$ and $q_x(r) = f\,p(r)$. Finally, in the stick disk $q_x(r) < f\,p(r)$, as required. Therefore, the shear traction distribution satisfies the boundary conditions for partial slip and stick.

Since the shear tractions are all acting in the x direction, Mindlin's solution does not satisfy the orthogonality condition for slip, i.e. the requirement for shear tractions to oppose relative slip is not precisely satisfied. The solution is accurate when the Poisson's ratio is zero and the error increases with ν. Munisamy et al. [49] obtained a corrected numerical solution to this problem, where the tractions are correctly aligned.

2.6 Dislocation Densities as Strain Nuclei

Models with higher level of complexity can be obtained by introducing modifications to the half-space geometry through nuclei of strain. This opens the possibility of analysing the contact between two semi-infinite bodies subjected to various loadings, such as a semi-infinite shaft shrink fitted unto a hub or a semi-infinite layer pressed against a half-space.

The basic idea for obtaining a solution is to start with a simple geometry for the contact pair. As the bodies are put in contact, we assume that the normal and shear tractions that arise at the contact interface are such that the contact remains closed and stuck throughout this region, i.e. the contact pressure is compressive everywhere and the shear traction is limited by Coulomb friction. This is equivalent to the bodies being 'adhered' to each other and behaving elastically as one. We then apply superposition of the stress fields in the bilateral (adhered) solution together with an unknown distribution of 'strain nuclei' chosen so that separation and slip boundary conditions are recovered.

The choice of strain nucleus can be any point source of strain (or stress), such as a dislocation, a force-pair or a dipole. In this work, we focus on the use of dislocations as strain nuclei. One of the advantages of using dislocations is that solutions may be obtained for the stress fields and displacements for a range of geometries, such as in an infinite plane, a half-plane, a quarter-plane or around wedges, amongst others

[50–53]. This allows us to maintain the boundary conditions of the problem while introducing the dislocations.

Even though the quantities we wish to employ have precisely the same characteristics as the edge dislocations arising in defect lattices (such as the introduction of a sheet of atoms in a previously perfect lattice structure), *the presence of those flaws is not implied in any way*. The dislocations are used solely as a mathematical means of introducing a controlled and consistent state of stress within the body. A detailed exposition of this method is given by Hills et al. [17].

In a two-dimensional plane context, a dislocation may be formed by making a slit in an infinite solid, from the *core* of the dislocation to any infinitely remote point. The dislocation is formed by imposing a constant displacement between adjacent points located on either side of the slit, followed by inserting or removing material as necessary, and then welding the material back together. The Burgers vector is defined as the constant relative displacement imposed. This will induce a state of stress that is dependent on the components of the Burgers vector (b_x, b_y) but *independent* of the path cut taken.

Figure 2.8 shows two methods of creating an edge dislocation with a Burgers vector b_x. In Figure 2.8a, the material is cut along the *y-axis* and pulled apart, followed by the insertion of a thin strip of thickness b_x. Then, the material is welded together again. In Figure 2.8b, a cut is made along the *x-axis* and the material is slipped by an amount b_x in the positive x direction before being re-joined. An impressive characteristic of these operations is that the induced stress fields and displacements are the same for both cases. As long as the material is displaced a constant amount b_x along the positive x axis, the solutions will be the same. The dislocation is *path-cut independent*. Also, since we are specifying a *constant* displacement along the length of the cut, the dislocation is said to be of the Volterra type.

Dislocations can be classified through the jargon ‘climb’ or ‘glide’, defined as follows: if a strip of material is inserted (Figure 2.8a), so that the Burgers vector is *perpendicular* to the path cut, the dislocation is said to be ‘climb’; if the material is displaced in

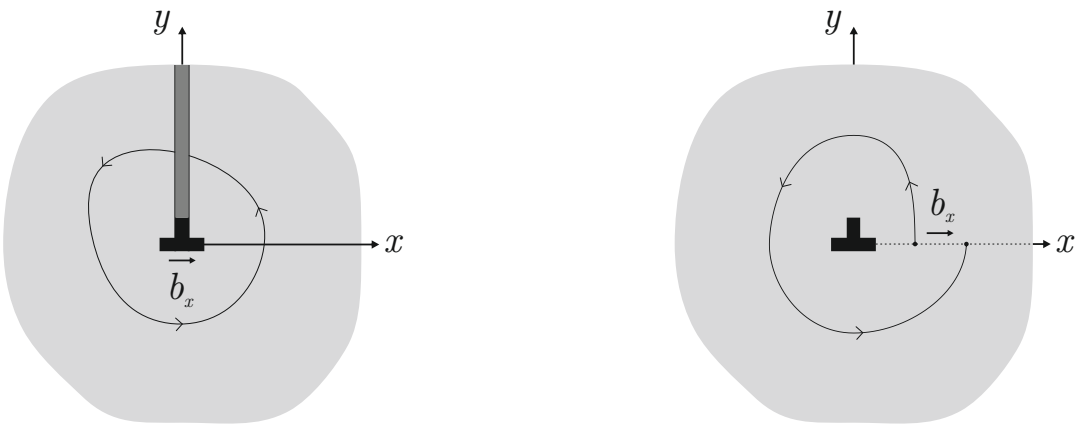

Climb Dislocation *Glide Dislocation*

(a) **(b)**

Figure 2.8: Path cuts for a climb (a) and glide (b) plane dislocation.

shear, so that the Burgers vector is *parallel* to the path cut, the dislocation is said to be 'glide' (Figure 2.8b).

2.7 Solution of Cracks and Contact Problems

The study of stress intensity factors in a crack subjected to external loading can be made by applying **Bueckner's Principle** [54], which may be stated as [17, 55]:

The mode I stress intensity factor for a crack in a body subjected to external forces is identical to that for a similar crack, subjected to internal pressure in a similar body which has no external forces acting on it where the internal pressure acting on the crack is equal to the stress that would exist normal to the crack-line in the uncracked body subjected to the external forces. An analogous procedure exists for shear stresses and the calculation of sliding-mode stress intensity factors.

Bueckner's principle can be exploited to model cracks by the distribution of strain nuclei along crack lines in otherwise perfect bodies. Figure 2.9 illustrates this process. The solution is a superposition of two problems. First, the stresses are found for the uncracked body (Figure 2.9b). Then, stresses are found for the unloaded body due to the application

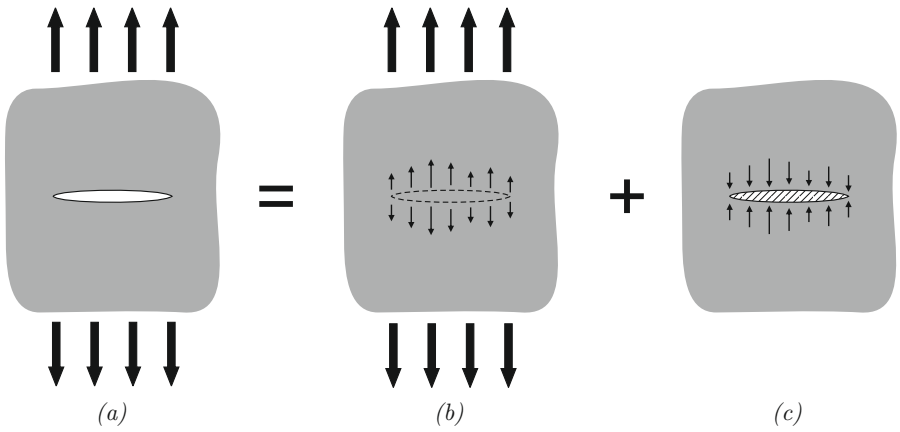

Figure 2.9: Application of Bueckner's principle: (a) overall problem, (b) stress in uncracked body, (c) inclusion of material.

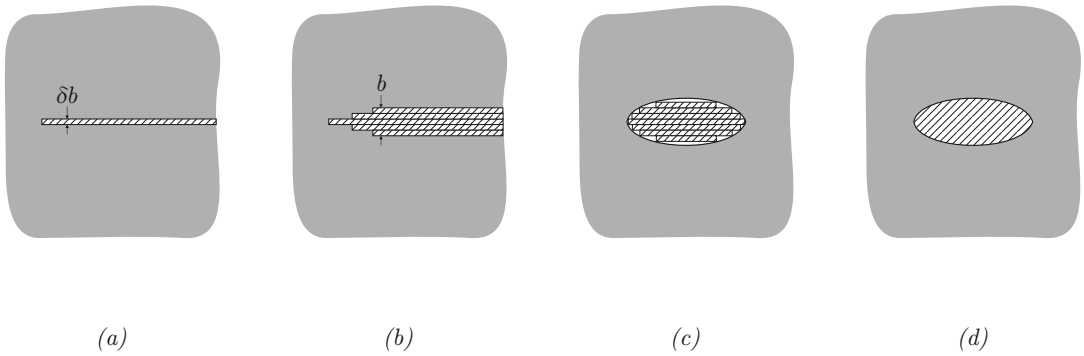

Figure 2.10: Insertion of material between the crack faces.

of equal and opposite tractions to those present along the line of the crack in the first solution (Figure 2.9c). The superposition of those two states result in the crack faces being traction free (Figure 2.9a). The generation of corrective tractions consists in making a slit along the line of the crack, separating the two sides of the cut and then 'inserting material to fill the crack'. A real crack has no material in its interior, of course, thus the insertion of material is just a mathematical device to introduce corrective tractions.

The insertion of material can be visualised as a combination of infinitesimally thin strips, illustrated in Figure 2.10. The first strip is put at one of the crack-ends, extending

from there to infinity. More strips are added and strips are taken away until the geometry of the crack is recovered. The single thin strip of material is an edge dislocation and the geometry of the problem can be recovered by integrating the effects of each thin strip along the crack line.

Mathematically, the problem is defined as finding corrective tractions to satisfy the boundary conditions along the crack line. Consider, for instance, a crack with semi-width a along the x axis, being loaded by tractions $p(x)$ and $q(x)$. Along its faces, the tractions have to be null, i.e.

$$p(x) = 0, \quad q(x) = 0 \quad -a \leq x \leq a \tag{2.78}$$

When this condition is violated, the stresses are corrected by introducing glide $B_x(\xi)$ and climb $B_y(\xi)$ dislocation densities, resulting in

$$p(x) = \sigma_{yy}(x) + \int_{-a}^{a} \Big[G^x_{yy}(x,\xi)\, B_x(\xi) + G^y_{yy}(x,\xi)\, B_y(\xi) \Big] d\xi \tag{2.79}$$

$$q(x) = \sigma_{xy}(x) + \int_{-a}^{a} \Big[G^x_{xy}(x,\xi)\, B_x(\xi) + G^y_{xy}(x,\xi)\, B_y(\xi) \Big] d\xi, \tag{2.80}$$

where the functions G^k_{ij}, $i, j, k = x, y$, are the influence functions of a dislocation.

Equations (2.79) and (2.80) are substituted in eq. (2.78), resulting in two simultaneous integral equations in $B_x(\xi)$ and $B_y(\xi)$. More details about the usage of dislocations to solve crack problems can be found in [17].

The same procedure can also be used to model frictional contact problems. The stresses in the contact region can be corrected by using integrals of dislocation densities in order to satisfy the boundary conditions for a contact, shown in Section 2.5.

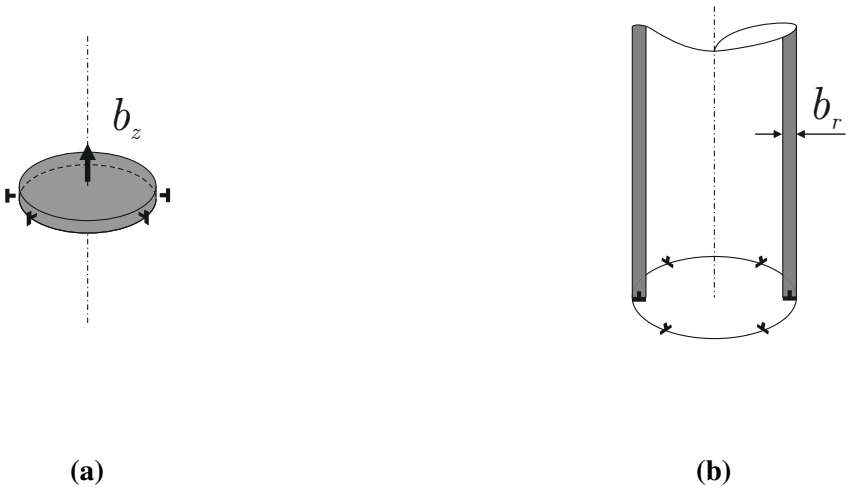

Figure 2.11: Path cuts for an axial prismatic dislocation (a) and a radial dislocation (b).

2.7.1 Circular Dislocation Loops

The construction of circular edge dislocations follows a similar procedure to the plane dislocations. An axial edge dislocation may be formed, for example, by making a path cut along the cylinder $r = c$ and sliding the outer wall with respect to the inner wall by a constant amount b_z (Figure 2.11a). This generates a glide dislocation which is of the Volterra kind and *independent* of the choice of path cut. A $b_r(\xi)$ radial dislocation loop, of radius c and with the dislocation lying at a depth ξ may be formed by making a path cut along the cylinder $r = c$ between the dislocation and the free surface of the half-space and inserting a tube of wall thickness b_r (Figure 2.11b). Even though the amount that the material displaces (b_r) is the same in all directions, the Burgers vector changes direction since it points towards the exterior of the tube. Therefore, the radial dislocation is not of the Volterra kind, as the Burgers vector changes direction along the path cut (the Burgers vector is not constant). As a consequence, it *depends* on the chosen path cut.

In addition to edge dislocations, it is necessary to consider as well a screw loop. It may be created by making a path cut along the cylinder $r = c$ between the dislocation and the free surface of the half-space and twisting the outer wall with respect to the inner wall by b_θ.

3

Numerical Solution of Singular Integral Equations

The application of dislocation densities in cracks and contact problems results in the need of solving Singular Integral Equations (SIEs). The imposition of distributions of circular edge dislocations to correct stress fields relies on imposing integrals of those dislocations along the contact interface (or the crack line). We then obtain the values of those dislocations that satisfy a certain condition. Since the dislocation values appear inside the integrals, those problems constitute Integral Equations. Besides, some of the influence functions contain singular Cauchy terms ($1/(t-s)$). This section presents the solution for Singular Integral Equations with Cauchy terms.

3.1 Finite Contacts

For a finite contact, a general singular integral equation of the first kind with a simple Cauchy kernel can be written in standard form (with the contact lying along $[-1, 1]$) as

$$F(t) = \int_{-1}^{1} \frac{w(s)\,\phi(s)}{t-s}\mathrm{d}s, \qquad |t| < 1 \tag{3.1}$$

where $F(t)$ is the bilateral traction in a contact (or the normalised traction component on the line of the crack), $B(s) = w(s)\,\phi(s)$ is the dislocation density, $\phi(s)$ is a smooth continuous function and $w(s)$ is a weight function of the form

$$w(s) = (1+s)^{\alpha}\,(1-s)^{\beta}. \tag{3.2}$$

Muskhelishvili [60] proved that, for solids, α and β must each be either $1/2$ or $-1/2$, resulting in four classes of SIEs, depending on the behaviour of $B(s)$ at the end points.

If the function $F(t)$ is simple, eq. (3.1) can be inverted analytically. Several methods for analytical inversion and known solutions are presented in [61, 62]. When $F(t)$ presents significant complexity, however, the inversion must be done numerically.

3.1.1 Gauss-Chebyshev Quadrature

Several quadratures have been developed to numerically solve singular integral equations, including the use of piecewise quadratic polynomials [63] and closed-type schemes, such as the Lobatto-Chebyshev quadrature [64].

Presented here is the standard Gauss-Chebyshev quadrature, devised by Erdogan, Gupta and Cook [22]. Its main advantage is the closed form solution for the quadrature points and weights, which results in its implementation being simple and straightforward. For this quadrature, the weight function is associated with the Chebyshev polynomials of the first kind T_N. The solution for eq. (3.1) is given as

$$F(t_k) = \sum_{i=1}^{N} W_i\,\frac{\phi(s_i)}{t_k - s_i}, \qquad k = 1, \ldots, N+n \tag{3.3}$$

where s_i are the integration points, t_k the collocation points and W_i the weights. These are all dependent on the behaviour of the dislocation density function at the end points. Since

Table 3.1: Gauss-Chebyshev quadrature formulae for Cauchy kernels

Case	$w(s)$	s_i	t_k	W_i	n
A	$\frac{1}{\sqrt{1-s^2}}$	$\cos\left(\pi\frac{2i-1}{2N}\right)$	$\cos\left(\pi\frac{k}{N}\right)$	$\frac{1}{N}$	-1
B	$\sqrt{\frac{1-s}{1+s}}$	$\cos\left(\pi\frac{2i}{2N+1}\right)$	$\cos\left(\pi\frac{2k-1}{2N+1}\right)$	$\frac{2(1-s_i)}{2N+1}$	0
C	$\sqrt{\frac{1+s}{1-s}}$	$\cos\left(\pi\frac{2i-1}{2N+1}\right)$	$\cos\left(\pi\frac{2k}{2N+1}\right)$	$\frac{2(1+s_i)}{2N+1}$	0
D	$\sqrt{1-s^2}$	$\cos\left(\pi\frac{i}{N+1}\right)$	$\cos\left(\pi\frac{2k-1}{2(N+1)}\right)$	$\frac{1-s_i^2}{2N+1}$	+1

the function's behaviour is dictated by $w(s)$, there are four sets of s_i, t_k and W_i. These are shown in Table 3.1. Case A corresponds to a function with singular behaviour at both ends. Case D corresponds to a function bounded at both ends of the integration interval. Cases B and C describe functions bounded at one on end and singular at the other.

3.2 Semi-infinite contacts

While the majority of complete and incomplete contacts will happen over a finite region, the modelling of receding contacts often involves imposing integrals over a semi-infinite region, in order to account for the initial configuration of the contact.

In this case, a general singular integral equation of the first kind with a simple Cauchy kernel can be written in standard form (with the contact lying along $[0, \infty]$) as

$$F(v) = \int_0^\infty \frac{w(u)\,\phi(u)}{v-u}\mathrm{d}u, \qquad 0 \leq v \leq \infty \tag{3.4}$$

where $F(v)$ is the bilateral traction in a contact, $B(u) = w(u)\,\phi(u)$ is the dislocation density, $\phi(u)$ is a smooth continuous function and $w(u)$ is a weight function.

Two numerical methods are considered here to solve these integrals: a standard Gauss-Laguerre quadrature; and the application of a transformation function.

3.2.1 Gauss-Laguerre Quadrature

For this quadrature, we take $w(u)$ as

$$w(u) = u^{\alpha}\, e^{-u}, \tag{3.5}$$

where α must be $1/2$ when the contact is bounded at both ends of the interval or $-1/2$ when it is bounded at $u = 0$ and singular at $u = \infty$.

Ioakimidis [65] shows that the solution of eq. (3.4) is given by

$$F(v_k) = \sum_{i=1}^{N} X_i \, \frac{\phi(u_i)}{v_k - u_i}, \qquad k = 1, \ldots, N + n \tag{3.6}$$

where u_i are the integration points, v_k the collocation points and X_i the weights for the Gauss-Laguerre quadrature. When the solution is expected to be bounded at both ends of the interval, $n = 1$, while $n = 0$ for the case where $w(u)$ is bounded at infinity and singular at $u = 0$.

The integration points u_i are given as the roots of the Laguerre polynomial $L_N^{(\alpha)}(u)$. The weights X_i are given by:

$$X_i = \frac{N!\,\Gamma\left(N + \alpha + 1\right)}{u_i \left[L_N^{(\alpha)\prime}(u_i)\right]^2}, \tag{3.7}$$

where $\Gamma\left(\cdot\right)$ represents the gamma function [66] and $L_N^{(\alpha)\prime}(u)$ is the first derivative of the Laguerre polynomial with respect to u.

The collocation points v_k are selected as the zeros of the function $\lambda(v)$:

$$\lambda_N^{(\alpha)}(v) = \pi \, \cot\left(\pi\,\alpha\right) \, v^{\alpha}\, e^{-v}\, L_N^{(\alpha)}(v) - \Gamma\left(\alpha\right) \, {}_1F_1\left(N + 1, 1 - \alpha; -v\right), \tag{3.8}$$

where ${}_1F_1(a,b;z)$ represents the Kummer confluent hypergeometric function [66].

For $\alpha = \pm 1/2$, eq. (3.8) simplifies to:

$$\lambda_N^{(-1/2)}(v) = 2\sqrt{\pi}\,{}_1F_1\left(N+1, 3/2; -v\right) \tag{3.9}$$

$$\lambda_N^{(1/2)}(v) = -\sqrt{\pi}\,{}_1F_1\left(N+1, 1/2; -v\right). \tag{3.10}$$

In each case, this reduces to finding the zeros of the confluent hypergeometric function ${}_1F_1(a,b;z)$, which can be achieved through a Newton-Raphson algorithm. In addition, there must be a v_k point between a pair of consecutive u_i [65]. Hence, we can take the initial guess for each v_k as the average of consecutive integration points. Tables D.1 to D.4 in Appendix D show the Gauss-Laguerre quadrature points and weights for $N = 1, 10, 20$ and 40.

The Gauss-Laguerre quadrature has some drawbacks when implemented in a computer program. First, there are no explicit equations to determine the quadrature points and the computational time to obtain them is significant for large N ($N \gtrsim 40$). In addition, for large N, some of the weights are of order of magnitude 10^{-60} and cannot be operated on properly using standard double precision arithmetic in a computer code. The need for quadruple precision (or variable precision in MATLAB) increases computational costs significantly.

3.2.2 Modified Gauss-Chebyshev Quadrature

An alternative to Gauss-Laguerre quadrature consists in modifying the Gauss-Chebyshev scheme through a transformation function, which maps the semi-infinite interval $[0, \infty]$ to the regular interval $[-1, 1]$. Suitable mapping functions include polynomials, exponentials and trigonometric functions.

Consider, for instance, the following transformations to map the coordinate v ($0 \leq v \leq \infty$) to the normalised coordinate t ($-1 \leq t \leq 1$):

$$t = \frac{v-1}{v+1} \tag{3.11}$$

$$t = 1 - 2\,e^{-v} \tag{3.12}$$

$$t = 2\,\tanh(v) - 1. \tag{3.13}$$

The solution to eq. (3.4) is, then, given by eq. (3.3), where $\alpha = 1/2$ corresponds to case D (bounded-bounded) and $\alpha = -1/2$ corresponds to case B (singular-bounded) and can be later mapped back to the interval $0 \leq v \leq \infty$ by using the inverse of the relationship chosen in eq. (3.11).

3.2.3 Quadrature Comparison

Consider the following illustrative singular equation with a Cauchy kernel:

$$\int_0^\infty \frac{s^{1/2}\,e^{-s}\,\phi(s)\,ds}{s-x} = \frac{e\,\pi\,\mathrm{erfc}(1) - 2\sqrt{\pi\,x}\,\mathrm{F}\left(\sqrt{x}\right)}{x+1}, \tag{3.14}$$

where $\mathrm{erfc}(1)$ is the complementary error function ($\mathrm{erfc}(x) = 1 - \mathrm{erf}(x)$) and $F(x)$ represents the Dawson integral [66], given as

$$\mathrm{F}(x) = e^{-x^2} \int_0^x e^{y^2} dy. \tag{3.15}$$

The analytical solution $g(x) = w(x)\,\phi(x)$ to eq. (3.14) is given by

$$g(x) = \frac{w(x)}{1+x}, \quad w(x) = x^{1/2}\,e^{-x}, \quad \phi(x) = \frac{1}{1+x}. \tag{3.16}$$

The numerical quadratures shown in the previous sections can also be applied to find $\phi(x)$. The solution is expected to be bounded at both ends of the interval.

Figure 3.1 compares the analytical solution with the numerical inversions for the Gauss-Laguerre and Gauss-Chebyshev quadratures, with $N = 40$. For the Gauss-

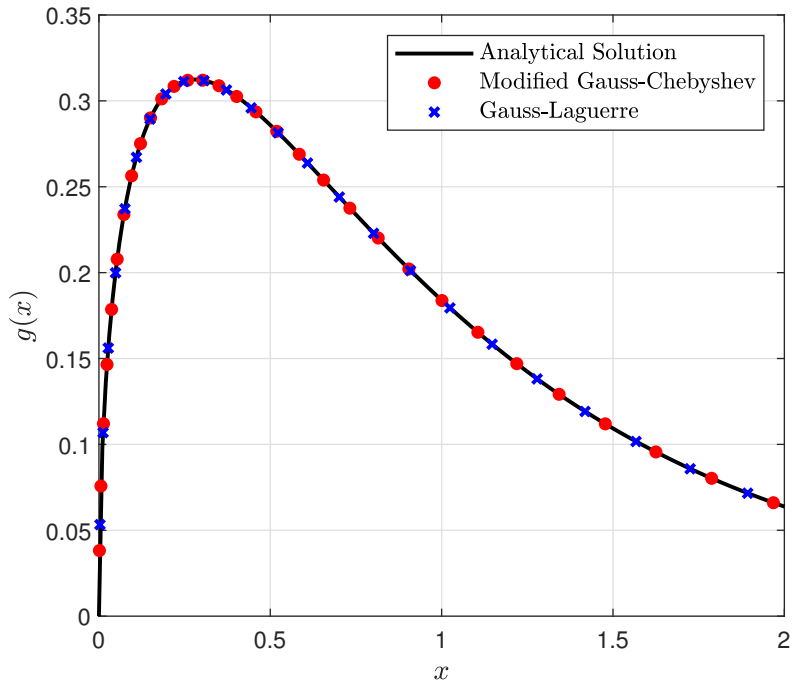

Figure 3.1: Comparison between analytical and numerical solutions of illustrative singular integral equation.

Laguerre quadrature, a scaling parameter $\alpha = 0.05$ was used to ensure proper distribution of points around the interval of interest. Note that there is no loss of accuracy by using the modified Gauss-Chebyshev quadrature on this example.

However, computational time is significantly improved when using the modified Gauss-Chebyshev quadrature, due to the need of extra precision in the computation when using Gauss-Laguerre. Resolving this problem 100 times in a MATLAB implementation, the Gauss-Laguerre scheme is approximately 26 times slower than the modified Gauss-Chebyshev, even when the quadrature points are pre-calculated.

Part I

Preliminary Problems

The application of circular dislocations to solve contact problems often fails because of implementation errors of the influence functions. Because of the complexity of the kernel functions, the literature for the circular dislocation kernels and Lipschitz-Hankel integrals are often ridden with typos and errors, which result in erroneous influence functions.

To circumvent this problem and bring a verified set of circular dislocations into public domain, Part I presents a verification of the methodology of using dislocation densities as modifiers of interfacial tractions and of the implementation of the axisymmetric influence functions, through the solution of three simpler problems.

Chapter 4 uses a distribution of ring dislocations to determine the crack tip stress intensity factors for a ring crack at the surface of a half-space subjected to a concentrated normal force P put at the axis of symmetry. This solution will show that the circular edge dislocations are suitable quantities to be used as stress correctors (nuclei of strain) and will provide a verification for the implementation of the axial and radial kernels, together with MATLAB code provided as supplementary material. For a short crack, the stress intensity factors for a plane crack at the surface of a half-space under remote tension is recovered ($K_I = 1.1215$, $K_{II} = 0$).

Next, two 'simpler' axisymmetric frictional problems are proposed, where no opening is expected. The first problem is presented in Chapter 5, where a shaft-hub system is subjected to a concentrated normal force. This illustrates the use of circular dislocations to obtain the stress fields of a frictional contact in partial slip. Because this problem can be solved using only the axial dislocation loop, it provides a 'controlled environment' to test its implementation.

In the second problem (presented in Chapter 6), the same shaft-hub system is subjected to a monotonically increasing torque after being shrink fitted in assembly. This shows the use of dislocation densities in frictional contacts that involve orthogonal components of shear stress, as the application of torque induces a shear stress which is perpendicular to the one induced by the shrink fit assembly. Careful consideration must be taken to ensure that the solution satisfies the orthogonality condition at each time step, i.e. that the direction of the equivalent shear stress is collinear but opposed to the slip velocity. In

addition to the implementation of the screw dislocation, a new algorithm for the solution of contact problems involving orthogonal shearing stress is proposed.

A comparison between the analytical solutions presented in Part I and their respective finite element solutions are presented in Appendix C.

4

Ring Cracks in a Half-Space

Ring Cracks at the Surface of a Half-Space

J.P. Lopes[a,*], D.A. Hills[a]

[a] *Department of Engineering Science, University of Oxford, Parks Road, Oxford OX1 3PJ, United Kingdom*

Abstract

This paper uses a distribution of ring dislocations to determine the crack tip stress intensity factors for a ring crack at the surface of a half-space subjected to a point force at the axis of symmetry. Three cases are considered: a short crack (relative to its radius), fully open to its root; a longer crack open at the surface but closed and slipping to the root; and a longer crack open at the surface and slipping to some self-determining point in the closing region. The stress intensity factors and points of closure and stick are determined.

Keywords: Ring dislocations, Axisymmetric, Crack, Stress intensity factor

1. Introduction

A powerful method for solving for crack tip stress intensity factors and slip conditions for cracks in simple geometries, but where there may be at least some crack closure, is to use a combination of the nominal stress field in the crack's absence, together with arrays of strain nuclei in the form of dislocations. This expedient is numerically very efficient and is well established for plane problems [1]. In principle, the same ideas may be applied both to general three dimensional problems (where a cruder discretisation of the crack face is needed [2]) and to axi-symmetric problems. Here we address the latter, using circular dislocation loops. This permits all the quadratures and techniques developed for plane problems to be used but suffers from a drawback associated with the nature of the dislocation solution: straight dislocations (that is, those used in plane elasticity) are of the Volterra kind, because they have a constant Burgers vector and, as a consequence, the solution is independent of the path cut used to form the dislocation, so that we may tacitly assume that this follows the line of the crack, without detailed considerations of how we actually form the dislocation solution. Turning to circular dislocations, we see that the ring edge dislocation with axial Burgers vector (b_z) is also Volterra in nature, but the same is *not* true of the radial dislocation (b_r), although a number of crack solutions have either been sent to journals or actually appeared in the literature in which this need has been ignored. In order to circumvent this problem, some authors resort to using dislocation dipoles [3], but this results in singular integral equations with hypersingular kernels (i.e., kernels with $1/(t-s)^2$ terms), requiring a much more powerful quadrature scheme to be solved. The purpose of this paper is to solve an illustrative axi-symmetric crack problem using the path-cut dependent approach, by making use of the dislocation kernels for a circular dislocation in a homogeneous elastic half-space where the plane of the ring is parallel with the free surface, and due to Paynter [4, 5]. Supplementary material will be attached giving MATLAB code to enable others to use these results in further problems without the need to transcribe the solutions manually, we hope, thereby, avoiding errors.

*Corresponding author

Email addresses: jhonatan.dapontelopes@eng.ox.ac.uk (J.P. Lopes), david.hills@eng.ox.ac.uk (D.A. Hills)

2. Bilateral Problem

The basic, illustrative, bilateral problem is shown in Figure 1. A point force, P is applied acting into an elastic half-space whose Poisson's ratio is ν. In the cylindrical coordinate set of Figure 1, the state of stress within the half-space is given by Timoshenko [6], and the tractions arising on any cylindrical cut (an $r =$ constant surface), $\tilde{\sigma}_{ij}(r,z)$ are given by

$$\tilde{\sigma}_{rr}(r,z) = \frac{P}{2\,\pi}\left\{(1-2\,\nu)\left[\frac{1}{r^2} - \frac{z}{r^2\,(r^2+z^2)^{1/2}}\right] - \frac{3\,r^2\,z}{(r^2+z^2)^{5/2}}\right\} \tag{1}$$

$$\tilde{\sigma}_{rz}(r,z) = -\frac{3\,P}{2\,\pi}\left\{\frac{r\,z^2}{(r^2+z^2)^{5/2}}\right\}. \tag{2}$$

As we would expect the stress field is self-similar, as there are no length dimensions in the problem, and the stresses decay as $[L^{-2}]$. For a force acting inwards there is a band, making an angle of approximately 83° with respect to the axis of symmetry where the radial stress is tensile, and a band between the angles of 83° and 15°

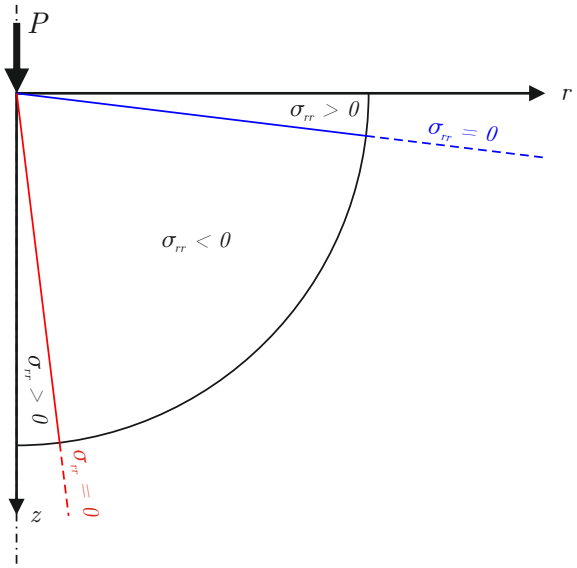

Figure 1: Bands of stress given by the bilateral solution for an inwards force.

where the radial stress is compressive, and then the narrow cone around the axis where it again becomes tensile.

Therefore, a short crack (relative to its radius) will be fully open to its root, Figure 2b, and denoted case I. A longer crack, Figure 2c, and where the inter-face coefficient of friction is small, will be open at the surface but closed and slipping to the root, case II, but, if the coefficient of friction is high enough slip will not penetrate to the root but will stop at some self-determining point in the closed region, case III, Figure 2d. Thus, case I will give rise to both modes I and II stress intensities, case II will give to a mode II stress intensity only, and case III will give rise to a wholly bounded state of stress everywhere. This set of cases is not exhaustive, and we explicitly exclude the case where the crack is so deep relative to its radius that its tip penetrates into the near-axis tension region.

3. Formulation

The general principle in obtaining a solution will be to develop expressions for the tractions on the surface of the crack, $N(z), S(z)$, representing the normal and shear components, respectively, as the sum of the bilateral solution together with an integral representation of slip in the form of a distribution of climb and glide dislocations. The dislocations needed are all 'edge' in character, with their Burgers vectors lying in a $\theta = constant$ plane. A $b_r(\xi)$ climb dislocation loop, of radius c and with the dislocation lying at a depth ξ may be formed by making a path cut along the cylinder $r = c$ between the dislocation and the free surface of the half-space and inserting a tube of wall thickness b_r. It models crack opening, and

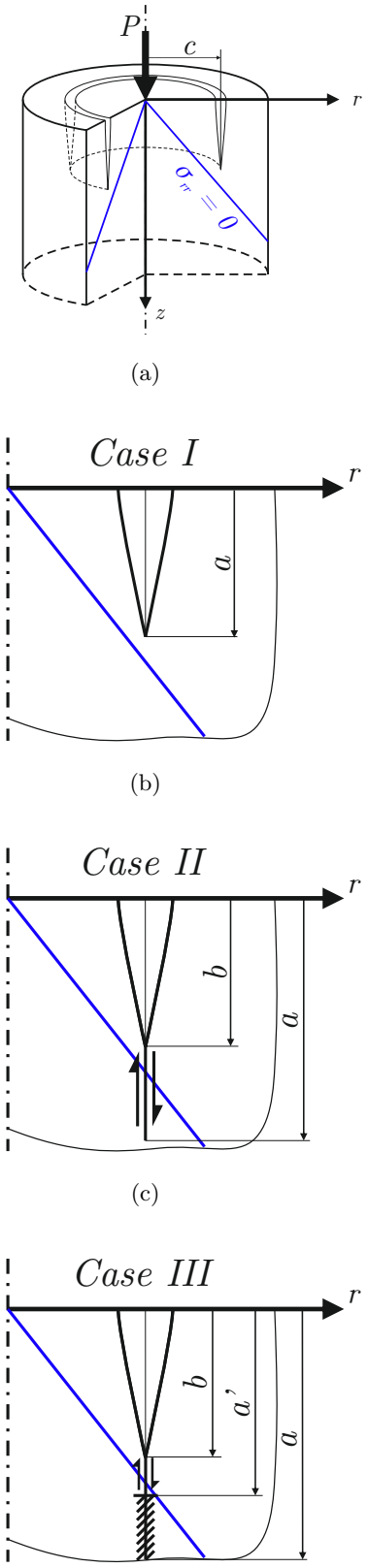

Figure 2: A radial crack subjected to a point force.

will induce tractions along the same cylinder $\hat{\sigma}_{ri}(z)$,where $i = r, z$, given by

$$\hat{\sigma}_{ri}(z) = G^r_{ri}(z,\xi) b_r(\xi). \tag{3}$$

The functions $G^r_{ri}(z,\xi)$ are extremely complicated in form and are defined in [5], as well as being explicitly provided in the supplementary material and in Appendix A. They are bounded ('regular') when $i = z$ but display a Cauchy singularity when $i = r$.

In a similar way, a second edge dislocation may be formed by (for example) making the same path cut on the same surface as above, but now sliding the outer wall with respect to the inner wall by a constant amount b_z. This generates a glide dislocation which is of the Volterra kind and will be used to represent crack slip displacement. It will induce tractions along the same cylinder $\hat{\sigma}_{zi}(z)$, where $i = r, z$, given by

$$\hat{\sigma}_{zi}(z) = G^z_{zi}(z,\xi) b_z(\xi). \tag{4}$$

The functions $G^z_{zi}(z,\xi)$ are again extremely complicated in form and are also defined in [5], as well as being explicitly provided in the supplementary material and in Appendix A. This time they are bounded ('regular') when $i = r$ but display a Cauchy singularity when $i = z$. The resulting tractions on the plane of the crack surface are given by

$$N(z) = \tilde{\sigma}_{rr}(z) + \int_{opening} G^r_{rr}(z,\xi)\, B_r(\xi) d\xi + \int_{slip} G^z_{rr}(z,\xi)\, B_z(\xi) d\xi \tag{5}$$

$$S(z) = \tilde{\sigma}_{rz}(z) + \int_{opening} G^r_{rz}(z,\xi)\, B_r(\xi) + \int_{slip} G^z_{rz}(z,\xi)\, B_z(\xi) d\xi \tag{6}$$

where $B_i(\xi) = db_i/d\xi$, $i = r, z$. Glide dislocations are installed over the whole of the length of the crack where slipping occurs, including the open portion, and climb dislocations are installed over that part of the crack which is open. Equations (5) and (6) form the basis of the solution and integral equations may be generated in slightly different forms for the three cases of response described in §2.

3.1. Case I

This is the most straightforward problem to consider, and is hence dealt with first, Figure 2b. The crack is of depth a, which is sufficiently small (relative to c) for it to be open to the root. The boundary conditions for the crack faces to be traction-free are

$$N(z) = 0 \tag{7}$$

$$S(z) = 0 \qquad 0 \le z \le a \tag{8}$$

which, with eqs. (5) and (6) define the two simultaneous Cauchy integral equations

$$\int_0^a \Big[G^r_{rr}(z,\xi)\, B_r(\xi) + G^z_{rr}(z,\xi)\, B_z(\xi)\Big] \mathrm{d}\xi = -\tilde{\sigma}_{rr}(z) \qquad 0 \le z \le a \tag{9}$$

$$\int_0^a \Big[G^r_{rz}(z,\xi)\, B_r(\xi) + G^z_{rz}(z,\xi)\, B_z(\xi)\Big] \mathrm{d}\xi = -\tilde{\sigma}_{rz}(z) \qquad 0 \le z \le a. \tag{10}$$

These equations possess the property that the range of the integrals is the same as the range of imposition of the right hand side, so that they constitute two well-posed integral equations with generalized Cauchy kernels. They must be solved numerically using a standard numerical quadrature devised by Erdogan, Gupta and Cook [7]. First, we put them in standard form over the intervals $[-1\,, 1]$ utilizing the substitutions

$$s = \frac{2\,\xi}{a} - 1\,, \qquad t = \frac{2\,z}{a} - 1 \qquad 0 \le z, \xi \le a \tag{11}$$

which give

$$\int_{-1}^1 \Big[G^r_{rr}(t,s)\, B_r(s) + G^z_{rr}(t,s)\, B_z(s)\Big] \mathrm{d}s = -\tilde{\sigma}_{rr}(t) \qquad -1 \le t \le 1 \tag{12}$$

$$\int_{-1}^1 \Big[G^r_{rz}(t,s)\, B_r(s) + G^z_{rz}(t,s)\, B_z(s)\Big] \mathrm{d}s = -\tilde{\sigma}_{rz}(t) \qquad -1 \le t \le 1. \tag{13}$$

The next step is to consider the general form of the solution required, and here we note that, at the crack root ($t = 1$), the displacement gradient must be square root singular in nature, while at the surface it must bounded. The quadratures available do not give us the option of letting the gradients take a finite value, so we instead choose it to be square root bounded. This is slightly over restrictive – it means that the crack faces must parallel, for example – but is known to have only a very tiny effect on the crack root [1], and so we assume fundamental functions $B_i(s)$ as shown below, which leaves the unknown dislocation densities being represented by the functions $\phi_i(s)$:

$$B_i(s) = \phi_i(s) \sqrt{\frac{1+s}{1-s}} \qquad i = r,\, z \tag{14}$$

$$\tag{15}$$

and eqs. (12) and (13) become, in normalised form

$$\sum_{i=1}^{N}\left\{W_i\left[G^r_{rr}(t_k,s_i)\,\phi_r(s_i)+G^z_{rr}(t_k,s_i)\,\phi_z(s_i)\right]\right\} = -\frac{2}{\pi\,a}\tilde{\sigma}_{rr}(t_k) \qquad k=1,\ldots,N \tag{16}$$

$$\sum_{i=1}^{N}\left\{W_i\left[G^r_{rz}(t_k,s_i)\,\phi_r(s_i)+G^z_{rz}(t_k,s_i)\,\phi_z(s_i)\right]\right\} = -\frac{2}{\pi\,a}\tilde{\sigma}_{rz}(t_k) \qquad k=1,\ldots,N \tag{17}$$

where the integration points s_i, collocation points t_k and weights W_i for the quadrature are given in Appendix B.

Thus, we have a set of $2N$ equations for $2N$ unknowns. Once the vector $[\phi_r(s_i),\phi_z(s_i)]$ is known the crack tip stress intensities may be found from the following relations

$$K_I = \sqrt{2\,\pi\,a}\,\frac{2\,\mu}{(\kappa+1)}\,\phi_r(1) \tag{18}$$

$$K_{II} = \sqrt{2\,\pi\,a}\,\frac{2\,\mu}{(\kappa+1)}\,\phi_z(1), \tag{19}$$

where μ is the modulus of rigidity (shear modulus) and κ Kolosov's constant ($\kappa = 3-4\nu$ for plane strain).

3.2. Case II

The solution described above will be valid for sufficiently small a/c. As this ratio is increased the mode I crack tip stress intensity factor will decrease until it reaches zero at a unique value of a/c, which corresponds to crack-tip closure. In this section we look at what happens for larger values of a/c, and denote the closure point by b, Figure 2c. Notice that, in this problem, point a is specified but point b is an output of the problem. The boundary conditions on the tractions are now rather different. In the open part we require, as before,

$$N(z) = 0 \tag{20}$$

$$S(z) = 0 \qquad 0 \le z \le b \tag{21}$$

whereas, in the closed, slipping region, the shearing traction is limited by friction:

$$N(z) < 0 \tag{22}$$

$$S(z) = f\,N(z) \qquad b \le z \le a. \tag{23}$$

These two sets of conditions may be combined into one by making use of the Heaviside step function, $H(\cdot)$, giving

$$N(z) = 0 \qquad 0 \le z \le b \tag{24}$$

$$S(z) - f\,H(z-b)\,N(z) = 0 \qquad 0 \le z \le a. \tag{25}$$

A further complication is that the climb dislocations are non-zero only over the interval $0 \le z \le b$, whereas the glide dislocations must be distributed over the whole interval $0 \le z \le a$:

$$N(z) = \tilde{\sigma}_{rr}(z) + \int_0^b G^r_{rr}(z,\xi)\,B_r(\xi)\mathrm{d}\xi + \int_0^a G^z_{rr}(z,\xi)\,B_z(\xi)\mathrm{d}\xi \tag{26}$$

$$S(z) = \tilde{\sigma}_{rz}(z) + \int_0^b G^r_{rz}(z,\xi)\,B_r(\xi)\mathrm{d}\xi + \int_0^a G^z_{rz}(z,\xi)\,B_z(\xi)\mathrm{d}\xi \tag{27}$$

or

$$\int_0^b G^r_{rr}(z,\xi)\,B_r(\xi)\mathrm{d}\xi + \int_0^a G^z_{rr}(z,\xi)\,B_z(\xi)\mathrm{d}\xi = -\tilde{\sigma}_{rr}(z) \tag{28}$$

$$\int_0^b B_r(\xi)\left[G^r_{rz}(z,\xi) - f\,H(z-b)\,G^r_{rr}(z,\xi)\right]\mathrm{d}\xi + \int_0^a B_z(\xi)\left[G^z_{rz}(z,\xi) - f\,H(z-b)\,G^z_{rr}(z,\xi)\right]\mathrm{d}\xi = -\left[\tilde{\sigma}_{rz}(z) - f\,H(z-b)\,\tilde{\sigma}_{rr}(z)\right]. \tag{29}$$

Notice that, as required, the region of imposition of the integral equations (eqs. (24) and (25)) matches those integrals in eqs. (28) and (29) which are Cauchy in character.

Since there are two regions of imposition for the integral equations, two sets of quadrature points are needed. Again, the equation must be solved numerically, using Gauss-Chebyshev quadrature [7]. Putting them in standard form over the intervals $[-1\,,1]$ using the substitutions

$$u = \frac{2\,\xi}{b} - 1\,, \qquad v = \frac{2\,z}{b} - 1 \qquad 0 \le z,\xi \le b \tag{30}$$

$$s = \frac{2\,\xi}{a} - 1\,, \qquad t = \frac{2\,z}{a} - 1 \qquad 0 \le z,\xi \le a \tag{31}$$

gives

$$\int_{-1}^{1} G^r_{rr}(v,u)\,B_r(u)\mathrm{d}u + \int_{-1}^{1} G^z_{rr}(v,s)\,B_z(s)\mathrm{d}s = -\tilde{\sigma}_{rr}(v) \qquad -1 \le v \le 1 \tag{32}$$

$$\int_{-1}^{1} B_r(u)\left[G^r_{rz}(t,u) - f\,H(\zeta)\,G^r_{rr}(t,u)\right]\mathrm{d}u + \int_{-1}^{1} B_z(s)\left[G^z_{rz}(t,s) - f\,H(\zeta)\,G^z_{rr}(t,s)\right]\mathrm{d}s = -\left[\tilde{\sigma}_{rz}(t) + f\,H(\zeta)\,\tilde{\sigma}_{rr}(s)\right] \quad -1 \le t \le 1 \tag{33}$$

where $\zeta = (t+1) - 2\,b\,/\,a$.

For the general form of the solution, the behaviour of the climb and glide dislocations are distinct. At the surface, both climb and glide solutions must be bounded. At

the closure point b ($v = 1$), the climb solution must be bounded, since this point is a cusp. At the crack root ($z = a$, $t = 1$), the glide solution must be square root singular. Thus, we choose

$$B_r(u) = \phi_r(u)\,\sqrt{1-u^2} \tag{34}$$

$$B_z(s) = \phi_z(s)\,\sqrt{\frac{1+s}{1-s}} \tag{35}$$

and eqs. (32) and (33) become, in normalised form,

$$\sum_{i=1}^{N}\Big\{X_i\,b\,\phi_r(u_i)\,G^r_{rr}(v_k,u_i) + W_i\,a\,\phi_z(s_i)\,G^z_{rr}(v_k,s_i)\Big\} = -\frac{2}{\pi}\tilde{\sigma}_{rr}(v_k) \qquad k = 1,\ldots,N+1 \tag{36}$$

$$\sum_{i=1}^{N}\Big\{X_i\,b\,\Big[G^r_{rz}(t_k,u_i) - f\,H(\zeta_k)\,G^r_{rr}(t_k,u_i)\Big]\,\phi_r(u_i)\Big\} + \sum_{i=1}^{N}\Big\{W_i\,a\,\Big[G^z_{rz}(t_k,s_i) - f\,H(\zeta_k)\,G^z_{rr}(t_k,s_i)\Big]\,\phi_z(s_i)\Big\} = -\frac{2}{\pi}\Big[\tilde{\sigma}_{rz}(t_k) - f\,H(\zeta_k)\,\tilde{\sigma}_{rr}(t_k)\Big] \quad k = 1,\ldots,N \tag{37}$$

where $\zeta_k = (t_k + 1) - 2\,b\,/\,a$. The integration points (s_i, u_i), collocation points (t_k, v_k) and weights (W_i, X_i) for the quadrature are given in Appendix B.

Equations (36) and (37) form a system of $2N+1$ equations and $2N+1$ unknowns. These are the N values of $\phi_r(u_i)$, N values of $\phi_z(s_i)$ and the closure point b. Once the vector $[\phi_r(u_i), \phi_z(s_i)]$ is known the crack tip stress intensity may be found from the following relation

$$K_{II} = \sqrt{2\,\pi\,a}\,\frac{2\,\mu}{(\kappa+1)}\,\phi_z(1). \tag{38}$$

The value of the mode II crack tip stress intensity will depend on the coefficient of friction. It will reduce in magnitude as the friction is increased. When it vanishes, there is no longer a mode II stress intensity factor, and the solution is as detailed in the following section.

3.3. Case III

The problem we look at now is that of a relatively deep crack (but not so deep that it approaches the region of radial tension, Figure 1), and the general format of the problem is depicted in Figure 2d. We denote the closure point by b and the stick point by a' (Figure 2d). In this problem, point a does not appear in the solution and points b and a' are outputs of the problem. The boundary conditions are similar to those applied in case II. In the open region we require, as in case I,

$$N(z) = 0 \tag{39}$$

$$S(z) = 0 \qquad 0 \le z \le b \tag{40}$$

and in the closed, slipping region, the shearing traction is limited by friction:

$$N(z) < 0 \tag{41}$$

$$S(z) = f\,N(z) \qquad b \le z \le a'. \tag{42}$$

Combining the sets of conditions into one, we have

$$N(z) = 0 \qquad 0 \le z \le b \tag{43}$$

$$S(z) - f\,H(z-b)\,N(z) = 0 \qquad 0 \le z \le a'. \tag{44}$$

The same procedure used for case II can be applied here, giving

$$N(z) = \tilde{\sigma}_{rr}(z) + \int_0^b G^r_{rr}(z,\xi)\,B_r(\xi)\mathrm{d}\xi + \int_0^{a'} G^z_{rr}(z,\xi)\,B_z(\xi)\mathrm{d}\xi \tag{45}$$

$$S(z) = \tilde{\sigma}_{rz}(z) + \int_0^b G^r_{rz}(z,\xi)\,B_r(\xi)\mathrm{d}\xi + \int_0^{a'} G^z_{rz}(z,\xi)\,B_z(\xi)\mathrm{d}\xi, \tag{46}$$

or

$$\int_0^b G^r_{rr}(z,\xi)\,B_r(\xi)\mathrm{d}\xi + \int_0^{a'} G^z_{rr}(z,\xi)\,B_z(\xi)\mathrm{d}\xi = -\tilde{\sigma}_{rr}(z) \tag{47}$$

$$\int_0^b B_r(\xi)\Big[G^r_{rz}(z,\xi) - f\,H(z-b)\,G^r_{rr}(z,\xi)\Big]\mathrm{d}\xi + \int_0^{a'} B_z(\xi)\Big[G^z_{rz}(z,\xi) - f\,H(z-b)\,G^z_{rr}(z,\xi)\Big]\mathrm{d}\xi = -\Big[\tilde{\sigma}_{rz}(z) - f\,H(z-b)\,\tilde{\sigma}_{rr}(z)\Big]. \tag{48}$$

Equations (47) and (48) need to be solved numerically as before. Normalising the integrals over the intervals $[-1\,,1]$ using the substitutions

$$u = \frac{2\,\xi}{b} - 1\,, \qquad v = \frac{2\,z}{b} - 1 \qquad 0 \le z,\xi \le b \tag{49}$$

$$s = \frac{2\,\xi}{a'} - 1\,, \qquad t = \frac{2\,z}{a'} - 1 \qquad 0 \le z,\xi \le a' \tag{50}$$

give

$$\int_{-1}^{1} G^r_{rr}(v,u)\, B_r(u)\mathrm{d}u + \int_{-1}^{1} G^z_{rr}(v,s)\, B_z(s)\mathrm{d}s = -\tilde{\sigma}_{rr}(v) \qquad -1 \le v \le 1 \tag{51}$$

$$\int_{-1}^{1} B_r(u)\left[G^r_{rz}(t,u) - f\, H(\zeta)\, G^r_{rr}(t,u)\right]\mathrm{d}u + \int_{-1}^{1} B_z(s)\left[G^z_{rz}(t,s) - f\, H(\zeta)\, G^z_{rr}(t,s)\right]\mathrm{d}s = -\left[\tilde{\sigma}_{rz}(t) + f\, H(\zeta)\, \tilde{\sigma}_{rr}(s)\right] \quad -1 \le t \le 1 \tag{52}$$

where $\zeta = (t+1) - 2\,b\,/\,a'$.

The integral equations in eqs. (51) and (52) for case III are the same as those found in case II (eqs. (32) and (33)), with a' in place of a. The difference in cases lies in the general form of the solution. For case III, both the climb and glide dislocations must be bounded at both ends of the interval. Therefore,

$$B_r(u) = \phi_r(u)\,\sqrt{1-u^2} \tag{53}$$

$$B_z(s) = \phi_z(s)\,\sqrt{1-s^2} \tag{54}$$

and eqs. (51) and (52) become, in normalised form,

$$\sum_{i=1}^{N}\left\{X_i\, b\, \phi_r(u_i)\, G^r_{rr}(v_k,u_i) + W_i\, a'\, \phi_z(s_i)\, G^z_{rr}(v_k,s_i)\right\} = -\frac{2}{\pi}\tilde{\sigma}_{rr}(v_k) \qquad k = 1,\ldots,N+1 \tag{55}$$

$$\sum_{i=1}^{N}\left\{X_i\, b\left[G^r_{rz}(t_k,u_i) - f\, H(\zeta)\, G^r_{rr}(t_k,u_i)\right]\phi_r(u_i)\right\} + \sum_{i=1}^{N}\left\{W_i\, a'\left[G^z_{rz}(t_k,s_i) - f\, H(\zeta)\, G^z_{rr}(t_k,s_i)\right]\phi_z(s_i)\right\} = -\frac{2}{\pi}\left[\tilde{\sigma}_{rz}(t_k) - f\, H(\zeta)\, \tilde{\sigma}_{rr}(t_k)\right] \quad k = 1,\ldots,N+1 \tag{56}$$

where $\zeta_k = (t_k+1) - 2\,b\,/\,a'$. The integration points (s_i, u_i), collocation points (t_k, v_k) and weights (W_i, X_i) for the quadrature are given in Appendix B.

Equations (55) and (56) form a system of $2N+2$ equations and $2N+2$ unknowns: N values of $\phi_r(u_i)$, N values of $\phi_z(s_i)$, the closure point b and the stick point a'. For this case, there are no mode I or II stress intensity factors.

4. Results

Each of the three classes of problem was coded up using the numerical processor MATLAB. Setting N to 80 makes the solution converge for all cases, i.e. the changes in the stress intensity factors become negligible when N is increased beyond 80. The results are for $\nu = 0.3$. In problems where a length dimension is an unknown of the problem (b in case II and both b, a' in case III), there are additional collocation equations which need to be satisfied and which enable the values of b/c and a'/c to be found. In practice, we guess values of the lengths to be found and omit the central equations from the $N+1$ generated. The column vector of ϕ is found. The omitted equation is then evaluated and the lengths needed are adjusted to minimise the residue.

Consider case I first, the crack fully open to the root, where the results are portrayed in Figure 4. We choose as a non-dimensionalising constant the crack tip stress intensity factor for a crack of length $2a$ embedded in a half-plane, and choose as a reference stress the radial stress at the surface (eq. (1)), so that

$$K_0 = \frac{P\,(1-2\nu)}{2\pi c^2}\sqrt{\pi a}. \tag{57}$$

This means that, as expected, when $a/c \to 0$ we recover the standard result for a plane surface breaking crack under uniform tension ($K_I/K_0 = 1.1215$). As the crack is made longer the normalised mode I stress intensity falls, and goes to zero when $a/c \to 0.207$. This contrasts with the depth at which the radial stress becomes zero (eq. (1)) of $a/c = 0.122$. The same non-dimensionalising constant is also used for mode II loading. Of course the mode II stress intensity vanishes for short cracks and increases as the crack length is increased.

Figure 3 shows what happens when we make the crack longer than those just considered (case II). At the left of the figure ($a/c < 0.207$) the mode II stress intensity for the open crack is re-plotted, and then the right hand part of the figure shows what happens as the crack is made longer, and hence remains closed, with no mode I intensification. First, look at the response with no friction. The K_{II} value, in normalised form, first increases in magnitude, until $a/c \sim 1.1$, beyond which it decreases. We do not attempt to investigate what happens for very large values of a/c, when the crack tip approaches the tension region. Secondly, consider the curves for increasing values of the coefficient of friction. The crack faces are closed along part of their length, including the crack tip, and some of the shear traction is sustained by friction, with the unsatisfied part contributing to a stress intensity of lower magnitude, as expected. The case II solution remains valid until the coefficient of friction reaches the value 0.625. At this point K_{II} falls to zero and, if we attempt to obtain a solution for long cracks slipping at higher coefficients of friction we find that the crack slip displacement changes sign, and this is inconsistent with our assumption that the sign of slip is constant along the whole of the closed portion of the crack. Thus, the solution for a short crack with an interfacial coefficient of friction of 0.7 is valid only for cracks which penetrate a very short distance into the compression region, and the mode II stress intensity vanishes when $a/c \to \sim 0.3$.

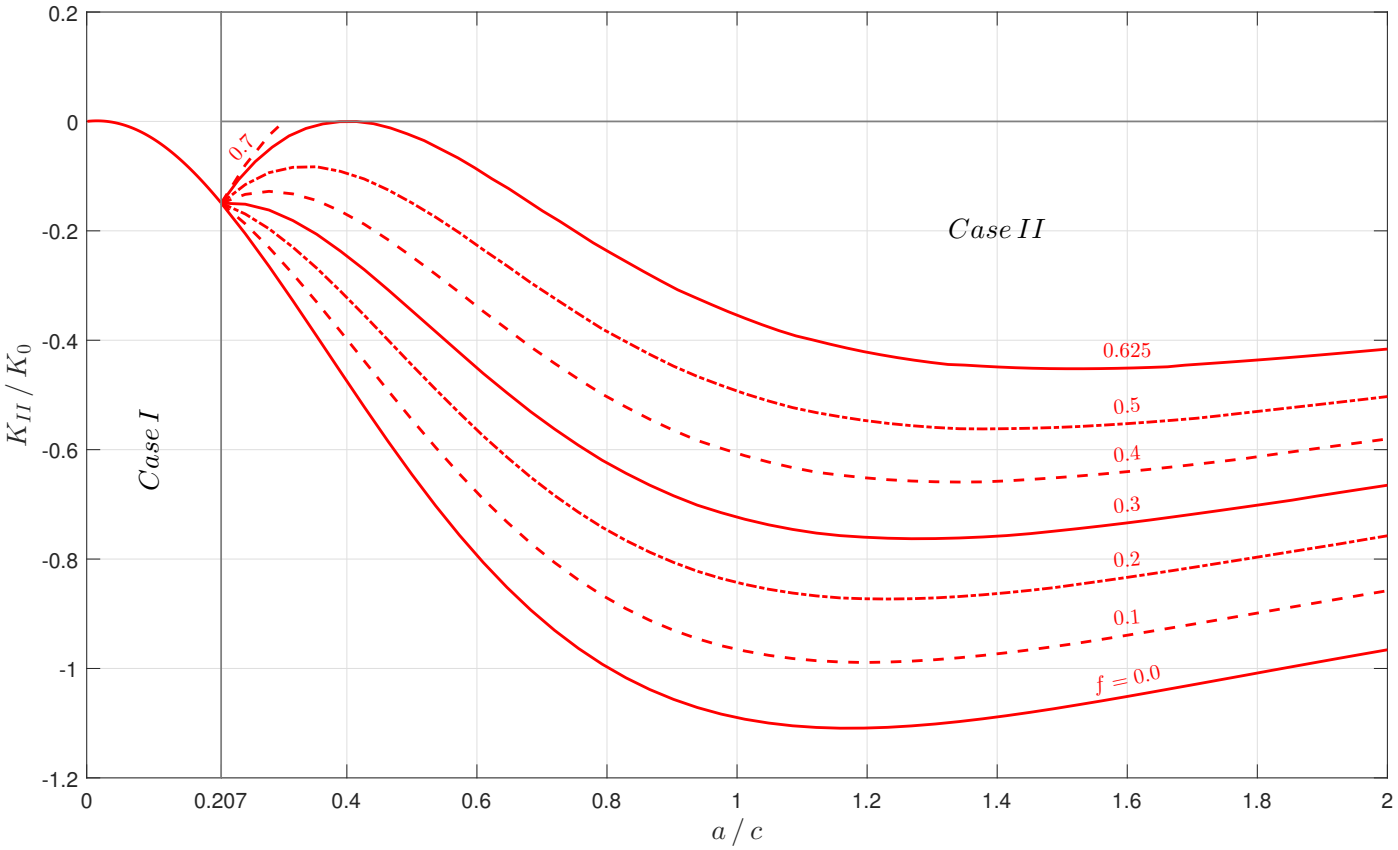

Figure 3: Non-dimensional mode II stress intensity factors for cases I and II.

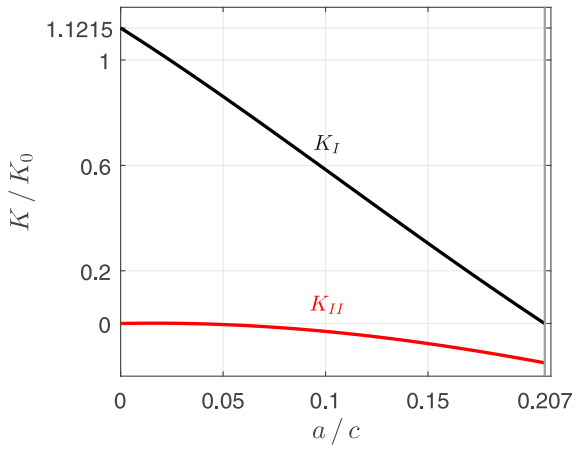

Figure 4: Non-dimensional mode I and II stress intensity factors for case I.

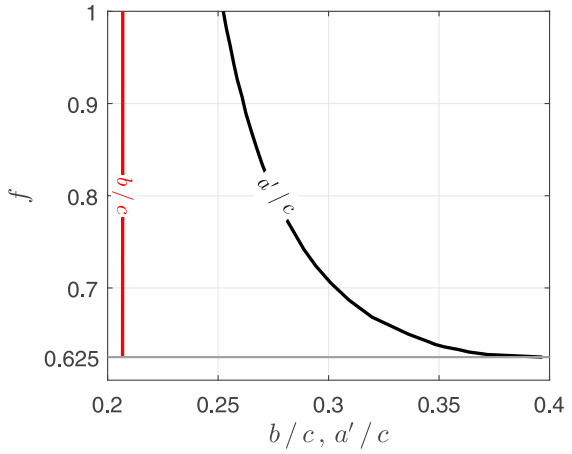

Figure 5: Non-dimensional closure and stick points as a function of the coefficient of friction for case III.

The next question which arises is 'What happens when we have a crack which is longer than $0.207c$, and where the coefficient of friction is greater than 0.625? These are case III problems, in which the crack does not slip all the way to the root, but sticks at some self-determining depth. The depth at which this occurs (a'/c), is shown in Figure 5 as a function of the coefficient of friction. If the coefficient of friction is less than 0.625 the crack will slip to the root. Note that, because of the coupling inherent in the kernels, glide dislocations modify the contact pressure between the crack faces, that is, they induce a change in the direct traction $\sigma_{rr}(z)$, so that we would expect the point of crack closure, b/c, to change. In fact, there is practically no change in this value for realistic coefficients of friction, Figure 5.

5. Conclusions

The crack tip stress intensity factors have been found for a surface-breaking ring crack loaded by a point force. This problem shows the interesting properties that there are regions in which the crack tip suffers both opening and shear loading modes of stress intensity (case I), regions in which the crack tip is closed but it suffers shear mode stress intensity only (case II), and regions in which the crack is closed and the crack root does not slip (case III). The transition from cases I to II was found to occur at a unique value of crack length a/c, and is independent of the applied load. The transition to case III, however, was found to be dependent both on the crack length (only occurs for short cracks) and on the coefficient of friction.

One of the prime motivations for carrying out this calculation was to show that the ring dislocation is a viable quantity to use as a kernel in studying axi-symmetric cracks problems, and also to bring the kernel functions into the public domain. They are attached to this paper as supplementary material suitable for use with MATLAB.

Acknowledgements

J. L. gratefully acknowledges the financial support of Christ Church Oxford, Rolls Royce PLC and CAPES [grant number 88881.128590/2016-01].

References

[1] D. A. Hills, P. A. Kelly, D. N. Dai, A. M. Korsunsky, Solution of crack problems: the distributed dislocation technique, Vol. 44 of Solid Mechanics and Its Applications, Springer Netherlands, Dordrecht, 1996. doi:10.1007/978-94-015-8648-1.

[2] Y. Murakami, Analysis of stress intensity factors of modes I, II and III for inclined surface cracks of arbitrary shape, Engineering Fracfure Mechanics 22 (I) (1985) 101–114.

[3] E. Gordeliy, E. Detournay, Displacement discontinuity method for modeling axisymmetric cracks in an elastic half-space, International Journal of Solids and Structures 48 (19) (2011) 2614–2629. doi:10.1016/j.ijsolstr.2011.05.009.

[4] R. J. H. Paynter, D. A. Hills, A. M. Korsunsky, The effect of path cut on Somigliana ring dislocation elastic fields, International Journal of Solids and Structures 44 (2) (2007) 6653–6677. doi:10.1016/j.ijsolstr.2008.09.001.

[5] R. J. H. Paynter, D. A. Hills, The effect of path cut on Somigliana ring dislocations in a half-space, International Journal of Solids and Structures 46 (2) (2009) 412–432. doi:10.1016/j.ijsolstr.2008.09.001.

[6] S. Timoshenko, J. N. Goodier, Theory of Elasticity, Vol. 49, 1986. doi:10.1007/BF00046464.

[7] F. Erdogan, G. D. Gupta, T. Cook, Numerical solution of singular integral equations, in: Methods of analysis and solutions of crack problems, 1973, pp. 368–425.

[8] G. Eason, B. Noble, I. N. Sneddon, On certain integrals of Lipschitz-Hankel type involving products of Bessel functions, Philosophical Transactions of the Royal Society of London A: Mathematical, Physical and Engineering Sciences 247 (935) (1955) 529–551.

[9] N. I. Muskhelishvili, Some Basic Problems of the Mathematical Theory of Elasticity, 1977. doi:10.1007/978-94-017-3034-1.

Appendix A. State of stress induced by circular edge dislocation loops

This section presents the influence functions due to circular edge dislocation loops. An axial edge dislocation may be formed, for example, by making a path cut along the cylinder $r = c$ and sliding the outer wall with respect to the inner wall by a constant amount b_z. This generates a glide dislocation which is of the Volterra kind and *independent* of the choice of path cut. A $b_r(\xi)$ radial dislocation loop, of radius c and with the dislocation lying at a depth ξ may be formed by making a path cut along the cylinder $r = c$ between the dislocation and the free surface of the half-space and inserting a tube of wall thickness b_r. The radial dislocation, however, is not of the Volterra kind, since the Burgers vector changes direction along the path cut (the Burgers vector is not constant) and, therefore, it *depends* on the chosen path cut.

Appendix A.1. Axial dislocation

Consider a glide axial dislocation loop of radius a put at a position (r, z) in a cylindrical coordinate system and being observed at a depth d, with a Burgers vector component b_z. The stress fields at a position (r, z) are given by

$$\sigma^z_{ri}(r, z) = G^z_{rj}(r, z, d)\, b_z(d) \quad i = r, z. \tag{A.1}$$

The influence functions $G^z_{ri}(\rho, \zeta, \delta)$ $(i = r, z)$ for the glide dislocation in a half-space are given as [5]:

$$G^z_{rr}(\rho,\zeta,\delta) = \frac{2\,\mu}{c\,(\kappa+1)}\Bigg[- J_{1,0;1} + I_{1,0;1} + (\zeta-\delta)\,J_{1,0;2} + (\zeta-3\,\delta)\,I_{1,0;2} + \frac{(\kappa-1)}{2\,\rho}\,J_{1,1;0} - \frac{(\kappa-1)}{2\,\rho}\,I_{1,1;0} - \frac{(\zeta-\delta)}{\rho}\,J_{1,1;1} + \frac{(\zeta\,\kappa-\delta)}{\rho}\,I_{1,1;1} + \frac{(2\,\zeta\,\delta)}{\rho}\,I_{1,1;2} - 2\,\zeta\,\delta\,I_{1,0;3}\Bigg] \tag{A.2}$$

$$G^z_{rz}(\rho,\zeta,\delta) = \frac{2\,\mu}{c\,(\kappa+1)}\Bigg[- (\zeta-\delta)\,J_{1,1;2} + (\zeta-\delta)\,I_{1,1;2} - 2\,\zeta\,\delta\,I_{1,1;3}\Bigg] \tag{A.3}$$

where ρ, ζ and δ are the normalised coordinates, given as

$$\rho = r/c, \qquad \zeta = z/c, \qquad \delta = d/c, \tag{A.4}$$

μ is the modulus of rigidity and κ is the Kolosov's constant.

Appendix A.2. Radial dislocation

The radial dislocation is not of Volterra kind and, thus, is path-cut dependent. There are four possible path-cuts to create a climb dislocation of Burgers vector b_r, defined by Paynter & Hills [5] and shown in Figure A.6. These result in significantly different solutions for the influence functions and should match the path in which the integrals are being evaluated.

Appendix A.2.1. Outer cut (b^o_r)

An 'outside ring' path cut is made by inserting a ring of material at the depth $z = d$, from $r = c$ to infinity, displacing the materials by an amount b_r (Figure A.6a). The angle parameter α designates the angle of the cut with respect to the r axis. For the outer cut, $\alpha = 0$. The influence functions are given as [5]:

$${}^oG^r_{rz}(\rho,\zeta,\delta,\alpha) = \frac{2\,\mu}{c\,(\kappa+1)}\Bigg[J_{0,1;1} - I_{0,1;1} - (\zeta-\delta)\,J_{0,1;2} + (\zeta+\delta)\,I_{0,1;2} - 2\,\zeta\,\delta\,I_{0,1;3}\Bigg] \tag{A.5}$$

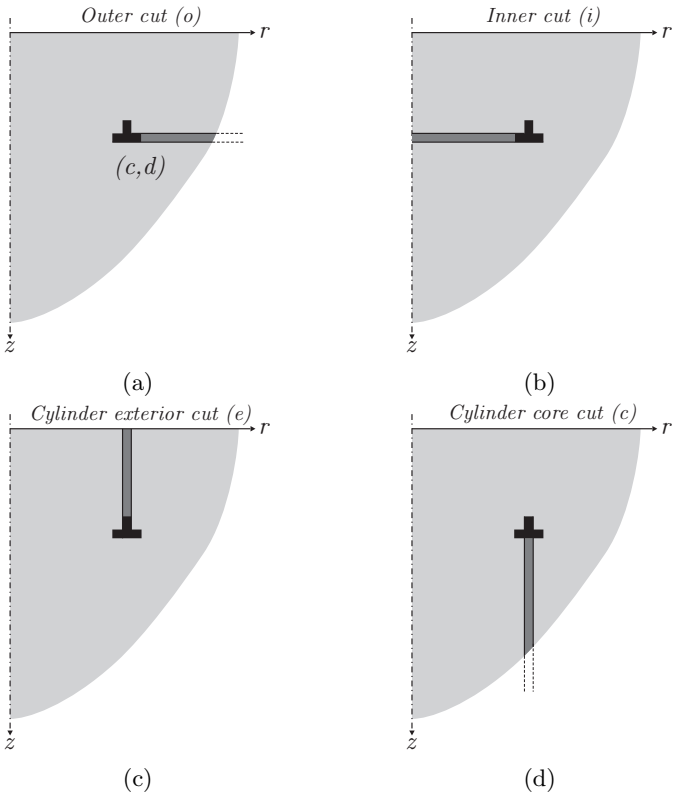

Figure A.6: Path cuts for a radial climb dislocation.

$${}^oG^r_{rz}(\rho,\zeta,\delta,\alpha) = \frac{2\,\mu}{c\,(\kappa+1)}\Bigg[J_{0,1;1} - I_{0,1;1} - (\zeta-\delta)\,J_{0,1;2} + (\zeta+\delta)\,I_{0,1;2} - 2\,\zeta\,\delta\,I_{0,1;3}\Bigg] \tag{A.6}$$

Appendix A.2.2. Inner cut (b^i_r)

An 'inside disk' path cut (Figure A.6b) can be formed by inserting a disk of material at a depth $z = d$, from $r = 0$ to $r = c$, displacing the material by the same amount b^i_r (thickness of the disk). For the inner cut, $\alpha = 0$.

$${}^iG^r_{rr}(\rho,\zeta,\delta,\alpha) = \frac{2\,\mu}{c\,(\kappa+1)}\Bigg[2\,J_{2,0;1}(\alpha) + 2\,I_{2,0;1}(|\alpha|) - (\zeta-\delta)\,J_{2,0;2} + (\zeta+3\,\delta)\,I_{2,0;2} - \frac{(\kappa+1)}{2\,\rho}\,J_{2,1;0}(\alpha) - \frac{(\kappa+1)}{2\,\rho}\,I_{2,1;0}(|\alpha|) + \frac{(\zeta-\delta)}{\rho}\,J_{2,1;1} - \frac{(\zeta+\kappa\,\delta)}{\rho}\,I_{2,1;1} - \frac{(2\,\zeta\,\delta)}{\rho}\,I_{2,1;2} + 2\,\zeta\,\delta\,I_{2,0;3}\Bigg] \tag{A.7}$$

$$
{}^{i}G^{r}_{rz}(\rho,\zeta,\delta,\alpha) = \frac{2\,\mu}{c\,(\kappa+1)}\Bigg[- J_{2,1;1} + I_{2,1;1} + (\zeta-\delta)\,J_{2,1;2} + (\zeta+\delta)\,I_{2,1;2} + 2\,\zeta\,\delta\,I_{2,1;3}\Bigg] \tag{A.8}
$$

Appendix A.2.3. Cylindrical cuts ($b^{c,e}_r$)

The two other path cuts involve cylindrical cuts. The 'exterior' path cut is made by inserting a cylinder of material of wall thickness b^e_r at a position $(r,z) = (c,d)$ extending along the z axis from $z = d$ to $z = 0$, i.e. towards the 'exterior' of the half-space (Figure A.6c). The 'core' path cut is made by inserting a cylinder of material of wall thickness b^c_r at a position $(r,z) = (c,d)$ extending along the z axis from $z = d$ to infinity, i.e. towards the 'core' of the half-space (Figure A.6d). These are dependent of radial dislocations with inside and outside path-cuts (b^i_r and b^o_r) and the corrective Kelvin and Boussinesq terms (b^k_r and b^b_r). The radial dislocations are also dependent of the angle argument α. For an 'exterior' cut, $\alpha = -\pi\,/\,2$ and for a 'core' cut, $\alpha = \pi\,/\,2$. From Paynter & Hills [5]:

$$
{}^{c}G^{j}_{rj}(\rho,\zeta,\delta) = \frac{(\kappa-1)}{(\kappa+1)}\,{}^{i}G^{j}_{rj}(\rho,\zeta,\delta,\pi/2) + \frac{2}{(\kappa+1)}\,{}^{o}G^{j}_{rj}(\rho,\zeta,\delta,\pi/2) - \frac{2\,\mu\,(3-\kappa)}{c\,(\kappa+1)}\,{}^{k}G^{j}_{rj}(\rho,\zeta,\delta,\pi/2) \quad j = r,z \tag{A.9}
$$

$$
{}^{e}G^{j}_{rj}(\rho,\zeta,\delta) = \frac{(\kappa-1)}{(\kappa+1)}\,{}^{i}G^{j}_{rj}(\rho,\zeta,\delta,-\pi/2) + \frac{2}{(\kappa+1)}\,{}^{o}G^{j}_{rj}(\rho,\zeta,\delta,-\pi/2) - \frac{2\,\mu\,(\kappa-1)}{c\,(\kappa+1)}\Bigg[{}^{k}G^{j}_{rj}(\rho,\zeta,\delta,-\pi/2) - {}^{b}G^{j}_{rj}(\rho,\zeta,-\pi/2)\Bigg] \quad j = r,z \tag{A.10}
$$

where ${}^{c}G^{j}_{rj}$, ${}^{e}G^{j}_{rj}$, ${}^{i}G^{j}_{rj}$, ${}^{o}G^{j}_{rj}$, ${}^{k}G^{j}_{rj}$ and ${}^{b}G^{j}_{rj}$ are, respectively, the influence functions for a radial dislocation with core, exterior, inner and outer cuts, and the Kelvin and Boussinesq corrective terms. These corrective terms are given as:

Kelvin term (b^k_r)

$$
{}^{k}G^{r}_{rr}(\rho,\zeta,\delta,\alpha) = \frac{c}{(\kappa+1)}\Bigg[- \frac{(3-\kappa)}{2}\,J_{1,0;0}(\alpha) + \frac{(3\,\kappa-1)}{2}\,I_{1,0;0}(|\alpha|) + (\zeta-\delta)\,J_{1,0;1} + (\kappa\zeta - 3\,\delta)\,I_{1,0;1} - \frac{(\zeta-\delta)}{\rho}\,J_{1,1;0} - \frac{(\zeta-\delta)\,\kappa}{\rho}\,I_{1,1;0} + \frac{(2\,\zeta\,\delta)}{\rho}\,I_{1,1;1} + \frac{(1-\kappa^2)}{2\,\rho}\,I_{1,1;-1}(|\alpha|) - 2\,\zeta\,\delta\,I_{1,0;2}\Bigg] \tag{A.11}
$$

$$
{}^{k}G^{r}_{rz}(\rho,\zeta,\delta,\alpha) = \frac{c}{(\kappa+1)}\Bigg[- \frac{(\kappa-1)}{2}\,J_{1,1;0} + \frac{(\kappa-1)}{2}\,I_{1,1;0} - (\zeta-\delta)\,J_{1,1;1} + (\kappa\zeta-\delta)\,I_{1,1;1} - 2\,\zeta\,\delta\,I_{1,1;2}\Bigg] \tag{A.12}
$$

Boussinesq term (b^b_r)

Kelvin term with depth set to zero ($\delta = 0$).

$$
{}^{b}G^{r}_{rr}(\rho,\zeta) = c\Bigg[- J_{1,0;0}(\alpha) + \zeta\,J_{1,0;1} - \frac{\zeta}{\rho}\,J_{1,1;0} + \frac{(\kappa-1)}{2\,\rho}\,J_{1,1;-1}(\alpha)\Bigg] \tag{A.13}
$$

$$
{}^{b}G^{r}_{rz}(\rho,\zeta) = c\Bigg[- \zeta\,J_{1,1;1}\Bigg] \tag{A.14}
$$

Appendix A.3. Lipschitz-Hankel integrals

In the influence functions, the terms $J_{n,p;q}$ and $I_{n,p;q}$ represent Lipschitz-Hankel integrals. The standard definition for these functions is as an integral of the product of Bessel functions ($J_i(\cdot)$), an exponential term and a power term. Using normalised coordinate variables, it is given as [8]

$$
P_{\mu,\nu;\lambda}(\rho,\zeta) = \int_0^\infty J_\mu(t)\,J_\nu(\rho\,t)\,e^{-\zeta\,t}\,t^{\lambda}\,\mathrm{d}t. \tag{A.15}
$$

In the kernels, the follow definition is applied:

$$
J_{n,p;q} = P_{n,p;q}(\rho,\zeta-\delta) \tag{A.16}
$$

$$
I_{n,p;q} = P_{n,p;q}(\rho,-\zeta-\delta) \tag{A.17}
$$

The Lipschitz-Hankel integrals needed in the kernels are given in [4, 5].

Appendix B. Gaussian Quadrature for SIEs with Cauchy Kernel

A general singular integral equation of the first kind with a simple Cauchy kernel can be written in standard form (with the crack lying along $[-1, 1]$) as

$$F(t) = \int_{-1}^{1} \frac{w(s)\,\phi(s)}{t-s}\mathrm{d}s, \qquad |t| < 1 \tag{B.1}$$

where $F(t)$ is the normalised traction component on the line of the crack, $B(s) = w(s)\,\phi(s)$ is the dislocation density, $\phi(s)$ is a smooth continuous function and $w(s)$ is a weight function of the form

$$w(s) = (1+s)^{\alpha}\,(1-s)^{\beta}. \tag{B.2}$$

It can be proved that the exponents α and β must be either $-1/2$ or $+1/2$ [9], resulting in four classes of SIEs, depending on the behaviour of the $B(s)$ at the end points. Solutions were presented by Erdogan, Gupta and Cook [7]. In those cases, the weight function is associated with the Chebyshev polynomials of the first kind T_N. The solution for eq. (B.1) is given as

$$F(t_k) = \sum_{i=1}^{N} W_i\,\frac{\phi(s_i)}{t_k - s_i}, \qquad k = 1, \ldots, N+n \tag{B.3}$$

where s_i are the integration points, t_k the collocation points and W_i the weights. These are all dependent on the behaviour of the dislocation density function at the end points. Since the function's behaviour is dictated by $w(s)$, there are also four sets of s_i, t_k and W_i. These are shown in Table B.1.

For the cracks solved in this paper, the behaviour of $w(s)$ is either bounded at both ends, which corresponds to case C in Table B.1, or bounded at $s = -1$ and singular at $s = 1$, which corresponds to case D in Table B.1.

Table B.1: Gauss-Chebyshev quadrature formulae for Cauchy kernels

Case	$w(s)$	s_i	t_k	W_i	n
A	$\frac{1}{\sqrt{1-s^2}}$	$\cos\left(\pi\frac{2i-1}{2N}\right)$	$\cos\left(\pi\frac{k}{N}\right)$	$\frac{1}{N}$	-1
B	$\sqrt{\frac{1-s}{1+s}}$	$\cos\left(\pi\frac{2i}{2N+1}\right)$	$\cos\left(\pi\frac{2k-1}{2N+1}\right)$	$\frac{2(1-s_i)}{2N+1}$	0
C	$\sqrt{\frac{1+s}{1-s}}$	$\cos\left(\pi\frac{2i-1}{2N+1}\right)$	$\cos\left(\pi\frac{2k}{2N+1}\right)$	$\frac{2(1+s_i)}{2N+1}$	0
D	$\sqrt{1+s^2}$	$\cos\left(\pi\frac{i}{N+1}\right)$	$\cos\left(\pi\frac{2k-1}{2(N+1)}\right)$	$\frac{1-s_i^2}{2N+1}$	+1

5

The Axisymmetric Shrink Fit Problem Subject to Axial Force

The Axisymmetric Shrink Fit Problem Subjected to Axial Force

J.P. Lopes[a,*], D.A. Hills[a], R.J.H. Paynter[a]

[a]*Department of Engineering Science, University of Oxford, Parks Road, Oxford OX1 3PJ, United Kingdom*

Abstract

A solution for the stress fields in a shaft-hub shrink-fit assembly subjected to an axial force is presented. The assembly is modelled as a semi-infinite shaft embedded within an elastic half-space. The stress field for a bilateral solution is obtained, considering that the contact interface is everywhere subjected to pressure and that the coefficient of friction is sufficient to prevent slip everywhere. This solution is then corrected to satisfy the slip condition using an array of strain nuclei in the form of glide ring dislocations. The contact pressure, shear traction and their ratio is presented as a function of the coefficient of friction and the ratio of shrink-fit to axial force stresses. Finally, the solution is extended to a finite shaft.

Keywords: Ring dislocations, Axisymmetric, Shrink Fit, Contact

1. Introduction

The classical solution for the contact pressure induced in an axisymmetric shrink fit problem is the well-know Lamé solution [1]. It is normally used in plane strain, and represents a very satisfactory solution at interior points well away from the edges, i.e. when $z \gg a$, Figure 1, where a is the radius of the shaft, and when the outer radius of the 'hub' (the part incorporating the hole) is much greater than the radius of the shaft, which is often at least approximately true. The question arises of how that pressure should be modified at the point of insertion of the shaft into the hub, and where the shaft and hub terminate. The latter problem was solved in closed form [2] providing a true local three dimensional correction for the presence of the free surface, and here we enquire how such an assembly responds to the application of a normal force (Figure 1) tending either to push the central shaft in, as shown, or tending to pull it out. In practice the details of the solution will depend, of course, on how the loading is distributed across the end of the shaft but providing that the points we are considering are not too close the details will not matter.

The general idea will be first to use the bilateral solution, that is one where we assume that the interface between shaft and socket is everywhere subjected to pressure and that the coefficient of friction is sufficient to prevent slip everywhere, so that the presence of the interface is not 'felt'. We will then probe the limits of this assumption, and go on to consider problems where a slip zone of finite extent develops by deploying distributions of circular glide dislocations to represent the effects of slip.

2. Adhered Solution

The geometry of the problem is shown in Figure 1. Upon assembly, an infinitely long shaft of radius $a + \Delta_0$ is inserted in a hub with a cylindrical hole of radius a, present in an elastic half-space. Both the shaft and the hub have Poisson's ratio ν and Young's modulus E. The assembly can be thought as inserting a shaft of radius a into a hole of same size under isothermal conditions and then heating only the shaft through a temperature differential ΔT, or by cooling the oversized shaft until it fits and then letting it warm back up. This results in an induced radial strain ϵ^* in the shaft, given by

$$\epsilon^* = \frac{\Delta_0}{a} = \alpha \Delta T \tag{1}$$

where α is the coefficient of thermal expansion for the shaft.

If the coefficient of friction is sufficiently high to prevent any slip, the state of stress that arises from this shrink-fit assembly is given by Paynter et al [2], and the stresses σ_{ij}^{SF} in a point (r,z), $z \geq 0$, are given by

*Corresponding author

Email addresses: jhonatan.dapontelopes@eng.ox.ac.uk (J.P. Lopes), david.hills@eng.ox.ac.uk (D.A. Hills), robert.paynter@eng.ox.ac.uk (R.J.H. Paynter)

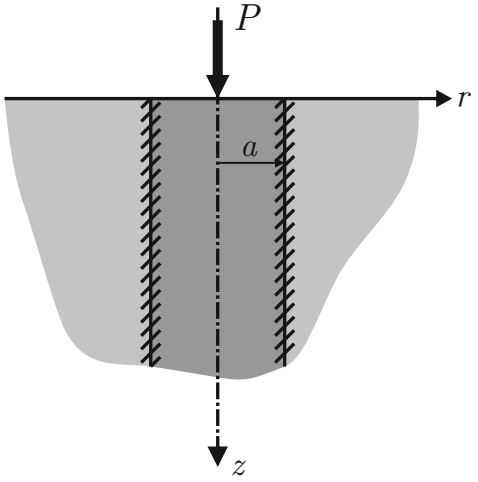

Figure 1: A semi infinite shaft of radius a in a half-space $z > 0$.

$$\sigma_{rr}^{SF}(r,z) = \sigma_0 \left[a\Big(J_{1,0;0} - z\, J_{1,0;1} + \frac{z}{r}\, J_{1,1;0} - \frac{\kappa - 1}{2r}\, J_{1,1;-1} \Big) + \begin{cases} -1/2 & r \le a \\ -a^2/(2\,r^2) & r > a \end{cases} \right] \tag{2}$$

$$\sigma_{zz}^{SF}(r,z) = \sigma_0\, a\Big(J_{1,0;0} + z\, J_{1,0;1} \Big) - \Big\{ \sigma_0 \quad r \le a \tag{3}$$

$$\sigma_{rz}^{SF}(r,z) = \sigma_0\, a\, z\, J_{1,1;1} \tag{4}$$

where $\sigma_0 = E\,\epsilon^*/(1-\nu)$ is the reference axial stress and $J_{m,n;p}$ are Lipschitz-Hankel integrals, defined in Appendix A.

The third kind elliptic integrals present in the Lipschitz-Hankel integrals in Equations (2) and (4) are singular when $(r,z) = (a,0)$. For this point, we obtain the stress values by taking the limit as $z \to 0$:

$$\sigma_{rr}^{SF}(a,0) = \sigma_0 \left(\nu - \frac{1}{2} \right) \tag{5}$$

$$\sigma_{zz}^{SF}(a,0) = \frac{\sigma_0}{2} \tag{6}$$

$$\sigma_{rz}^{SF}(a,0) = -\frac{\sigma_0}{\pi}. \tag{7}$$

After assembling the shrink-fit, a point force P is applied acting into the elastic half-space. In the cylindrical coordinate set of Figure 1, the state of stress within the half-space is given by Timoshenko [3], and the tractions arising on any cylindrical cut (an $r =$ constant surface), $\sigma_{ij}^P(r,z)$ are given by

$$\sigma_{rr}^P(r,z) = \frac{P}{2\,\pi} \left\{ (1-2\,\nu) \left[\frac{1}{r^2} - \frac{z}{r^2\,(r^2+z^2)^{1/2}} \right] - \frac{3\,r^2\,z}{(r^2+z^2)^{5/2}} \right\} \tag{8}$$

$$\sigma_{zz}^P(r,z) = -\frac{3\,P}{2\,\pi} \left\{ \frac{z^3}{(r^2+z^2)^{5/2}} \right\} \tag{9}$$

$$\sigma_{rz}^P(r,z) = -\frac{3\,P}{2\,\pi} \left\{ \frac{r\,z^2}{(r^2+z^2)^{5/2}} \right\}. \tag{10}$$

Considering a fully stuck solution, the stresses $\tilde{\sigma}_{ij}(r,z)$ for the bilateral solution can be obtained as a sum of the shrink-fit stresses (eqs. (2) to (4)) and the tractions due to the application of the load P (eqs. (8) to (10)):

$$\tilde{\sigma}_{rr}(r,z) = \sigma_{rr}^{SF}(r,z) + \sigma_{rr}^P(r,z) \tag{11}$$

$$\tilde{\sigma}_{zz}(r,z) = \sigma_{zz}^{SF}(r,z) + \sigma_{zz}^P(r,z) \tag{12}$$

$$\tilde{\sigma}_{rz}(r,z) = \sigma_{rz}^{SF}(r,z) + \sigma_{rz}^P(r,z). \tag{13}$$

Figure 2 shows the radial normal stress ($\tilde{\sigma}_{rr}(a,z)$), the shear stress ($\tilde{\sigma}_{rz}(a,z)$) and the ratio between those at the shaft-hole interface ($r = a$). The stresses are normalised by the the reference axial stress σ_0. A normalised variable λ is chosen as a measurement of the shrink-fit to applied load stress ratio, given by

$$\lambda = \frac{P}{a^2\,\sigma_0}. \tag{14}$$

Therefore, $\lambda = 0$ represents the contact assembly, i.e. only the shrink-fit stresses are present. A positive λ implies that the shaft is being 'pushed in', towards the core of the half-space, while $\lambda < 0$ represents the shaft being 'pulled out', towards the exterior of the half-space.

Analysing the radial stress (Figure 2 (a)), we notice that as we push the shaft in ($\lambda > 0$), σ_{rr} is compressive and increases in absolute value inside the contact interface (underneath the surface). However, at the surface, as λ increases, the radial stress decreases in absolute value until it reaches zero for $\lambda = 3.1$, which would indicate contact separation at the surface. As we pull the shaft out ($\lambda < 0$), σ_{rr} is still compressive but increases in absolute value at the surface as the load P is increased. Beneath the surface, as λ increases in absolute value, the radial stress decreases until it reaches zero for $\lambda = -2.9$, which would indicate sub-surface contact separation.

Now, looking at the shear to normal stress ratio (Figure 2 (c)), we notice that for a realistic coefficient of friction ($0 \le f \le 1$) the slip condition is violated even on assembly. For instance, if $\lambda = 0$, a coefficient of friction of 1.6 would be required to guarantee that the shaft-hole interface does not slip. Therefore, the assumption of a fully

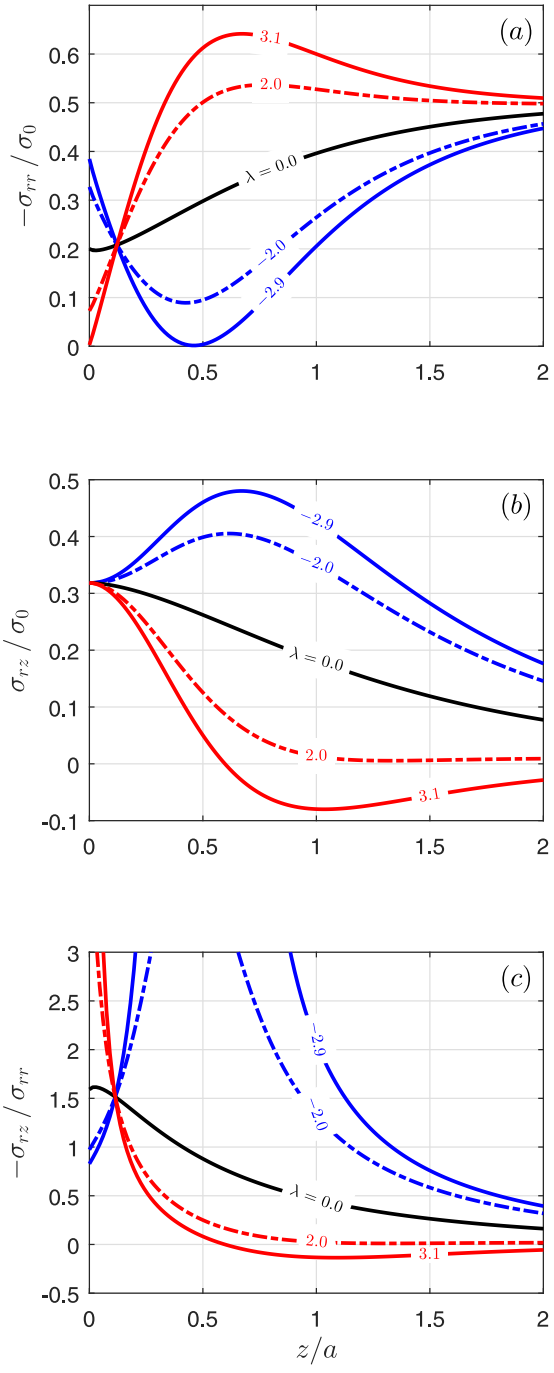

Figure 2: Stresses at the interface radius ($r = a$) versus depth z/a for varying λ. Adhered solution: (a) pressure, (b) shear and (c) traction ratio.

stuck contact interface does not hold. Slip would penetrate from the surface to a self determining point c. The traction ratio $-\sigma_{rz}/\sigma_{rr}$ increases even further in value as the force P is applied, at the surface if $\lambda > 0$ and subsurface if $\lambda < 0$.

3. Formulation

The general principle in obtaining a solution will be to develop expressions for the tractions on the shaft-hole interface, $N(z), S(z)$, representing the normal and shear components, respectively, as the sum of the bilateral solutions together with an integral representation of slip in the form of a distribution of glide dislocations. The dislocations needed are all 'edge' in character, with their Burgers vectors lying in a $\theta = constant$ plane. Only glide dislocations are needed in this problem.

A $b_z(\xi)$ dislocation loop, of radius a and with the dislocation lying at a depth ξ may be formed by making a path cut along the cylinder $r = a$ between the dislocation and the free surface of the half-space and sliding the outer wall with respect to the inner wall by a constant amount b_z. This generates a glide dislocation which is of the Volterra kind (path-cut independent) and will be used to represent slip displacement. It will induce tractions along the same cylinder $\bar{\sigma}_{zi}(z)$, where $i = r, z$, given by

$$\bar{\sigma}_{zi}(z) = G^z_{zi}(z, \xi) b_z(\xi). \tag{15}$$

The functions $G^z_{zi}(z, \xi)$ are extremely complicated in form and are defined for an isotropic half-space in [4], as well as being explicitly provided in Appendix A and as a supplementary material in [5]. They are bounded ('regular') when $i = z$ but display a Cauchy singularity when $i = r$.

3.1. Pulling the shaft out

We first look at the problem where the shaft is being 'pulled out' ($\lambda < 0$). In this case, the resulting tractions on the plane of the shaft-hole interface are given by

$$N(z) = \tilde{\sigma}_{rr}(z) + \int_{slip} G^z_{rr}(z, \xi)\, B_z(\xi) \mathrm{d}\xi \tag{16}$$

$$S(z) = \tilde{\sigma}_{rz}(z) + \int_{slip} G^z_{rz}(z, \xi)\, B_z(\xi) \mathrm{d}\xi \tag{17}$$

where $B_i(\xi) = db_i/d\xi$, $i = r, z$. Glide dislocations are installed over the interface region where slipping occurs.

The condition of slip states that the shear traction is limited by normal traction at the contact interface, giving, if the bilateral shear traction is positive,

$$N(z) < 0 \tag{18}$$

$$S(z) = -f\, N(z) \qquad 0 \le z \le c \tag{19}$$

where f is the coefficient of friction between the shaft and the hole, and c the depth to which slip penetrates.

The boundary conditions in eqs. (18) and (19) together with eqs. (16) and (17) define the following Cauchy integral equation

$$\int_0^c \left[G^z_{rz}(z,\xi) + f\, G^z_{rr}(z,\xi)\right]\, B_z(\xi)\mathrm{d}\xi = \\ -\left[\tilde{\sigma}_{rz}(z) + f\tilde{\sigma}_{rr}(z)\right] \qquad 0 \le z \le c. \tag{20}$$

This equation possesses the property that the range of the integrals is the same as the range of imposition of the right hand side, so that it constitutes a well-posed integral equation with a generalized Cauchy kernel. It must be solved numerically using a standard numerical quadrature devised by Erdogan et al. [6].

First, we put it in standard form over the interval $[-1\,,1]$ utilising the substitutions

$$s = \frac{2\,\xi}{c} - 1\,, \qquad t = \frac{2\,z}{c} - 1 \qquad 0 \le z, \xi \le c \tag{21}$$

which give

$$\int_{-1}^{1} \left[G^z_{rz}(t,s) + f\, G^z_{rr}(t,s)\right]\, B_z(s)\mathrm{d}s = \\ -\left[\tilde{\sigma}_{rz}(t) + f\,\tilde{\sigma}_{rr}(t)\right]. \tag{22}$$

Now, we must consider the general form of the solution required, noting that the displacement gradient must be square root bounded at both ends of the interval, at the surface ($t = -1$) and at the sticking point ($t = 1$). Thus, we assume a fundamental function as

$$B_z(s) = \phi_z(s)\,\sqrt{1 - s^2} \tag{23}$$

which leaves the unknown dislocation density being represented by the function $\phi_z(s)$.

Equation (22) can be expressed now, in normalised form, as

$$\sum_{i=1}^{N} \pi\, W_i\, \phi_z(s) \left[G^z_{rz}(s_i,t_k) + fG^z_{rr}(s_i,t_k)\right] = \\ -\left[\tilde{\sigma}_{rz}(t_k) + f\,\tilde{\sigma}_{rr}(t_k)\right] \qquad t_k = 1,\ldots,N+1 \tag{24}$$

where the integration points s_i, collocation points t_k and weights W_i for the quadrature are given as

$$s_i = \cos\left(\pi \frac{i}{N+1}\right) \qquad i = 1,\ldots,N \tag{25}$$

$$t_k = \cos\left(\frac{\pi}{2}\frac{2k-1}{(N+1)}\right) \qquad k = 1,\ldots,N+1 \tag{26}$$

$$W_i = \frac{1 - s_i^2}{2\,(N+1)}. \tag{27}$$

From eq. (24), we have a set of $N+1$ equations for $N+1$ unknowns. These are the N values of $\phi_z(s_i)$ and the stick point c. Once ϕ_z is known, the stresses at a point (r,z) can be found as

$$\sigma_{ij}(r,z) = \sigma_{ij}(r,z) + \int_0^c G^z_{ij}(r,z,\xi)\, B_z(\xi)\mathrm{d}\xi \\ i,j = r,z. \tag{28}$$

3.2. Pushing the shaft in

When the shaft is pushed towards the core of the half space ($\lambda > 0$), there is further forward slip at the interface, extending from the surface to a self-determining point b ($b < c$). The set of dislocations used before is not sufficient to correct the additional slip. This requires the imposition of a new set of dislocations at the shaft-hole interface inside the slip zone.

The resulting tractions on the plane of the shaft-hole interface are now given by

$$N(z) = \tilde{\sigma}_{rr}(z) + \int_{initial\ slip} G^z_{rr}(z,\xi)\, B_z(\xi)\mathrm{d}\xi + \\ \int_{slip} G^z_{rr}(z,\xi)\, B_z(\xi)\mathrm{d}\xi \tag{29}$$

$$S(z) = \tilde{\sigma}_{rz}(z) + \int_{initial\ slip} G^z_{rz}(z,\xi)\, B_z(\xi)\mathrm{d}\xi + \\ \int_{slip} G^z_{rz}(z,\xi)\, B_z(\xi)\mathrm{d}\xi. \tag{30}$$

The boundary conditions remain those in eqs. (18) and (19), that together with eqs. (29) and (30) define the following Cauchy integral equation

$$\int_0^c \left[G^z_{rz}(z,\xi) + f\, G^z_{rr}(z,\xi)\right]\, B_z(\xi)\mathrm{d}\xi + \\ \int_0^b \left[G^z_{rz}(z,\xi) + f\, G^z_{rr}(z,\xi)\right]\, B_z(\xi)\mathrm{d}\xi = \\ -\left[\tilde{\sigma}_{rz}(z) + f\,\tilde{\sigma}_{rr}(z)\right] \qquad 0 \le z \le b. \tag{31}$$

Once again, the integrals have to be put in standard form over the interval $[-1\,,1]$ utilising the substitutions

$$s = \frac{2\,\xi}{c} - 1\,, \qquad t = \frac{2\,z}{c} - 1 \qquad 0 \le z, \xi \le c \tag{32}$$

$$u = \frac{2\,\xi}{b} - 1\,, \qquad v = \frac{2\,z}{b} - 1 \qquad 0 \le z, \xi \le b \tag{33}$$

which give

$$\int_{-1}^{1} \left[G^z_{rz}(t,s) + f\, G^z_{rr}(t,s)\right]\, B_z(s)\mathrm{d}s + \\ \int_{-1}^{1} \left[G^z_{rz}(v,u) + f\, G^z_{rr}(v,u)\right]\, B_z(u)\mathrm{d}u = \\ -\left[\tilde{\sigma}_{rz}(v) + f\,\tilde{\sigma}_{rr}(v)\right]. \tag{34}$$

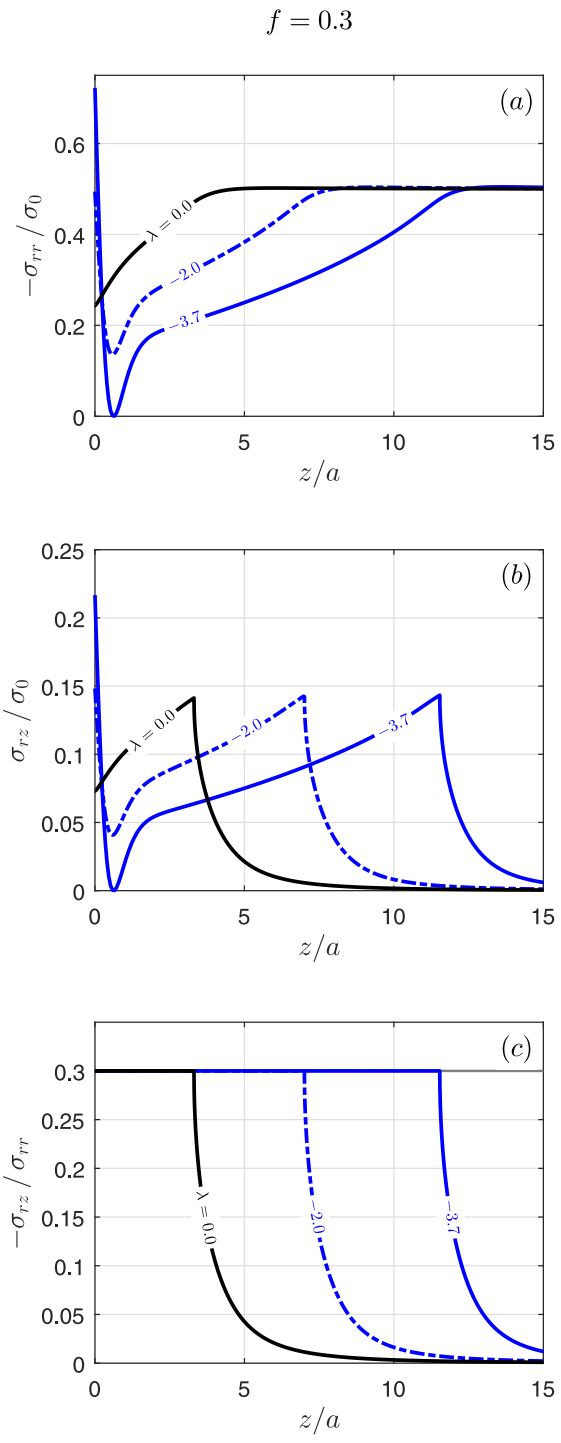

Figure 3: Stresses at the interface radius ($r = a$) versus depth z/a for $\lambda \leq 0$ and $f = 0.3$. Corrected solution: (a) pressure, (b) shear and (c) traction ratio.

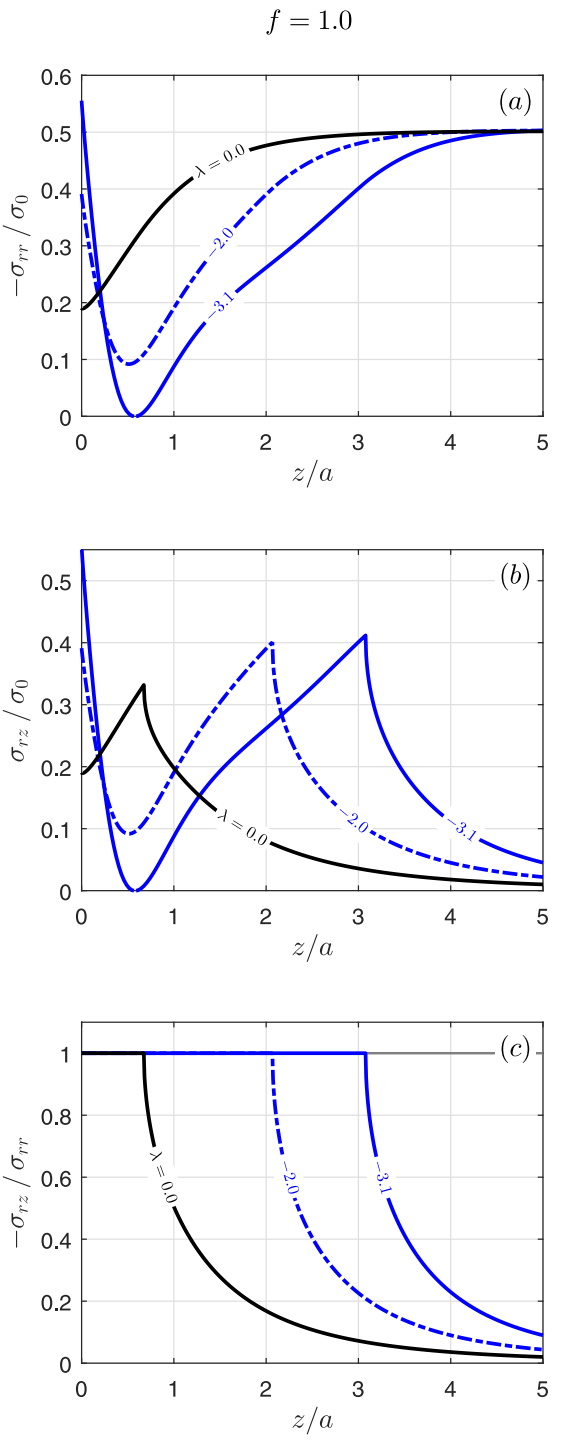

Figure 4: Stresses at the interface radius ($r = a$) versus depth z/a for $\lambda \leq 0$ and $f = 1.0$. Corrected solution: (a) pressure, (b) shear and (c) traction ratio.

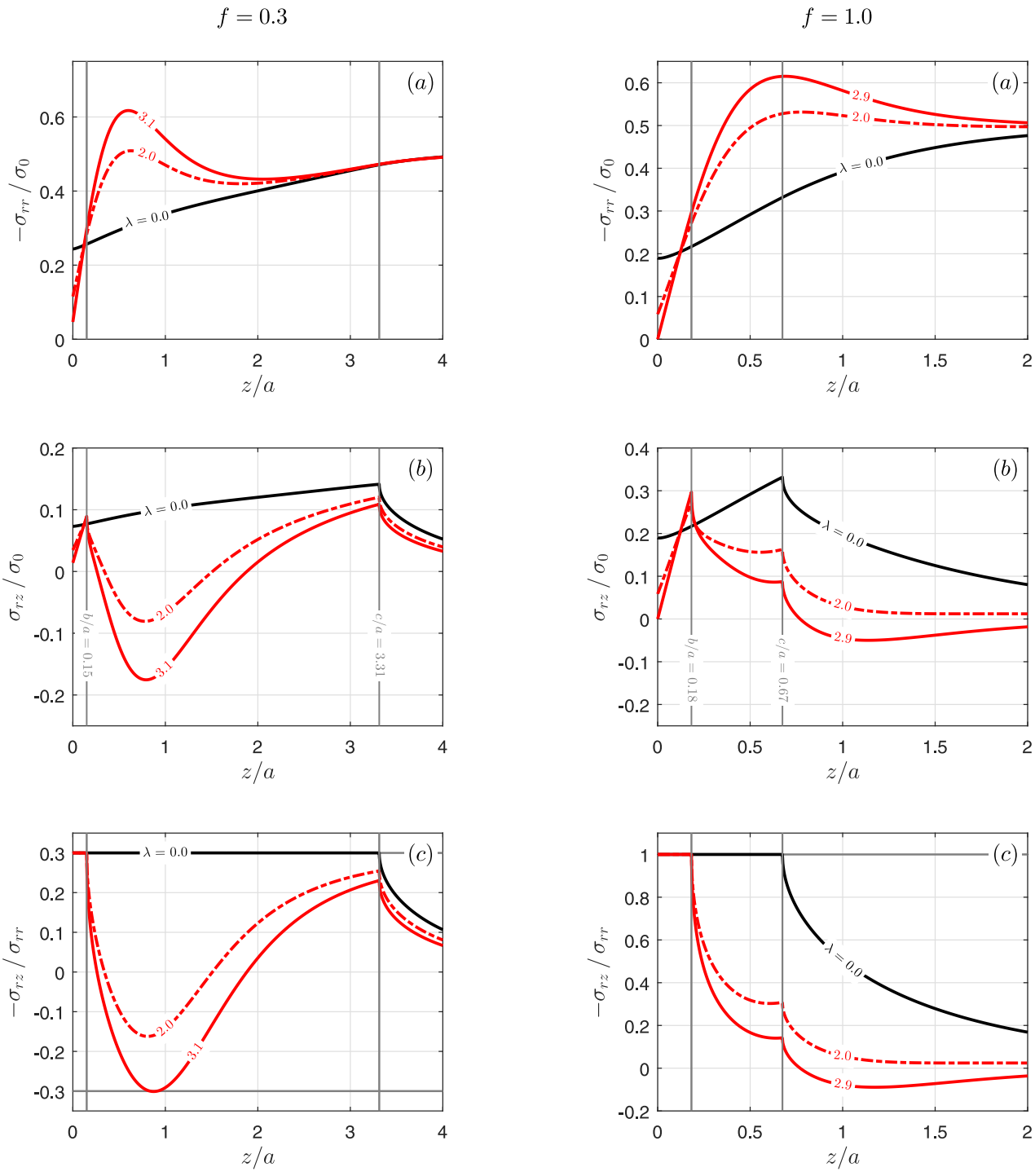

Figure 5: Stresses at the interface radius ($r = a$) versus depth z/a for $\lambda \geq 0$ and $f = 0.3$. Corrected solution: (a) pressure, (b) shear and (c) traction ratio.

Figure 6: Stresses at the interface radius ($r = a$) versus depth z/a for $\lambda \geq 0$ and $f = 1.0$. Corrected solution: (a) pressure, (b) shear and (c) traction ratio.

The displacement gradient again must be square root bounded at both ends of the interval ($v = \pm 1$) and we assume

$$B_z(u) = \psi_z(u)\,\sqrt{1-u^2}. \tag{35}$$

Equation (34) can be expressed now, in normalised form, as

$$\sum_{i=1}^{N} \pi\, W_i\, \phi_z(s) \left[G^z_{rz}(s_i,t_k) + f G^z_{rr}(s_i,t_k) \right] + \sum_{i=1}^{N} \pi\, X_i\, \psi_z(u) \left[G^z_{rz}(u_i,v_k) + f G^z_{rr}(u_i,v_k) \right] = - \left[\tilde{\sigma}_{rz}(v_k) + f\, \tilde{\sigma}_{rr}(v_k) \right] \qquad t_k = 1,\ldots,N+1 \tag{36}$$

where the integration points u_i, collocation points v_k and weights X_i for the quadrature are given as

$$u_i = \cos\left(\pi \frac{i}{N+1}\right) \qquad i = 1,\ldots,N \tag{37}$$

$$v_k = \cos\left(\frac{\pi}{2}\frac{2k-1}{(N+1)}\right) \qquad k = 1,\ldots,N+1 \tag{38}$$

$$X_i = \frac{1-u_i^2}{2\,(N+1)}. \tag{39}$$

From eq. (36), we have a set of $N+1$ equations for $N+1$ unknowns. These are the N values of $\psi_z(u_i)$ and the point b. The function $\phi_z(s_i)$ is obtained from the solution of eq. (24). Once ψ_z is known, the stresses at the bodies can be found as

$$\sigma_{ij}(r,z) = \sigma_{ij}(r,z) + \int_{-1}^{1} G^z_{ij}(t,s)\,\phi_z(s)\mathrm{d}s + \int_{-1}^{1} G^z_{ij}(v,u)\,\psi_z(u)\mathrm{d}u \qquad i,j = r,z. \tag{40}$$

4. Results

The problem was coded up using the numerical processor MATLAB. Convergence of the solution was obtained when N was set to 80. The results are for $\nu = 0.3$. In the problem, there are two length dimensions to be determined (c and b, if $\lambda > 0$) from the additional collocation equations that need to be satisfied. In practice, we guess the value of the length to be found and omit the central equation from the $N+1$ generated. The column vector of ϕ_z or ψ_z is found and the omitted equation is evaluated. The length to be found is adjusted to minimize the residue obtained from the omitted equation.

Consider first the shear stress (Figures 3 to 6 (b)). For the case where the shaft is being 'pulled out' ($\lambda < 0$) we notice that the more we 'pull the shaft out' (as λ becomes more negative), the larger the slip zone. Therefore, as we extract the shaft, the size of the slip zone increases with the magnitude of the extraction load P. When the shaft is being 'pushed in' ($\lambda > 0$) we notice that the size of the slip zone is independent of λ. As λ increases, the slip zone remains 'locked' at the assembly position (when $\lambda = 0$). To account for this effect there is additional forward slip closer to the surface ($0 \le z \le b$). For all values of λ, as the coefficient of friction f decreases, the slip zone increases, as expected. Figures 3 to 6 (a) show the contact pressure. If $\lambda < 0$ (shaft being 'pulled out'), we notice that, as the extraction force increases in magnitude, the pressure increases at the surface but decreases sub-surface. When λ reaches a critical value (-3.7 for $f = 0.3$ or -3.1 for $f = 1.0$), the contact pressure becomes null, which results in contact opening in a sub-surface point. This is in line with what was expected from the adhered solution. The ratio between the shear traction and contact pressure (Figures 3 and 4 (c)) remains positive and does not violates the slip condition as λ increases in magnitude.

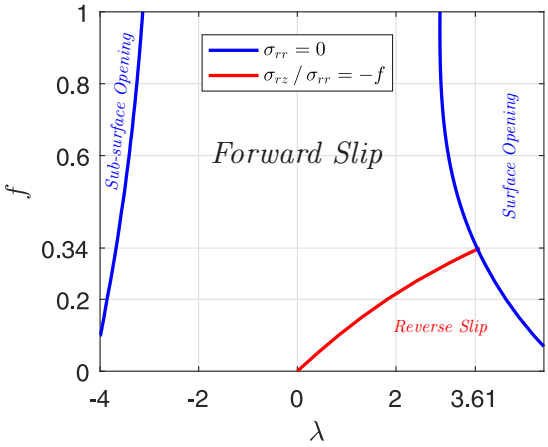

Figure 7: Values of load ratio λ required to cause contact opening or reverse slip for a given f. The solution is valid in the region marked 'Forward Slip'.

If $\lambda > 0$ ('pushing the shaft in'), it is noted that as the force increases in magnitude, the pressure now increases sub-surface but decreases at the surface. For $f = 1.0$, a value of λ equal to 2.9 results in contact opening at the surface ($\sigma_{rr}(a,0) = 0$). However, for $f = 0.3$, as λ increases, the slip condition is violated before there is contact opening at the surface ($\sigma_{rz}/\sigma_{rr} > -f$). This would result in a sub-surface patch of reverse slip.

Figure 7 summarises the region where the solution is valid for a given coefficient of friction, labelled 'Forward Slip'. The blue lines represent contact opening at the surface (for $\lambda > 0$) or sub-surface (for $\lambda < 0$). The red line represent the values of λ that result in a patch of reverse slip for a given f. For $f = 0.34$ and $\lambda = 3.61$, reverse slip and contact opening happen simultaneously. For $f < 0.34$, reverse slip occurs before the contact opens at the surface.

4.1. Finite Shaft

The next step is to consider what happens if the shaft is of finite length and terminates at a depth d, by the introduction of a 'free' surface at a depth d outside the slip zone ($d > c$). Figures 8 and 9 show the stresses at a constant depth (obtained from eqs. (28) and (40)) for the two values of λ that would cause contact separation at the shaft-hole interface. From these results, we notice that, at a potential surface of depth d, the axial stress is compressive for all depths, *even if the shaft is being extracted from the hole* (Figures 8 and 9 (a)). This is due to the compressive nature of the shrink-fit assembly that results in the axial stresses due to shrink-fit being at least six times the values of axial stresses for the application of the load P, when $\lambda \sim 3$. Besides, the ratio between the shear and axial stress does not surpasses the coefficient of friction, which means that the potential surface would be stuck to the half space beneath it. Even though these results are only for $f = 1.0$, the same behaviour is observed for all values of f. Therefore, the introduction of a free surface at any depth would result in this surface being stuck to the half-space underneath it (Figure 10) and the solution found in Section 3 remains valid.

5. Conclusions

The slip present in a shrink fit, axisymmetric problem, devoid of torsion, subjected to an axial force, has been solved by using a bilateral solution for a shrink fitted shaft finishing flush with the surface of the surrounding material. Slip surfaces are represented by using arrays of axisymmetric dislocations. Conventional Gauss-Chebyshev quadrature is used to find their density. It was shown that, when the shaft is being 'pulled out' towards the exterior of the hub, the size of the slip zone increases with the load magnitude, but as we 'push the shaft in', towards the core of the hub, the slip zone remains locked at the assembly position. Also, the solution for a semi-infinite shaft is still valid for a finite shaft of depth d, as long as the surface extends beyond the slip zone.

Besides obtaining the stress fields for the shaft-hub assembly, one of the prime motivations for carrying out this calculation is to show that the glide ring dislocation is a viable quantity to use as a kernel in studying axisymmetric contact problems.

Acknowledgements

J. L. gratefully acknowledges the financial support of Christ Church Oxford, Rolls Royce PLC and CAPES [grant number 88881.128590/2016-01].

References

[1] J. R. Barber, Elasticity, Springer, 1992.

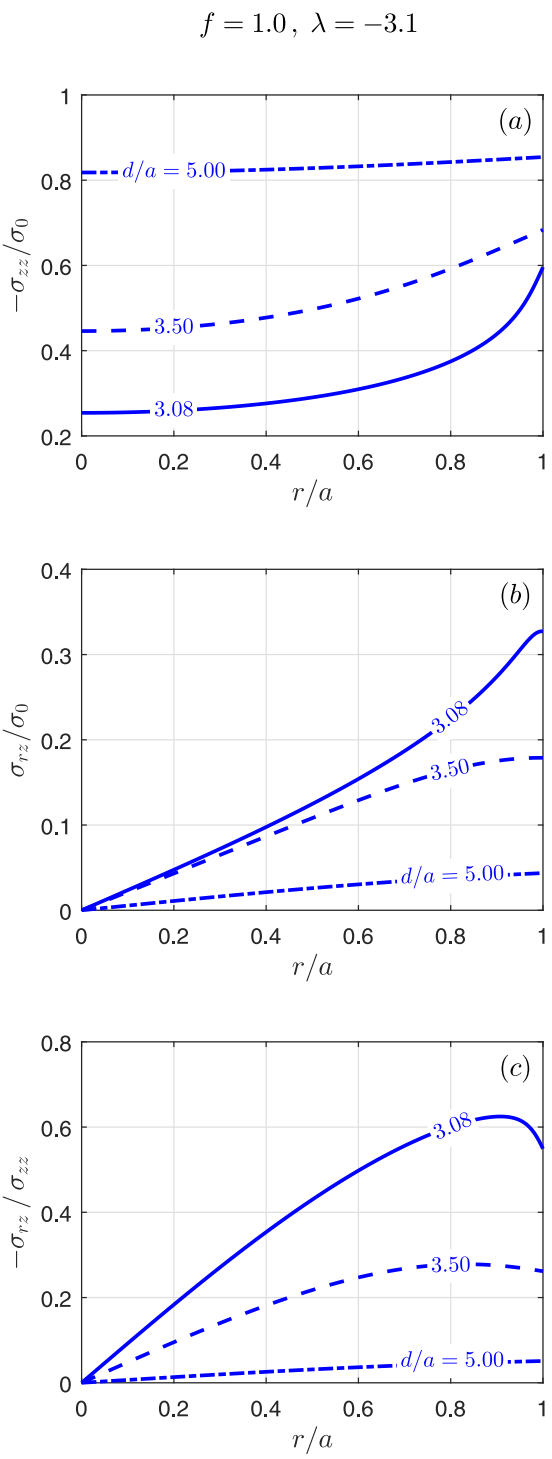

Figure 8: Stresses at a depth d/a for $f = 1.0$ and $\lambda = -3.1$: (a) axial pressure, (b) shear and (c) traction ratio.

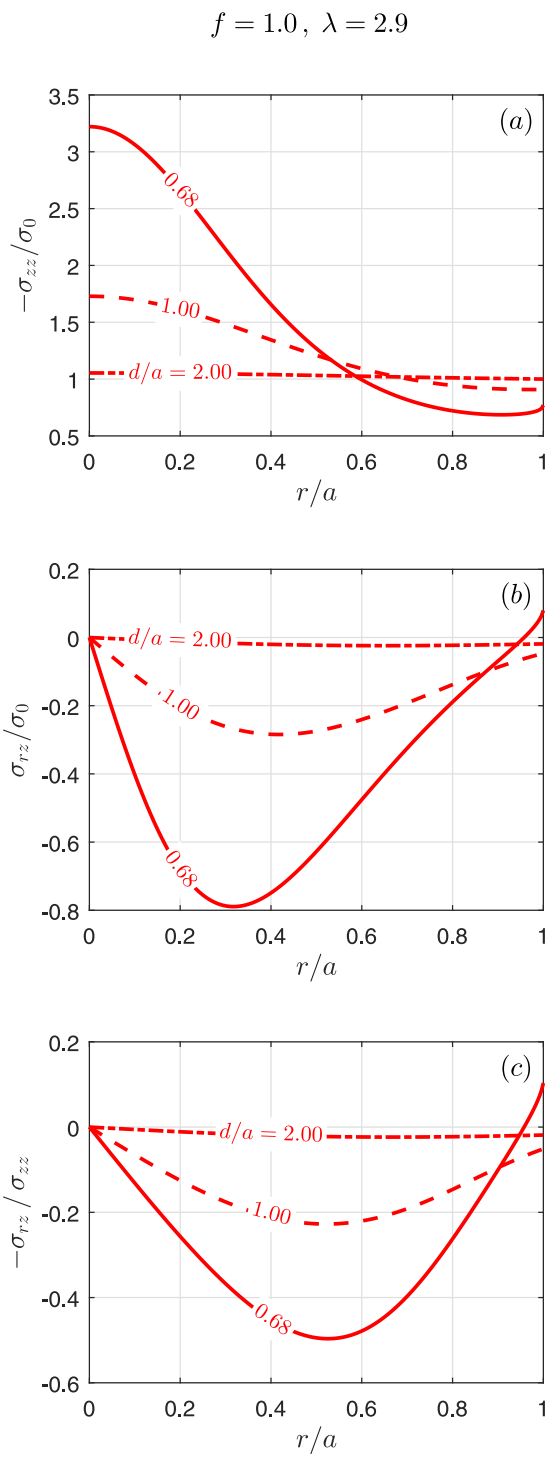

Figure 9: Stresses at a depth d/a for $f = 1.0$ and $\lambda = 2.9$: (a) axial pressure, (b) shear and (c) traction ratio.

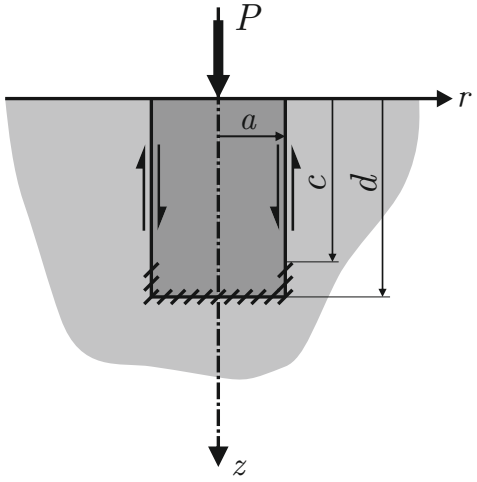

Figure 10: A finite shaft of radius a in a half-space $z > 0$.

[2] R. Paynter, D. Hills, J. Barber, Features of the stress field at the surface of a flush shrink-fit shaft, Proceedings of the Institution of Mechanical Engineers, Part C: Journal of Mechanical Engineering Science 223 (10) (2009) 2241–2247. doi:10.1243/09544062JMES1403.

[3] S. Timoshenko, J. N. Goodier, Theory of Elasticity, Vol. 49, 1986. doi:10.1007/BF00046464.

[4] R. Paynter, D. Hills, The effect of path cut on Somigliana ring dislocations in a half-space, International Journal of Solids and Structures 46 (2) (2009) 412–432. doi:10.1016/j.ijsolstr.2008.09.001.

[5] J. Lopes, D. Hills, Ring cracks at the surface of a half-space, Engineering Fracfure Mechanics.

[6] F. Erdogan, G. D. Gupta, T. Cook, Numerical solution of singular integral equations, in: Methods of analysis and solutions of crack problems, 1973, pp. 368–425.

[7] G. Eason, B. Noble, I. N. Sneddon, On certain integrals of Lipschitz-Hankel type involving products of Bessel functions, Philosophical Transactions of the Royal Society of London A: Mathematical, Physical and Engineering Sciences 247 (935) (1955) 529–551.

[8] R. Paynter, D. Hills, A. Korsunsky, The effect of path cut on Somigliana ring dislocation elastic fields, International Journal of Solids and Structures 44 (2) (2007) 6653–6677. doi:10.1016/j.ijsolstr.2008.09.001.

Appendix A. State of stress induced by circular edge dislocation loops

Consider a dislocation loop put at a position (r, z) in a cylindrical coordinate system and being observed at a depth d. To calculate the influence functions, the coordinates are normalised with respect to the dislocation ring radius a:

$$\rho = r/a \qquad \zeta = z/a \qquad \delta = d/a. \tag{A.1}$$

The influence functions G^z_{zi} $(i = r, z)$ for the glide dislocation in a half-space are given as [4]:

$$G^z_{rr} = \frac{2\,\mu}{a\,(\kappa+1)}\Bigg[- J_{1,0;1} + I_{1,0;1} + (\zeta-\delta)\,J_{1,0;2} + (\zeta-3\,\delta)\,I_{1,0;2} + \frac{(\kappa-1)}{2\,\rho}\,J_{1,1;0} - \frac{(\kappa-1)}{2\,\rho}\,I_{1,1;0} - \frac{(\zeta-\delta)}{\rho}\,J_{1,1;1} + \frac{(\zeta\,\kappa-\delta)}{\rho}\,I_{1,1;1} + \frac{(2\,\zeta\,\delta)}{\rho}\,I_{1,1;2} - 2\,\zeta\,\delta\,I_{1,0;3}\Bigg] \tag{A.2}$$

$$G^z_{rz} = \frac{2\,\mu}{a\,(\kappa+1)}\Bigg[- (\zeta-\delta)\,J_{1,1;2} + (\zeta-\delta)\,I_{1,1;2} - 2\,\zeta\,\delta\,I_{1,1;3}\Bigg] \tag{A.3}$$

Appendix A.1. Lipschitz-Hankel integrals

In the influence functions, the terms $J_{n,p;q}$ and $I_{n,p;q}$ represent Lipschitz-Hankel integrals. The standard definition for these functions is as an integral of the product of Bessel functions ($J_i(\cdot)$), an exponential term and a power term. Using normalised coordinate variables, it is given as [7]

$$P_{\mu,\nu;\lambda}(\rho,\zeta) = \int_0^\infty J_\mu(t)\,J_\nu(\rho\,t)\,e^{-\zeta\,t}\,t^\lambda\,\mathrm{d}t \tag{A.4}$$

In the kernels, the follow definition is applied:

$$J_{n,p;q} = P_{n,p;q}(\rho,\zeta-\delta) \tag{A.5}$$

$$I_{n,p;q} = P_{n,p;q}(\rho,-\zeta-\delta). \tag{A.6}$$

The Lipschitz-Hankel integrals needed in the kernels are given in [8, 4] and by Lopes and Hills [5] as a supplementary material.

6

The Axisymmetric Shrink Fit Problem Subject to Torsion

The axisymmetric shrink fit problem subjected to torsion

J.P. Lopes[a,*], D.A. Hills[a]

[a] *Department of Engineering Science, University of Oxford, Parks Road, Oxford OX1 3PJ, United Kingdom*

Abstract

The problem of an elastic shaft fitted into an under-sized hole in an elastically identical body, the latter in the form of a half-space, has been studied when the assembly is subject to increasing and then subsequently reducing torque. The solution has been found as the superposition of a unilateral solution for an adhered contact pair and a set of ring dislocations along the contact interface to represent slip. The dislocations needed are prismatic (b_z) and twist or screw (b_θ), and by using continuous distributions of them the modified traction may be represented very effectively in a way which enables the local orthogonality requirement of slip to be followed rigorously. The residual interface tractions left when the applied torque has been completely removed are found. The whole calculation was carried out on a quasi-static basis.

Keywords: Axisymmetric, Contact, Shrink fit, Torsion, Orthogonality, Frictional slip, Plane/anti-plane slip

1. Introduction

The problem of a cylinder shrink fitted into an under-sized cavity arises in a a number of engineering problems such as when a disk (pulley, gear etc) is shrink fitted onto a shaft, or in the domestic environment of, for example, a cork or stopper closure. The relationship between the degree of interference and the contact pressure generated in a plane problem has been known for a very long time and is associated with the name Lamé, but the presence of a free surface, where the contact terminates, produces interesting complicating three dimensional effects which can be solved in closed form [1]. The gradients along the axis of the shaft which the free surface induces means that axial shear tractions arise, and these have been shown [1] to be sufficiently severe for slip always to be present when the contact is formed, for realistic coefficients of friction.

The object of the present paper is to extend this solution to problems in which a torque is inserted at the free surface itself, and to see how this modifies the interfacial shear tractions present. Although the solution has relevance to engineering assemblies it also has relevance to the cork closure refereed to: a corkscrew is normally twisted and released before an axial force is applied, and this paper shows how a self-equilibrating residual interface shear traction is developed by the twisting action. Although the axial force part of the problem is not considered, it is is clear that the torque pre-load will reduce the value of the axial force needed to achieve extraction of the cork.

*Corresponding author

Email addresses: jhonatan.dapontelopes@eng.ox.ac.uk (J.P. Lopes), david.hills@eng.ox.ac.uk (D.A. Hills)

The formulation presented in this work relies on two idealisations that might lead to gross aproximations when applied to practical applications but have to be made due to the current state of knowledge of the tools for analytical modelling of shrink fit under partial slip.

The method used to introduce interfacial slip relies on the knowledge of the state of stress induced in a half-space by a ring dislocation lying in a plane parallel with the surface (kernel or core of the solution). In practical applications, the hub and the shaft might be made of different materials and this would imply knowing the kernel for a mismatched half-space, which is not available in the literature. We assume, therefore, that the hub and the shaft are made of the same material, and consider the the case where the half-space is homogeneous [2].

In addition, the application of a torque is usually distributed over the surface of the shaft. However, a point torque was chosen to be applied because; (a) the solution was available in the literature in an elegant format for a homogeneous half-space [3], (b) the only mathematical singularity in the stress fields appears at the origin (away from the contact interface), (c) and it presents no intrinsic length dimension, i.e. it introduces no extra parameters in the model.

2. Shrink fit assembly

The stresses due to the shrink fit assembly (shown in Figure 1) are given by Paynter et al. [1] and are reproduced here. Upon assembly, an infinitely long oversized shaft of radius $a+\Delta_0$ is inserted in a hub with a cylindrical hole of radius a, present in an elastic half-space. Both the shaft and the hub have Poisson's ratio ν and Young's modulus

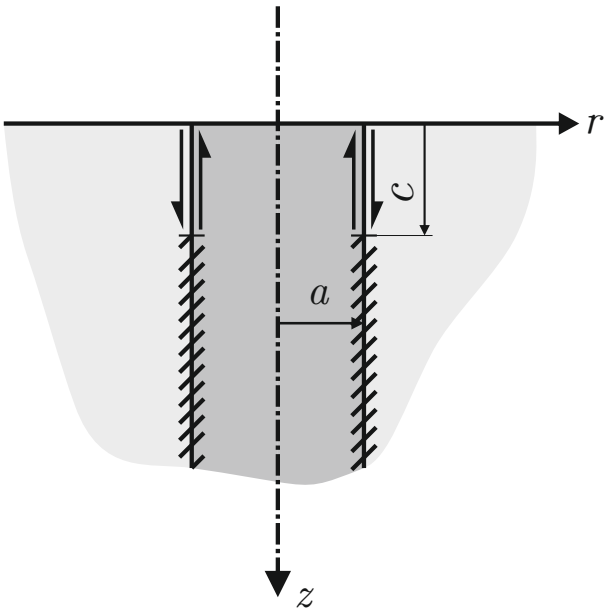

Figure 1: A semi infinite shaft of radius a in a half-space $z > 0$ subjected to shrink fit.

E. The assembly can be achieved by cooling the oversized shaft through a temperature differential ΔT until it fits in the hub and then letting it warm back up. This results in an induced radial strain ϵ^* in the shaft, given by

$$\epsilon^* = \frac{\Delta_0}{a} = \alpha \Delta T \tag{1}$$

where α is the coefficient of thermal expansion for the shaft.

If the coefficient of friction is sufficiently high to prevent any slip, the stresses σ_{ij}^{SF} at a point (r,z), $z \geq 0$, are given by

$$\begin{aligned}\sigma_{rr}^{SF}(r,z) = \sigma_0 \Bigg[a\Big(& P_{1,0;0}(\rho,\zeta) - z\, P_{1,0;1}(\rho,\zeta) + \\ & \frac{z}{r} P_{1,1;0}(\rho,\zeta) - \frac{\kappa-1}{2r} P_{1,1;-1}(\rho,\zeta)\Big) + \\ & \begin{cases} -1/2 & r \leq a \\ -a^2/(2\,r^2) & r > a \end{cases} \Bigg] \end{aligned} \tag{2}$$

$$\sigma_{rz}^{SF}(r,z) = \sigma_0\, a\, z\, P_{1,1;1}(\rho,\zeta), \tag{3}$$

where $\sigma_0 = E\,\epsilon^*/(1-\nu)$ is a reference axial stress and $P_{m,n;p}(\rho,\zeta)$ are Lipschitz-Hankel integrals, defined in Appendix A.

The third kind elliptic integrals present in the Lipschitz-Hankel integrals in eqs. (2) and (3) are singular when $(r,z) = (a,0)$. For this point, we obtain the stress values by taking the limits as $z \to 0$, which give

$$\sigma_{rr}^{SF}(a,0) = \sigma_0 \left(\nu - \frac{1}{2}\right) \tag{4}$$

$$\sigma_{rz}^{SF}(a,0) = -\frac{\sigma_0}{\pi}. \tag{5}$$

For the stresses in eqs. (2) and (3) to be valid, they cannot violate the slip condition, i.e.

$$|\sigma_{rz}^{SF}(z)| \leq f\, \sigma_{rr}^{SF}(z) < 0 \qquad z \geq 0. \tag{6}$$

However, Paynter et al. [1] show that a realistic coefficient of friction ($f \lesssim 1.0$) will result in the violation of eq. (6) and, consequently, the contact must be in partial slip.

Because the coefficient of friction is insufficient to maintain complete adhesion, a region of slip will develop when the assembly is put together, whose extent we wish to know. In order to satisfy slipping conditions, a modified solution can be developed by representing the tractions at the contact interface as a sum of the bilateral (adhered) solution together with a correction in the form of an integral representation of slip as a distribution of glide dislocations.

We emphasise that the introduction of dislocations is used only as a mathematical device to correct the tractions in the formulation as a distribution of strain nuclei. This does not mean that physical defects are being inserted in the micro-structure of the material. Detailed explanations of the method can be found in [4, 5].

The modelling of contact slip is achieved by introducing an axial glide dislocation loop $b_z(\xi)$ of radius a, placed at a depth ξ. This loop has a Burgers vector which is constant in magnitude and orientation so that it is of the Volterra kind and may be formed by making a path cut along the cylinder $r = a$ between the dislocation and the free surface of the half-space and sliding the outer wall with respect to the inner wall by a constant amount b_z. This will introduce tractions $\hat{\sigma}_{iz}(z)$, $i = r, z$, along the same path cut, given by

$$\hat{\sigma}_{iz}(z) = G_{ri}^{z}(z,\xi)\, b_z(\xi). \tag{7}$$

The influence functions $G_{ri}^{z}(z,\xi)$ are described as sums of Lipschitz-Hankel integrals, and for a half-space are given by Paynter et al. [2, 6] and in the Appendix A.

We can now write the contact pressure $p^{(0)}(z)$ and shear stress $q_{rz}^{(0)}(z)$ at the interface as

$$p^{(0)}(z) = \sigma_{rr}^{SF}(z) + \int_{slip} G_{rr}^{z}(z,\xi)\, B_z(\xi) \mathrm{d}\xi \tag{8}$$

$$q_{rz}^{(0)}(z) = \sigma_{rz}^{SF}(z) + \int_{slip} G_{rz}^{z}(z,\xi)\, B_z(\xi) \mathrm{d}\xi. \tag{9}$$

The slip condition requires that the shear stress must be limited by friction in the slip zone, i.e.

$$p^{(0)}(z) < 0 \tag{10}$$

$$q_{rz}^{(0)}(z) = -f\,p^{(0)}(z) \qquad 0 \le z \le c \tag{11}$$

where f is the coefficient of friction between the shaft and the hole, and c the depth to which slip penetrates.

Substituting eqs. (8) and (9) into eq. (11), we have the following singular integral equation:

$$\int_0^c \left[G_{rz}^z(z,\xi) + f\,G_{rr}^z(z,\xi)\right] B_z(\xi)\mathrm{d}\xi = -\left[\sigma_{rz}^{SF}(z) + f\,\sigma_{rr}^{SF}(z)\right] \qquad 0 \le z \le c, \tag{12}$$

which can be solved using standard Gauss-Chebyshev quadrature [7, 4].

After solving eq. (12) for $B_z(\xi)$, the stresses can be recovered from integration (eqs. (8) and (9)) and the slip displacement is given by:

$$h_{rz}^{(0)}(z) = -\int_z^c B_z(\xi)\mathrm{d}\xi. \tag{13}$$

3. Formulation of twist problem

After assembling the shrink fit, a point torque T is applied acting into the elastic half-space. In the cylindrical coordinate set of Figures 2a and 2b, the state of stress within the half-space is given by Chowdhury [3, 8], and the non-zero tractions arising on any cylindrical cut (an $r =$ constant surface), $\sigma_{ij}^T(r,z)$ are given by

$$\sigma_{r\theta}^T(r,z) = -\frac{3\,T}{4\,\pi}\left\{\frac{r\,z}{(r^2+z^2)^{5/2}}\right\} \tag{14}$$

$$\sigma_{z\theta}^T(r,z) = -\frac{3\,T}{4\,\pi}\left\{\frac{r^2}{(r^2+z^2)^{5/2}}\right\}. \tag{15}$$

A normalised variable γ is chosen as a measure of the shrink fit to applied torque stress ratio, given by

$$\gamma = \frac{T}{a^3\,\sigma_0}. \tag{16}$$

Therefore, $\gamma = 0$ represents the contact assembly, i.e. only the shrink fit stresses are present. A positive γ implies that the shaft is being twisted clockwise (when looking from the free surface), while a negative γ represents the shaft being twisted anticlockwise.

Notice that, on any cylindrical cuts ($r =$ constant surfaces), the shrink fit assembly produces only q_{rz} shear stress, acting in the z direction, while the application of the torque results in a shear stress $q_{r\theta}$ in the θ direction, perpendicular to the direction of slip in the assembly.

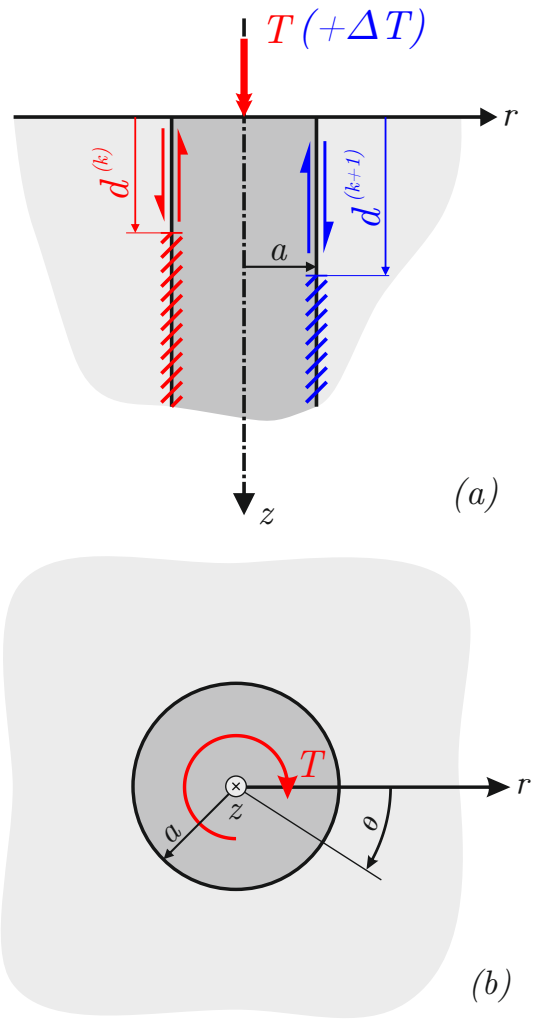

Figure 2: A semi-infinite shaft of radius a in a half-space $z > 0$ subjected to shrink fit. (a) State (k) on the left: the system holds a torque T. State $(k+1)$ on the right: an increment of torque ΔT is applied. (b) View from free surface showing a positive torque.

Close to the contact edge, q_{rz} acts as an 'in-plane' component of shear, while $q_{r\theta}$ represents an 'anti-plane' component. While over the whole contact these components are acting along a constant $r = a$ cylinder instead of a plane, we shall employ the nomenclature in-plane/anti-plane to reference the shear components $q_{rz}/q_{r\theta}$ respectively.

Because there are now two components of shear stress in perpendicular directions being applied to the bodies, the slip condition needs to be modified. In the stick zone, the total shearing traction at each point must be less than that needed to cause slip, i.e.

$$p(z) < 0, \qquad [q_{rz}(z)]^2 + [q_{r\theta}(z)]^2 < [f\,p(z)]^2 \tag{17}$$

and in the slip zone, the total shearing traction is limited by friction:

$$p(z) < 0, \qquad [q_{rz}(z)]^2 + [q_{r\theta}(z)]^2 = [f\, p(z)]^2 . \tag{18}$$

In addition, the direction of the equivalent shearing traction must be such that it is collinear with, but opposed to, the slip velocity (orthogonality condition) [9]:

$$\frac{q_{r\theta}(z)}{q_{rz}(z)} = \frac{\dot{h}_{r\theta}(z)}{\dot{h}_{rz}(z)}, \tag{19}$$

where $\dot{h}_{ri}(z)$ represents the slip velocity in the direction $i = r, \theta$.

Consequently, it is necessary to solve the problem incrementally, to ensure that this condition is met instantaneously at each time step.

3.1. Incremental solution

In order to find the solution for a general time step $k+1$, we assume that we have a solution for the stresses and slip displacements for the shaft/hub system in the current step k, where the system holds a torque T. The solution at step k is characterized by the normal stress $p^{(k)}(\gamma, z)$, in-plane shear stress $q_{rz}^{(k)}(\gamma, z)$, in-plane tangential displacement $h_{rz}^{(k)}(\gamma, z)$, anti-plane shear stress $q_{r\theta}^{(k)}(\gamma, z)$ and anti-plane tangential displacement $h_{r\theta}^{(k)}(\gamma, z)$. It is also assumed that in this step a slip zone was developed, extending from $z = 0$ to a point $z = d^{(k)}$ (left side of Figure 2a).

When $k + 1 = 1$, the k state is defined as the shrink fit assembly, where $p^{(0)}(z)$, $q_{rz}^{(0)}$ and $h_{rz}^{(0)}(z)$ were obtained in Section 2, and $q_{r\theta}^{(0)} = h_{r\theta}^{(0)}(z) = 0$.

The solution for the state k must obey the slip condition, i.e. the magnitude of the shear stress must be limited by friction:

$$\left[\sigma_{rz}^{(k)}(\gamma, z)\right]^2 + \left[\sigma_{r\theta}^{(k)}(\gamma, z)\right]^2 = \left[f\, \sigma_{rr}^{(k)}(\gamma, z)\right]^2 \; 0 \le z \le d^{(k)}. \tag{20}$$

An increment of torque $\Delta\gamma$ is applied, giving rise to the new state of stress $k + 1$. The torque in the system is now $\gamma + \Delta\gamma$. Due to a bilateral change caused by the increase in torque, the current solution (state k) is no longer valid, since it now violates the slip condition in eq. (20). We also expect the increment of torque to increase the size of the slip zone, which will now extend from $z = 0$ to a point $z = d^{(k+1)}$, where $d^{(k+1)} > d^{(k)}$ (right side of Figure 2a). This self-determining stick-slip transition point is an output of the problem. For simplicity, we shall drop the superscripts for the new state and write $d = d^{(k+1)}$, $p(z) = p^{(k+1)}(z)$, $q_{rz}(z) = q_{rz}^{(k+1)}(z)$ and $q_{r\theta}(z) = q_{r\theta}^{(k+1)}(z)$.

A modified solution for the new state $k + 1$ can be obtained as described in Section 2, by developing expressions for the tractions at the contact interface as the sum of the solution in the current state k together with a correction in the form of an integral representation of slip as a distribution of glide dislocations. Because of the introduction of $\sigma_{r\theta}$ stresses, a screw glide dislocation loop $b_\theta(z)$ is needed in addition to the axial glide loop $b_z(z)$. The screw glide loop may be created by making a path cut along the cylinder $r = a$ between the dislocation and the free surface of the half-space and twisting the outer wall with respect to the inner wall by b_θ. This will introduce the following tractions along the same path cut

$$\hat{\sigma}_{i\theta}(z) = G_{\theta i}^{\theta}(z, \xi)\, b_\theta(\xi). \tag{21}$$

The influence functions $G_{\theta i}^{\theta}(z, \xi)$, $i = r, z$, are also described as sums of Lipschitz-Hankel integrals, and for a half-space are given by Sackfield et al. [10] and in the Appendix A.

The resulting normal $p(z)$, in-plane shear $q_{rz}(z)$ and anti-plane shear $q_{r\theta}(z)$ tractions along the contact interface for the current step are given by

$$p(\gamma + \Delta\gamma, z) = p^{(k)}(\gamma, z) + \int_0^d G_{rr}^{z}(z, \xi)\, B_z(\xi) \mathrm{d}\xi, \tag{22}$$

$$q_{rz}(\gamma + \Delta\gamma, z) = q_{rz}^{(k)}(\gamma, z) + \int_0^d G_{rz}^{z}(z, \xi)\, B_z(\xi) \mathrm{d}\xi \tag{23}$$

$$q_{r\theta}(\gamma + \Delta\gamma, z) = \tilde{\sigma}_{r\theta}(\gamma + \Delta\gamma, z) + \int_0^d G_{r\theta}^{\theta}(z, \xi)\, B_\theta(\xi) \mathrm{d}\xi \tag{24}$$

where $B_i(\xi) = db_i/d\xi$, $i = z, \theta$ represents the dislocation density and $\tilde{\sigma}_{r\theta}(\gamma + \Delta\gamma, z)$ represents the sum of the anti-plane shear stress in the previous state $q_{r\theta}^{(k)}(\gamma, z)$ and the contribution due to the increase in torque $\sigma_{r\theta}^{T}(\Delta\gamma, z)$,

$$\tilde{\sigma}_{r\theta}(\gamma + \Delta\gamma, z) = q_{r\theta}^{(k)}(\gamma, z) + \sigma_{r\theta}^{T}(\Delta\gamma, z). \tag{25}$$

Equations (22) to (25) form the basis of the solution and integral equations may be generated to restore Signorini and orthogonality conditions.

In the closed, slipping region, the equivalent shearing traction must be limited by friction:

$$p(z) < 0 \qquad [q(z)]^2 = [f\, p(z)]^2 \qquad 0 \le z \le d, \tag{26}$$

where

$$q(z) = \sqrt{[q_{rz}(\gamma + \Delta\gamma, z)]^2 + [q_{r\theta}(\gamma + \Delta\gamma, z)]^2}. \tag{27}$$

In addition, the in-plane and anti-plane shear tractions must be subjected to the orthogonality condition (eq. (19)).

Even though the loading is quasi-static, there is still the need to correlate the application of the torque with the pseudo time derivatives:

$$\frac{\mathrm{d}h(T, z)}{\mathrm{d}t} = \frac{\mathrm{d}T}{\mathrm{d}t} \frac{\mathrm{d}h(T, z)}{\mathrm{d}T}. \tag{28}$$

Therefore, for a finite time step ΔT, we can approximate eq. (19) by

$$\frac{q_{r\theta}(z)}{q_{rz}(z)} = \frac{\Delta h_{r\theta}(z)}{\Delta h_{rz}(z)}. \tag{29}$$

Equations (26) and (29) form a system of non-linear singular integral equations with Cauchy kernels. There are two unknown functions to be determined, $B_z(z)$ and $B_\theta(z)$, and an unknown stick-slip transition point, d. However, obtaining a solution in this non-linear format is extremely difficult. Previous attempts at solving plane/antiplane frictional problems involved the use of special elements of strain nuclei, such as triangular elements of dislocation densities [11, 12, 13, 14]. We propose, instead, a simple modification to the system that allows for an iterative solution using standard Gauss-Chebyshev quadrature devised by Erdogan et al. [7].

3.2. Numerical scheme

The angle of slip at each point $\alpha(z)$ can be given either as the ratio between the components of shear stress or the velocity components. Hence, each side of eq. (29) gives the tangent of the angle of slip $\alpha(z)$ at each point and we can rewrite the equation as:

$$\frac{q_{r\theta}(z)}{q_{rz}(z)} = \tan(\alpha(z)), \tag{30}$$

$$\frac{\Delta h_{r\theta}(z)}{\Delta h_{rz}(z)} = \tan(\alpha(z)). \tag{31}$$

Substitution of eq. (30) in eq. (26), together with eq. (31), leads to the following linear system of singular integral equations:

$$q_{rz}(z) = -f\,\cos(\alpha(z))\,p(z), \tag{32}$$

$$q_{r\theta}(z) = -f\,\sin(\alpha(z))\,p(z), \tag{33}$$

$$\frac{\Delta h_{r\theta}(z)}{\Delta h_{rz}(z)} = \tan(\alpha(z)). \tag{34}$$

Applying eqs. (22) to (24) to eqs. (32) to (34), gives

$$\int_0^d \Big[G^z_{rz}(z,\xi) + f\,\cos(\alpha(z))\,G^z_{rr}(z,\xi)\Big]\,B_z(\xi)\,\mathrm{d}\xi + = -\Big[q^{(k)}_{rz}(z) + f\,\cos(\alpha(z))\,p^{(k)}(z)\Big] \quad 0 \le z \le d \tag{35}$$

$$\int_0^d G^\theta_{r\theta}(z,\xi)\,B_\theta(\xi)\,\mathrm{d}\xi + f\,\sin(\alpha(z))\int_0^d G^z_{rr}(z,\xi)\,B_z(\xi)\,\mathrm{d}\xi + = -\Big[\tilde\sigma_{r\theta}(z) + f\,\sin(\alpha(z))\,p^{(k)}(z)\Big] \quad 0 \le z \le d. \tag{36}$$

Owing to the nature of the functions present in eqs. (35) and (36), there is no hope of analytically inverting the integral equations. However, there are no explicit non-linearities in them and, assuming that $\alpha(z)$ is known, the singular integral equations (SIE's) can be solved numerically, using Gauss-Chebyshev quadrature [7]. The two equations are imposed over one region ($0 \le z \le d$), and, as long as $B_z(z)$ and $B_\theta(z)$ can each be described by the same fundamental function (same behaviour at the ends of the interval), only one set of quadrature points is needed.

The first step in solving the SIE's is to put the integrals in standard form over the interval $[-1\,,1]$. We choose the following substitution

$$s = \frac{2\,\xi}{d} - 1 \tag{37}$$

$$t = \frac{2\,z}{d} - 1 \tag{38}$$

$$\tag{39}$$

which gives

$$\int_{-1}^{1} \Big[G^z_{rz}(t,s) + f\,\cos(\alpha(t))\,G^z_{rr}(t,s)\Big]\,B_z(s)\,\mathrm{d}s + = -\frac{2}{d}\Big[q^{(k)}_{rz}(t) + f\,\cos(\alpha(t))\,p^{(k)}(t)\Big] \quad -1 \le t \le 1 \tag{40}$$

$$\int_{-1}^{1} G^\theta_{r\theta}(t,s)\,B_\theta(s)\,\mathrm{d}s + f\,\sin(\alpha(t))\int_{-1}^{1} G^z_{rr}(t,s)\,B_z(s)\,\mathrm{d}s + = -\frac{2}{d}\Big[\tilde\sigma_{r\theta}(t) + f\,\sin(\alpha(t))\,p^{(k)}(t)\Big] \quad -1 \le t \le 1. \tag{41}$$

For the general form of the solution, the two dislocation densities must be bounded at both ends of the interval. Thus, we choose

$$B_z(s) = \phi_z(s)\,\sqrt{1-s^2} \tag{42}$$

$$B_\theta(s) = \phi_\theta(s)\,\sqrt{1-s^2} \tag{43}$$

and eqs. (40) and (41) become, in normalised form,

$$\sum_{i=1}^{N}\Big\{\Big[G^z_{rz}(t_j,s_i) + f\,\cos(\alpha(t_j))\,G^z_{rr}(t_j,s_i)\Big]\,W_i\phi_z(s_i)\Big\} + = -\frac{2}{\pi\,d}\Big[q^{(k)}(t_j) + f\,\cos(\alpha(t_j))\,p^{(k)}(t_j)\Big] \quad j = 1,\ldots,N+1 \tag{44}$$

$$\sum_{i=1}^{N}\left\{\left[G^{\theta}_{r\theta}(t_j,s_i)\right]\phi_\theta(s_i)\right\}+$$
$$\sum_{i=1}^{N}\left\{\left[f\,\sin(\alpha(t_j))\,G^{z}_{rr}(t_j,s_i)\right]\phi_z(s_i)\right\}$$
$$=-\frac{2}{\pi\,d}\left[\tilde{\sigma}_{r\theta}(t_j)+f\,\sin(\alpha(t_j))\,p^{(k)}(t_j)\right] \qquad (45)$$
$$j=1,\ldots,N+1$$

where the integration points s_i, collocation points t_j and weights W_i for the quadrature are given as

$$s_i=\cos\left(\pi\frac{i}{N+1}\right) \qquad i=1,\ldots,N \qquad (46)$$
$$t_j=\cos\left(\frac{\pi}{2}\frac{2j-1}{(N+1)}\right) \qquad j=1,\ldots,N+1 \qquad (47)$$
$$W_i=\frac{1-s_i^2}{2\,(N+1)}. \qquad (48)$$

Equation (31) can be rewritten in terms of the displacements. Note that

$$\Delta h_{rz}(z)=-\int_z^d B_z(\xi)\mathrm{d}\xi-h_z^{(k)}(z) \qquad (49)$$
$$\Delta h_{r\theta}(z)=-\int_z^d B_\theta(\xi)\mathrm{d}\xi-h_\theta^{(k)}(z). \qquad (50)$$

which gives

$$\tan(\alpha(z))=\frac{-\int_z^d B_\theta(\xi)\mathrm{d}\xi-h_\theta^{(k)}(z)}{-\int_z^d B_z(\xi)\mathrm{d}\xi-h_z^{(k)}(z)}. \qquad (51)$$

Equation (34) can also be rewritten in a discretised form, viz.

$$\Delta h_{r\theta}(t_j)-\Delta h_{rz}(t_j)\tan(\alpha(t_j))=0,$$
$$j=1,\ldots,N+1.. \qquad (52)$$

For a given angle of slip $\alpha(z)$, Equations (44), (45) and (52) form a system of $3N+3$ equations and $3N+2$ unknowns. These are the N values of $\phi_z(s_i)$, N values of $\phi_\theta(s_i)$, $N+1$ values of $\alpha(t_j)$ and the stick point d.

We can solve the system in eqs. (44), (45) and (52) by giving an initial guess for $\alpha(t_j)$ and d, solving the system in eqs. (44) and (45) for ϕ_z and ϕ_θ and using an iterative procedure to adjust $\alpha(t_j)$ and d to make sure that the solution satisfies the orthogonality condition in eq. (52).

4. Results

The problem was coded using the numerical processor MATLAB. Convergence was obtained using $N=80$. A

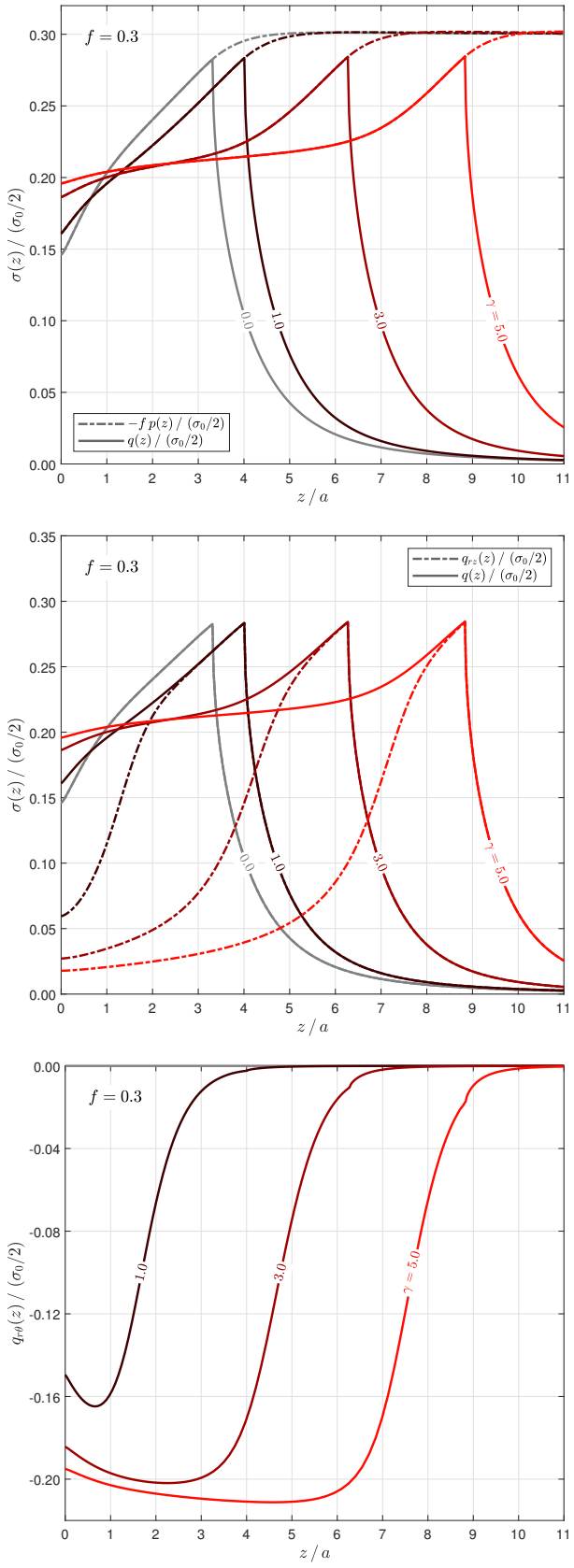

Figure 3: Normalised tractions at the contact interface for $f=0.3$, $\gamma=0.0, 1.0, 3.0$ and 5.0. (a) Contact pressure and equivalent shear stress. (b) In-plane and equivalent shear stress. (c) Anti-plane shear stress.

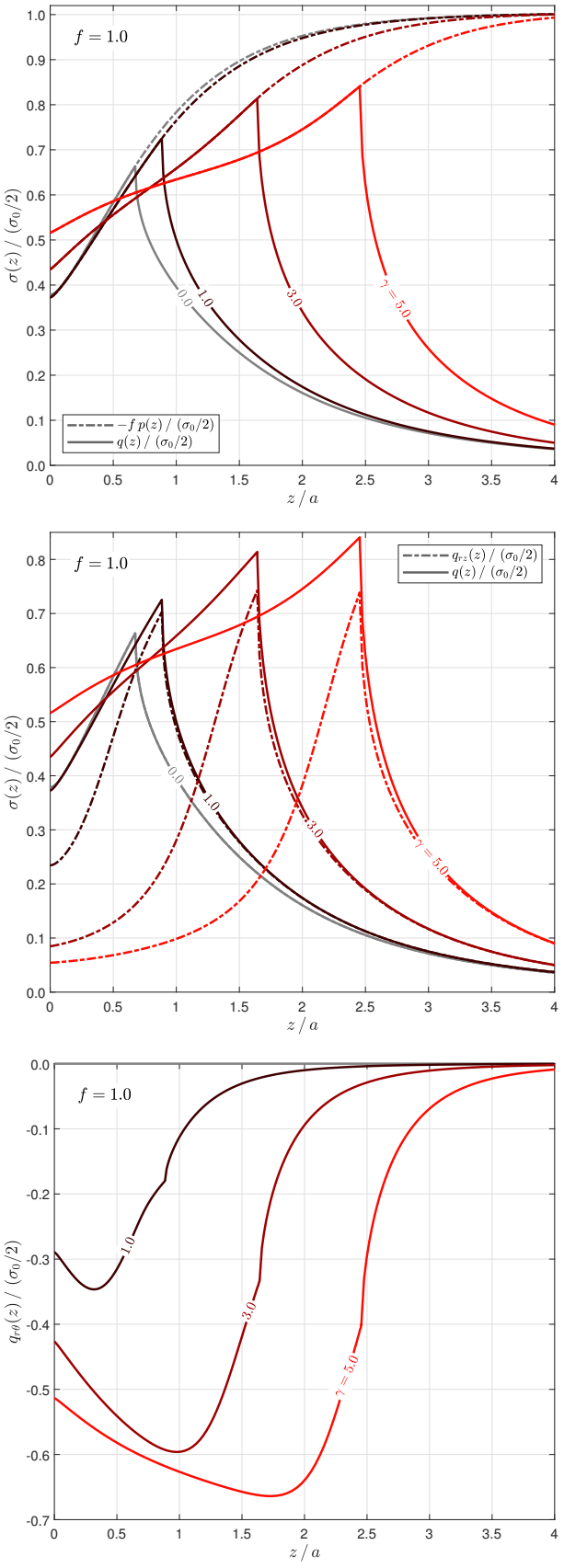

Figure 4: Normalised tractions at the contact interface for $f = 1.0$, $\gamma = 0.0, 1.0, 3.0$ and 5.0. (a) Contact pressure and equivalent shear stress. (b) In-plane and equivalent shear stress. (c) Anti-plane shear stress.

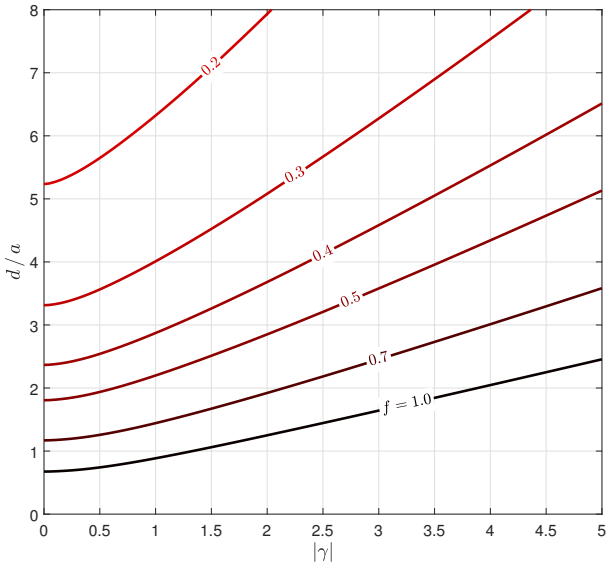

Figure 5: Normalised slip zone size d/a versus applied torque γ.

pseudo-time step of $\Delta\gamma = 0.05$ was used in all calculations. It was noted that changes in stresses and displacements for large γ was negligible when $\Delta\gamma$ was made smaller than 0.10. All the results presented in this paper are for $\nu = 0.3$.

Figures 3 and 4 show the tractions at the contact interface for $f = 0.3$ and 1.0 for $\gamma = 0.0$, 1.0, 3.0 and 5.0, normalised by the reference stress $\sigma_0/2$. The stresses at the assembly are given by $\gamma = 0$ and represented by the curves in light grey.

Figures 3a and 4a show the variation with depth of the equivalent shear stress $q(z)$ (solid lines) together with the product of the contact pressure and the coefficient of friction $f\,p(z)$ (dash-dotted lines). Far away from the surface ($z >> d$), the contact is fully stuck and, as expected, $|q(z)| < f\,p(z)$. As we move closer to the surface, the equivalent shear stress increases until it reaches $f\,p(z)$. At this point ($z = d$), the contact enters partial slip. For $0 \le z \le d$, the quantities $q(z)$ and $-f\,p(z)$ follow the same curve, since the contact is slipping. As γ increases, the slip-stick transition point d moves farther down, i.e. as more torque is applied to the shaft, it slips more deeply. Also, notice that the contact pressure itself at the surface changes significantly with the application of torque, increasing when γ increases. Even though the application of a torque produces no σ_{rr} stresses to change $p(z)$, the frictional behaviour of the contact results in a coupling effect, causing the pressure to change.

Figures 3b and 4b depict the variation with depth of the in-plane shear stress $q_{rz}(z)$ (dashed lines) together with the equivalent shear stress (solid lines). At assembly, $q_{r\theta}(z) = 0$ and, consequently, $q(z) = q_{rz}(z)$, which results in the two curves being the same. We notice that close to the surface the effect of the torque is more pronounced, and the difference between $q(z)$ and $q_{rz}(z)$ is higher. For greater depths, the effects of the torque vanish and the two curves converge. This is also shown in Figures 3c and 4c,

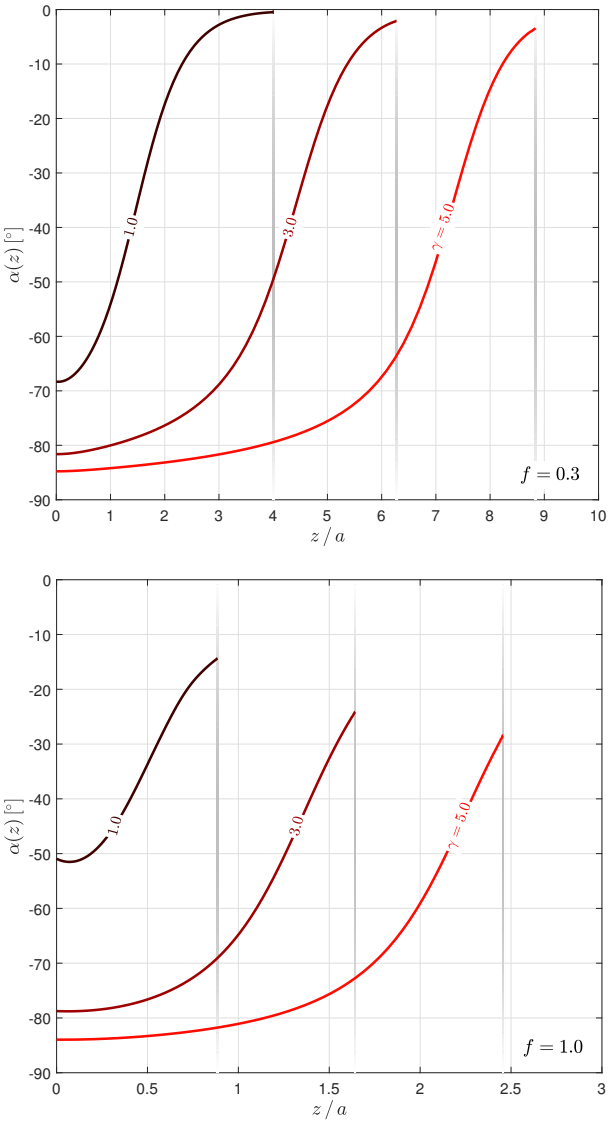

Figure 6: Angle of slip at the contact interface. (a) $f = 0.3$. (b) $f = 1.0$.

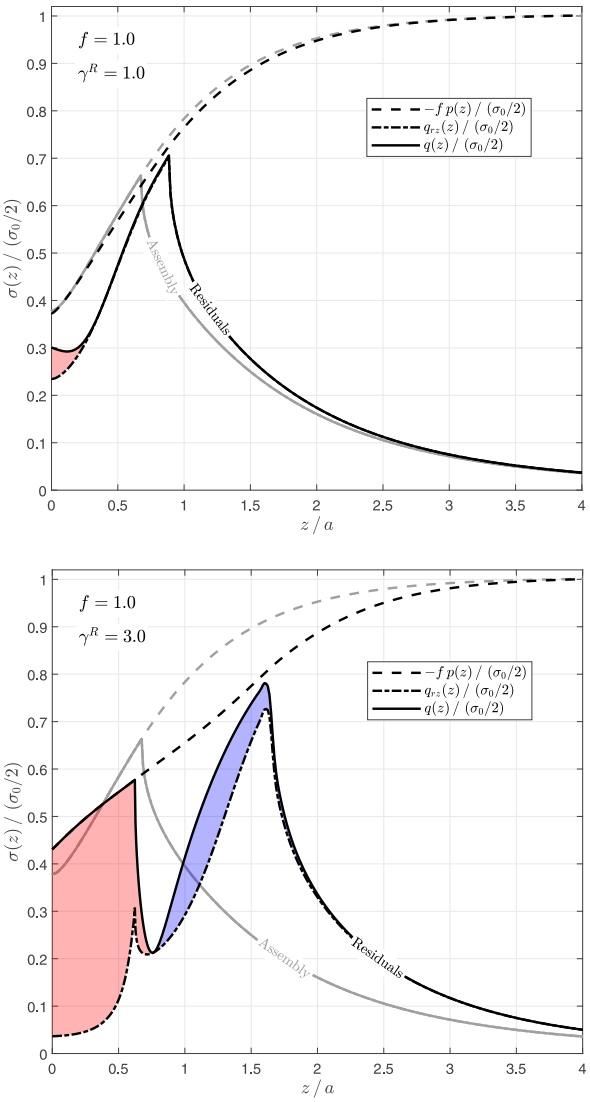

Figure 7: Normalised residual stresses at the contact interface for $f = 1.0$. (a) After applying $\gamma^R = 1.0$. (b) After applying $\gamma^R = 3.0$.

which represents the anti-plane shear stress $q_{r\theta}(z)$ as a function of z. We can see that $q_{r\theta}(z)$ is greater in magnitude closer to the surface and has a maximum inside the contact for both values of f and all γ.

Figure 5 shows the normalised slip zone size d/a as a function of the applied normalised torque γ for different values of coefficient of friction. As expected, as more torque is applied, the slip zone gets bigger. This effect is more pronounced for smaller coefficients of friction. Also, as expected, a higher value of f results in overall smaller slip zones than lower f. Furthermore, d/a is symmetric in γ, i.e. applying a negative torque would result in the same value of d/a. Since the shaft is semi-infinite, a finite torque can never cause spin, as it would require overcoming an infinite shear force.

Figure 6 depicts the angle of slip $\alpha(z)$ at the contact interface for $f = 0.3$ and 1.0. The vertical lines represent the normalised slip-stick transition points (d/a). For the shrink fit assembly ($\gamma = 0$), since there is no q_{rt} stress, slip is only in-plane and, consequently, the angle of slip is 0° throughout the slip zone. Notice that, as expected, close to the surface $\alpha(z)$ is higher and closer to $-90°$, since $q_{r\theta}$ is dominant and results in slip being predominantly in the anti-plane direction. However, because the shrink fit assembly results in the development of an in-plane q_{rz} stress, slip can never be purely in the anti-plane direction ($\alpha(z) = \pm 90°$) for $0 \leq z \leq c$. This can be seen in Figure 6b, for $f = 1.0$ and $\gamma = 5.0$. Even though a considerable amount of torque is being applied, $\alpha(z)$ presents an asymptotic behaviour close to the surface, and it does not reach $-90°$. In addition, at the slip-stick transition point, the anti-plane shear stress is not required to be zero, as shown in Figures 3c and 4c. Hence, $\alpha(d)$ will not necessarily be equal to zero.

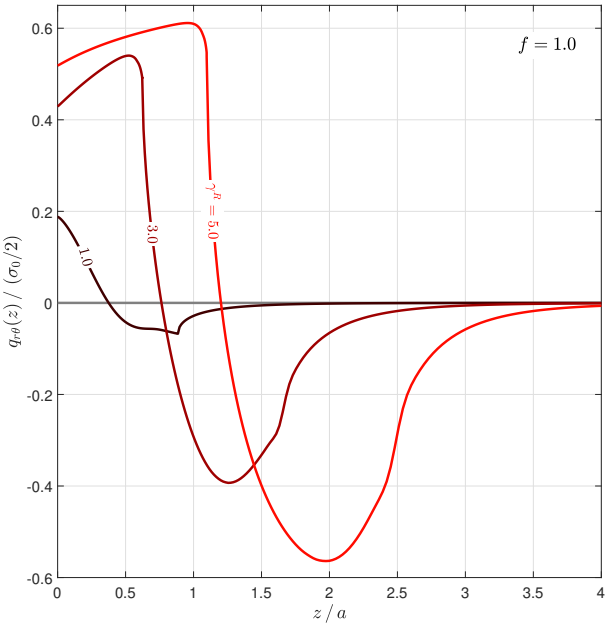

Figure 8: Normalised residual anti-plane stress at the contact interface.

4.1. Residual stresses

The next step in the analysis is to look at the residual stresses when a torque is monotonically applied to the system and subsequently relaxed. After assembling the shaft/hub system, a torque $\gamma = \gamma^R$ is monotonically applied. Subsequently, the torque is released (equivalent to applying $\gamma = -\gamma^R$), until the system is back to a no net torque state.

In the loading phase ($|\gamma|$ increasing), the slip zone size will extend from 0 to d and increase as γ increases. When γ is a maximum, d/a will be a maximum as well. As soon as the torque starts to decrease, the contact will stick everywhere instantaneously. As $|\gamma|$ decreases even further, new regions of slip will develop in the contact.

For simplicity, we shall consider only two cases, when the coefficient of friction is high ($f = 1.0$, Figure 7). In Figure 7a, a torque of $\gamma^R = 1.0$ is applied and then relaxed. In this case, after reaching the maximum torque, the contact sticks everywhere instantaneously, as soon as the torque starts to decrease. After unloading the torque completely, the final state is fully stuck. The curves in light grey represent the stresses at assembly, when no torque was applied, while the black curves represent the residual stresses. Notice that the equivalent shear stress is everywhere smaller than $-f\,p(z)$. Even though the two states represent no net torque, upon assembly the contact slips from $z = 0$ until $0.674\,a$, while this new state is completely stuck. There is also a considerable difference in the equivalent shear stress but not a lot of variation in contact pressure. We also note that the point where the shear stress peaks moved farther inside the contact.

In Figure 7b, a higher value of torque $\gamma^R = 3.0$ is applied and later relaxed. Similarly to the previous case, the contact sticks everywhere as soon as the torque starts to decrease. However, as γ decreases, the equivalent shear stress close to the surface increases and results in violation of the slip condition. A new slip zone is formed, extending from $z = 0$ to $z = 0.620\,a$. After unloading the torque completely, the new state is now in partial slip but in a different configuration from assembly. The contact pressure and equivalent shear are significantly different from assembly.

The shaded areas in Figure 7 highlight the locked-in anti-plane shear stress $q_{r\theta}$. Because all states hold no net torque, the integral of $q_{r\theta}(z)$ over the surface area of the shaft must be zero. The red shaded areas represent the places where $q_{r\theta}(z) > 0$, while the blue shaded areas represent $q_{r\theta}(z) < 0$. In both figures, the areas are the same. In Figure 7a, the blue area is 'hidden' between the $q(z)$ and $q_{rz}(z)$ curves, which are very similar but not exactly the same. This is shown more clearly in Figure 8.

5. Conclusions

A solution was obtained for the tractions, displacements and geometric parameters for an oversized shaft shrink fitted to an elastically identical hub and subjected to torsion. Due to the torque, there are in-plane and anti-plane components of shear and, consequently, an incremental solution was needed.

It was shown that the problem exhibits considerable frictional coupling. Even though the torsion of the shaft does not explicitly induce σ_{rz} and σ_{rr} stresses, the solution shows that the contact pressure and in-plane shear stress are significantly affected by the application of the torque.

In addition, it was shown that in monotonic loading the size of the slip zone is proportional to the magnitude of the applied torque.

Finally, when unloading the system back to zero net torque it was shown that the residual stresses are history dependent. Although the final state represents no net torque, it still had locked-in anti-plane shear stress.

Acknowledgements

J. L. gratefully acknowledges the financial support of Christ Church Oxford, Rolls Royce PLC and Coordenação de Aperfeiçoamento de Pessoal de Nível Superior - CAPES.

References

[1] R. Paynter, D. Hills, J. Barber, Features of the stress field at the surface of a flush shrink-fit shaft, Proceedings of the Institution of Mechanical Engineers, Part C: Journal of Mechanical Engineering Science 223 (10) (2009) 2241–2247.

[2] R. Paynter, D. Hills, The effect of path cut on Somigliana ring dislocations in a half-space, International Journal of Solids and Structures 46 (2) (2009) 412–432.

[3] K. Chowdhury, Solution of the problem of a concentrated torque on a semi-space by similarity transformations, Journal of Elasticity 13 (1) (1983) 87–90.

[4] D. Hills, P. Kelly, D. Dai, A. Korsunsky, Solution of crack problems: the distributed dislocation technique, Vol. 44 of Solid Mechanics and Its Applications, Springer Netherlands, Dordrecht, 2013.
[5] M. Comninou, D. Schmueser, J. Dundurs, Frictional Slip Between a Layer and a Substrate Caused by a Normal Load, International Journal of Engineering Science 18 (9) (1980) 131–137. doi:10.1016/0020-7225(80)90115-9.
[6] J. Lopes, D. Hills, Ring cracks at the surface of a half-space, Engineering Fracture Mechanics 194 (2018) 105–116.
[7] F. Erdogan, G. D. Gupta, T. Cook, Numerical solution of singular integral equations, in: Methods of analysis and solutions of crack problems, 1973, pp. 368–425.
[8] C. Chow, F. Yang, On the solution of a concentrated torque on an orthotropic half-space, International Journal of Engineering Science 28 (9) (1990) 871–874.
[9] J. Barber, Contact Mechanics, Solid Mechanics and Its Applications, Springer International Publishing, 2018.
[10] A. Sackfield, J. Barber, D. Hills, C. Truman, A shrink-fit shaft subject to torsion, European Journal of Mechanics-A/Solids 21 (1) (2002) 73–84.
[11] H. Qiu, D. Hills, D. Nowell, D. Dini, Skew sliding of an elastic cylinder: An investigation of convection in contact, International Journal of Mechanical Sciences 50 (2) (2008) 293–298.
[12] H. Qiu, D. Dini, D. Hills, Torsional contact of an elastic flat-ended cylinder, Journal of the Mechanics and Physics of Solids 56 (12) (2008) 3352–3362.
[13] H. Qiu, D. Hills, D. Dini, An investigation of convection effects in complete and almost complete contact problems, European Journal of Mechanics-A/Solids 28 (4) (2009) 680–687.
[14] R. Bentall, K. Johnson, An elastic strip in plane rolling contact, International Journal of Mechanical Sciences 10 (8) (1968) 637–663.
[15] G. Eason, B. Noble, I. N. Sneddon, On certain integrals of Lipschitz-Hankel type involving products of Bessel functions, Philosophical Transactions of the Royal Society of London A: Mathematical, Physical and Engineering Sciences 247 (935) (1955) 529–551.
[16] R. Paynter, D. Hills, A. Korsunsky, The effect of path cut on Somigliana ring dislocation elastic fields, International Journal of Solids and Structures 44 (2) (2007) 6653–6677.

Appendix A. State of stress induced by circular edge dislocation loops

Appendix A.1. Axial prismatic dislocation

Consider a glide axial dislocation loop of radius a at a depth d and being observed at a position (r, z) in a cylindrical coordinate system, with a Burgers vector component b_z. The stress fields at a position (r, z) are given by

$$\sigma^z_{iz}(r,z) = G^z_{iz}(r,z,d)\, b_z(a) \quad i = r, z. \tag{A.1}$$

The influence functions $G^z_{iz}(\rho,\zeta,\delta)$ $(i = r,\ z)$ for the glide dislocation in a half-space are given as [2]:

$$G^z_{zz}(\rho,\zeta,\delta) = \frac{2\,\mu}{a\,(\kappa+1)}\Bigg[- J_{1,0;1} + I_{1,0;1} - (\zeta-\delta)\, J_{1,0;2} - (\zeta+\delta)\, I_{1,0;2} + 2\,\zeta\,\delta\, I_{1,0;3}\Bigg] \tag{A.2}$$

$$G^z_{rz}(\rho,\zeta,\delta) = \frac{2\,\mu}{a\,(\kappa+1)}\Bigg[- (\zeta-\delta)\, J_{1,1;2} + (\zeta-\delta)\, I_{1,1;2} - 2\,\zeta\,\delta\, I_{1,1;3}\Bigg] \tag{A.3}$$

where ρ, ζ and δ are the normalised coordinates, given by

$$\rho = r/a, \qquad \zeta = z/a, \qquad \delta = d/a, \tag{A.4}$$

μ is the modulus of rigidity and κ is the Kolosov's constant.

The axial dislocation loop does not induce shear stresses in the θ direction, i.e. $G^z_{\theta z}(\rho,\zeta,\delta) = 0$.

Appendix A.2. Screw dislocation

Consider a glide screw dislocation loop of radius a at a depth d with a Burgers vector component b_θ and being observed at a position (r, z) in a cylindrical coordinate system. The stress field at a position (r, z) is given by

$$\sigma^\theta_{i\theta}(r,z) = G^\theta_{i\theta}(r,z,d)\, b_\theta(a) \quad i = r, z. \tag{A.5}$$

The influence functions $G^\theta_{r\theta}(\rho,\zeta,\delta)$ $(i = r,\ z)$ for the glide dislocation in a half-space are given as [10]:

$$G^\theta_{r\theta}(\rho,\zeta,\delta) = \frac{\mu\, a}{2}\Bigg[J_{0,2;1} - 2\, J_{1,2;0} - (I_{0,2;1} - 2\, I_{1,2;0})\Bigg] \tag{A.6}$$

$$G^\theta_{z\theta}(\rho,\zeta,\delta) = \frac{\mu\, a}{2}\Bigg[J_{1,2;1} - I_{1,2;1}\Bigg] \tag{A.7}$$

Appendix A.3. Lipschitz-Hankel integrals

In the influence functions, the terms $J_{n,p;q}$ and $I_{n,p;q}$ represent Lipschitz-Hankel integrals. The standard definition for these functions is as an integral of the product of Bessel functions $(J_i(\cdot))$, an exponential term and a power term. Using normalised coordinate variables, it is given as [15]

$$P_{\mu,\nu;\lambda}(\rho,\zeta) = \int_0^\infty J_\mu(t)\, J_\nu(\rho\, t)\, e^{-\zeta\, t}\, t^\lambda\, \mathrm{d}t. \tag{A.8}$$

In this paper, the follow definition is applied:

$$J_{n,p;q} = P_{n,p;q}(\rho, \zeta-\delta) \tag{A.9}$$

$$I_{n,p;q} = P_{n,p;q}(\rho, -\zeta-\delta) \tag{A.10}$$

The Lipschitz-Hankel integrals needed in the paper are given by Paynter et al. [16, 2] and are available in MATLAB in [6].

Part II

Receding Contacts

Part II corresponds to the solution of receding contacts involving a thin sheet of material being pressed against an elastic substrate. In these problems, the sheet is modelled by a semi-infinite layer of thickness a, which rests against an elastically similar half-space (substrate). For each problem, a different loading is applied to the upper surface of the layer, which will result in different frictional behaviour.

The main difficulty in solving these problems is that the contact area is infinite and, consequently, the singular integral equations must be posed over an infinite domain. In Chapter 7, a stamping receding contact is proposed, where uniform pressure is applied over the whole surface of the sheet, except for a disk of radius b. In this case, the contact may recede over the unloaded region, depending on the radius of the unloaded region and the coefficient of friction. Because this area is finite, this constitutes a receding contact where the singular integrals are finite, and corresponds to an intermediate case of complexity between the problems in Part I and the problems in Chapters 8 and 9.

The simplest axisymmetric frictional receding contact model is when the layer is subjected to a concentrated force applied at its axis of symmetry (Chapter 8). Because there are no intrinsic length dimensions associated with the loading, the only independent parameter of the problem is the interfacial coefficient of friction.

In order to construct a better model for a bolted joint, Chapter 9 considers the case where the layer is subjected to uniform pressure over a disk, which represents the washer pressure. Limit considerations show that the application of distributed pressure is inherently different from applying a point force, even when the radius of the circular patch tends to zero.

The modified Gauss-Chebyshev quadrature was chosen to numerically invert the singular integral equations in Chapters 8 and 9, since it was shown in Chapter 3 that its usage does not hinder the accuracy of the solution for singular integral equations posed over a semi-infinite interval when compared to the Gauss-Laguerre quadrature, while providing a much better computational cost. The choice of transformation function for the interval mapping was carefully considered in both problems.

A comparison between the analytical solutions presented in Part I and their respective

finite element solutions are presented in Appendix C.

7

The Axisymmetric Frictional Receding Contact of a Layer Pressed Against a Half-Space by Pressure Outside a Disk

The axisymmetric frictional receding contact of a layer pressed against a half-space by pressure outside a disk

J.P. Lopes[a,*], D.A. Hills[a]

[a] *Department of Engineering Science, University of Oxford, Parks Road, Oxford OX1 3PJ, United Kingdom*

Abstract

This paper uses a distribution of ring dislocations to find the solution for the frictional axisymmetric receding contact of a semi-infinite layer pressed against a half-space by a uniform surface pressure exerted outside a disk. Three cases are considered: the contact is fully closed and stuck; the contact is fully closed and slipping; the contact is partially open and slipping. The tractions in the contact interface are obtained, as well as the self-determining points of closure and stick.

Keywords: Axisymmetric, Receding Contact, Ring dislocations

1. Introduction

The main characterization of contacts is done by comparing the extent of the contact in the deformed configuration with the initial configuration in the unloaded state. While the initial state is determined by the geometric features of the bodies and their fixtures, the deformed contact state generally depends on the nature of the applied loads, the level of loading and the elastic constants of the materials [1].

The classification is done by observing whether or not new surface points come in contact as the bodies deform. In advancing contacts, new surface points come in contact as the load is applied and, as a consequence, the deformed contact is not contained in the initial state. However, in receding contacts, the contact shrinks resulting in the deformed contact being contained in the initial state.

In machines or structures with carefully fitted parts, receding contacts are more likely to appear than advancing contacts, because of the opening of gaps between the individual parts as they distort under application of loads.

A property of some receding contacts is that the contact area in the deformed configuration is independent of the applied load and, consequently, the change between undeformed/deformed configurations is discontinuous, i.e. the contact 'snaps' to the deformed configuration upon applying a load [1, 2]. This presents a challenge in obtaining solutions through the finite element method, as a large portion of the nodes change status from being in contact to being free with any increment of load.

One of the applications of receding contacts in industry is the analysis of frictional contacts in bolted joints, which are naturally axisymmetric, either for the whole joint or for its individual elements. However, the scarce work currently present in the literature for receding contacts is focused either on plane contacts [3, 4] or on frictionless cases [5, 6, 7].

This paper proposes the study of the frictional axisymmetric receding contact of a homogeneous semi-infinite layer of thickness a, Poisson's ratio ν and modulus of rigidity μ, pressed against an elastically similar half-space $z \geq a$ (Figure 1a) by a semi-infinite patch of pressure applied to the layer's surface ($z = 0$), such that

$$\sigma_{zz}(r,0) = -p, \qquad r \geq b \tag{1}$$

$$\sigma_{zz}(r,0) = 0, \qquad 0 \leq r < b. \tag{2}$$

Furthermore, the objective of this study is to find the solution to the proposed problem using ring dislocations to introduce corrections to the stresses in the contact interface as a distribution of strain nuclei. Initially, we assume that the contact is in a fully closed and stuck configuration. Then, dislocation densities are applied to correct the stresses when this condition is violated.

2. Adhered Solution

First, we assume that the unloaded region of radius b is small enough to prevent contact opening and that the coefficient of friction f is high enough to prevent slip throughout the contact area, as shown in Figure 1a (Case I). In this case, the two bodies behave as one, since the contact is closed and stuck everywhere. Therefore, the state of stress in the bodies is equivalent to a half-space $z \geq 0$ under the same loading. In the cylindrical coordinate set shown in the figure, the state of stress is given by the superposition

*Corresponding author

Email addresses: jhonatan.dapontelopes@eng.ox.ac.uk (J.P. Lopes), david.hills@eng.ox.ac.uk (D.A. Hills)

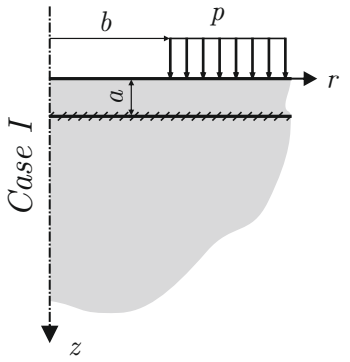

(a)

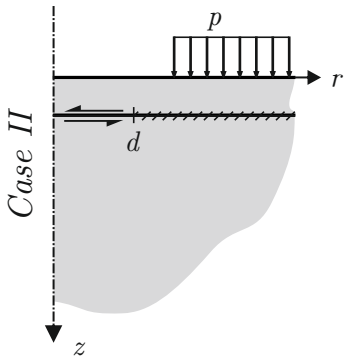

(b)

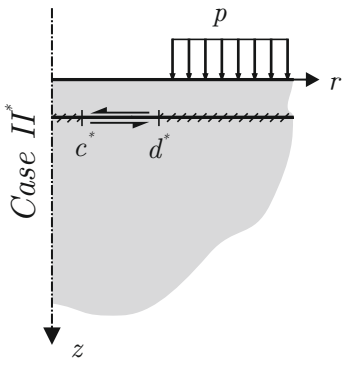

(c)

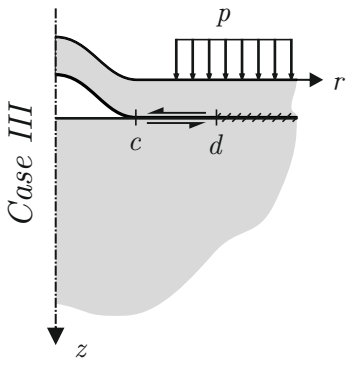

(d)

Figure 1: A layer subjected to semi-infinite pressure. (a) Fully closed and stuck. (b) Closed and slipping. (c) Closed and slipping inside contact. (d) Partially open and slipping.

of a uniform pressure p throughout the surface of the half-space and a circular patch of uniform normal traction $-p$ and radius b [8, 9, 10]. The tractions $\tilde{\sigma}_{ij}(r,z)$ arising on any radial cut ($z = constant$ surface) are given by:

$$\tilde{\sigma}_{zz}(r,z) = -p\left\{1+\frac{2z}{\pi}\left[\frac{r^2+z^2-b^2}{(l_2)^3(1-k^2)^2}\boldsymbol{E}(k)+\frac{b^2-(l_1)^2}{(l_2)^3(1-k^2)}\boldsymbol{K}(k)-\frac{1}{l_2}\boldsymbol{\Pi}(n;k)\right]\right\} \quad (3)$$

$$\tilde{\sigma}_{rz}(r,z) = p\left\{\frac{2z^2}{\pi}\left[\frac{\left(1+k^2\right)\boldsymbol{E}(k)-\left(1-k^2\right)\boldsymbol{K}(k)}{\left(k^2-1\right)^2 l_2\, r}\right]\right\} \quad (4)$$

where

$$l_1 = \frac{1}{2}\left\{\sqrt{(r+b)^2+z^2}-\sqrt{(r-b)^2+z^2}\right\} \quad (5)$$

$$l_2 = \frac{1}{2}\left\{\sqrt{(r+b)^2+z^2}+\sqrt{(r-b)^2+z^2}\right\} \quad (6)$$

$$k = \frac{l_1}{l_2} \quad (7)$$

$$n = \left(\frac{l_1}{r}\right)^2 \quad (8)$$

and $\boldsymbol{K}(k)$, $\boldsymbol{E}(k)$, $\boldsymbol{\Pi}(n;k)$ are the complete elliptic integrals of the first, second and third kind respectively. These functions are continuous and bounded at every point inside the half-space, but $\boldsymbol{\Pi}(n;k)$ cannot be evaluated numerically along the z-axis, since $r = 0$ there. In this region, we take the limits as $r \to 0$, giving:

$$\tilde{\sigma}_{zz}(0,z) = -p\left\{\frac{z^3}{(b^2+z^2)^{3/2}}\right\} \quad (9)$$

$$\tilde{\sigma}_{rz}(0,z) = 0. \quad (10)$$

If the contact is, indeed, fully closed and adhered, the normal $N(r)$ and shear $S(r)$ tractions at the layer/half-space interface are given by:

$$N(r) = \tilde{\sigma}_{zz}(r,a) \quad (11)$$

$$S(r) = \tilde{\sigma}_{rz}(r,a). \quad (12)$$

Figure 2 shows the normalised contact pressure and shear to normal stress ratio for the adhered solution. Analysing the stress ratio (Figure 2b), there is a minimum coefficient of friction that results in the contact being fully stuck for each b/a. When b/a is relatively large, however, there is no realistic coefficient of friction that prevents slip. Thus, we expect that some pairs of b/a and f result in a case where the contact is closed but slipping from the axis

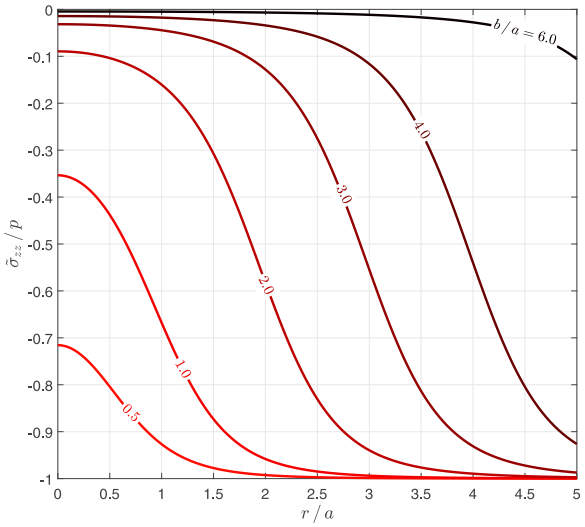

(a)

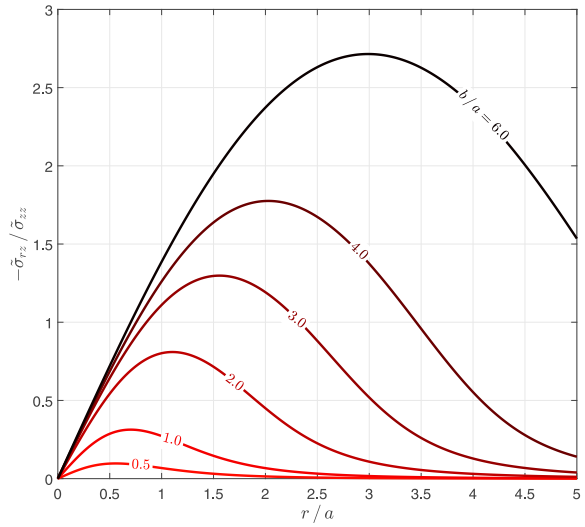

(b)

Figure 2: Normalised tractions for the adhered (bilateral) solution. (a) Normalised contact pressure. (b) Shear to normal stress ratio.

of symmetry to a self-determining radius d (Case II, Figure 1b). Analysing the contact pressure (Figure 2a), we expect the contact to be closed when the normalised radius of the unloaded disk b/a is small. As the unloaded region widens, the contact pressure becomes zero at the interface, which results in the development of an open region. Therefore, for some pairs of b/a and f, we expect the contact to be partially open from the axis of symmetry to a radius c and closed and slipping from c to d (Case III).

3. Formulation

If the contact is not fully stuck and closed, the bilateral solution obtained in Section 2 is no longer valid. A modified solution can be obtained by developing expressions for the tractions at the contact interface as the sum of the adhered (bilateral) solution together with a correction in the form of an integral representation of slip and opening as a distribution of climb and glide dislocations. The dislocations needed are all 'edge' in character, with their Burgers vector lying in a $\theta = constant$ plane. We emphasise that the introduction of dislocations is used solely as a mathematical device to introduce corrections in our formulation as a distribution of strain nuclei and do not imply the introduction of physical defects in the micro-structure of the material. A more detailed explanation can be found in [11].

First, we introduce a $b_r(\xi)$ glide dislocation loop of radius ξ, lying at a depth a. It may be formed by making a path cut along the disk $0 \le r \le \xi$ and sliding the surfaces by a constant amount b_r. This models contact slip and will induce the following tractions $\hat{\sigma}_{iz}(r)$ $(i = r, z)$ along the same disk

$$\hat{\sigma}_{iz}(r) = G^r_{iz}(r,\xi)\, b_r(\xi). \tag{13}$$

The influence functions $G^r_{iz}(r,\xi)$ are functions of Lipschitz-Hankel integrals and have extremely complicated forms. For a half-space, these are given by Paynter et al. [12] (see also [13, 14]). They are bounded ('regular') when $i = z$ and display a Cauchy singularity when $i = r$.

Next, we introduce a $b_z(\xi)$ climb dislocation loop of radius ξ, lying at a depth a. Now, the dislocation loop may be formed by making a path cut along $0 \le r \le \xi$ and inserting a disk of thickness b_z. This models contact opening and will induce the following tractions $\hat{\sigma}_{iz}(r)$ $(i = r, z)$ along the same disk

$$\hat{\sigma}_{iz}(r) = G^z_{iz}(r,\xi)\, b_z(\xi). \tag{14}$$

Once again, the influence functions $G^z_{iz}(r,\xi)$ are functions of Lipschitz-Hankel integrals and have extremely complicated forms. For a half-space, these are also given by Paynter et al. [12]. This time, they are bounded ('regular') when $i = r$ and display a Cauchy singularity when $i = z$.

The resulting normal $N(r)$ and shear $S(r)$ tractions along the contact interface are given by

$$N(r) = \tilde{\sigma}_{zz}(r) + \int_{opening} G^z_{zz}(r,\xi)\, B_z(\xi)\mathrm{d}\xi + \int_{slip} G^r_{zz}(r,\xi)\, B_r(\xi)\mathrm{d}\xi \tag{15}$$

$$S(r) = \tilde{\sigma}_{rz}(r) + \int_{opening} G^z_{rz}(r,\xi)\, B_z(\xi)\mathrm{d}\xi + \int_{slip} G^r_{rz}(r,\xi)\, B_r(\xi)\mathrm{d}\xi \tag{16}$$

where $B_i(\xi) = db_i/d\xi$, $i = r, z$. Glide dislocations are installed over the whole of the length of the contact interface where slipping occurs, including the open portion, and climb dislocations are installed over the part of the contact interface which is open. Equations (15) and (16) form the basis of the solution and integral equations may be generated in slightly different forms for the cases II and III of response described in Section 2.

3.1. Case II

Case II represents the situation where there is a region of slip of radius d but there is no separation. The coefficient of friction f is small enough so that slip occurs but is high enough to prevent contact opening. The point d where the contact sticks is self-determining and, thus, is an output of the problem.

In the slip region, the boundary conditions require that the normal stress must be compressive and the shear stress must be limited by friction:

$$S(r) = -fN(r), \qquad N(r) < 0, \qquad 0 \le r \le d. \quad (17)$$

Since there are no open regions in Case II, only glide dislocations b_r are needed to correct the stresses. Applying eqs. (15) and (16) to eq. (17), we obtain the following Cauchy integral equation

$$\int_0^d \Big[G^r_{rz}(r,\xi) + f\, G^r_{zz}(r,\xi)\Big]\, B_r(\xi)\mathrm{d}\xi = -\Big[\tilde{\sigma}_{rz}(r) + f\,\tilde{\sigma}_{zz}(r)\Big] \qquad 0 \le r \le d \quad (18)$$

The problem consists now in finding the dislocation density $B_r(\xi)$ that satisfies eq. (18). Since the functions present in eq. (18) are of extreme complexity, there is no hope of analytically inverting the singular integral equation. It must be solved numerically using a standard numerical quadrature devised by Erdogan, Gupta and Cook [15]. First, we put them in standard form over the intervals $[-1\,,1]$ utilizing the substitutions

$$s = \frac{2\,\xi}{d} - 1\,, \qquad t = \frac{2\,r}{d} - 1 \qquad 0 \le r, \xi \le d \quad (19)$$

which gives

$$\int_{-1}^{1} \Big[G^r_{rz}(t,s) + f\, G^r_{zz}(t,s)\Big]\, B_r(s)\mathrm{d}s = -\frac{2}{d}\Big[\tilde{\sigma}_{rz}(t) + f\,\tilde{\sigma}_{zz}(t)\Big] \qquad -1 \le t \le 1. \quad (20)$$

Next, we need to consider the general form of the solution required. We note, first, that at $r = d$ the contact transitions smoothly from slip to stick. Thus, at this point ($t = 1$) the shear displacement gradient must be zero (both upper and lower surfaces displace the same amount tangentially), which means that the dislocation density must be bounded. At the other end of the integration interval ($r = 0, t = -1$), by symmetry, the tangential displacement gradient must be zero and, thus, the dislocation density is also bounded. Hence, we assume a fundamental function $B_r(s)$ as shown below, which leaves the unknown dislocation density being represented by the function $\phi_r(s)$:

$$B_r(s) = \phi_r(s)\,\sqrt{1 - s^2} \quad (21)$$

and eq. (20) becomes, in normalised form,

$$\sum_{i=1}^{N} \left\{ \left[G^r_{rz}(t_k, s_i) + f\, G^r_{zz}(t_k, s_i) \right] W_i\, \phi_r(s_i) \right\} = -\frac{2}{\pi\, d}\left[\tilde{\sigma}_{rz}(r,z)(t_k) + f\,\tilde{\sigma}_{zz}(r,z)(t_k) \right] \qquad k = 1, \ldots, N+1 \quad (22)$$

where the integration points s_i, collocation points t_k and weights W_i for the quadrature are given as [15]

$$s_i = \cos\left(\pi \frac{i}{N+1}\right) \qquad i = 1, \ldots, N \quad (23)$$

$$t_k = \cos\left(\frac{\pi}{2}\,\frac{2k-1}{(N+1)}\right) \qquad k = 1, \ldots, N+1 \quad (24)$$

$$W_i = \frac{1 - s_i^2}{2\,(N+1)}. \quad (25)$$

From eq. (22), we have a set of $N + 1$ equations for $N + 1$ unknowns. These are the N values of $\phi_r(s_i)$ and the stick point d. Once ϕ_z is known, the stresses at a point (r, z) can be found as

$$\sigma_{iz}(r,z) = \tilde{\sigma}_{iz}(r,z) + \int_0^d G^r_{iz}(r,z,\xi)\, B_r(\xi)\mathrm{d}\xi \qquad i = r, z. \quad (26)$$

3.2. Case III

The problem we look at now is when b/a is large and f is small, which allows for the contact to have an open region extending from the origin to a radius $r = c$ and a slip region from $r = c$ to $r = d$. Both the closure point c and stick point d are outputs of the problem (self-determining points).

In the open region, we require the surfaces to be traction-free

$$N(r) = 0, \qquad S(r) = 0, \qquad 0 \le r \le c \quad (27)$$

whereas, in the closed, slipping region, the shearing traction is again limited by friction:

$$N(r) < 0 \qquad S(r) = -f\,N(r) \qquad c \le r \le d. \tag{28}$$

The three sets of conditions in eqs. (27) and (28) may be combined into two by making use of the Heaviside step function, $H(\cdot)$, giving

$$N(r) = 0 \qquad 0 \le r \le c \tag{29}$$
$$S(r) + f\,H(r-c)\,N(r) = 0 \qquad 0 \le r \le d. \tag{30}$$

The climb dislocations are non-zero only over the interval $0 \le r \le c$, whereas the glide dislocations must be distributed over the whole interval $0 \le r \le d$. Applying eqs. (15) and (16) to eqs. (29) and (30), gives

$$\int_0^d G^r_{zz}(r,\xi)\,B_r(\xi)\mathrm{d}\xi + \int_0^c G^z_{zz}(r,\xi)\,B_z(\xi)\mathrm{d}\xi = -\tilde{\sigma}_{zz}(r) \qquad 0 \le r \le c \tag{31}$$

$$\int_0^d \Big[G^r_{rz}(r,\xi) + f\,H(r-c)\,G^r_{zz}(r,\xi)\Big]\,B_r(\xi)\,\mathrm{d}\xi + \int_0^c \Big[G^z_{rz}(r,\xi) + f\,H(r-c)\,G^z_{zz}(r,\xi)\Big]\,B_z(\xi)\,\mathrm{d}\xi = -\Big[\tilde{\sigma}_{rz}(r) + f\,H(r-c)\,\tilde{\sigma}_{zz}(r)\Big] \quad 0 \le r \le d. \tag{32}$$

Since there are two regions of imposition for the integral equations, two sets of quadrature points are needed. Again, the equation must be solved numerically, using Gauss-Chebyshev quadrature [15]. Putting them in standard form over the intervals $[-1\,,1]$ using the substitutions

$$u = \frac{2\,\xi}{c} - 1\,, \qquad v = \frac{2\,r}{c} - 1 \qquad 0 \le r, \xi \le c \tag{33}$$
$$s = \frac{2\,\xi}{d} - 1\,, \qquad t = \frac{2\,r}{d} - 1 \qquad 0 \le r, \xi \le d \tag{34}$$

gives

$$\int_{-1}^1 G^r_{zz}(v,s)\,B_r(s)\,d\,\mathrm{d}s + \int_{-1}^1 G^z_{zz}(v,u)\,B_z(u)\,c\,\mathrm{d}u = -\tilde{\sigma}_{zz}(v) \qquad -1 \le v \le 1 \tag{35}$$

$$\int_{-1}^1 B_r(s)\,\Big[G^r_{rz}(t,s) + f\,H(\gamma)\,G^r_{zz}(t,s)\Big]\,d\,\mathrm{d}s + \int_{-1}^1 B_z(u)\,\Big[G^z_{rz}(t,u) + f\,H(\gamma)\,G^z_{zz}(t,u)\Big]\,c\,\mathrm{d}u = -\Big[\tilde{\sigma}_{rz}(t) + f\,H(\gamma)\,\tilde{\sigma}_{zz}(t)\Big] \quad -1 \le t \le 1 \tag{36}$$

where $\gamma = (t+1)d\,/\,(2c) - 1$.

For the general form of the solution, both the climb and glide dislocations must be bounded at both ends of the interval. Thus, we choose

$$B_r(s) = \phi_r(s)\,\sqrt{1-s^2} \tag{37}$$
$$B_z(u) = \phi_z(u)\,\sqrt{1-u^2} \tag{38}$$

and eqs. (35) and (36) become, in normalised form,

$$\sum_{i=1}^N \Big\{W_i\,d\,\phi_r(s_i)\,G^r_{zz}(v_k,s_i) + X_i\,c\,\phi_z(u_i)\,G^z_{zz}(v_k,u_i)\Big\} = -\frac{2}{\pi}\tilde{\sigma}_{zz}(v_k) \qquad k = 1,\ldots,N+1 \tag{39}$$

$$\sum_{i=1}^N \Big\{\Big[G^r_{rz}(t_k,s_i) + f\,H(\gamma_k)\,G^r_{zz}(t_k,s_i)\Big]\,W_i\,d\,\phi_r(s_i)\Big\} + \sum_{i=1}^N \Big\{\Big[G^z_{rz}(t_k,u_i) + f\,H(\gamma_k)\,G^z_{zz}(t_k,u_i)\Big]\,X_i\,c\,\phi_z(u_i)\Big\} = -\frac{2}{\pi}\Big[\tilde{\sigma}_{rz}(t_k) + f\,H(\gamma_k)\,\tilde{\sigma}_{zz}(t_k)\Big] \quad k = 1,\ldots,N+1 \tag{40}$$

where $\gamma_k = (t_k+1)d\,/\,(2c) - 1$. Since both dislocations have the same behaviour, $s_i = u_i$, $t_k = v_k$ and $W_i = X_i$. Furthermore, they are the same as those presented in Section 3.1 and are given in eqs. (23) to (25).

Equations (39) and (40) form a system of $2N+2$ equations and $2N+2$ unknowns. These are the N values of $\phi_r(s_i)$, N values of $\phi_z(u_i)$, the closure point c and the stick point d. Once ϕ_r and ϕ_z are known, the stresses at a point (r,z) can be found as

$$\sigma_{iz}(r,z) = \tilde{\sigma}_{iz}(r,z) + \int_0^d G^r_{iz}(r,z,\xi)\,B_r(\xi)\mathrm{d}\xi + \int_0^c G^z_{iz}(r,z,\xi)\,B_z(\xi)\mathrm{d}\xi \qquad i = r,z. \tag{41}$$

4. Results

The two problems relating to cases II and III were coded up using the numerical processor MATLAB. Setting N to 80 makes the solution converge for both cases, i.e. the changes in the closure point c and stick point d, as well as changes in stress, are negligible when N is increased beyond 80. All the results presented in this paper are for $\nu = 0.3$. In problems where a length dimension is an unknown of the problem (d in case II and both c, d in case III), there are additional collocation equations which need to be satisfied and which enable the values of c/a and d/a to be found. In practice, we guess values of the lengths to be found and omit the last equations from the $N+1$ generated. The column vector of ϕ is found. The omitted equations are then evaluated and the lengths needed are adjusted to minimise the residues.

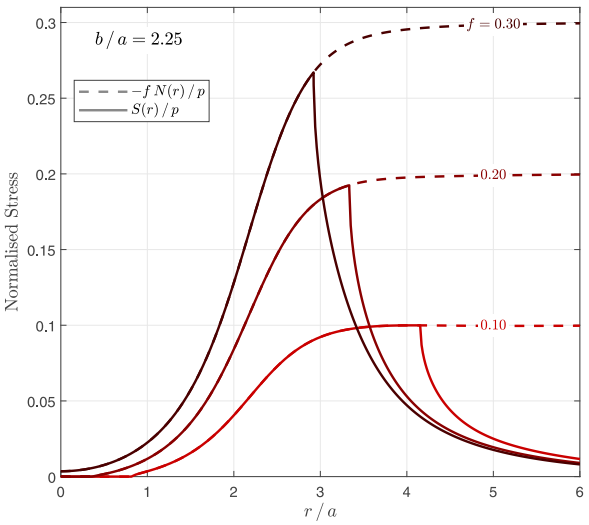

(a)

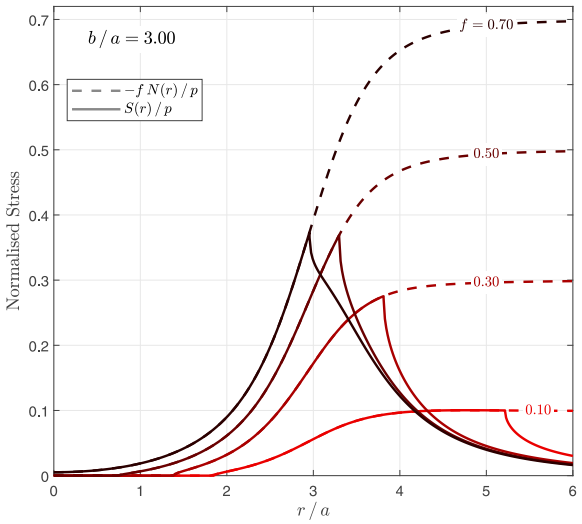

(b)

Figure 3: Normalised tractions in the contact interface. (a) $b/a = 2.25$. (b) $b/a = 3.00$.

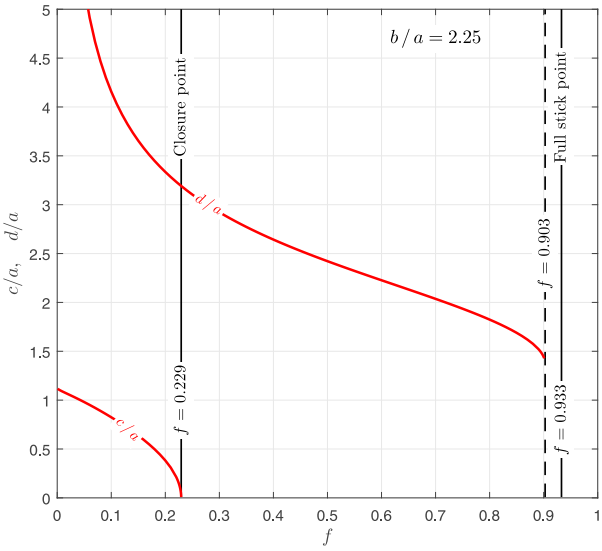

Figure 4: Normalised closure point c/a and stick point d/a as a function of the coefficient of friction for $b/a = 2.25$.

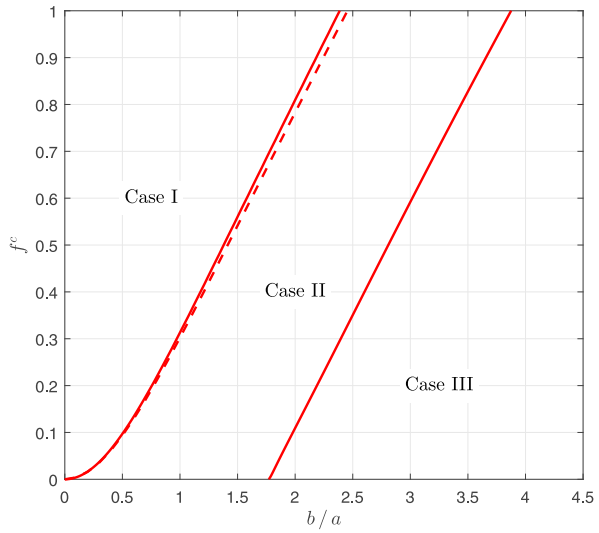

Figure 5: Transition between cases.

Figure 3 shows the contact pressure and shear stress normalised by the applied pressure p for $b/a = 2.25$ and 3.00. We notice that the stresses are proportional to the applied pressure, i.e. for a given b/a doubling the applied pressure p would result in the stresses being doubled, such that the normalised traction distributions remain constant. Since the distributions do not change, the points of stick and closure do not change as well. The contact size is, therefore, independent of p and varies only with the coefficient of friction and the normalised radius of the unloaded disk b/a. For any increment of load the contact 'snaps' from the undeformed unloaded condition to the deformed configuration, which means that, as expected, the contact area changes discontinuously from an infinite size when unloaded to a finite size upon applying any increment of load [1, 2, 16].

Consider, now, the values of normalised stick point d/a and closure point c/a as a function of the coefficient of friction for $b/a = 2.25$ (Figure 4). For $0 \leq f < 0.229$, the contact is in Case III. As f increases, the opening and slip regions decrease, but the contact remains in Case III (there is an open region). When f reaches 0.229, $c/a = 0$ and the contact closes. For $0.229 < f < 0.903$, the contact is in Case II and as f increases the radius of the slip zone decreases. For $0.903 < f < 0.933$, there are no solutions for d/a in Case II. This region characterizes an intermediate state between Cases II and I where the

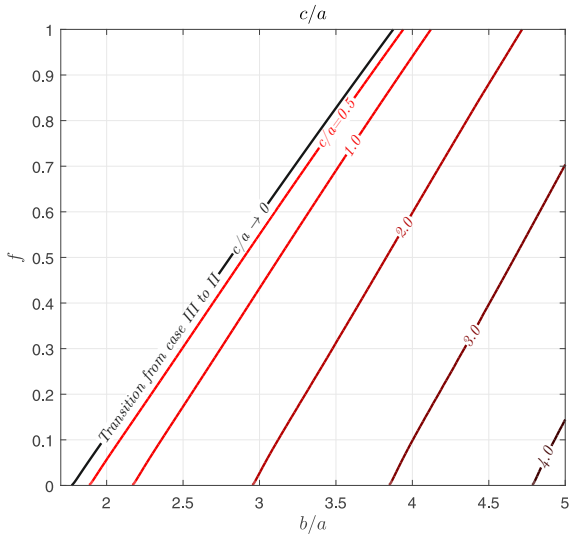

Figure 6: Normalised point of closure c/a.

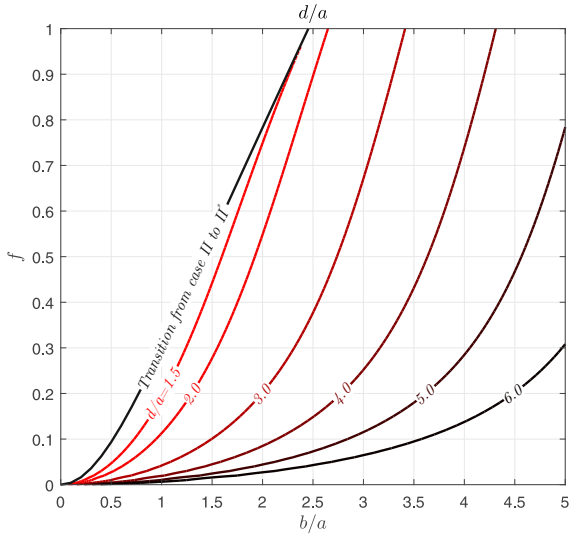

Figure 7: Normalised point of stick d/a.

contact has a finite region of slip inside the contact (Case II^*). Because this case represents only a small portion of the results, its solution was not found. The line $f = 0.933$ represents the minimum coefficient of friction that results in the contact being fully stuck. For $f > 0.933$, the contact is in Case I (fully closed and stuck).

This same procedure can be used to find the transition values between cases for pairs of b/a and f (Figure 5). From Cases II to III, the transition is characterized by contact opening at the origin. Therefore, we look for the value of b/a that results in $N(0) = 0$ for a given f (rightmost solid line in Figure 5). In Case I, the transition is given by the minimum coefficient of friction required to guarantee no slip for each b/a (leftmost solid line in Figure 5). Finally, the dashed line represents the limit in solution for Case II. The region inside the solid and dashed lines between Cases I and II represents the intermediate Case II^*.

Figures 6 and 7 show the contours of normalised point of closure c/a and point of stick d/a as functions of f and b/a. It may be noted that the normalised closure point is always smaller than the unloaded radius b/a, i.e. contact opening never extends into the loaded region. Also, c/a decreases as the coefficient of friction increases and/or b/a becomes smaller. The contact closes at the line of $c/a = 0$ (black line in Figure 6). The point of stick d/a also decreases when f increases and/or b/a becomes smaller.

If there is no friction, from Figure 5, the contact is in case II if $b/a < 1.771$ and in Case III otherwise. In Case II, the point of stick is finite and increases as b/a increases (Figure 7). In Case III, the point of closure is finite and increases as b/a increases (Figure 6) but $d/a \to \infty$, which means that the contact would be sliding and not in elastic equilibrium (Figures 4 and 7).

5. Conclusions

The contact properties and tractions were obtained for a receding contact between a layer subjected to axisymmetric 'external' semi-infinite pressure and an elastically similar half-space. It was shown that the problem is fully characterised by two variables, the coefficient of friction between interfaces f and the normalised length of the unloaded radius b/a. Depending on the relationship between f and b/a, the contact may be fully closed and stuck (Case I), closed and partially slipping from the axis of symmetry (Case II), closed and partially slipping inside the contact interface (Case II^*), or partially open and slipping (Case III). The curves that characterise the transition between cases were also found.

In addition, it was shown that, as expected, the interfacial tractions are proportional to the applied load while the contact area is independent of it and changes discontinuously from the unloaded to loaded configuration with the application of an incremental load

Finally, in Case III it was found that contact opening never penetrates into the loaded regions, as d/a is always smaller than the unloaded radius b/a.

Acknowledgements

J. L. gratefully acknowledges the financial support of Christ Church Oxford, Rolls Royce PLC and Coordenação de Aperfeiçoamento de Pessoal de Nível Superior - CAPES.

References

[1] J. Dundurs, Properties of elastic bodies in contact, The Mechanics of the Contact between Deformable bodies (1975) 54–66.
[2] J. Barber, Contact Mechanics, Solid Mechanics and Its Applications, Springer International Publishing, 2018.

[3] T. Chaise, R. Paynter, D. Hills, Contact analysis of a semi-infinite strip pressed onto a half plane by a line force, International Journal of Mechanical Sciences 81 (2014) 60–64.
[4] K. Parel, D. Hills, Frictional receding contact analysis of a layer on a half-plane subjected to semi-infinite surface pressure, International Journal of Mechanical Sciences 108 (2016) 137–143.
[5] L. Keer, J. Dundurs, K. Tsai, Problems involving a receding contact between a layer and a half space, Journal of Applied Mechanics 39 (4) (1972) 1115–1120.
[6] K. Tsai, J. Dundurs, L. Keer, Contact between an elastic layer with a slightly curved bottom and a substrate, Journal of Applied Mechanics, Transactions ASME 39 (3) (1972) 821–823.
[7] K. Tsai, J. Dundurs, L. Keer, Elastic layer pressed against a half space, Journal of Applied Mechanics 41 (3) (1974) 703–707.
[8] K.-i. Terazawa, On the elastic equilibrium of a semi-infinite solid under given boundary conditions, Journal of the College of Science (1916) 14–24.
[9] A. E. H. Love, The stress produced in a semi-infinite solid by pressure on part of the boundary, Philosophical Transactions of the Royal Society of London. Series A, Containing Papers of a Mathematical or Physical Character 228 (659-669) (1929) 377–420.
[10] M. T. Hanson, I. W. Puja, Love's circular patch problem revisited: Closed form solutions for transverse isotropy and shear loading, Quarterly of applied mathematics 54 (2) (1996) 359–384.
[11] D. Hills, P. Kelly, D. Dai, A. Korsunsky, Solution of crack problems: the distributed dislocation technique, Vol. 44 of Solid Mechanics and Its Applications, Springer Netherlands, Dordrecht, 2013.
[12] R. Paynter, D. Hills, The effect of path cut on Somigliana ring dislocations in a half-space, International Journal of Solids and Structures 46 (2) (2009) 412–432.
[13] R. Paynter, D. Hills, A. Korsunsky, The effect of path cut on Somigliana ring dislocation elastic fields, International Journal of Solids and Structures 44 (2) (2007) 6653–6677.
[14] J. Lopes, D. Hills, Ring cracks at the surface of a half-space, Engineering Fracture Mechanics 194 (2018) 105–116.
[15] F. Erdogan, G. D. Gupta, T. Cook, Numerical solution of singular integral equations, in: Methods of analysis and solutions of crack problems, 1973, pp. 368–425.
[16] J. Dundurs, M. Stippes, Role of elastic constants in certain contact problems, Journal of Applied Mechanics 37 (4) (1970) 965–970.
[17] G. Eason, B. Noble, I. N. Sneddon, On certain integrals of Lipschitz-Hankel type involving products of Bessel functions, Philosophical Transactions of the Royal Society of London A: Mathematical, Physical and Engineering Sciences 247 (935) (1955) 529–551.
[18] E. Gordeliy, E. Detournay, Displacement discontinuity method for modeling axisymmetric cracks in an elastic half-space, International Journal of Solids and Structures 48 (19) (2011) 2614–2629.

Appendix A. State of stress induced by circular edge dislocation loops

Appendix A.1. Axial dislocation

Consider a climb axial dislocation loop of radius a put at a depth d and being observed at a position (r, z) in a cylindrical coordinate system , with a Burgers vector component b_z. The stress fields at a position (r, z) are given by

$$\sigma^z_{iz}(r,z) = G^z_{iz}(r,z,d)\, b_z(a) \quad i = r, z. \tag{A.1}$$

The influence functions $G^z_{iz}(\rho,\zeta,\delta)$ $(i = r,\, z)$ for the glide dislocation in a half-space are given as [12]:

$$G^z_{zz}(\rho,\zeta,\delta) = \frac{2\,\mu}{a\,(\kappa+1)}\Bigg[- J_{1,0;1} + I_{1,0;1} - (\zeta-\delta)\, J_{1,0;2} - (\zeta+\delta)\, I_{1,0;2} + 2\,\zeta\,\delta\, I_{1,0;3}\Bigg] \tag{A.2}$$

$$G^z_{rz}(\rho,\zeta,\delta) = \frac{2\,\mu}{a\,(\kappa+1)}\Bigg[- (\zeta-\delta)\, J_{1,1;2} + (\zeta-\delta)\, I_{1,1;2} - 2\,\zeta\,\delta\, I_{1,1;3}\Bigg] \tag{A.3}$$

where ρ, ζ and δ are the normalised coordinates, given as

$$\rho = r/a, \qquad \zeta = z/a, \qquad \delta = d/a, \tag{A.4}$$

μ is the modulus of rigidity and κ is the Kolosov's constant.

Appendix A.2. Radial dislocation

The radial dislocation is not of Volterra kind and, thus, is path-cut dependent. In this paper, an 'inside disk' path cut is used [12]. This path cut can be formed by inserting a disk of material at a depth $z = d$, from $r = 0$ to $r = a$, displacing the material by the same amount b_r (thickness of the disk). The stress fields at a position (r, z) are given by

$$\sigma^r_{iz}(r,z) = G^r_{iz}(r,z,d)\, b_r(a) \quad i = r, z. \tag{A.5}$$

The influence functions $G^r_{iz}(\rho,\zeta,\delta)$ $(i = r,\, z)$ for the glide dislocation in a half-space are given as [12]:

$$G^r_{zz}(\rho,\zeta,\delta) = \frac{2\,\mu}{a\,(\kappa+1)}\Bigg[- (\zeta-\delta)\, J_{2,0;2} + (\zeta-\delta) I_{2,0;2} - 2\,\zeta\,\delta\, I_{2,0;3}\Bigg] \tag{A.6}$$

$$G^r_{rz}(\rho,\zeta,\delta) = \frac{2\,\mu}{a\,(\kappa+1)}\Bigg[- J_{2,1;1} + I_{2,1;1} + (\zeta-\delta)\, J_{2,1;2} + (\zeta+\delta)\, I_{2,1;2} + 2\,\zeta\,\delta\, I_{2,1;3}\Bigg] \tag{A.7}$$

Appendix A.3. Lipschitz-Hankel integrals

In the influence functions, the terms $J_{n,p;q}$ and $I_{n,p;q}$ represent Lipschitz-Hankel integrals. The standard definition for these functions is as an integral of the product of Bessel functions ($J_i(\cdot)$), an exponential term and a power term. Using normalised coordinate variables, it is given as [17]

$$P_{\mu,\nu;\lambda}(\rho,\zeta) = \int_0^\infty J_\mu(t)\, J_\nu(\rho\, t)\, e^{-\zeta\, t}\, t^\lambda \,\mathrm{d}t. \tag{A.8}$$

In the kernels, the follow definition is applied:

$$J_{n,p;q} = P_{n,p;q}(\rho, \zeta - \delta) \tag{A.9}$$
$$I_{n,p;q} = P_{n,p;q}(\rho, -\zeta - \delta) \tag{A.10}$$

The Lipschitz-Hankel integrals needed in the kernels are given by Paynter et al. [13, 12] (see also [18]).

8

The Axisymmetric Frictional Receding Contact of a Layer Pressed Against a Half-Space by a Point Force

The axisymmetric frictional receding contact of a layer pressed against a half-space by a point force

J.P. Lopes[a,*], D.A. Hills[a]

[a] *Department of Engineering Science, University of Oxford, Parks Road, Oxford OX1 3PJ, United Kingdom*

Abstract

This paper uses a distribution of ring dislocations to find the solution for the frictional axisymmetric receding contact of a semi-infinite layer pressed against a half-space by a point force. The frictional behaviour between the surfaces of the layer and the half-space is modelled via Coulomb friction. The problem is fully characterized by the coefficient of friction between the interfaces. For a realistic coefficient of friction and finite load, the contact will always be partially open and partially slipping, even if there is no friction. It is shown that the interfacial tractions are proportional to the applied load while the contact area is independent of it. The transition from the unloaded to loaded configuration is discontinuous.

Keywords: Axisymmetric, Receding Contact, Ring dislocations

1. Introduction

Receding contacts are those where the application of a normal load causes a reduction in the size of the contact. In some problems, for example that of an over-sized pin shrink fitted into a hole in a plate have the property that the contact contracts smoothly as the applied load is gradually increased [1], but in others the contact 'snaps' to the final size on application of the normal load. So, for example, if the pin just referred to was mathematically of precisely the same size as the hole in which it is journalled, this property would be observed.

In machines or structures with carefully fitted parts, receding contacts are more likely to appear than advancing contacts, because of the opening of gaps between the individual parts as they distort under application of loads. Despite its importance, the literature in receding contacts was often limited to cases where there is no friction between the bodies [2, 3, 4]. More recently, Ahn and Barber [5] studied a frictional receding contact between an elastic block and a rigid substrate under cyclic loading.

Further examples include the simple, plane problem of a layer resting on a frictional, elastically similar half-plane, and with a normal line load gradually applied [6]. This problem is the axisymmetric equivalent, where we have a layer resting on a frictional, elastically similar half-space, and a normal point load applied. The problem is so fundamental in character that it is worth studying to learn its general properties. If the thickness of the layer is a then, from St Venant's principle, if pressure is applied over a small disk of radius ρ ($\rho << a$) the results to be found may be expected to apply. Qualitatively, we would expect the axisymmetric problem to have much in common with the plane problem, but with one major distinction – in the plane problem the lifted-off layer, being free of stress becomes straight at points remote from the contact, and the separation from the half-plane becomes infinitely great at infinitely remote distances. In the axisymmetric case this is inhibited by the development of circumferential ($\sigma_{\theta\theta}$) stress so that the surface layer has a decreasing gradient which falls smoothly at remote points.

As well as its fundamental nature the solution to be presented may be expected to have relevance to bolted plates. In reality the bolt load is spread over a washer which distributes pressure over a finite disk, as mentioned above, and the bolt must pass through a hole, of course, in both layer and half-space but, nevertheless, this idealisation may be expected to show a lot of the key properties for the bolted problem.

This paper proposes the study of the frictional axisymmetric receding contact of a homogeneous infinite layer of thickness a, Poisson's ratio ν and modulus of rigidity μ, pressed against an elastically similar half-space $z \geq a$ by a point force applied to the layer's axis of symmetry (Figure 1). This represents a 'fundamental' axisymmetric receding contact problem, with only one characteristic length (the layer's thickness a). The only independent parameter in this problem is the coefficient of friction between the layer and the half-space.

The objective of this study is to find the solution to the proposed problem using ring dislocations to introduce corrections to the stresses in the contact interface as a distri-

*Corresponding author

Email addresses: jhonatan.dapontelopes@eng.ox.ac.uk (J.P. Lopes), david.hills@eng.ox.ac.uk (D.A. Hills)

bution of strain nuclei. First, we assume that the contact is in a fully closed and stuck configuration. Then, dislocation densities are applied to correct the stresses when this condition is violated.

2. Adhered Solution

We start our analysis by assuming that the applied force induces normal and shear tractions at the layer/half-space interface such that the contact remains closed and stuck throughout this region, i.e. the contact pressure is compressive everywhere and the shear traction is limited by Coulomb friction. Following this assumption, the state of stress in the bodies is equivalent to a half-space $z \geq 0$ under the same loading. In the cylindrical coordinate set shown in Figure 1, the tractions $\tilde{\sigma}_{iz}(r,z)$, $i = r, z$ arising on any radial cut ($z = constant$ surface) are given by [7]:

$$\tilde{\sigma}_{zz}(r,z) = -\frac{3\,P}{2\,\pi}\left\{\frac{z^3}{(r^2+z^2)^{5/2}}\right\} \tag{1}$$

$$\tilde{\sigma}_{rz}(r,z) = -\frac{3\,P}{2\,\pi}\left\{\frac{r\,z^2}{(r^2+z^2)^{5/2}}\right\}. \tag{2}$$

If the contact is, indeed, fully closed and adhered, the normal $N(r)$ and shear $S(r)$ tractions at the layer/half-space interface are given by:

$$N(r) = \tilde{\sigma}_{zz}(r,a) \tag{3}$$

$$S(r) = \tilde{\sigma}_{rz}(r,a). \tag{4}$$

From eqs. (1) and (2), the ratio between the normal and shear tractions at the contact interface is given by:

$$\frac{S(r)}{N(r)} = \frac{\tilde{\sigma}_{rz}(r,a)}{\tilde{\sigma}_{zz}(r,a)} = \frac{r}{a}. \tag{5}$$

Analysing eq. (5), we note that as $r \to \infty$ the shear to normal traction ratio also goes to ∞, which means that no realistic coefficient of friction would be high enough to prevent contact slip. Furthermore, as $r \to \infty$ the contact pressure goes to zero (eq. (1)), resulting in contact opening.

3. Formulation

Since our assumption that the contact is fully stuck and closed does not hold true, the bilateral solution obtained in Section 2 is no longer valid. We expect the contact to develop regions where it is closed and partially slipping and regions where it is open as shown in Figure 1.

A modified solution can be obtained by developing expressions for the tractions at the contact interface as the sum of the adhered (bilateral) solution together with a correction in the form of an integral representation of slip and opening as a distribution of glide and climb dislocations, respectively. The dislocations needed are all 'edge' in character, with their Burgers vector lying in a $\theta = constant$ plane. We emphasise that the introduction of dislocations is used solely as a mathematical device to introduce corrections in our formulation as a distribution of strain nuclei and do not imply the introduction of physical defects in the micro-structure of the material. A more detailed explanation can be found in [8].

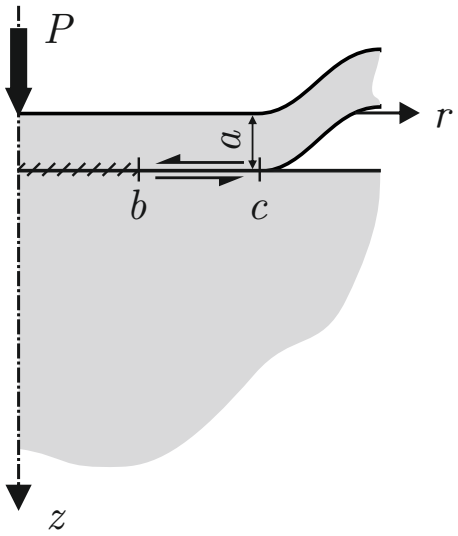

Figure 1: A layer resting in a half-space subjected to a point force.

First, we introduce a $b_r(\xi)$ glide dislocation loop of radius ξ, lying at a depth a. It may be formed by making a path cut along the annular disk $\xi \leq r \leq \infty$ and sliding the surfaces by a constant amount b_r. This models contact slip and will induce the following tractions $\hat{\sigma}_{iz}(r)$ $(i = r, z)$ along the same disk

$$\hat{\sigma}_{iz}(r) = G^r_{iz}(r,\xi)\, b_r(\xi). \tag{6}$$

The influence functions $G^r_{iz}(r,\xi)$ are functions of Lipschitz-Hankel integrals and have extremely complicated forms. For a half-space, these are given by Paynter et al. [9] (see also [10, 11]). They are bounded ('regular') when $i = z$ and display a Cauchy singularity when $i = r$.

Next, we introduce a $b_z(\xi)$ climb dislocation loop of radius ξ, lying at a depth a. Now, the dislocation loop may be formed by making a path cut along $\xi \leq r \leq \infty$ and inserting a disk of thickness b_z. This models contact opening and will induce the following tractions $\hat{\sigma}_{iz}(r)$ $(i = r, z)$ along the same disk

$$\hat{\sigma}_{iz}(r) = G^z_{iz}(r,\xi)\, b_z(\xi). \tag{7}$$

Once again, the influence functions $G^z_{iz}(r,\xi)$ are functions of Lipschitz-Hankel integrals and have extremely complicated forms. For a half-space, these are also given by

Paynter et al. [9]. This time, they are bounded ('regular') when $i = r$ and display a Cauchy singularity when $i = z$.

From the bilateral solution, we expect the contact to be closed and stuck from the origin to a radius $r = b$, closed and slipping in the region $b \leq r \leq c$, and open in a region extending from a radius c to infinity. Both the closure point c and stick point b are outputs of the problem (self-determining points).

The resulting normal $N(r)$ and shear $S(r)$ tractions along the contact interface are given by

$$N(r) = \tilde{\sigma}_{zz}(r) + \int_c^\infty G^z_{zz}(r,\xi)\, B_z(\xi)\mathrm{d}\xi + \int_b^\infty G^r_{zz}(r,\xi)\, B_r(\xi)\mathrm{d}\xi, \tag{8}$$

$$S(r) = \tilde{\sigma}_{rz}(r) + \int_c^\infty G^z_{rz}(r,\xi)\, B_z(\xi)\mathrm{d}\xi + \int_b^\infty G^r_{rz}(r,\xi)\, B_r(\xi)\mathrm{d}\xi, \tag{9}$$

where $B_i(\xi) = db_i/d\xi,\ i = r, z$ represents the dislocation density. Glide dislocations are installed over the whole of the length of the contact interface where slipping occurs, including the open portion, and climb dislocations are installed over the part of the contact interface which is open. Equations (8) and (9) form the basis of the solution and integral equations may be generated to restore conventional Signorini inequalities.

In the open region, we require the surfaces to be traction-free

$$N(r) = 0, \qquad S(r) = 0, \qquad c \leq r \leq \infty \tag{10}$$

whereas, in the closed, slipping region, the shearing traction is limited by friction:

$$N(r) < 0 \qquad S(r) = f\, N(r) \qquad b \leq r \leq c. \tag{11}$$

The three sets of conditions in eqs. (10) and (11) may be combined into two by making use of the Heaviside step function, $H(\cdot)$, giving

$$N(r) = 0 \qquad c \leq r \leq \infty \tag{12}$$

$$S(r) - f\, H(c-r)\, N(r) = 0 \qquad b \leq r \leq \infty. \tag{13}$$

Applying eqs. (8) and (9) to eqs. (12) and (13), gives

$$\int_b^\infty G^r_{zz}(r,\xi)\, B_r(\xi)\mathrm{d}\xi + \int_c^\infty G^z_{zz}(r,\xi)\, B_z(\xi)\mathrm{d}\xi = -\tilde{\sigma}_{zz}(r) \qquad c \leq r \leq \infty \tag{14}$$

$$\int_b^\infty \Big[G^r_{rz}(r,\xi) - f\, H(c-r)\, G^r_{zz}(r,\xi)\Big] B_r(\xi)\,\mathrm{d}\xi + \int_c^\infty \Big[G^z_{rz}(r,\xi) - f\, H(c-r)\, G^z_{zz}(r,\xi)\Big] B_z(\xi)\,\mathrm{d}\xi = -\Big[\tilde{\sigma}_{rz}(r) - f\, H(c-r)\, \tilde{\sigma}_{zz}(r)\Big] \quad b \leq r \leq \infty. \tag{15}$$

Due to the nature of the functions present in eqs. (14) and (15), there is no hope of analytically inverting the integral equations. The Singular Integral Equations (SIEs) must be solved numerically, and we choose to use Gauss-Chebyshev quadrature [12]. Since there are two regions of imposition for the integral equations, two sets of quadrature points are needed. Notice that in eq. (14), the kernel $G^z_{zz}(r,\xi)$ is Cauchy singular over the region $c \leq r, \xi \leq \infty$ while $G^r_{zz}(r,\xi)$ is regular. In eq. (15), the kernel $G^r_{rz}(r,\xi)$ is Cauchy singular over the region $b \leq r, \xi \leq \infty$ while all the other terms are regular.

The first step in solving the SIEs is to put the integrals in standard form over the interval $[-1\,, 1]$. The following transformation functions were proposed to map a normalised coordinate t to a physical coordinate r:

$$r = \frac{\lambda\,(t+1) + 2\,\hat{r}}{1-t} \tag{16}$$

$$r = \hat{r} + \lambda\, \log\left(\frac{2}{1-t}\right) \tag{17}$$

$$r = \hat{r}\, \left[1 + \lambda\, \tanh^{-1}\left(\frac{2}{1-t}\right)\right], \tag{18}$$

where $\hat{r}$ corresponds to the lower bound of the physical interval $[\hat{r}\,, \infty]$ ($\hat{r} = b \mathrm{or} c$) and λ is a scaling parameter.

From the proposed mappings, the logarithm transformation resulted in the best description of the solution as well as the best convergence. Hence, normalising the integrals using the following substitutions:

$$u = 1 - 2\, \exp\left(\frac{c-\xi}{\lambda}\right), \qquad c \leq \xi \leq \infty \tag{19}$$

$$v = 1 - 2\, \exp\left(\frac{c-r}{\lambda}\right), \qquad c \leq r \leq \infty \tag{20}$$

$$s = 1 - 2\, \exp\left(\frac{b-\xi}{\lambda}\right), \qquad b \leq \xi \leq \infty \tag{21}$$

$$t = 1 - 2\, \exp\left(\frac{b-r}{\lambda}\right), \qquad b \leq r \leq \infty. \tag{22}$$

gives

$$\int_{-1}^{1} G^r_{zz}(v,s)\, B_r(s) \left(\frac{\mathrm{d}\xi}{\mathrm{d}s}\right) \mathrm{d}s + \int_{-1}^{1} G^z_{zz}(v,u)\, B_z(u) \left(\frac{\mathrm{d}\xi}{\mathrm{d}u}\right) \mathrm{d}u = -\tilde{\sigma}_{zz}(v) \qquad -1 \le v \le 1 \tag{23}$$

$$\int_{-1}^{1} B_r(s) \left[G^r_{rz}(t,s) + f\, H(\gamma)\, G^r_{zz}(t,s)\right] \left(\frac{\mathrm{d}\xi}{\mathrm{d}s}\right) \mathrm{d}s + \int_{-1}^{1} B_z(u) \left[G^z_{rz}(t,u) + f\, H(\gamma)\, G^z_{zz}(t,u)\right] \left(\frac{\mathrm{d}\xi}{\mathrm{d}u}\right) \mathrm{d}u = -\left[\tilde{\sigma}_{rz}(t) + f\, H(\gamma)\, \tilde{\sigma}_{zz}(t)\right] \quad -1 \le t \le 1 \tag{24}$$

where

$$\gamma = 1 - \frac{b}{c} + \frac{\lambda}{c} \log\left(\frac{1-t}{2}\right) \tag{25}$$

$$\frac{\mathrm{d}\xi}{\mathrm{d}s} = \frac{\lambda}{1-s} \tag{26}$$

$$\frac{\mathrm{d}\xi}{\mathrm{d}u} = \frac{\lambda}{1-u}. \tag{27}$$

For the general form of the solution, both the climb and glide dislocations must be bounded at both ends of the interval. Thus, we choose

$$B_r(s) = \phi_r(s)\sqrt{1-s^2} \tag{28}$$

$$B_z(u) = \phi_z(u)\sqrt{1-u^2} \tag{29}$$

and eqs. (23) and (24) become, in normalised form,

$$\sum_{i=1}^{N} \left\{\frac{\lambda W_i}{1-s_i}\, \phi_r(s_i)\, G^r_{zz}(v_k,s_i)\right\} + \sum_{i=1}^{N} \left\{\frac{\lambda X_i}{1-u_i}\, \phi_z(u_i)\, G^z_{zz}(v_k,u_i)\right\} = -\frac{2}{\pi}\tilde{\sigma}_{zz}(v_k) \qquad k = 1,\ldots,N+1 \tag{30}$$

$$\sum_{i=1}^{N} \left\{\left[G^r_{rz}(t_k,s_i) - f\, H(\gamma_k)\, G^r_{zz}(t_k,s_i)\right] \frac{\lambda W_i}{1-s_i} \phi_r(s_i)\right\} + \sum_{i=1}^{N} \left\{\left[G^z_{rz}(t_k,u_i) - f\, H(\gamma_k)\, G^z_{zz}(t_k,u_i)\right] \frac{\lambda X_i}{1-u_i} \phi_z(u_i)\right\} = -\frac{2}{\pi}\left[\tilde{\sigma}_{rz}(t_k) - f\, H(\gamma_k)\, \tilde{\sigma}_{zz}(t_k)\right] \quad k = 1,\ldots,N+1 \tag{31}$$

where

$$\gamma_k = 1 - \frac{b}{c} + \frac{\lambda}{c} \log\left(\frac{1-t_k}{2}\right) \tag{32}$$

and the integration points s_i, u_i, collocation points t_k, v_k and weights W_i, X_i for the quadrature are given as [12]

$$s_i = u_i = \cos\left(\pi \frac{i}{N+1}\right) \qquad i = 1,\ldots,N \tag{33}$$

$$t_k = v_k = \cos\left(\frac{\pi}{2}\frac{2k-1}{(N+1)}\right) \qquad k = 1,\ldots,N+1 \tag{34}$$

$$W_i = X_i = \frac{1-s_i^2}{2\,(N+1)}. \tag{35}$$

Equations (30) and (31) form a system of $2N+2$ equations and $2N+2$ unknowns. These are the N values of $\phi_r(s_i)$, N values of $\phi_z(u_i)$, the closure point c and the stick point b. Once ϕ_r and ϕ_z are known, the stresses at a point (r,z) can be found by the discrete versions of eqs. (8) and (9)

$$N(v) = \tilde{\sigma}_{zz}(v) + \sum_{i=1}^{N} \left\{\frac{\lambda W_i}{1-s_i}\, \phi_r(s_i)\, G^r_{zz}(v,s_i)\right\} + \sum_{i=1}^{N} \left\{\frac{\lambda X_i}{1-u_i}\, \phi_z(u_i)\, G^z_{zz}(v,u_i)\right\} \tag{36}$$

$$S(t) = \tilde{\sigma}_{rz}(t) + \sum_{i=1}^{N} \left\{\frac{\lambda W_i}{1-s_i}\, \phi_r(s_i)\, G^r_{rz}(t,s_i)\right\} + \sum_{i=1}^{N} \left\{\frac{\lambda X_i}{1-u_i}\, \phi_z(u_i)\, G^z_{zz}(t,u_i)\right\}. \tag{37}$$

Finally, the axial dislocation density B_z is related to the axial displacement of the contact $u_z(r)$ through the following relationship [8]:

$$B_z(r) = -\frac{\mathrm{d}u_z(r)}{\mathrm{d}r}. \tag{38}$$

Thus, $u_z(r)$ can be found by integration:

$$u_z(r) = -\int_c^r B_z(\xi)\mathrm{d}\xi. \tag{39}$$

4. Results

The problem was coded up using the numerical processor MATLAB. Due to the semi-infinite nature of the integrals and, consequently, of the mapping functions, the problem is highly non-linear and obtaining a convergent solution is not trivial. First, due to the unknown length dimensions there are two additional collocation equations which need to be satisfied and which enable the values of b/a and c/a to be found. In practice, we guess values of the lengths b/a and c/a to be found and omit the central equations corresponding to $k = N/2+1$ from the

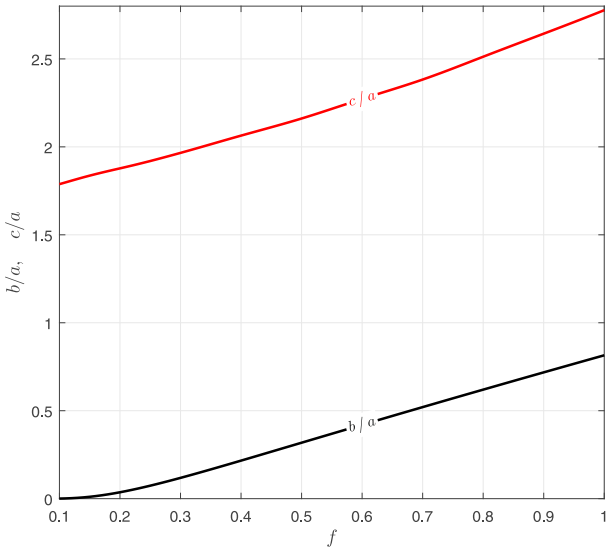

Figure 2: Normalised closure point c/a and stick point b/a as a function of the coefficient of friction.

$N+1$ generated for each dislocation in eqs. (30) and (31). The column vectors of ϕ_r and ϕ_z are found. The omitted equations are then evaluated and residues are taken as the difference between the left and the right-hand sides of eqs. (30) and (31) for $k = N/2+1$. A programme is then used to find the values of b/a and c/a that result in the residuals being as close to zero as numerically possible.

Convergence is dependent on obtaining adequate values of quadrature points N and the scaling parameter λ. For the present solution, convergence was obtained for $N = 150$ and $\lambda = 8\,a$, i.e. changes in the stresses, b/a and c/a were negligible when N was increased beyond 150 and λ varied slightly around $8\,a$. All results present in this paper are for $\nu = 0.3$.

Figure 2 shows the stick and opening points normalised with respect to the layer's thickness as a function of the coefficient of friction. As f increases, both b/a and c/a increase as well, resulting in the contact area becoming larger. This is followed by an increase in the stick zone, characterized by its radius (b/a) becoming larger. However, the size of the slip zone is practically insensitive to the variation of the coefficient of friction, corresponding to an annulus of width $\approx 1.8\,a$ for $0.2 \leq f \leq 1.0$. This behaviour was also observed in the equivalent plane receding contact problem of a layer subjected to a line loading [6]. On the other hand, when f is small ($f \leq 0.2$), $b \to 0$ as f decreases resulting in the stick region collapsing to a point, and the decrease in c/a results in a smaller slip zone.

Consider, now, the the contact pressure and shear stress normalised by the reference stress $\sigma_0 = P\,/\,a^2$ for different coefficients of friction (Figure 3). Note that the stresses are proportional to the applied pressure. The contact size, however, is independent of it and varies only with the coefficient of friction. Therefore, for any increment of load the

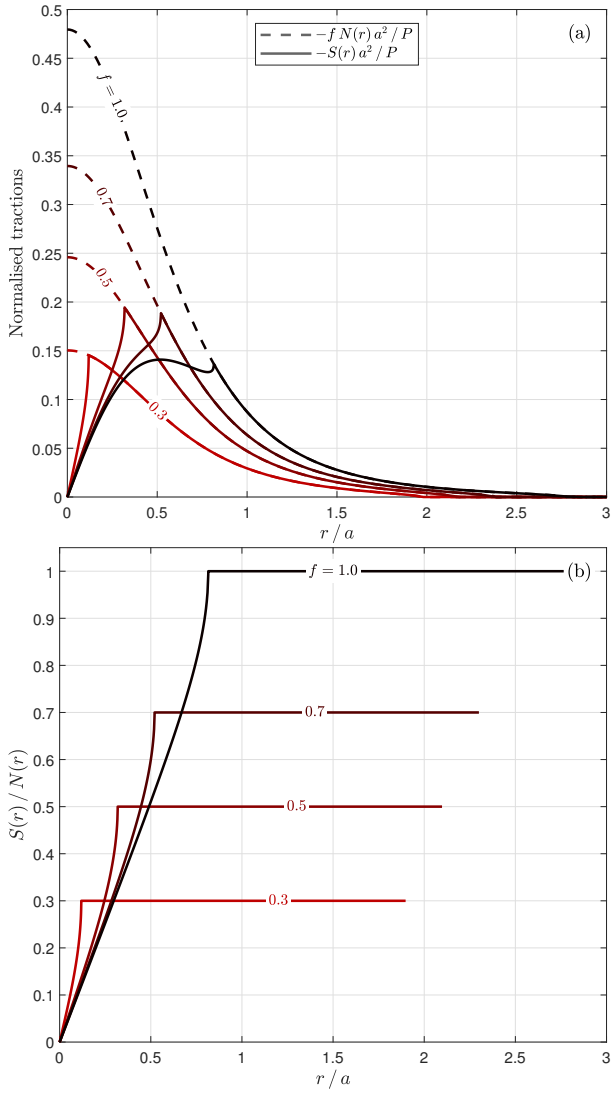

Figure 3: Tractions in the contact interface. (a) Normalised contact pressure and shear stress. (b) Ratio between shear and normal stresses.

contact 'snaps' from the undeformed unloaded condition to the deformed configuration, which means that, as expected, the contact area changes discontinuously from an infinite size when unloaded to a finite size upon applying any increment of load [13, 14]. For $f = 1.0$, even though the shear stress seems to have a peak inside the stick zone, we can see from Figure 3(b) that the ratio between $S(r)$ and $N(r)$ is still less than f, i.e. the slip condition is not violated.

Another property of this problem is that since the bilateral stresses in eqs. (1) and (2) are independent of the Poisson's ratio, so does the stresses in our solution. Therefore, the tractions at the contact surface are independent of ν and, consequently, so are the points of stick and opening.

Figure 4 shows the normalised tractions and dislocations densities for a sample coefficient of friction ($f = 0.7$). Note that the radial dislocation $B_r(r)$ goes to zero at both

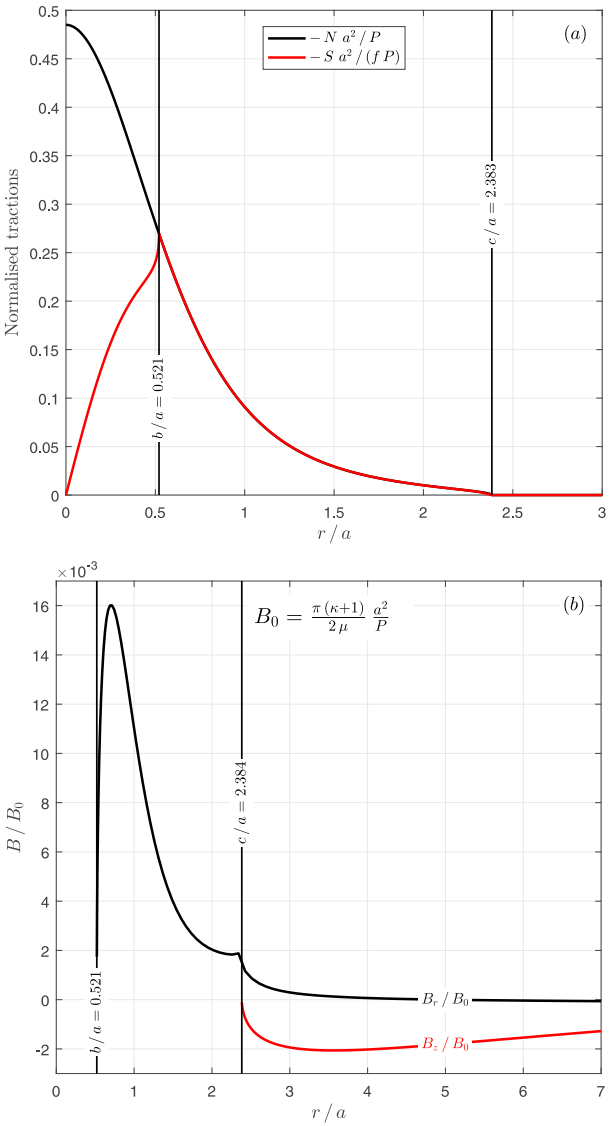

Figure 4: Results for $f = 0.7$ at the contact interface. (a) Normalised tractions. (b) Normalised dislocation densities.

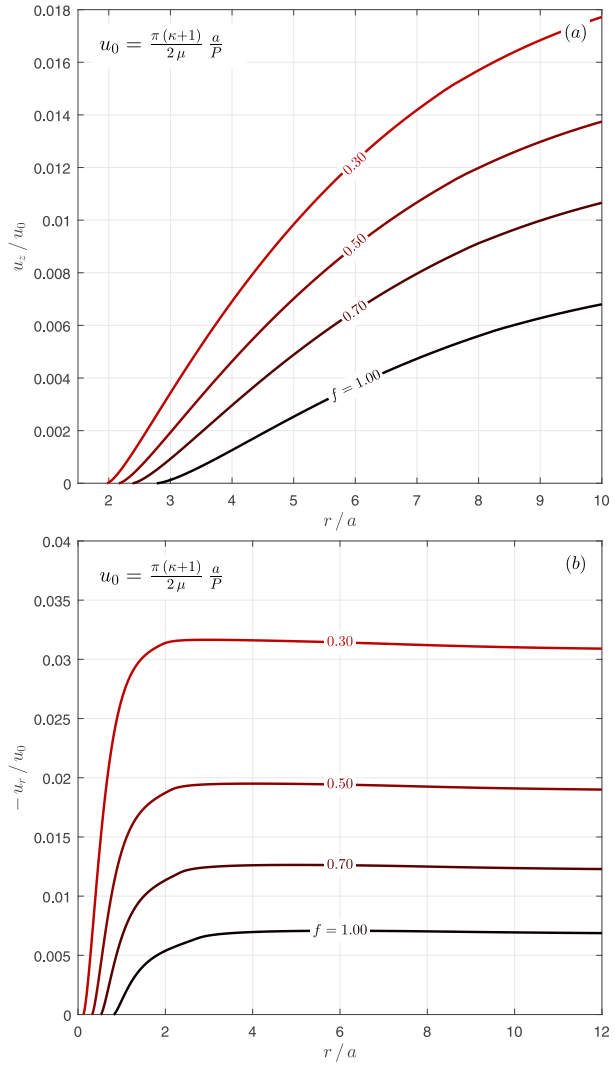

Figure 5: Normalised displacements at the contact interface. (a) Axial displacement. (b) Radial displacement.

ends of the interval and is, therefore, bounded-bounded, as imposed in the solution. Also, since $B_r(r)$ models contact slip, it has a maximum inside the region $b \leq r \leq c$, where slip occurs. The axial dislocation B_z also tends to zero as r becomes larger, but decays slower than the radial dislocation. Also, while the shear stress distribution varies significantly with respect to the coefficient of friction, the pressure distribution only changes slightly as f varies.

Figure 5 shows the normalised displacements at the contact interface for different values of f ($\nu = 0.3$). In the equivalent plane receding contact problem, as the load is applied the normal contact displacement 'snaps' to a straight line, corresponding to a constant angle [6]. In this problem, however, the presence of a non-zero hoop strain ϵ_θ makes the normal contact displacement present a logarithmic curvature. As the coefficient of friction increases, it is noted that the contact opening becomes smaller.

Finally, due to the symmetry of the problem, the contact is in partial slip even for $f = 0$. Note from eq. (5) that when $r = 0$, $S(r)/N(r) = 0$, which means that the point $(r, z) = (0, a)$ needs no friction to be stuck.

5. Conclusions

The contact properties and tractions were obtained for a receding contact between a layer subjected to a point force and an elastically similar half-space. It was shown that the problem is fully characterised by the coefficient of friction between interfaces. For a realistic coefficient of friction, the contact will always be partially open and partially slipping, even if there is no friction.

In addition, it was shown that, as expected, the interfacial tractions are proportional to the applied load while the contact area is independent of it and changes discontinuously from the unloaded to loaded configuration with

the application of an incremental load. Also, the stresses at the contact interface are independent of Poisson's ratio.

With regards to the contact area, for $0.2 \leq f \leq 1.0$, it was shown that an increase in the coefficient of friction results in an increase in the stick zone but no significant variance in the size of the slip annulus. Finally, due to the presence of a non-zero hoop strain, the contact opening presents a logarithmic curvature.

Acknowledgements

D. H. thanks Rolls-Royce PLC and the EPSRC for the support under the ProsperityPartnership Grant/ Cornerstone: Mechanical Engineering Science to Enable Aero-Propulsion Futures [Grant Ref: EP/R004951/1]. J. L. gratefully acknowledges the financial support of Christ Church Oxford, Rolls Royce PLC and Coordenação de Aperfeiçoamento de Pessoal de Nível Superior - CAPES.

[1] M. Ciavarella, P. Decuzzi, The state of stress induced by the plane frictionless cylindrical contact. i. the case of elastic similarity, International Journal of Solids and Structures 38 (26-27) (2001) 4507–4523.

[2] L. Keer, J. Dundurs, K. Tsai, Problems involving a receding contact between a layer and a half space, Journal of Applied Mechanics 39 (4) (1972) 1115–1120.

[3] K. Tsai, J. Dundurs, L. Keer, Elastic layer pressed against a half space, Journal of Applied Mechanics 41 (3) (1974) 703–707.

[4] S. El-Borgi, R. Abdelmoula, L. Keer, A receding contact plane problem between a functionally graded layer and a homogeneous substrate, International Journal of Solids and Structures 43 (3-4) (2006) 658–674.

[5] Y. J. Ahn, J. Barber, Response of frictional receding contact problems to cyclic loading, International Journal of Mechanical Sciences 50 (10-11) (2008) 1519–1525.

[6] T. Chaise, R. Paynter, D. Hills, Contact analysis of a semi-infinite strip pressed onto a half plane by a line force, International Journal of Mechanical Sciences 81 (2014) 60–64.

[7] S. Timoshenko, J. N. Goodier, Theory of Elasticity, Vol. 49, 1986.

[8] D. Hills, P. Kelly, D. Dai, A. Korsunsky, Solution of crack problems: the distributed dislocation technique, Vol. 44 of Solid Mechanics and Its Applications, Springer Netherlands, Dordrecht, 2013.

[9] R. Paynter, D. Hills, The effect of path cut on Somigliana ring dislocations in a half-space, International Journal of Solids and Structures 46 (2) (2009) 412–432. doi:10.1016/j.ijsolstr.2008.09.001.

[10] R. Paynter, D. Hills, A. Korsunsky, The effect of path cut on Somigliana ring dislocation elastic fields, International Journal of Solids and Structures 44 (2) (2007) 6653–6677.

[11] J. Lopes, D. Hills, Ring cracks at the surface of a half-space, Engineering Fracture Mechanics 194 (2018) 105–116.

[12] F. Erdogan, G. D. Gupta, T. Cook, Numerical solution of singular integral equations, in: Methods of analysis and solutions of crack problems, 1973, pp. 368–425.

[13] J. Dundurs, Properties of elastic bodies in contact, The Mechanics of the Contact between Deformable bodies (1975) 54–66.

[14] J. Dundurs, M. Stippes, Role of elastic constants in certain contact problems, Journal of Applied Mechanics 37 (4) (1970) 965–970.

[15] G. Eason, B. Noble, I. N. Sneddon, On certain integrals of Lipschitz-Hankel type involving products of Bessel functions, Philosophical Transactions of the Royal Society of London A: Mathematical, Physical and Engineering Sciences 247 (935) (1955) 529–551.

Appendix A. State of stress induced by circular edge dislocation loops

Appendix A.1. Axial dislocation

Consider a climb axial dislocation loop of radius a put at a depth d and being observed at a position (r, z) in a cylindrical coordinate system, with a Burgers vector component b_z. The stress fields at a position (r, z) are given by

$$\sigma^z_{iz}(r,z) = G^z_{iz}(r,z,d)\, b_z(a) \quad i = r, z. \tag{A.1}$$

The influence functions $G^z_{iz}(\rho,\zeta,\delta)$ $(i = r,\ z)$ for the glide dislocation in a half-space are given as [9]:

$$G^z_{zz}(\rho,\zeta,\delta) = \frac{2\,\mu}{a\,(\kappa+1)}\Big[- J_{1,0;1} + I_{1,0;1} - (\zeta-\delta)\, J_{1,0;2} - (\zeta+\delta)\, I_{1,0;2} + 2\,\zeta\,\delta\, I_{1,0;3}\Big] \tag{A.2}$$

$$G^z_{rz}(\rho,\zeta,\delta) = \frac{2\,\mu}{a\,(\kappa+1)}\Big[- (\zeta-\delta)\, J_{1,1;2} + (\zeta-\delta)\, I_{1,1;2} - 2\,\zeta\,\delta\, I_{1,1;3}\Big] \tag{A.3}$$

where ρ, ζ and δ are the normalised coordinates, given as

$$\rho = r/a, \qquad \zeta = z/a, \qquad \delta = d/a, \tag{A.4}$$

μ is the modulus of rigidity and κ is the Kolosov's constant.

Appendix A.2. Radial dislocation

The radial dislocation is not of Volterra kind and, thus, is path-cut dependent. In this paper, an 'outside disk' path cut is used [9]. This path cut can be formed by inserting a disk of material at a depth $z = d$, from $r = a$ to $r = \infty$, displacing the material by the same amount b_r (thickness of the disk). The stress fields at a position (r, z) are given by

$$\sigma^r_{iz}(r,z) = G^r_{iz}(r,z,d)\, b_r(a) \quad i = r, z. \tag{A.5}$$

The influence functions $G^r_{iz}(\rho,\zeta,\delta)$ $(i = r,\ z)$ for the glide dislocation in a half-space are given as [9]:

$$G^r_{zz}(\rho,\zeta,\delta) = \frac{2\,\mu}{a\,(\kappa+1)}\Big[- (\zeta-\delta)\, J_{0,0;2} + (\zeta-\delta) I_{0,0;2} + 2\,\zeta\,\delta\, I_{0,0;3}\Big] \tag{A.6}$$

$$G^r_{rz}(\rho,\zeta,\delta) = \frac{2\,\mu}{a\,(\kappa+1)}\Big[J_{0,1;1} - I_{0,1;1} - (\zeta-\delta)\,J_{0,1;2} + (\zeta+\delta)\,I_{0,1;2} - 2\,\zeta\,\delta\,I_{0,1;3}\Big] \tag{A.7}$$

Appendix A.3. Lipschitz-Hankel integrals

In the influence functions, the terms $J_{n,p;q}$ and $I_{n,p;q}$ represent Lipschitz-Hankel integrals. The standard definition for these functions is as an integral of the product of Bessel functions ($J_i(\cdot)$), an exponential term and a power term. Using normalised coordinate variables, it is given as [15]

$$P_{\mu,\nu;\lambda}(\rho,\zeta) = \int_0^\infty J_\mu(t)\,J_\nu(\rho\,t)\,e^{-\zeta\,t}\,t^\lambda\,\mathrm{d}t. \tag{A.8}$$

In the kernels, the follow definition is applied:

$$J_{n,p;q} = P_{n,p;q}(\rho,\zeta-\delta) \tag{A.9}$$

$$I_{n,p;q} = P_{n,p;q}(\rho,-\zeta-\delta) \tag{A.10}$$

The Lipschitz-Hankel integrals needed in the kernels are given by Paynter et al. [10, 9].

9

An Idealised Description of the Frictional Receding Contact Behaviour of a Bolted Joint

An idealised description of the frictional receding contact behaviour of a bolted joint

J.P. Lopes[a,*], D.A. Hills[a]

[a] *Department of Engineering Science, University of Oxford, Parks Road, Oxford OX1 3PJ, United Kingdom*

Abstract

This paper proposes a description for the contact behaviour of bolted joints through the solution of the frictional axisymmetric receding contact of a semi-infinite layer pressed against an elastically similar half-space by uniform pressure over a disk of radius b. First, the contact is assumed to be adhered and closed, and a bilateral solution is obtained. The adhered solution is then corrected using an integral formulation based on a kernel of circular dislocation loop to describe the interfacial tractions at the regions where partial slip and opening occur. A numerical solution is obtained for the corrected tractions and radius of slip and opening.

Keywords: Axisymmetric, Receding Contact, Ring dislocations, Bolted joints

1. Introduction

One of the ways to classify contacts is to observe whether or not new points come in contact as the bodies deform. In receding contacts, the application of a normal load causes a reduction in the size of the contact. A property of some receding contacts is that the contact area in the deformed configuration is independent of the applied load and, consequently, the change between undeformed/deformed configurations is discontinuous, i.e. the contact 'snaps' to the deformed configuration upon applying a normal load [1]. This presents a challenge in obtaining solutions through the Finite Element Method, as a large portion of the nodes change status from being in contact to being free when an infinitesimal normal load is applied.

Amongst the examples of axisymmetric receding contacts is the contact in bolted joints. Even though this type of fixing is ubiquitous in industry, the description of axisymmetric receding contacts in the literature is still restricted to either plane problems [2, 3] or frictionless cases [4, 5, 6]. More recently, a solution for an axisymmetric receding contact of a layer pressed against a half-space by a point load has been presented [7]. Even though the fundamental nature of this solution is crucial to better understanding receding contacts, in reality the bolt load is spread over a washer which distributes pressure over a finite disk.

In order to model better the normal characteristics of a bolted joint, the effect of the bolt/washer loading over the layer will be modelled by a disk of pressure. This paper proposes, then, the study of the frictional axisymmetric receding contact of a homogeneous semi-infinite layer of thickness a, Poisson's ratio ν and modulus of rigidity μ, pressed against an elastically similar half-space $z \geq a$ (Figure 1a) by a disk of pressure applied to the layer's surface ($z = 0$), such that

$$\sigma_{zz}(r,0) = -p, \qquad 0 \leq r \leq b \tag{1}$$

$$\sigma_{zz}(r,0) = 0, \qquad r > b. \tag{2}$$

Furthermore, the objective of this study is to find the solution to the proposed problem using ring dislocations to introduce corrections to the stresses in the contact interface as a distribution of strain nuclei. First, we assume that the contact is in a fully closed and stuck configuration. We then apply dislocation densities to correct the stresses when this condition is violated. This methodology has been presented in previous papers by the authors [8, 7].

2. Adhered Solution

We start our analysis by assuming that the applied pressure induces normal and shear tractions at the layer/half-space interface such that the contact remains closed and stuck throughout this region, i.e. the contact pressure is compressive everywhere and the shear traction is limited by Coulomb friction. Following this assumption, the state of stress in the bodies is equivalent to an augmented half-space $z \geq 0$ under the same loading (Figure 1a). In the cylindrical coordinate set shown in the figure, the state of stress is given by Love [9, 10, 11] and the tractions $\tilde{\sigma}_{ij}(r,z)$ arising on any radial plane ($z = \textit{constant}$ surface) are given by:

*Corresponding author

Email addresses: jhonatan.dapontelopes@eng.ox.ac.uk (J.P. Lopes), david.hills@eng.ox.ac.uk (D.A. Hills)

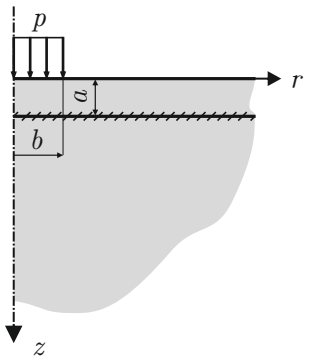

(a)

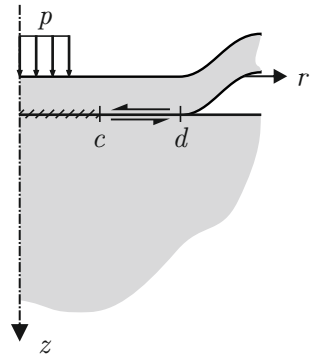

(b)

Figure 1: A layer subjected to semi-infinite pressure. (a) Fully closed and stuck. (b) Partially open and slipping.

$$\tilde{\sigma}_{zz}(r,z) = p\left\{\frac{2z}{\pi}\left[\frac{r^2+z^2-b^2}{(l_2)^3(1-k^2)^2}\boldsymbol{E}(k) + \frac{b^2-(l_1)^2}{(l_2)^3(1-k^2)}\boldsymbol{K}(k) - \frac{1}{l_2}\boldsymbol{\Pi}(n;k)\right]\right\} \quad (3)$$

$$\tilde{\sigma}_{rz}(r,z) = -\,p\left\{\frac{2z^2}{\pi}\left[\frac{\left(1+k^2\right)\boldsymbol{E}(k) - \left(1-k^2\right)\boldsymbol{K}(k)}{\left(k^2-1\right)^2 l_2\, r}\right]\right\} \quad (4)$$

where

$$l_1 = \frac{1}{2}\left\{\sqrt{(r+b)^2+z^2} - \sqrt{(r-b)^2+z^2}\right\} \quad (5)$$

$$l_2 = \frac{1}{2}\left\{\sqrt{(r+b)^2+z^2} + \sqrt{(r-b)^2+z^2}\right\} \quad (6)$$

$$k = \frac{l_1}{l_2} \quad (7)$$

$$n = \left(\frac{l_1}{r}\right)^2 \quad (8)$$

and $\boldsymbol{K}(k)$, $\boldsymbol{E}(k)$, $\boldsymbol{\Pi}(n;k)$ are the complete elliptic integrals of the first, second and third kind respectively. These functions are continuous and bounded at every point inside the half-space, but $\boldsymbol{\Pi}(n;k)$ cannot be evaluated numerically along the z-axis, since $r = 0$ there. In this region, we take the limits as $r \to 0$, giving:

$$\tilde{\sigma}_{zz}(0,z) = -\,p\left\{\frac{z^3}{(b^2+z^2)^{3/2}}\right\} \quad (9)$$

$$\tilde{\sigma}_{rz}(0,z) = 0. \quad (10)$$

When $b \to 0$ and $p \to \infty$, we would expect the bilateral loading due to the circular patch of pressure (eqs. (3) and (4)) to converge to the stress distribution due to a concentrated point force applied at the origin [7]. However, taking the limits results in:

$$\lim_{b\to 0} \tilde{\sigma}_{zz}(r,z) = 0 \quad (11)$$

$$\lim_{b\to 0} \tilde{\sigma}_{rz}(r,z) = 0. \quad (12)$$

Therefore, even if the pressure is infinite, the limiting stress distribution would be a constant over the half-space. Hence, the circular patch of pressure and the point force are inherently different loadings and result in distinct stress distributions even in the limiting case where $b \to 0$.

If the contact is, indeed, fully closed and adhered, the normal $N(r)$ and shear $S(r)$ tractions at the layer/half-space interface are given by:

$$N(r) = \tilde{\sigma}_{zz}(r,a) \quad (13)$$

$$S(r) = \tilde{\sigma}_{rz}(r,a). \quad (14)$$

Figure 2 shows the normalised contact pressure and shear to normal stress ratio for the adhered solution. Analysing the stress ratio (Figure 2b), we notice that no realistic value of coefficient of friction would be high enough to prevent slip as $r/a \to \infty$. Furthermore, for all values of b/a the contact pressure (Figure 2a) eventually falls to zero at the contact interface, which results in the development of an open region.

3. Formulation

The bilateral solution developed in Section 2 is, therefore, not valid, as the assumption that the contact is fully stuck and closed is violated for realistic values of f and b/a. The contact should develop regions where it is closed and partially slipping and regions where it is open, as shown in Figure 1b.

It is necessary to correct the bilateral solution in order to satisfy opening and slipping conditions. A modified solution can be developed by representing the tractions at the contact interface as a sum of the bilateral (adhered) solution with a correction in the form of an integral representation of slip and opening as a distribution of glide and

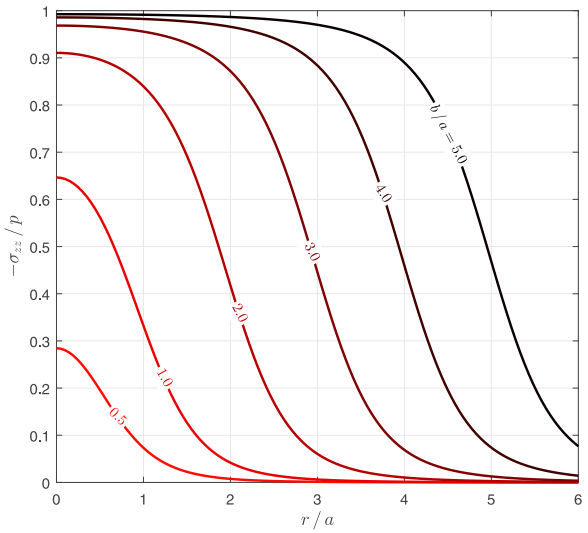

(a)

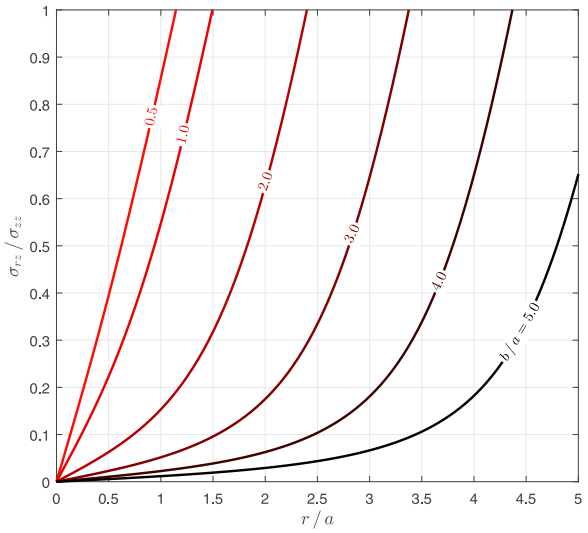

(b)

Figure 2: Normalised tractions for the adhered (bilateral) solution. (a) Normalised contact pressure. (b) Shear to normal stress ratio.

climb dislocations, respectively. The dislocations needed are all of 'edge' type, with their Burger's vectors resting in a $\theta = constant$ plane. We stress that the insertion of dislocations is used only as a mathematical device to correct the tractions in our formulation as a distribution of strain nuclei. This does not mean that physical defects are being inserted in the micro-structure of the material. Detailed explanations of the method can be found in [12, 7, 8].

In order to model contact slip, we introduce a radial $b_r(\xi)$ glide dislocation loop of radius ξ, placed at a depth a. It may be created by cutting a path along the annular disk $\xi \leq r \leq \infty$ and sliding the surfaces by a constant amount b_r. This will introduce the following tractions along the path cut disk

$$\hat{\sigma}_{iz}(r) = G^r_{iz}(r,\xi)\, b_r(\xi). \tag{15}$$

The influence functions $G^r_{iz}(r,\xi)$ are described as sums of Lipschitz-Hankel integrals and have extremely complicated forms. For a half-space, these are given by Paynter et al. [13] (see also [14, 15]) and in the Appendix A. They are bounded ('regular') when $i = z$ and display a Cauchy singularity when $i = r$.

The modelling of contact opening is done by introducing an axial $b_z(\xi)$ climb dislocation loop of radius ξ, lying at a depth a. Now, the dislocation loop may be formed by making a path cut along $\xi \leq r \leq \infty$ and inserting a disk of thickness b_z. This will induce the following tractions $\hat{\sigma}_{iz}(r)$ $(i = r, z)$ along the path cut disk

$$\hat{\sigma}_{iz}(r) = G^z_{iz}(r,\xi)\, b_z(\xi). \tag{16}$$

Once again, the influence functions $G^z_{iz}(r,\xi)$ are functions of Lipschitz-Hankel integrals. For a half-space, these are also given by Paynter et al. [13]. This time, they are bounded ('regular') when $i = r$ and display a Cauchy singularity when $i = z$.

From the bilateral solution, we expect the contact to be closed and stuck from the origin to a radius $r = c$, closed and slipping in the region $c \leq r \leq d$, and open in a region extending from a radius d to infinity. Both the closure point d and stick point c are outputs of the problem (self-determining points).

The resulting normal $N(r)$ and shear $S(r)$ tractions along the contact interface are given by

$$N(r) = \tilde{\sigma}_{zz}(r) + \int_d^\infty G^z_{zz}(r,\xi)\, B_z(\xi)\mathrm{d}\xi + \int_c^\infty G^r_{zz}(r,\xi)\, B_r(\xi)\mathrm{d}\xi, \tag{17}$$

$$S(r) = \tilde{\sigma}_{rz}(r) + \int_d^\infty G^z_{rz}(r,\xi)\, B_z(\xi)\mathrm{d}\xi + \int_c^\infty G^r_{rz}(r,\xi)\, B_r(\xi)\mathrm{d}\xi, \tag{18}$$

where $B_i(\xi) = db_i/d\xi$, $i = r, z$ represents the dislocation density. Glide dislocations are installed over the whole of the length of the contact interface where slipping occurs, including the open portion, and climb dislocations are installed over the part of the contact interface which is open. Equations (17) and (18) form the basis of the solution and integral equations may be generated to restore conventional Signorini inequalities.

In the open region, we require the surfaces to be traction-free

$$N(r) = 0, \qquad S(r) = 0, \qquad d \leq r \leq \infty \tag{19}$$

whereas, in the closed, slipping region, the shearing traction is limited by friction:

$$N(r) < 0 \qquad S(r) = f\,N(r) \qquad c \le r \le d. \tag{20}$$

The three sets of conditions in eqs. (19) and (20) may be combined into two by making use of the Heaviside step function, $H(\cdot)$, giving

$$N(r) = 0 \qquad d \le r \le \infty \tag{21}$$
$$S(r) - f\,H(d-r)\,N(r) = 0 \qquad c \le r \le \infty. \tag{22}$$

Applying eqs. (17) and (18) to eqs. (21) and (22), gives

$$\int_c^\infty G^r_{zz}(r,\xi)\,B_r(\xi)\mathrm{d}\xi + \int_d^\infty G^z_{zz}(r,\xi)\,B_z(\xi)\mathrm{d}\xi = -\tilde{\sigma}_{zz}(r) \qquad d \le r \le \infty \tag{23}$$

$$\int_c^\infty \Big[G^r_{rz}(r,\xi) - f\,H(d-r)\,G^r_{zz}(r,\xi)\Big]\,B_r(\xi)\,\mathrm{d}\xi + \int_d^\infty \Big[G^z_{rz}(r,\xi) - f\,H(d-r)\,G^z_{zz}(r,\xi)\Big]\,B_z(\xi)\,\mathrm{d}\xi = -\Big[\tilde{\sigma}_{rz}(r) - f\,H(d-r)\,\tilde{\sigma}_{zz}(r)\Big] \qquad c \le r \le \infty. \tag{24}$$

Due to the nature of the functions present in eqs. (23) and (24), there is no expectation of obtaining an analytical inversion of the integral equations. We must solve the singular integral equations numerically, choosing to use Gauss-Chebyshev quadrature [16]. Since there are two regions of imposition for the integral equations, two sets of quadrature points are needed. Notice that in eq. (23), the kernel $G^r_{zz}(r,\xi)$ is Cauchy singular over the region $d \le r,\xi \le \infty$ while $G^r_{zz}(r,\xi)$ is regular. In eq. (24), the kernel $G^r_{rz}(r,\xi)$ is Cauchy singular over the region $c \le r,\xi \le \infty$ while all the other terms are regular. Since there is no overlap of Cauchy regions, the two sets of quadrature are sufficient and no special interpolation is needed.

The first step in solving the SIEs is to put the integrals in standard form over the interval $[-1\,,1]$. The following transformation functions were proposed to map a normalised coordinate t to a physical coordinate r:

$$r = \frac{\lambda\,(t+1) + 2\,\hat{r}}{1-t} \tag{25}$$
$$r = \hat{r} + \lambda\,\log\left(\frac{2}{1-t}\right) \tag{26}$$
$$r = \hat{r}\,\left[1 + \lambda\,\tanh^{-1}\left(\frac{2}{1-t}\right)\right], \tag{27}$$

where $\hat{r}$ corresponds to the lower bound of the physical interval $[\hat{r}\,,\infty]$ and λ is a scaling parameter.

From the proposed mappings, the logarithm transformation resulted in the best description of the solution as well as the best convergence. Hence, normalising the integrals using the following substitutions:

$$u = 1 - 2\,\exp\left(\frac{d-\xi}{\lambda}\right), \qquad d \le \xi \le \infty \tag{28}$$
$$v = 1 - 2\,\exp\left(\frac{d-r}{\lambda}\right), \qquad d \le r \le \infty \tag{29}$$
$$s = 1 - 2\,\exp\left(\frac{c-\xi}{\lambda}\right), \qquad c \le \xi \le \infty \tag{30}$$
$$t = 1 - 2\,\exp\left(\frac{c-r}{\lambda}\right), \qquad c \le r \le \infty. \tag{31}$$

gives

$$\int_{-1}^1 G^r_{zz}(v,s)\,B_r(s)\left(\frac{\mathrm{d}\xi}{\mathrm{d}s}\right)\mathrm{d}s + \int_{-1}^1 G^z_{zz}(v,u)\,B_z(u)\left(\frac{\mathrm{d}\xi}{\mathrm{d}u}\right)\mathrm{d}u = -\tilde{\sigma}_{zz}(v) \qquad -1 \le v \le 1 \tag{32}$$

$$\int_{-1}^1 B_r(s)\left[G^r_{rz}(t,s) + f\,H(\gamma)\,G^r_{zz}(t,s)\right]\left(\frac{\mathrm{d}\xi}{\mathrm{d}s}\right)\mathrm{d}s + \int_{-1}^1 B_z(u)\left[G^z_{rz}(t,u) + f\,H(\gamma)\,G^z_{zz}(t,u)\right]\left(\frac{\mathrm{d}\xi}{\mathrm{d}u}\right)\mathrm{d}u = -\Big[\tilde{\sigma}_{rz}(t) + f\,H(\gamma)\,\tilde{\sigma}_{zz}(t)\Big] \qquad -1 \le t \le 1 \tag{33}$$

where

$$\gamma = 1 - \frac{c}{d} + \frac{\lambda}{d}\,\log\left(\frac{1-t}{2}\right) \tag{34}$$
$$\frac{\mathrm{d}\xi}{\mathrm{d}s} = \frac{\lambda}{1-s} \tag{35}$$
$$\frac{\mathrm{d}\xi}{\mathrm{d}u} = \frac{\lambda}{1-u}. \tag{36}$$

For the general form of the solution, both the climb and glide dislocations must be bounded at both ends of the interval. Thus, we choose

$$B_r(s) = \phi_r(s)\,\sqrt{1-s^2} \tag{37}$$
$$B_z(u) = \phi_z(u)\,\sqrt{1-u^2} \tag{38}$$

and eqs. (32) and (33) become, in normalised form,

$$\sum_{i=1}^{N}\left\{\frac{\lambda W_i}{1-s_i}\,\phi_r(s_i)\,G^r_{zz}(v_k,s_i)\right\}+ \sum_{i=1}^{N}\left\{\frac{\lambda X_i}{1-u_i}\,\phi_z(u_i)\,G^z_{zz}(v_k,u_i)\right\} = -\frac{2}{\pi}\tilde{\sigma}_{zz}(v_k) \qquad k=1,\dots,N+1 \tag{39}$$

$$\sum_{i=1}^{N}\left\{\left[G^r_{rz}(t_k,s_i)-f\,H(\gamma_k)\,G^r_{zz}(t_k,s_i)\right]\frac{\lambda W_i}{1-s_i}\phi_r(s_i)\right\}+ \sum_{i=1}^{N}\left\{\left[G^z_{rz}(t_k,u_i)-f\,H(\gamma_k)\,G^z_{zz}(t_k,u_i)\right]\frac{\lambda X_i}{1-u_i}\phi_z(u_i)\right\} = -\frac{2}{\pi}\left[\tilde{\sigma}_{rz}(t_k)-f\,H(\gamma_k)\,\tilde{\sigma}_{zz}(t_k)\right] \quad k=1,\dots,N+1 \tag{40}$$

where

$$\gamma_k = 1-\frac{c}{d}+\frac{\lambda}{d}\log\left(\frac{1-t_k}{2}\right) \tag{41}$$

and the integration points s_i, u_i, collocation points t_k, v_k and weights W_i, X_i for the quadrature are given as [16]

$$s_i = u_i = \cos\left(\pi\frac{i}{N+1}\right) \qquad i=1,\dots,N \tag{42}$$

$$t_k = v_k = \cos\left(\frac{\pi}{2}\frac{2k-1}{(N+1)}\right) \qquad k=1,\dots,N+1 \tag{43}$$

$$W_i = X_i = \frac{1-s_i^2}{2\,(N+1)}. \tag{44}$$

Equations (39) and (40) form a system of $2N+2$ equations and $2N+2$ unknowns. These are the N values of $\phi_r(s_i)$, N values of $\phi_z(u_i)$, the closure point d and the stick point c. Once ϕ_r and ϕ_z are known, the stresses at a point (r,z) can be found by the discrete versions of eqs. (17) and (18)

$$N(v) = \tilde{\sigma}_{zz}(v)+\sum_{i=1}^{N}\left\{\frac{\lambda W_i}{1-s_i}\,\phi_r(s_i)\,G^r_{zz}(v,s_i)\right\}+ \sum_{i=1}^{N}\left\{\frac{\lambda X_i}{1-u_i}\,\phi_z(u_i)\,G^z_{zz}(v,u_i)\right\} \tag{45}$$

$$S(t) = \tilde{\sigma}_{rz}(t)+\sum_{i=1}^{N}\left\{\frac{\lambda W_i}{1-s_i}\,\phi_r(s_i)\,G^r_{rz}(t,s_i)\right\}+ \sum_{i=1}^{N}\left\{\frac{\lambda X_i}{1-u_i}\,\phi_z(u_i)\,G^z_{zz}(t,u_i)\right\}. \tag{46}$$

Finally, the axial dislocation density B_z is related to the axial displacement of the contact $u_z(r)$ through the following relationship [12]:

$$B_z(r) = -\frac{\mathrm{d}u_z(r)}{\mathrm{d}r}. \tag{47}$$

Thus, $u_z(r)$ can be found by integration:

$$u_z(r) = -\int_d^r B_z(\xi)\mathrm{d}\xi. \tag{48}$$

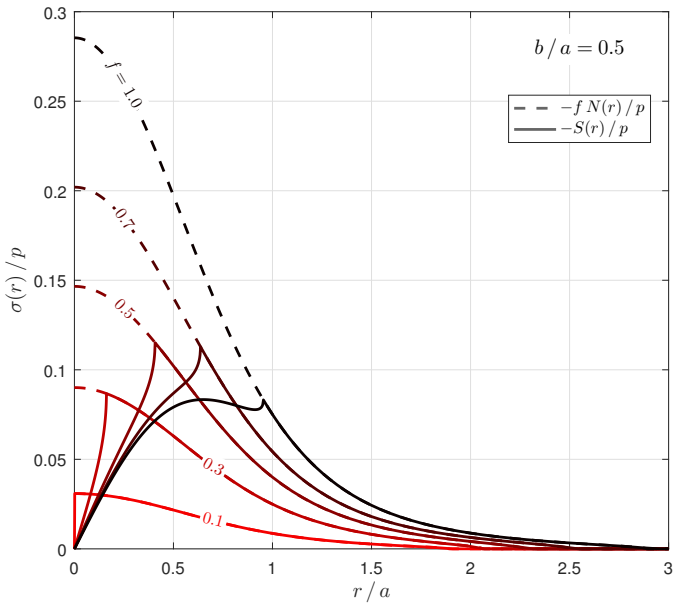

Figure 3: Normalised contact pressure and shear stress in the contact interface for $b/a = 0.5$

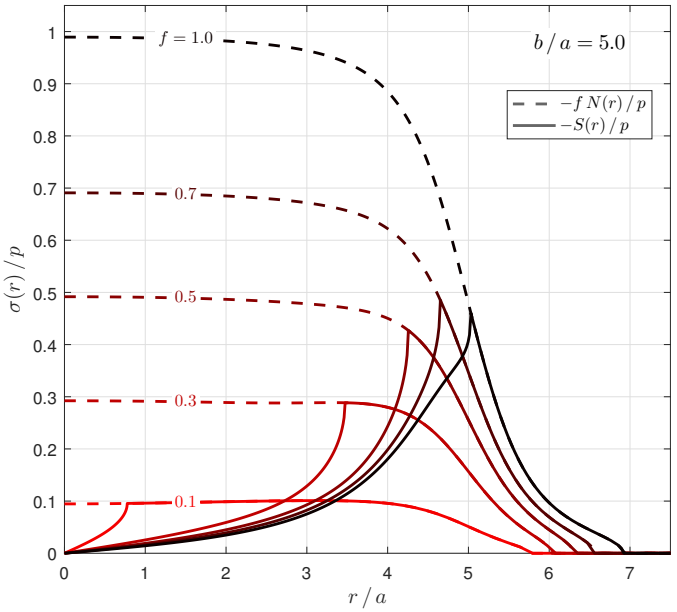

Figure 4: Normalised contact pressure and shear stress in the contact interface for $b/a = 5.0$.

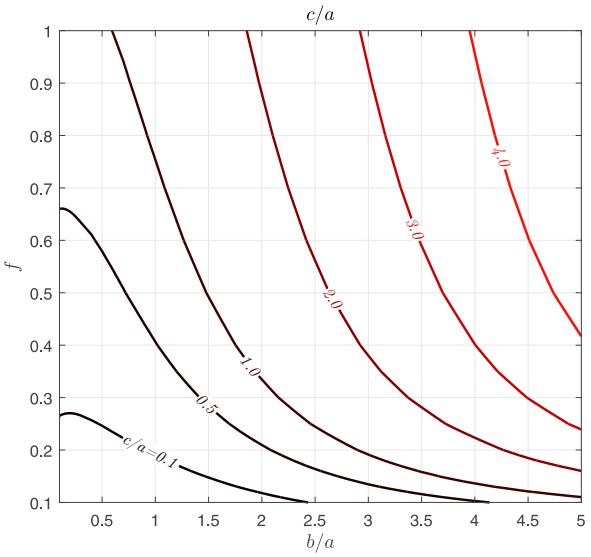

Figure 5: Normalised stick radius c/a.

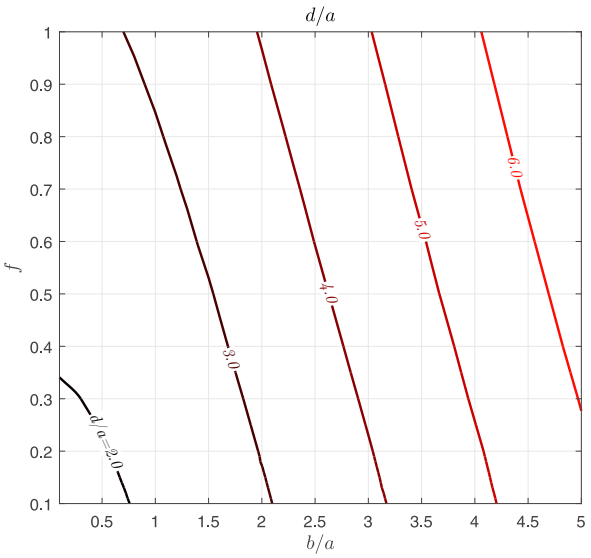

Figure 6: Normalised closure radius d/a.

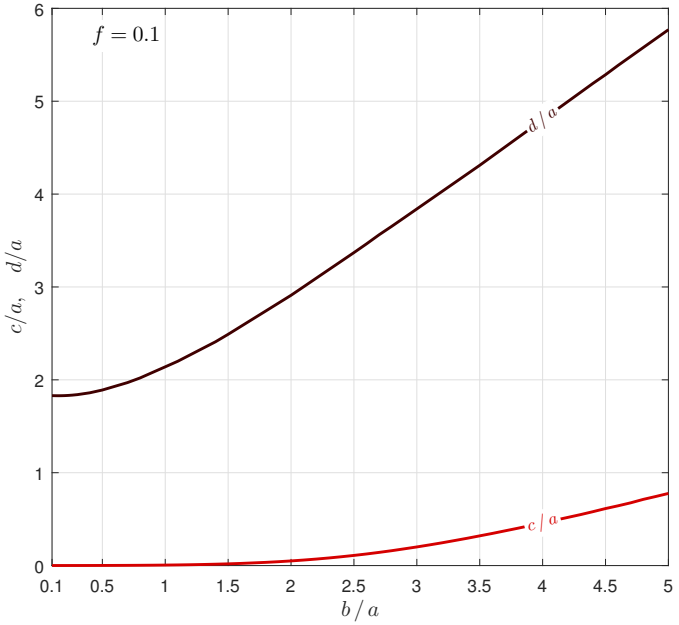

Figure 7: Normalised closure radius d/a and stick radius c/a for $f = 0.1$

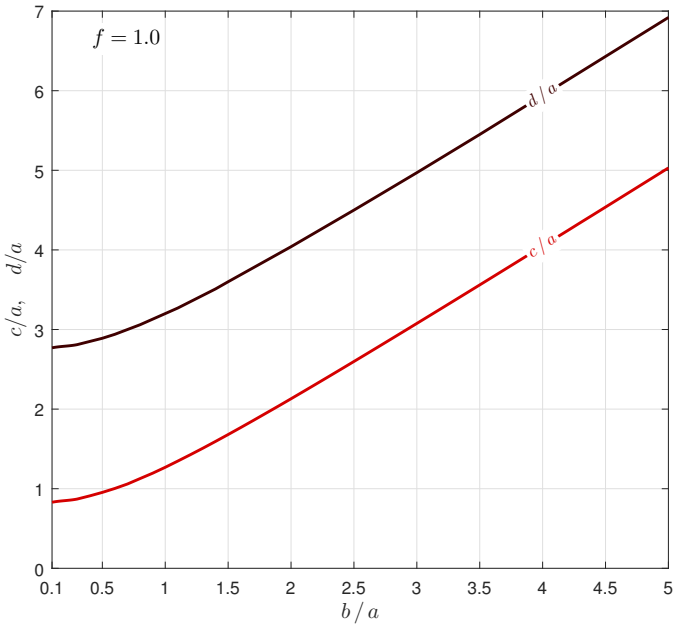

Figure 8: Normalised closure radius d/a and stick radius c/a for $f = 1.0$

4. Results

The problem was coded using the numerical processor MATLAB. Due to the semi-infinite nature of the integrals and, consequently, of the mapping functions, the problem is highly non-linear and obtaining a convergent solution is not trivial. First, due to the unknown length dimensions there are additional collocation equations which need to be satisfied and which enable the values of c/a and d/a to be found. In practice, we guess values of the radii to be found and omit the central equations from the $N + 1$ generated for each dislocation. The column vectors of ϕ_i are found. The omitted equations are then evaluated and the lengths needed are adjusted to minimise the residues. Convergence is dependent on obtaining adequate values of quadrature points N and the scaling parameter λ. For the present solution, convergence was obtained for $N = 150$ and λ varying between $5\,a$ and $11\,a$. Changes in the stresses, displacements, c/a and d/a were negligible when N was increased beyond 150. All results present in this paper are for $\nu = 0.3$.

Figures 3 and 4 show the normalised contact pressure $N(r)$ and shear traction $S(r)$ at the contact interface. As expected, for a fixed coefficient of friction f, the shear stress increases until it reaches $f\,N(r)$, at which point slip

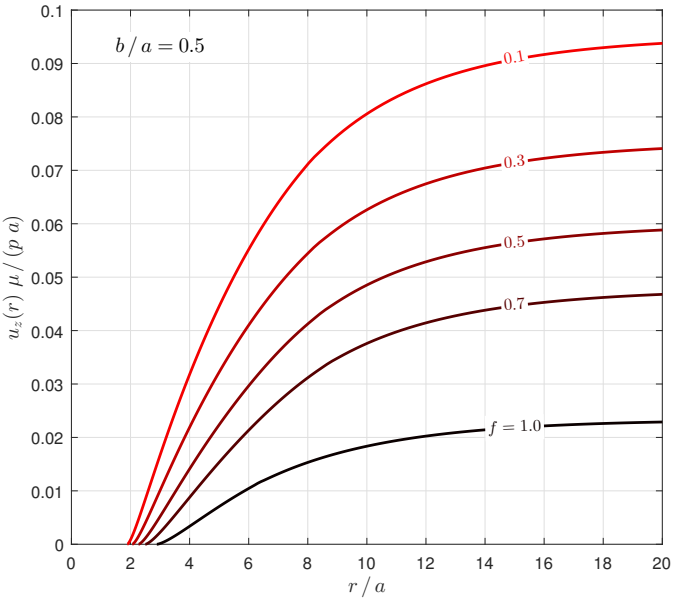

Figure 9: Normalised axial displacement at the contact interface for $b/a = 0.5$.

occurs. From there, the normal and shear tractions fall to zero, where opening occurs. Notice that the tractions are proportional to the magnitude of the applied pressure p. Therefore, the points of slip and opening are independent of p. As a consequence, as soon as an increment of pressure is applied, the contact changes discontinuously from an unloaded configuration to the loaded one [1].

We also note, from eqs. (3) and (4), that the bilateral stresses are independent of the Poisson's ratio. Consequently, this results in the tractions at the contact surface and the points of stick and opening being independent of ν. Therefore, to completely describe the interfacial stresses, only two parameters are needed: f and b/a.

The contours of the normalised points of slip and opening as functions of the coefficient of friction f and the normalised radius of the loaded disk b/a are shown in Figures 5 and 6. It can be noted that as f and b/a increase, c/a and d/a also increase. Figures 7 and 8 show the normalised slip and opening points as a function of b/a for $f = 0.1$ and $f = 1.0$. The region below the c/a curve represents the stick disk, while the region between the d/a and c/a curves shows the slip annulus. For low coefficients of friction ($f = 0.1$ for instance, Figure 7), we notice that as b/a increases the slip annulus becomes larger and accounts for a larger portion of the closed region. For higher f, however ($f = 1.0$, Figure 8), the slip annulus remains approximately of the same size as b/a increases. In this case, the increase in the closed region results in the stick disk becoming larger.

Finally, it is of special interest to look at the contact displacements, especially the axial component, which represents the layer's lifted shape, shown in Figure 9. Away from the origin, the layer is subjected to no shear force across its cross-section, which is similar to a circular plate under the same loading. As expected, this results in the layer's axial displacement following a logarithmic shape, due to the presence of a non-zero hoop strain. This behaviour was also observed when the bodies were subjected to a normal point force [7].

5. Conclusions

A solution was obtained for the tractions, displacements and geometric parameters for a receding contact between a layer subjected to a disk of pressure and an elastically similar half-space. It was shown that the problem is fully described by two parameters; the coefficient of friction between interfaces and the normalised radius of the loaded disk b/a. For a realistic coefficient of friction, the contact will always be partially open and partially slipping.

In addition, it was shown that the magnitude of pressure p applied to disk does not change the behaviour of the outputs of the problem, since the interfacial tractions are proportional to the applied pressure. The contact's geometric parameters are independent of the pressure which results in the contact changing discontinuously from the unloaded to loaded configuration with the application of an incremental pressure.

With regards to the geometry of the contact, it was noted that the variation of the size of the slip annulus changes considerably with the coefficient of friction. For low f, minimization of the slip annulus size is achieved by reducing the radius of the loaded disk b/a. For high f, however, changes in b/a do not result in significant changes in the slip region's size.

Finally, due to the presence of a non-zero hoop strain, the contact opening presents a logarithmic curvature.

Acknowledgements

J. L. gratefully acknowledges the financial support of Christ Church Oxford, Rolls Royce PLC and Coordenação de Aperfeiçoamento de Pessoal de Nível Superior - CAPES.

References

[1] J. Dundurs, Properties of elastic bodies in contact, The Mechanics of the Contact between Deformable bodies (1975) 54–66.
[2] T. Chaise, R. Paynter, D. Hills, Contact analysis of a semi-infinite strip pressed onto a half plane by a line force, International Journal of Mechanical Sciences 81 (2014) 60–64.
[3] K. Parel, D. Hills, Frictional receding contact analysis of a layer on a half-plane subjected to semi-infinite surface pressure, International Journal of Mechanical Sciences 108 (2016) 137–143.
[4] L. Keer, J. Dundurs, K. Tsai, Problems involving a receding contact between a layer and a half space, Journal of Applied Mechanics 39 (4) (1972) 1115–1120.
[5] K. Tsai, J. Dundurs, L. Keer, Contact between an elastic layer with a slightly curved bottom and a substrate, Journal of Applied Mechanics, Transactions ASME 39 (3) (1972) 821–823.
[6] K. Tsai, J. Dundurs, L. Keer, Elastic layer pressed against a half space, Journal of Applied Mechanics 41 (3) (1974) 703–707.

[7] J. Lopes, D. Hills, The axisymmetric frictional receding contact of a layer pressed against a half-space by a point force, International Journal of Solids and Structures 171 (2019) 47–53.
[8] J. Lopes, D. Hills, The axisymmetric frictional receding contact of a layer pressed against a half-space by pressure outside a disk, European Journal of Mechanics-A/Solids 77 (2019) 103787.
[9] A. E. H. Love, The stress produced in a semi-infinite solid by pressure on part of the boundary, Philosophical Transactions of the Royal Society of London. Series A, Containing Papers of a Mathematical or Physical Character 228 (659-669) (1929) 377–420.
[10] K.-i. Terazawa, On the elastic equilibrium of a semi-infinite solid under given boundary conditions, Journal of the College of Science (1916) 14–24.
[11] M. T. Hanson, I. W. Puja, Love's circular patch problem revisited: Closed form solutions for transverse isotropy and shear loading, Quarterly of applied mathematics 54 (2) (1996) 359–384.
[12] D. Hills, P. Kelly, D. Dai, A. Korsunsky, Solution of crack problems: the distributed dislocation technique, Vol. 44 of Solid Mechanics and Its Applications, Springer Netherlands, Dordrecht, 2013.
[13] R. Paynter, D. Hills, The effect of path cut on Somigliana ring dislocations in a half-space, International Journal of Solids and Structures 46 (2) (2009) 412–432.
[14] R. Paynter, D. Hills, A. Korsunsky, The effect of path cut on Somigliana ring dislocation elastic fields, International Journal of Solids and Structures 44 (2) (2007) 6653–6677.
[15] J. Lopes, D. Hills, Ring cracks at the surface of a half-space, Engineering Fracture Mechanics 194 (2018) 105–116.
[16] F. Erdogan, G. D. Gupta, T. Cook, Numerical solution of singular integral equations, in: Methods of analysis and solutions of crack problems, 1973, pp. 368–425.
[17] G. Eason, B. Noble, I. N. Sneddon, On certain integrals of Lipschitz-Hankel type involving products of Bessel functions, Philosophical Transactions of the Royal Society of London A: Mathematical, Physical and Engineering Sciences 247 (935) (1955) 529–551.

Appendix A. State of stress induced by circular edge dislocation loops

Appendix A.1. Axial dislocation

Consider a climb axial dislocation loop of radius a put at a depth d and being observed at a position (r, z) in a cylindrical coordinate system, with a Burgers vector component b_z. The stress fields at a position (r, z) are given by

$$\sigma^z_{iz}(r,z) = G^z_{iz}(r,z,d)\, b_z(a) \quad i = r, z. \tag{A.1}$$

The influence functions $G^z_{iz}(\rho,\zeta,\delta)$ $(i = r,\ z)$ for the glide dislocation in a half-space are given as [13]:

$$G^z_{zz}(\rho,\zeta,\delta) = \frac{2\,\mu}{a\,(\kappa+1)}\Bigg[- J_{1,0;1} + I_{1,0;1} - (\zeta-\delta)\, J_{1,0;2} - (\zeta+\delta)\, I_{1,0;2} + 2\,\zeta\,\delta\, I_{1,0;3}\Bigg] \tag{A.2}$$

$$G^z_{rz}(\rho,\zeta,\delta) = \frac{2\,\mu}{a\,(\kappa+1)}\Bigg[- (\zeta-\delta)\, J_{1,1;2} + (\zeta-\delta)\, I_{1,1;2} - 2\,\zeta\,\delta\, I_{1,1;3}\Bigg] \tag{A.3}$$

where ρ, ζ and δ are the normalised coordinates, given as

$$\rho = r/a, \qquad \zeta = z/a, \qquad \delta = d/a, \tag{A.4}$$

μ is the modulus of rigidity and κ is the Kolosov's constant.

Appendix A.2. Radial dislocation

The radial dislocation is not of Volterra kind and, thus, is path-cut dependent. In this paper, an 'outside disk' path cut is used [13]. This path cut can be formed by inserting a disk of material at a depth $z = d$, from $r = a$ to $r = \infty$, displacing the material by the same amount b_r (thickness of the disk). The stress fields at a position (r, z) are given by

$$\sigma^r_{iz}(r,z) = G^r_{iz}(r,z,d)\, b_r(a) \quad i = r, z. \tag{A.5}$$

The influence functions $G^r_{iz}(\rho,\zeta,\delta)$ $(i = r,\ z)$ for the glide dislocation in a half-space are given as [13]:

$$G^r_{zz}(\rho,\zeta,\delta) = \frac{2\,\mu}{a\,(\kappa+1)}\Bigg[- (\zeta-\delta)\, J_{0,0;2} + (\zeta-\delta) I_{0,0;2} + 2\,\zeta\,\delta\, I_{0,0;3}\Bigg] \tag{A.6}$$

$$G^r_{rz}(\rho,\zeta,\delta) = \frac{2\,\mu}{a\,(\kappa+1)}\Bigg[J_{0,1;1} - I_{0,1;1} - (\zeta-\delta)\, J_{0,1;2} + (\zeta+\delta)\, I_{0,1;2} - 2\,\zeta\,\delta\, I_{0,1;3}\Bigg] \tag{A.7}$$

Appendix A.3. Lipschitz-Hankel integrals

In the influence functions, the terms $J_{n,p;q}$ and $I_{n,p;q}$ represent Lipschitz-Hankel integrals. The standard definition for these functions is as an integral of the product of Bessel functions $(J_i(\cdot))$, an exponential term and a power term. Using normalised coordinate variables, it is given as [17]

$$P_{\mu,\nu;\lambda}(\rho,\zeta) = \int_0^\infty J_\mu(t)\, J_\nu(\rho\, t)\, e^{-\zeta\, t}\, t^\lambda\, \mathrm{d}t. \tag{A.8}$$

In the kernels, the follow definition is applied:

$$J_{n,p;q} = P_{n,p;q}(\rho, \zeta - \delta) \tag{A.9}$$
$$I_{n,p;q} = P_{n,p;q}(\rho, -\zeta - \delta) \tag{A.10}$$

The Lipschitz-Hankel integrals needed in the kernels are given by Paynter et al. [14, 13].

10

Conclusions

In Chapter 4, it was shown that the circular dislocations are viable quantities to use as kernels in studying axisymmetric cracks and contact problems. In addition, it provided a verification for the kernels that were brought into public domain in the paper [23] (as MATLAB code included as supplementary material), through the recovery of known results.

The viability of using the circular dislocation kernels as correctors of stresses in axisymmetric problems was further demonstrated in Chapter 5. It was shown that, as expected, the application of a normal extraction force to a semi-infinite shaft shrink fitted to a hub causes the slip zone to increase. Unexpectedly, because of the semi-infinite nature of the shaft, when it was pushed in towards the core of the hub, the slip zone remained of the same size and an additional zone of forward slip developed close to the surface.

Chapter 6 provided an integration scheme for solving frictional axisymmetric contact problems that involve orthogonal components of slip, i.e. the axisymmetric equivalent of the frictional 'in-plane/anti-plane' slip problem. Even though previous attempts at solving these kinds of problems involved the use of special elements of strain nuclei, such as triangular elements of dislocation densities, it was shown that a marching-in-time scheme with a standard Gauss-Chebyshev quadrature is suitable for obtaining the solution, provided that a simple modification is made to the system of equations. The

new method has several advantages, including the maintenance of consistency with the assumed functional forms from the quadrature; smoother representation of tractions and higher order variation with position; and computational efficiency, since there is no need to generate and store a 'look-up' table for the influence functions.

General properties of the axisymmetric frictional receding contact between a layer and a substrate were presented in Part II. For these types of receding contact, it was shown that the interfacial tractions are proportional to the applied load, which results in the slip-stick and closure-opening transition points being independent of the load. Consequently, the change from loaded to unloaded configurations was shown to be discontinuous, as expected, and the application of any increment of load results in the contact 'snapping'.

For the fundamental axisymmetric frictional receding contact problem, shown in Chapter 8, when the layer was subjected to a point force, it was noted that the only parameter in the model is the coefficient of friction between the contacting interfaces. Because the bilateral stresses are independent of the Poisson's ratio, the model is consequently also independent of ν. When the coefficient of friction was varied, an increase in f was followed by an increase in the size of stick disk but resulted in no significant changes in the size of the slip annulus.

In plane frictional receding contacts, the application of a knife-edge normal load to a layer resting on a substrate results in the layer curving at a constant angle (lift-off angle) away from the contact interface, as shown by Chaise et al. [13] and Parel & Hills [14]. However, it was shown that the presence of non-zero hoop strains in the axisymmetric equivalent problem (Chapter 8), results in the layer now displaying a logarithmic curvature away from the contact, which becomes asymptotically parallel with the free surface.

In Chapter 9, an idealised model of a bolted joint was constructed by applying uniform pressure to a disk at the surface of the layer. In this problem, it was also shown that the solution is independent of ν, since the bilateral tractions are independent of this parameter as well. The solution was fully characterised by two parameters: the interfacial coefficient of friction, and the normalised radius of the loaded disk. Additionally, it was shown that

the model exhibits different behaviours regarding the size of the slip annulus when the coefficient of friction is varied. For low f, minimization of the slip annulus was obtained by reducing the normalised radius of the loaded disk, while for high f changes in this parameter do not result in significant changes to the slip annulus size.

From this work, it was also possible to show that singular integral equations posed over semi-infinite regions can be properly inverted using the modified Gauss-Chebyshev quadrature, without suffering from loss of accuracy when compared to Gauss-Laguerre. In addition, there are no explicit formulae for the points and weights for Gauss-Laguerre quadrature, which have to be calculated beforehand. Also, taking more than 40 gaussian points in the implementation requires the use of higher precision floating point numbers, such as quadruple or variable precision, since the quadrature weights have a range of order of magnitude of 10^{-58}. These factors result in the implementation of the modified Gauss-Chebyshev quadrature being simpler and quicker when compared to Gauss-Laguerre.

Furthermore, in Chapter 2, a solution is presented for the application of a tangential shear force Q_x towards the x direction of a half-space (see Section 2.3.3). One proposed problem was to apply this tangential load to the surface of the layer together with a concentrated normal force, hence expanding the work done in Chapter 8. This would follow similar ideas to the work presented by Mindlin [47, 48], presented in Section 2.5.1.

Assuming that the layer and the half-space are adhered, the interfacial tractions are given by the bilateral solution obtained in Section 2.3.3, i.e. the two bodies behave as one. The normal $\sigma_{zz}(r,\theta)$ and shear $\sigma_{rz}(r,\theta)$ tractions along the interface are given, in this case, by the sum of the contributions of the normal load P and tangential load Q_x:

$$\sigma_{zz}(r,\theta,z) = -\frac{Q_x}{2\,\pi}\, r\, \cos(\theta) \left\{ \frac{3\,z^2}{R^5} \right\} - \frac{3\,P}{2\,\pi} \left\{ \frac{z^3}{R^5} \right\} \tag{10.1}$$

$$\sigma_{rz}(r,\theta,z) = -\frac{Q_x}{2\,\pi}\, r^2\, \cos(\theta) \left\{ \frac{3\,z}{R^5} \right\} - \frac{3\,P}{2\,\pi} \left\{ \frac{r\,z^2}{R^5} \right\}, \tag{10.2}$$

where $R = \sqrt{r^2 + z^2}$ is the spherical radius.

Taking γ as the ratio between applied shear to normal force ($\gamma = Q_x \,/\, P$), Equations (10.1) and (10.1) can be rewritten in a simplified format as:

$$\sigma_{zz}(r,\theta,z) = -\frac{3\,P}{2\,\pi}\left\{\frac{z^2\ (z+\gamma\, r\ \cos(\theta))}{R^5}\right\} \tag{10.3}$$

$$\sigma_{rz}(r,\theta,z) = -\frac{3\,P}{2\,\pi}\left\{\frac{r\,z\ (z+\gamma\, r\ \cos(\theta))}{R^5}\right\}. \tag{10.4}$$

From Equations (10.3) and (10.3), the ratio between shear and normal tractions along the adhered interface is given by:

$$\frac{\sigma_{rz}(r,\theta,z)}{\sigma_{zz}(r,\theta,z)} = \frac{r}{z}. \tag{10.5}$$

Even though the shear to normal stress ratio is axisymmetric, it was also expected that along the line $(r > 0, \theta = 0, z = a)$, that the σ_{rz} shear traction and the pressure σ_{zz} would be radially symmetric for the fully adhered case, similarly to Mindlin's problem. However, eqs. (10.3) and (10.4) shows that these components of stress are actually not axisymmetric, as they have a $\cos(\theta)$ term, which is proportional to the applied shear force. In this case, the contact would need to be represented by two coordinates (r, θ) and, therefore, would be beyond the scope of solution of the methodology presented in this thesis.

10.1 Further Work

One improvement to the bolted joint model could be made by considering the effects of introducing a torque loading, which could be represented by the concentrated torque applied to the half-space (see Section 2.3.4). The twisting of the receding layer will give rise to a shear stress $\sigma_{z\theta}$, which is perpendicular to the shear stress σ_{rz} due to the

application of the normal force only. Since there are, now, two components of shear stress which are perpendicular to each other, the solution must satisfy the orthogonality condition at each pseudo-time step. This can be achieved by employing the methodology developed in Chapter 6 to the solutions obtained in Chapters 8 and 9.

Semi-analytical methods could be used to solve the problem of the application of a normal and a non-axisymmetric tangential force to the frictional contact problem of a layer and a substrate, including the use of triangular elements of dislocation density over an area [17].

In addition, questions remain about the interaction between receding contacts, i.e. if the tightening sequence influences the contact behaviour of receding bolted joints, which is corroborated by empirical evidence of the maintenance of aircraft engines. It is observed that, when the engine is disassembled and reassembled, the vibration modes and, consequently, the contact behaviour is changed. An investigation of this effect can be done by looking at the interaction between a pair of fundamental receding contact models under normal load and torque. Because there are, now, two contacts interacting with each other, axisymmetry is lost and the analytical methods deployed earlier are no longer valid. The use of high quality Finite Elements Methods could be used to analyse this interaction. Two distinct problems can be considered, one where the bodies are tightened sequentially, and another where the bolts are tightened simultaneously.

Appendices

A

Influence Functions for Circular Dislocations

This section presents the solution for the state of stress induced by the axial prismatic, radial and screw circular dislocation loops in a half-space.

A.1 Axial prismatic dislocation

Consider a glide axial dislocation loop of radius a put at a depth d in a cylindrical coordinate system with a Burgers vector component b_z. The stress fields at a position (r, z) are given by

$$\sigma^z_{ri}(r, z) = G^z_{rj}(r, z, d)\, b_z \quad i = r, z. \tag{A.1}$$

The influence functions $G^z_{ri}(\rho, \zeta, \delta)$ $(i = r,\ z)$ for the glide dislocation in a half-space are given as [56]:

$$G^z_{rr}(\rho,\zeta,\delta) = \frac{2\,\mu}{a\,(\kappa+1)}\Bigg[- J_{1,0;1} + I_{1,0;1} + (\zeta-\delta)\,J_{1,0;2} + (\zeta-3\,\delta)\,I_{1,0;2} + \frac{(\kappa-1)}{2\,\rho}\,J_{1,1;0} - \frac{(\kappa-1)}{2\,\rho}\,I_{1,1;0} - \frac{(\zeta-\delta)}{\rho}\,J_{1,1;1} + \frac{(\zeta\,\kappa-\delta)}{\rho}\,I_{1,1;1} + \frac{(2\,\zeta\,\delta)}{\rho}\,I_{1,1;2} - 2\,\zeta\,\delta\,I_{1,0;3}\Bigg] \tag{A.2}$$

$$G^z_{rz}(\rho,\zeta,\delta) = \frac{2\,\mu}{a\,(\kappa+1)}\Bigg[- (\zeta-\delta)\,J_{1,1;2} + (\zeta-\delta)\,I_{1,1;2} - 2\,\zeta\,\delta\,I_{1,1;3}\Bigg] \tag{A.3}$$

$$G^z_{zz}(\rho,\zeta,\delta) = \frac{2\,\mu}{a\,(\kappa+1)}\Bigg[- J_{1,0;1} + I_{1,0;1} - (\zeta-\delta)\,J_{1,0;2} - (\zeta+\delta)\,I_{1,0;2} + 2\,\zeta\,\delta\,I_{1,0;3}\Bigg], \tag{A.4}$$

where ρ, ζ and δ are the normalised coordinates, given as

$$\rho = r/a, \qquad \zeta = z/a, \qquad \delta = d/a, \tag{A.5}$$

μ is the modulus of rigidity and κ is the Kolosov's constant. The terms $J_{n,p;q}$ and $I_{n,p;q}$ represent Lipschitz-Hankel integrals, detailed in Appendix B.

A.2 Radial dislocation

The radial dislocation is not of Volterra kind and, thus, is path-cut dependent. There are four possible path-cuts to create a climb dislocation of Burgers vector b_r, defined by Paynter & Hills [56] and shown in Figure A.1. These result in significantly different

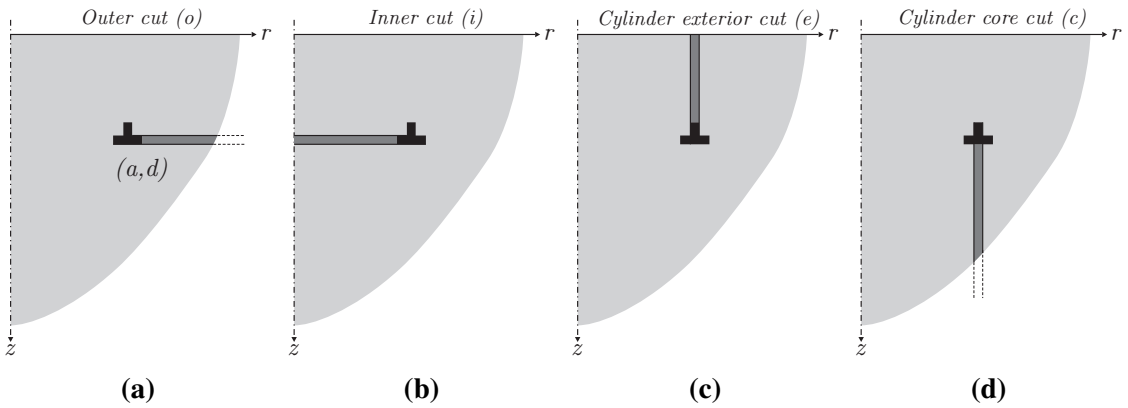

Figure A.1: Path cuts for a radial climb dislocation.

solutions for the influence functions and should match the path in which the integrals are being evaluated.

A.2.1 Outer cut (b_r^o)

An 'outside ring' path cut is made by inserting a ring of material at the depth $z = d$, from $r = a$ to infinity, displacing the materials by an amount b_r (Figure A.1a). The angle parameter α designates the angle of the cut with respect to the r axis. For the outer cut, $\alpha = 0$. The influence functions are given as [56]:

$$
\begin{aligned}
{}^{o}G^{r}_{rr}(\rho,\zeta,\delta,\alpha) = \frac{2\,\mu}{a\,(\kappa+1)} \Bigg[& -2\,J_{0,0;1} - 2\,I_{0,0;1} + (\zeta-\delta)\,J_{0,0;2} - (\zeta+3\,\delta)\,I_{0,0;2} + \\
& \frac{(\kappa+1)}{2\,\rho}\,J_{0,1;0}(\alpha) + \frac{(\kappa+1)}{2\,\rho}\,I_{0,1;0}(|\alpha|) - \frac{(\zeta-\delta)}{\rho}\,J_{0,1;1} + \\
& \frac{(\zeta+\kappa\,\delta)}{\rho}\,I_{0,1;1} + \frac{(2\,\zeta\,\delta)}{\rho}\,I_{0,1;2} - 2\,\zeta\,\delta\,I_{0,0;3} \Bigg]
\end{aligned}
\tag{A.6}
$$

$$
\begin{aligned}
{}^{o}G^{r}_{rz}(\rho,\zeta,\delta,\alpha) = \frac{2\,\mu}{a\,(\kappa+1)} \Bigg[& J_{0,1;1} - I_{0,1;1} - (\zeta-\delta)\,J_{0,1;2} + (\zeta+\delta)\,I_{0,1;2} - \\
& 2\,\zeta\,\delta\,I_{0,1;3} \Bigg]
\end{aligned}
\tag{A.7}
$$

$$ {}^{o}G^{r}_{zz}(\rho,\zeta,\delta) = \frac{2\,\mu}{a\,(\kappa+1)}\left[-(\zeta-\delta)\,J_{0,0;2} + (\zeta-\delta)I_{0,0;2} + 2\,\zeta\,\delta\,I_{0,0;3}\right]. \tag{A.8} $$

A.2.2 Inner cut (b^i_r)

An 'inside disk' path cut (Figure A.1b) can be formed by inserting a disk of material at a depth $z = d$, from $r = 0$ to $r = a$, displacing the material by the same amount b^i_r (thickness of the disk). For the inner cut, $\alpha = 0$.

$$ \begin{aligned} {}^{i}G^{r}_{rr}(\rho,\zeta,\delta,\alpha) = \frac{2\,\mu}{a\,(\kappa+1)}\Bigg[& 2\,J_{2,0;1}(\alpha) + 2\,I_{2,0;1}(|\alpha|) - (\zeta-\delta)\,J_{2,0;2} + \\ & (\zeta+3\,\delta)\,I_{2,0;2} - \frac{(\kappa+1)}{2\,\rho}\,J_{2,1;0}(\alpha) - \\ & \frac{(\kappa+1)}{2\,\rho}\,I_{2,1;0}(|\alpha|) + \frac{(\zeta-\delta)}{\rho}\,J_{2,1;1} - \\ & \frac{(\zeta+\kappa\,\delta)}{\rho}\,I_{2,1;1} - \frac{(2\,\zeta\,\delta)}{\rho}\,I_{2,1;2} + 2\,\zeta\,\delta\,I_{2,0;3}\Bigg] \end{aligned} \tag{A.9} $$

$$ \begin{aligned} {}^{i}G^{r}_{rz}(\rho,\zeta,\delta,\alpha) = \frac{2\,\mu}{a\,(\kappa+1)}\Bigg[& -J_{2,1;1} + I_{2,1;1} + (\zeta-\delta)\,J_{2,1;2} + (\zeta+\delta)\,I_{2,1;2} + \\ & 2\,\zeta\,\delta\,I_{2,1;3}\Bigg] \end{aligned} \tag{A.10} $$

$$ {}^{i}G^{r}_{zz}(\rho,\zeta,\delta) = \frac{2\,\mu}{a\,(\kappa+1)}\left[-(\zeta-\delta)\,J_{2,0;2} + (\zeta-\delta)I_{2,0;2} - 2\,\zeta\,\delta\,I_{2,0;3}\right]. \tag{A.11} $$

A.2.3 Cylindrical cuts $(b^{c,e}_r)$

The two other path cuts involve cylindrical path cuts. The 'exterior' path cut is made by inserting a cylinder of material of wall thickness b^e_r at a position $(r,z) = (a,d)$ extending along the z axis from $z = d$ to $z = 0$, i.e. towards the 'exterior' of

the half-space (Figure A.1c). The 'core' path cut is made by inserting a cylinder of material of wall thickness b_r^c at a position $(r, z) = (a, d)$ extending along the z axis from $z = d$ to infinity, i.e. towards the 'core' of the half-space (Figure A.1d). These are dependent of radial dislocations with inside and outside path-cuts (b_r^i and b_r^o) and the corrective Kelvin and Boussinesq terms (b_r^k and b_r^b). The radial dislocations are also dependent of the angle argument α. For an 'exterior' cut, $\alpha = -\pi\,/\,2$ and for a 'core' cut, $\alpha = \pi\,/\,2$. From Paynter & Hills [56]:

$$
\begin{aligned}
{}^{c}G^{j}_{rj}(\rho,\zeta,\delta) =& \frac{(\kappa-1)}{(\kappa+1)}\,{}^{i}G^{j}_{rj}(\rho,\zeta,\delta,\pi/2) + \frac{2}{(\kappa+1)}\,{}^{o}G^{j}_{rj}(\rho,\zeta,\delta,\pi/2) \\
&- \frac{2\,\mu\,(3-\kappa)}{a\,(\kappa+1)}\,{}^{k}G^{j}_{rj}(\rho,\zeta,\delta,\pi/2) \quad j = r, z
\end{aligned}
\tag{A.12}
$$

$$
\begin{aligned}
{}^{e}G^{j}_{rj}(\rho,\zeta,\delta) =& \frac{(\kappa-1)}{(\kappa+1)}\,{}^{i}G^{j}_{rj}(\rho,\zeta,\delta,-\pi/2) + \frac{2}{(\kappa+1)}\,{}^{o}G^{j}_{rj}(\rho,\zeta,\delta,-\pi/2) \\
&- \frac{2\,\mu\,(\kappa-1)}{a\,(\kappa+1)}\left({}^{k}G^{j}_{rj}(\rho,\zeta,\delta,-\pi/2) - {}^{b}\,G^{j}_{rj}(\rho,\zeta,-\pi/2)\right) \quad j = r, z
\end{aligned}
\tag{A.13}
$$

where ${}^{c}G^{j}_{rj}$, ${}^{e}G^{j}_{rj}$, ${}^{i}G^{j}_{rj}$, ${}^{o}G^{j}_{rj}$, ${}^{k}G^{j}_{rj}$ and ${}^{b}G^{j}_{rj}$ are, respectively, the influence functions for a radial dislocation with core, exterior, inner and outer cuts, and the Kelvin and Boussinesq corrective terms. These corrective terms are given as:

A.2.4 Kelvin term (b_r^k)

$$
\begin{aligned}
{}^{k}G^{r}_{rr}(\rho,\zeta,\delta,\alpha) = \frac{a}{(\kappa+1)}\Bigg[&- \frac{(3-\kappa)}{2}\,J_{1,0;0}(\alpha) + \frac{(3\,\kappa-1)}{2}\,I_{1,0;0}(|\alpha|) + \\
&(\zeta-\delta)\,J_{1,0;1} + (\kappa\zeta - 3\,\delta)\,I_{1,0;1} -
\end{aligned}
$$

$$\frac{(\zeta-\delta)}{\rho}\,J_{1,1;0}-\frac{(\zeta-\delta)\,\kappa}{\rho}\,I_{1,1;0}+\frac{(2\,\zeta\,\delta)}{\rho}\,I_{1,1;1}+\frac{(1-\kappa^2)}{2\,\rho}\,I_{1,1;-1}(|\alpha|)-2\,\zeta\,\delta\,I_{1,0;2}\Bigg] \tag{A.14}$$

$${}^{k}G^{r}_{rz}(\rho,\zeta,\delta,\alpha)=\frac{a}{(\kappa+1)}\Bigg[-\frac{(\kappa-1)}{2}\,J_{1,1;0}+\frac{(\kappa-1)}{2}\,I_{1,1;0}-(\zeta-\delta)\,J_{1,1;1}+(\kappa\zeta-\delta)\,I_{1,1;1}-2\,\zeta\,\delta\,I_{1,1;2}\Bigg] \tag{A.15}$$

$${}^{k}G^{r}_{zz}(\rho,\zeta,\delta,\alpha)=\frac{a}{(\kappa+1)}\Bigg[-\frac{(\kappa-1)}{2}\,J_{1,0;0}(\alpha)+\frac{(\kappa-1)}{2}\,I_{1,0;0}(|\alpha|)-(\zeta-\delta)\,J_{1,0;1}-(\delta+\zeta\,\kappa)\,I_{1,0;1}+2\,\zeta\,\delta\,I_{1,0;2}\Bigg] \tag{A.16}$$

A.2.5 Boussinesq term (b^b_r)

Kelvin term with depth set to zero ($\delta = 0$).

$${}^{b}G^{r}_{rr}(\rho,\zeta)=a\Bigg[-J_{1,0;0}(\alpha)+\zeta\,J_{1,0;1}-\frac{\zeta}{\rho}\,J_{1,1;0}+\frac{(\kappa-1)}{2\,\rho}\,J_{1,1;-1}(\alpha)\Bigg] \tag{A.17}$$

$${}^{b}G^{r}_{rz}(\rho,\zeta)=a\Bigg[-\zeta\,J_{1,1;1}\Bigg] \tag{A.18}$$

$${}^{b}G^{r}_{zz}(\rho,\zeta)=a\Bigg[-J_{1,0;0}(\alpha)-(\zeta-\delta)\,J_{1,0;1}\Bigg] \tag{A.19}$$

A.3 Screw dislocation

Consider a glide screw dislocation loop of radius a at a depth d with a Burgers vector component b_θ and being observed at a position (r, z) in a cylindrical coordinate system. The stress fields at a position (r, z) are given by

$$\sigma^{\theta}_{i\theta}(r, z) = G^{\theta}_{i\theta}(r, z, d)\, b_\theta \quad i = r, z. \tag{A.20}$$

The influence functions $G^{\theta}_{r\theta}(\rho, \zeta, \delta)$ $(i = r,\ z)$ for the glide dislocation in a half-space are given as [57]:

$$G^{\theta}_{r\theta}(\rho, \zeta, \delta) = \frac{\mu\, a}{2}\left[J_{0,2;1} - 2\, J_{1,2;0} - (I_{0,2;1} - 2\, I_{1,2;0})\right] \tag{A.21}$$

$$G^{\theta}_{z\theta}(\rho, \zeta, \delta) = \frac{\mu\, a}{2}\left[J_{1,2;1} - I_{1,2;1}\right] \tag{A.22}$$

B

Lipschitz-Hankel Integrals

In the influence functions presented in Appendix A, the terms $J_{n,p;q}$ and $I_{n,p;q}$ represent Lipschitz-Hankel integrals. The standard definition for these functions is as an integral of the product of Bessel functions ($J_i(\cdot)$), an exponential term and a power term. Using normalised coordinate variables, it is given as [58]

$$P_{\mu,\nu;\lambda}(\rho,\zeta) = \int_0^\infty J_\mu(t)\, J_\nu(\rho\, t)\, e^{-\zeta\, t}\, t^\lambda \,\mathrm{d}t, \tag{B.1}$$

where

$$\rho = r/a, \qquad \zeta = z/a. \tag{B.2}$$

In the kernels, the following definition is applied:

$$J_{n,p;q} = P_{n,p;q}(\rho, \zeta - \delta) \tag{B.3}$$

$$I_{n,p;q} = P_{n,p;q}(\rho, -\zeta - \delta). \tag{B.4}$$

The integral exists when $\mu + \nu + \lambda > -1$, $\rho \geq 0$, $\zeta \geq 0$ [58] and are expressed as functions of complete elliptic integrals of the first, second and third kind, defined as

$$\boldsymbol{E} = \mathbf{K}(k^2) = \int_0^{\pi/2} \frac{\mathrm{d}\theta}{\sqrt{1 - k^2 \sin^2 \theta}} \tag{B.5}$$

$$\boldsymbol{K} = \mathbf{E}(k^2) = \int_0^{\pi/2} \sqrt{1 - k^2 \sin^2 \theta}\, \mathrm{d}\theta \tag{B.6}$$

$$\boldsymbol{\Pi} = \boldsymbol{\Pi}(h, k^2) = \int_0^{\pi/2} \frac{\mathrm{d}\theta}{(1 - h \sin^2 \theta)\sqrt{1 - k^2 \sin^2 \theta}} \tag{B.7}$$

where the *modulus* (k) and the *parameter* (h) are given by

$$k = \sqrt{\frac{4\,\rho}{(\rho+1)^2 + \zeta^2}}, \quad k'^2 = 1 - k^2, \qquad h = \frac{4\,\rho}{(\rho+1)^2}. \tag{B.8}$$

The Lipschitz-Hankel integrals needed in the kernels are given by Paynter et al. in [56, 59] and reproduced here. After obtaining $P_{0,0;0}(\rho, \zeta)$, subsequent integral functions can be derived by differentiation

$$P_{\mu,\nu;\lambda+1}(\rho,\zeta) = -\frac{\partial}{\partial\zeta} P_{\mu,\nu;\lambda}(\rho,\zeta) \tag{B.9}$$

$$P_{\mu,\nu+1;\lambda+1}(\rho,\zeta) = -\rho^{\nu} \frac{\partial}{\partial\rho}\left[r^{-\nu} P_{\mu,\nu;\lambda}(\rho,\zeta)\right] \tag{B.10}$$

$$P_{\mu,\nu-1;\lambda+1}(\rho,\zeta) = \rho^{-\nu} \frac{\partial}{\partial\rho}\left[r^{\nu} P_{\mu,\nu;\lambda}(\rho,\zeta)\right], \tag{B.11}$$

or through recurrence relationships [58]:

$$P_{\mu+1,\nu;\lambda}(\rho,\zeta) = 2\,\mu\, P_{\mu,\nu;\lambda-1}(\rho,\zeta) - P_{\mu-1,\nu;\lambda}(\rho,\zeta) \tag{B.12}$$

$$P_{\mu,\nu+1;\lambda}(\rho,\zeta) = 2\,\nu\,\rho^{-1}\, P_{\mu,\nu;\lambda-1}(\rho,\zeta) - P_{\mu,\nu-1;\lambda}(\rho,\zeta) \tag{B.13}$$

$$P_{\mu+1,\nu;\lambda}(\rho,\zeta) = (\mu+\nu+\lambda)\,P_{\mu,\nu;\lambda-1}(\rho,\zeta) - \zeta\,P_{\mu,\nu;\lambda}(\rho,\zeta) - \rho\,P_{\mu,\nu+1;\lambda}(\rho,\zeta) \quad \text{(B.14)}$$

$$P_{\mu-1,\nu;\lambda}(\rho,\zeta) = (\mu+\nu-\lambda)\,P_{\mu,\nu;\lambda-1}(\rho,\zeta) + \zeta\,P_{\mu,\nu;\lambda}(\rho,\zeta) - \rho\,P_{\mu,\nu-1;\lambda}(\rho,\zeta) \quad \text{(B.15)}$$

$$P_{\mu-1,\nu;\lambda}(\rho,\zeta) = (\mu-\nu-\lambda)\,P_{\mu,\nu;\lambda-1}(\rho,\zeta) + \zeta\,P_{\mu,\nu;\lambda}(\rho,\zeta) + \rho\,P_{\mu,\nu+1;\lambda}(\rho,\zeta). \quad \text{(B.16)}$$

The Integrals $P_{0,0;\lambda}$

$$P_{0,0;0}(\rho,\zeta) = \frac{k}{\pi\sqrt{\rho}}\,\boldsymbol{K} \quad \text{(B.17)}$$

$$P_{0,0;1}(\rho,\zeta) = \frac{\zeta\,k^3}{4\,\pi\,k'^2\,\rho^{3/2}}\,\boldsymbol{E} \quad \text{(B.18)}$$

$$P_{0,0;2}(\rho,\zeta) = \frac{k^5}{16\,\pi\,k'^2\,\rho^{5/2}}\left[\left(\frac{2\,(1+k'^2)}{k'^2} - \frac{4\,\rho}{k^2}\right)\boldsymbol{E} - \zeta^2\,\boldsymbol{K}\right] \quad \text{(B.19)}$$

$$\begin{aligned} P_{0,0;3}(\rho,\zeta) = \frac{\zeta k^{11}}{1024\pi k'^6\rho^{11/2}}\Bigg\{ & \Big[11\zeta^6 + 10\zeta^4\left(\rho^2+1\right) + \\ & \zeta^2\left(-13\rho^4+58\rho^2-13\right) - 12\left(\rho^2-1\right)^2\left(\rho^2+1\right)\Big]\,\boldsymbol{E} + \\ & \left(\zeta^2+(\rho-1)^2\right)\left[-5\zeta^4 - 2\zeta^2\left(\rho^2+1\right) + 3\left(\rho^2-1\right)^2\right]\,\boldsymbol{K}\Bigg\} \end{aligned} \quad \text{(B.20)}$$

The Integrals $P_{0,1;\lambda}$

$$\begin{aligned} P_{0,1;0}(\rho,\zeta,\alpha) = & -\frac{k\zeta}{2\pi\rho^{3/2}}\left(\boldsymbol{K} + \frac{\rho-1}{\rho+1}\boldsymbol{\Pi}\right) + \\ & \operatorname{sign}\left(\arctan\frac{\zeta}{|\rho-1|} - \alpha\right)\begin{cases} 0, & \rho<1 \\ 1/2, & \rho=1 \\ 1/\rho, & r>1 \end{cases} \end{aligned} \quad \text{(B.21)}$$

$$P_{0,1;1}(\rho,\zeta) = -\frac{k}{2\pi\rho^{3/2}}\left(\boldsymbol{K} - \frac{\zeta^2+1-\rho^2}{\zeta^2+(1-\rho)^2}\boldsymbol{\Pi}\right) \quad \text{(B.22)}$$

$$\begin{aligned} P_{0,1;2}(\rho,\zeta) = & \frac{\zeta k^7}{128\pi k'^4\rho^{9/2}}\Bigg\{\left[6\left(\zeta^2-1\right)\rho^2 - \left(\zeta^2+1\right)^2 + 7\rho^4\right]\,\boldsymbol{E} + \\ & \left[\zeta^2+(\rho-1)^2\right]\left[\zeta^2-\rho^2+1\right]\,\boldsymbol{K}\Bigg\} \end{aligned} \quad \text{(B.23)}$$

$$
\begin{aligned}
P_{0,1;3}(\rho,\zeta) \quad = & \frac{k^{11}}{2048\pi k'^6\rho^{13/2}}\Bigg\{\Big[\left(23\zeta^2+20\right)\rho^6-\left(\zeta^2+1\right)^3\left(2\zeta^2-1\right)+ \\
& \left(65\zeta^4+51\zeta^2-18\right)\rho^4+\left(\zeta^2+1\right)\left(33\zeta^4-79\zeta^2+4\right)\rho^2-7\rho^8\Big]\boldsymbol{E}+ \\
& \left[\zeta^2+(\rho-1)^2\right]\left[2\zeta^6+\zeta^4\left(3-11\rho^2\right)-12\zeta^2\rho^2\left(\rho^2-1\right)+\right. \\
& \left.\left(\rho^2-1\right)^3\Big]\boldsymbol{K}\right\} \qquad \text{(B.24)}
\end{aligned}
$$

The Integrals $P_{0,2;\lambda}$

$$
\begin{aligned}
P_{0,2;1}(\rho,\zeta,\alpha) = & -\frac{\zeta k}{\pi\rho^{5/2}}\left[\frac{(k^2\rho)}{4k'^2}\boldsymbol{E}+\boldsymbol{K}+\frac{(\rho-1)}{(\rho+1)}\boldsymbol{\Pi}\right]+ \\
& \frac{2}{\rho}\,\mathrm{sign}\left(\arctan\frac{\zeta}{|\rho-1|}-\alpha\right)\begin{cases}0, & \rho<1\\ 1/2, & \rho=1\\ 1/\rho, & r>1\end{cases} \qquad \text{(B.25)}
\end{aligned}
$$

The Integrals $P_{1,0;\lambda}$

$$
\begin{aligned}
P_{1,0;0}(\rho,\zeta,\alpha) = & -\frac{k\zeta}{2\pi\rho^{1/2}}\left(\boldsymbol{K}+\frac{1-\rho}{1+\rho}\boldsymbol{\Pi}\right)+ \\
& \mathrm{sign}\left(\arctan\frac{\zeta}{|\rho-1|}-\alpha\right)\begin{cases}1, & \rho<1\\ 1/2, & \rho=1\\ 0, & r>1\end{cases} \qquad \text{(B.26)}
\end{aligned}
$$

$$
P_{1,0;1}(\rho,\zeta) \quad = -\frac{k}{2\pi\rho^{1/2}}\left(\frac{k^2(1-\zeta^2-\rho^2)}{4\rho k'^2}\boldsymbol{E}-\boldsymbol{K}\right) \qquad \text{(B.27)}
$$

$$
P_{1,0;2}(\rho,\zeta) \quad = -\frac{k^3\zeta}{8\pi k'^2\rho^{3/2}}\left[\frac{k^4\left(1-(\rho^2+\zeta^2)^2\right)}{4\rho^2k'^2}\boldsymbol{E}-\frac{k^2\left(1-\zeta^2-\rho^2\right)}{4\rho k'^2}\boldsymbol{K}\right] \qquad \text{(B.28)}
$$

$$
\begin{aligned}
P_{1,0;3}(\rho,\zeta) \quad = & \frac{k^{11}}{2048\pi k'^6\rho^{11/2}}\Bigg\{\Big[-2\zeta^8+\zeta^6\left(33-5\rho^2\right)+\zeta^4\left(-3\rho^4-46\rho^2+65\right)+ \\
& \zeta^2\left(\rho^6-75\rho^4+51\rho^2+23\right)+\left(\rho^2-1\right)^3\left(\rho^2+7\right)\Big]\boldsymbol{E}+ \\
& \left[-\zeta^2-(\rho-1)^2\right]\left[-2\zeta^6+\zeta^4\left(11-3\rho^2\right)-\right. \\
& \left.12\zeta^2\left(\rho^2-1\right)+\left(\rho^2-1\right)^3\Big]\boldsymbol{K}\right\} \qquad \text{(B.29)}
\end{aligned}
$$

The Integrals $P_{1,1;\lambda}$

$$P_{1,1;-1}(\rho,\zeta,\alpha) = -\frac{\zeta}{2\pi\rho^{1/2}}\left[\frac{2}{k}\boldsymbol{E} - \left(\frac{k\rho}{2}+\frac{k}{2\rho}+\frac{2-k^2}{k}\right)\boldsymbol{K} + \frac{k(1-\rho)^2}{2\rho}\boldsymbol{\Pi}\right] + \frac{1}{2}\operatorname{sign}\left(\arctan\frac{\zeta}{|\rho-1|}-\alpha\right)\begin{cases}1/\rho, & \rho<1\\ 1/2, & \rho=1\\ \rho, & r>1\end{cases} \tag{B.30}$$

$$P_{1,1;0}(\rho,\zeta) = -\frac{2}{\pi k\rho^{1/2}}\left(\frac{2-k^2}{2}\boldsymbol{K}-\boldsymbol{E}\right) \tag{B.31}$$

$$P_{1,1;1}(\rho,\zeta) = -\frac{k\zeta}{2\pi\rho^{1/2}}\left(\frac{2-k^2}{2k'^2}\boldsymbol{E}-\boldsymbol{K}\right) \tag{B.32}$$

$$P_{1,1;2}(\rho,\zeta) = \frac{k}{2\pi\rho^{3/2}}\left[\frac{k^2}{4\rho k'^2}\left(\frac{k^2}{k'^2}-1-\rho^2\right)\boldsymbol{E} - \left(1-\frac{k^2\zeta^2\left(2-k^2\right)}{8\rho k'^2}\right)\boldsymbol{K}\right] \tag{B.33}$$

$$\begin{aligned}P_{1,1;3}(\rho,\zeta) = -\frac{\zeta k^{11}}{2048\pi k'^6\rho^{13/2}}\Bigg\{&\Big[9\left(\zeta^2+4\right)\rho^6+\left(\zeta^2-6\right)\left(9\zeta^2+13\right)\rho^4+\\ &3\left(\zeta^2+1\right)^3+\left(\zeta^2+1\right)\left(3\zeta^4-77\zeta^2+36\right)\rho^2+3\rho^8\Big]\boldsymbol{E}+\\ &\Big[-\zeta^2-(\rho-1)^2\Big]\Big[3\zeta^4\left(\rho^2+1\right)+2\zeta^2\left(3\rho^4-10\rho^2+3\right)+\\ &3\left(\rho^2-1\right)^2\left(\rho^2+1\right)\Big]\boldsymbol{K}\Bigg\}\end{aligned} \tag{B.34}$$

The Integrals $P_{1,2;\lambda}$

$$P_{1,2;0}(\rho,\zeta,\alpha) = \frac{2}{\rho}P_{1,1;-1}(\rho,\zeta,\alpha) - P_{1,0;0}(\rho,\zeta,\alpha) \tag{B.35}$$

$$P_{1,2;1}(\rho,\zeta,\alpha) = \frac{2}{\rho}P_{1,1;0}(\rho,\zeta,\alpha) - P_{1,0;1}(\rho,\zeta,\alpha) \tag{B.36}$$

The Integrals $P_{2,0;\lambda}$

$$P_{2,0;1}(\rho,\zeta,\alpha) = 2\,P_{1,0;0}(\rho,\zeta,\alpha) - P_{0,0;1}(\rho,\zeta) \tag{B.37}$$

$$P_{2,0;2}(\rho,\zeta) = 2\,P_{1,0;1}(\rho,\zeta) - P_{0,0;2}(\rho,\zeta) \tag{B.38}$$

$$P_{2,0;3}(\rho,\zeta) = 2\,P_{1,0;2}(\rho,\zeta) - P_{0,0;3}(\rho,\zeta) \tag{B.39}$$

The Integrals $P_{2,1;\lambda}$

$$P_{2,1;0}(\rho,\zeta,\alpha) = 2\,P_{1,1;-1}(\rho,\zeta,\alpha) - P_{0,1;0}(\rho,\zeta,\alpha) \tag{B.40}$$
$$P_{2,1;1}(\rho,\zeta) = 2\,P_{1,1;0}(\rho,\zeta) - P_{0,1;1}(\rho,\zeta) \tag{B.41}$$
$$P_{2,1;2}(\rho,\zeta) = 2\,P_{1,1;1}(\rho,\zeta) - P_{0,1;2}(\rho,\zeta) \tag{B.42}$$
$$P_{2,1;3}(\rho,\zeta) = 2\,P_{1,1;2}(\rho,\zeta) - P_{0,1;3}(\rho,\zeta) \tag{B.43}$$

Limits for $\rho \to 0$

Some of the Lipschitz-Hankel integrals appear in the kernels as $P_{\mu,\nu;\lambda}(\rho,\zeta)\,/\,\rho$. When $\rho \to 0$, the denominator goes to zero as well and the fraction appears to be unbounded. It is necessary, therefore, to define the values of this fraction as a limit, i.e.

$$\left(\frac{P_{\mu,\nu;\lambda}(\rho,\zeta)}{\rho}\right)\Bigg|_{\rho=0} = \lim_{\rho\to 0}\left[\frac{P_{\mu,\nu;\lambda}(\rho,\zeta)}{\rho}\right]. \tag{B.44}$$

The limits which are relevant to the circular dislocation kernels are given by:

$$\left(\frac{P_{0,1;0}(\rho,\zeta)}{\rho}\right)\Bigg|_{\rho=0} = \frac{\zeta}{2}\left(\frac{1}{1+\zeta^2}\right)^{3/2} \tag{B.45}$$
$$\left(\frac{P_{0,1;1}(\rho,\zeta)}{\rho}\right)\Bigg|_{\rho=0} = \frac{2\zeta^2-1}{2}\left(\frac{1}{1+\zeta^2}\right)^{5/2} \tag{B.46}$$
$$\left(\frac{P_{0,1;2}(\rho,\zeta)}{\rho}\right)\Bigg|_{\rho=0} = \frac{6\zeta^2-9}{2}\left(\frac{1}{1+\zeta^2}\right)^{7/2} \tag{B.47}$$

$$\left(\frac{P_{1,1;-1}(\rho,\zeta,\alpha)}{\rho}\right)\Bigg|_{\rho=0} = \frac{1}{2}\left[\operatorname{sign}(\arctan\zeta - \alpha) - \frac{\zeta}{\sqrt{1+\zeta^2}}\right] \tag{B.48}$$
$$\left(\frac{P_{1,1;0}(\rho,\zeta)}{\rho}\right)\Bigg|_{\rho=0} = \frac{1}{2}\left(\frac{1}{1+\zeta^2}\right)^{3/2} \tag{B.49}$$
$$\left(\frac{P_{1,1;1}(\rho,\zeta)}{\rho}\right)\Bigg|_{\rho=0} = \frac{3\zeta}{2}\left(\frac{1}{1+\zeta^2}\right)^{5/2} \tag{B.50}$$
$$\left(\frac{P_{1,1;2}(\rho,\zeta)}{\rho}\right)\Bigg|_{\rho=0} = \frac{3(4\zeta^2-1)}{2}\left(\frac{1}{1+\zeta^2}\right)^{7/2} \tag{B.51}$$

$$\left(\frac{P_{2,1;0}(\rho,\zeta,\alpha)}{\rho}\right)\Bigg|_{\rho=0} = -\frac{\zeta(2\zeta^2+3)}{2(\zeta^2+1)^{3/2}} + \operatorname{sign}\left(\arctan\zeta - \alpha\right) \tag{B.52}$$

$$\left(\frac{P_{2,1;1}(\rho,\zeta)}{\rho}\right)\Bigg|_{\rho=0} = \frac{3}{2(\zeta^2+1)^{5/2}} \tag{B.53}$$

$$\left(\frac{P_{2,1;2}(\rho,\zeta)}{\rho}\right)\Bigg|_{\rho=0} = \frac{15\zeta}{2(\zeta^2+1)^{7/2}} \tag{B.54}$$

C

Finite Element Analysis

The problems presented in this thesis were also modelled independently through a Finite Elements approach, using ABAQUS software (Dassault Systems, version 6.16).

Three models were constructed to solve the problems. The solution to each individual problem can be done by modifying only the loading to either the 'shaft' body or the 'layer' body. Since Finite Elements cannot handle infinite domains, the infinite half-space must be modelled as a finite domain. In this work, a rectangular block was chosen. At the far edges of the block, proper boundary conditions must be set to ensure the same behaviour at infinity as the half-space would experience. A sensitivity analysis was conducted to determine the proper size of the finite models. The shrink fitted shaft-hub contact problem was solved considering three sizes of half-space: 100, 70 and 50 times the radius of the shaft. The effects of the boundary conditions were negligible only when the block was 100 the radius of the shaft.

Figure C.1 depicts the models. The half-space was modelled as a 100 units wide, isotropic, homogeneous square block, represented by the white regions in Figure C.1. The shaft/layer bodies were modelled as 1 unit x 100 units, isotropic, homogeneous rectangles, represented by the grey regions in Figure C.1. Axisymmetry is imposed through the z-axis, which results in a 2D FE model. The black lines inside the domain represent regions of mesh refinement.

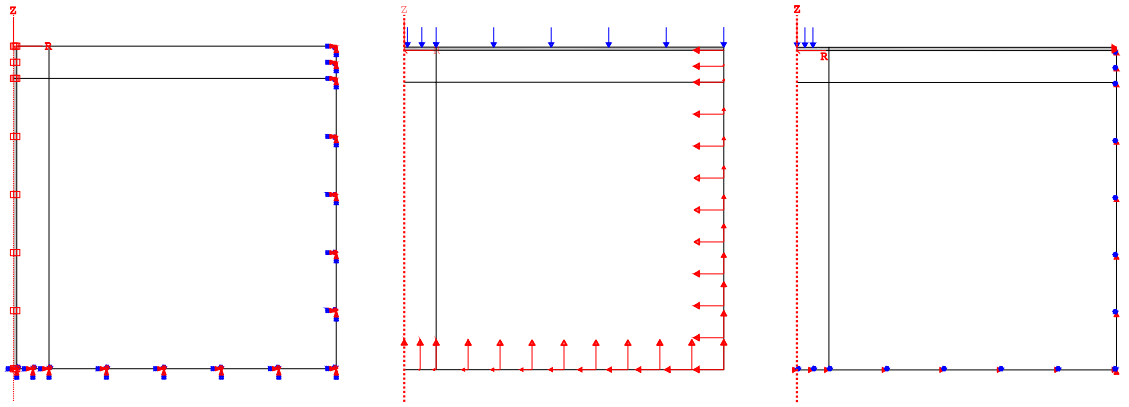

(a) **(b)** **(c)**

Figure C.1: Axisymmetric Finite Element models. (a) Semi-infinite 'shaft' shrink fitted to infinite hub (half-space). (b) Receding contact between a thin layer pressed against a half-space by pressure outside a disk. (c) Receding contact between a thin layer pressed against a half-space.

For the shaft-hub model (Figure C.1a), the displacements due to the shrink fit, point force, and point torque loadings are zero at infinity. Therefore, an encastre boundary condition was imposed to the far edges of the half-space. A frictional contact interface is modelled between the two bodies. The shrink fit assembly was modelled through am imposed temperature differential to the shaft body. The point force or point torque loadings were applied after assembly.

The model for the receding contact of a layer pressed against a half-space by a point force or pressure inside a disk is shown in Figure C.1c. An encastre boundary condition is applied to the far faces of the half-space block. The far face of the layer needs to be able to move vertically but not horizontally, which results in a $u_r = 0$ boundary condition. In order to improve convergence, contact is modelled only between the refined mesh zones of the two bodies, where $0 \leq r \leq 15a$. Initially, the refined zone was chosen to be 15 times the thickness of the layer in order to ensure that contact opening was occuring in the refined mesh zone. After getting the results, the size of the contact is of order of magnitude $\approx 1b$, and, therefore, can be reduced, in order to decrease the mesh size and improve convergence.

When the layer is pressed against the half-space by pressure outside a disk (Figure C.1b), the displacements due to the bilateral loading at infinity are not zero and,

therefore, an encastre boundary condition is not adequate. The expected displacements were calculated and inputed as appropriate boundary conditions at the far faces of the half-space block. In this case, because most of the contact is closed and recession only occurs in a small area close to the origin, the contact region was modelled as the whole interface between the two bodies.

For all three models, quadrilateral elements of 0.01 mm size were seeded through the length of the shaft or layer and the refined portion of the half-space. At least 100 elements were placed through the thickness of the shaft/layer. The mesh was gradually coarsened towards the far boundaries.

A Lagrange multiplier formulation was chosen for modelling the tangential frictional behaviour of the contact, while the normal behaviour was modelled as a 'hard' contact.

Figures C.2 to C.8 depict a comparison between the results obtained through finite element models and the analytical results presented in this thesis. In all figures, the analytical results are represented by solid lines, while the finite element results are represent by dots. Each dot represents the contact stresses at the face of an element of the layer/shaft body, except in Figures C.4 and C.5, where the points were 'filtered' for clarity. Therefore, the dots show not only the contact stresses along the interface but also the relative size of the mesh along the same line.

Even though there is almost a perfect agreement between the two results, it must be noted that the finite element calculations presented were set up in an academic context, where accuracy was paramount. The mesh is extremely refined and computationally expensive, even for a 2D problem. If the same mesh requirements were applied to a 3D problem, the computational cost would be too onerous. Convergence of the semi-infinite receding contacts was difficult, regardless of the mesh refinement.

The deficiencies of the finite element method can be seen even with such refined mesh, as evidenced by the spread of the points in regions where there are sharp gradients in the stresses, such as the shear stress distribution close to the slip/stick transition point and the contact pressure distribution close to the surface for the shrink fit problems (Figures C.2

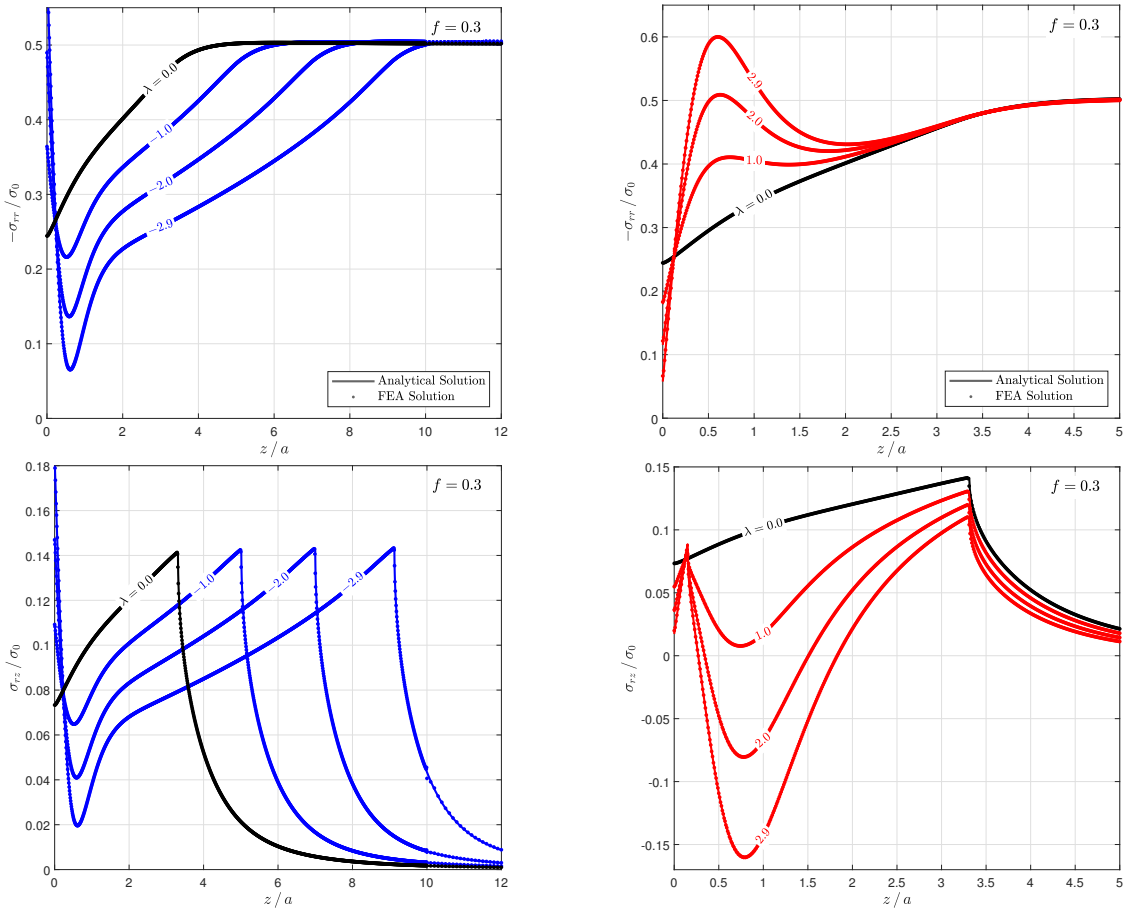

Figure C.2: Comparison between Analytical and Finite Element solutions for shaft/hub system subjected to shrink fit and concentrated normal force and ($f = 0.3$).

and C.3). Also, in Figures C.6 and C.8, it can be noted that the finite element method fails to capture the maximum shear stress for high coefficients of friction.

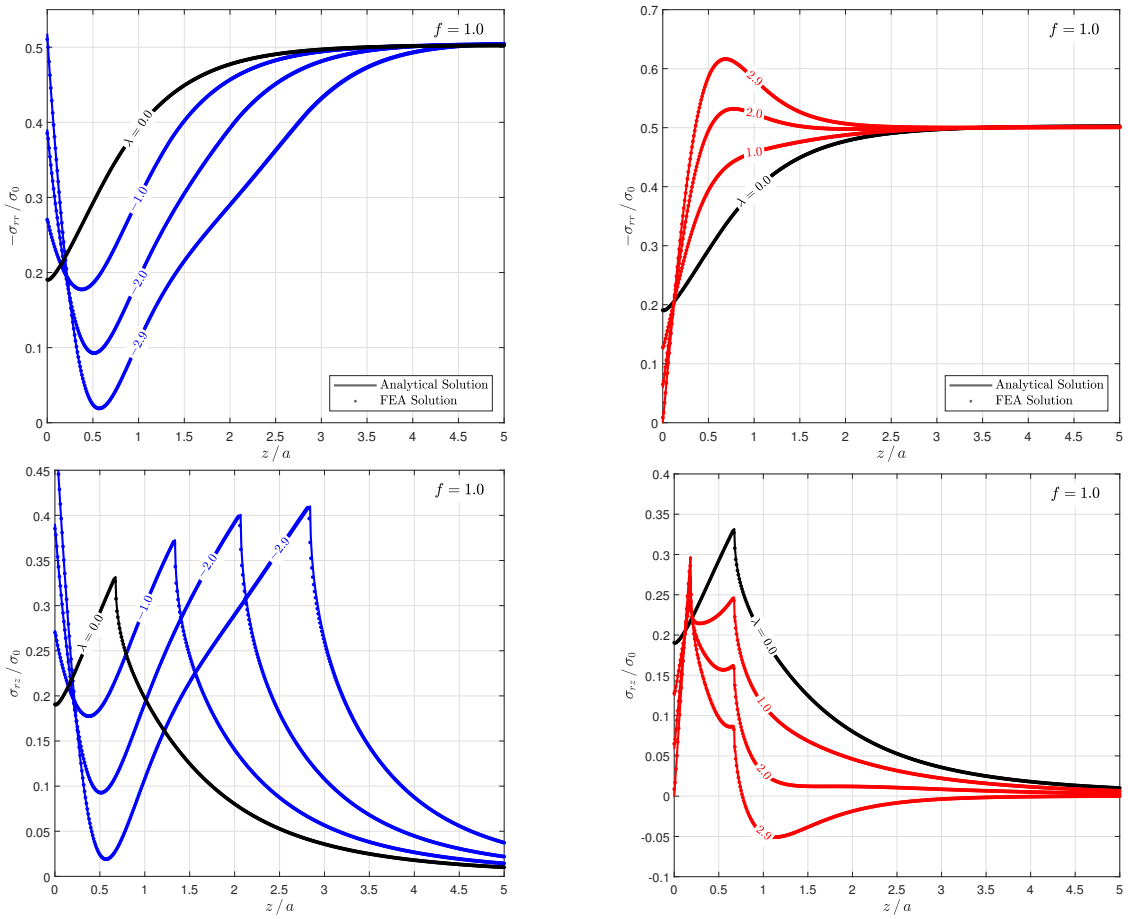

Figure C.3: Comparison between analytical and finite element solutions for shaft/hub system subjected to shrink fit and concentrated normal force ($f = 1.0$).

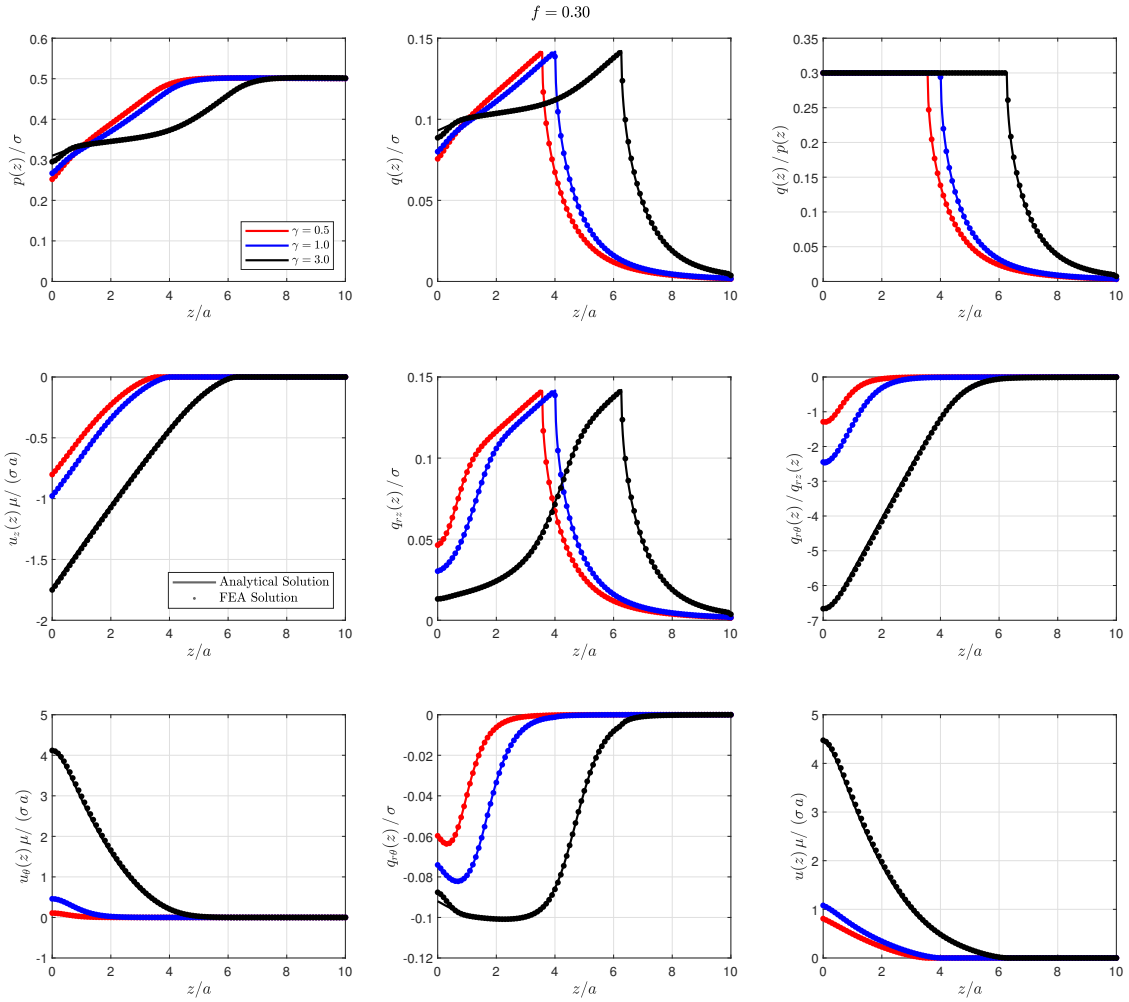

Figure C.4: Comparison between analytical and finite element solutions for shaft/hub system subjected to shrink fit and concentrated torque ($f = 0.3$).

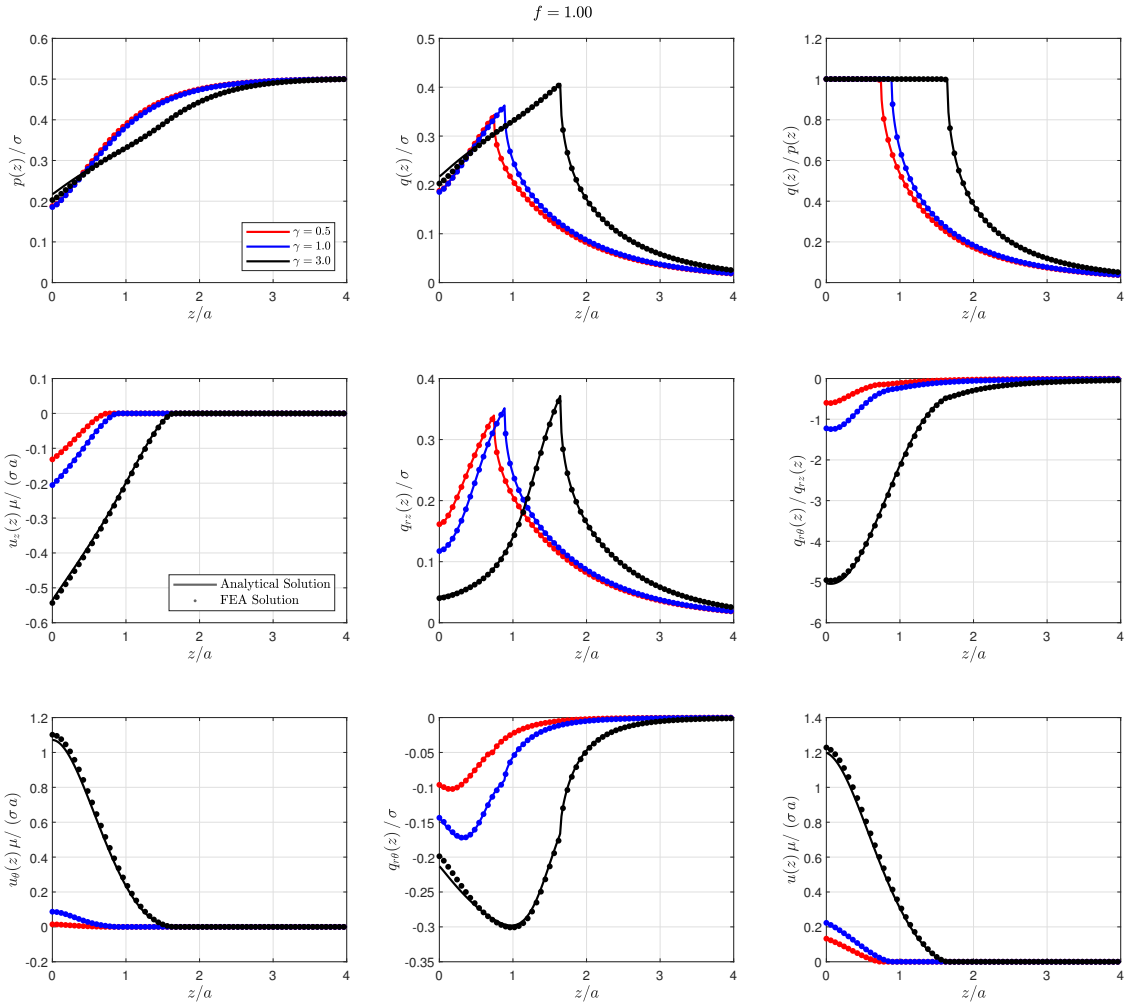

Figure C.5: Comparison between analytical and finite element solutions for shaft/hub system subjected to shrink fit and concentrated torque ($f = 1.0$).

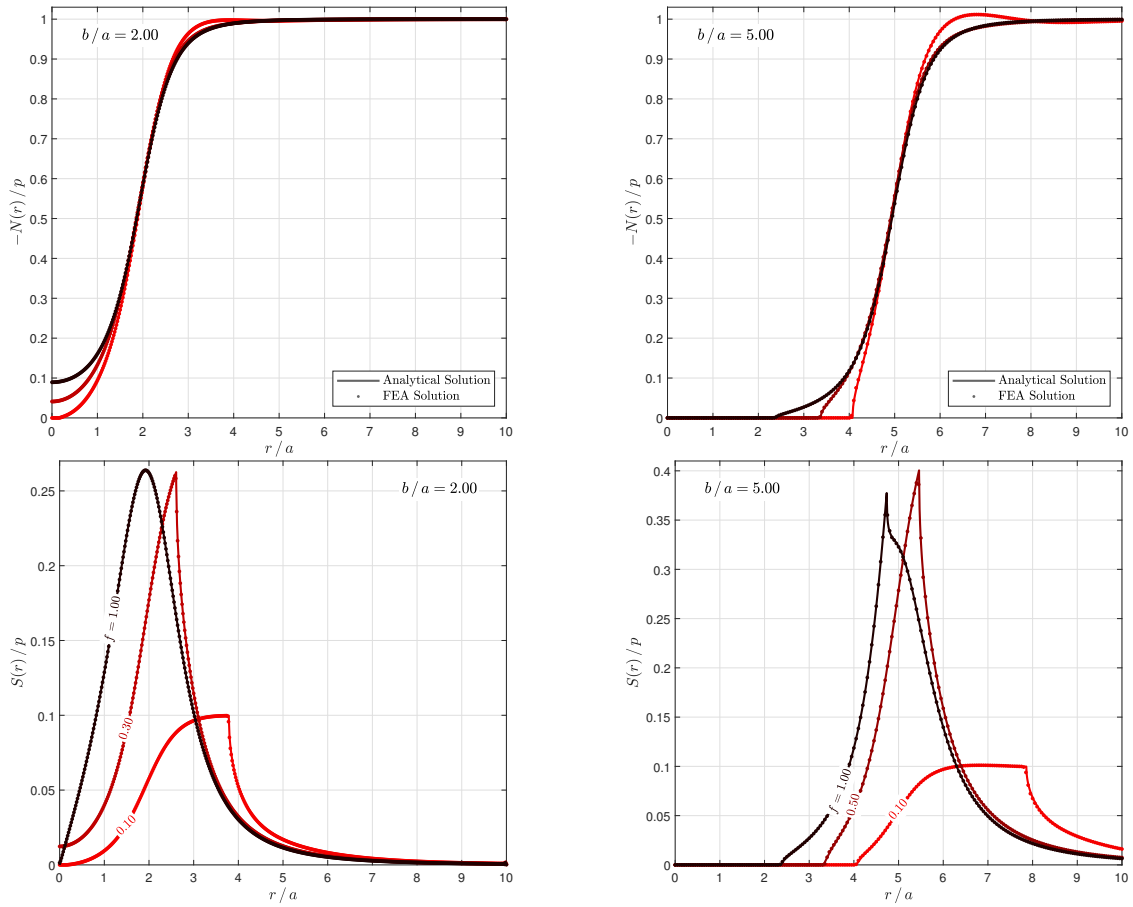

Figure C.6: Comparison between analytical and finite element solutions for layer pressed against half-space by pressure outside a disk.

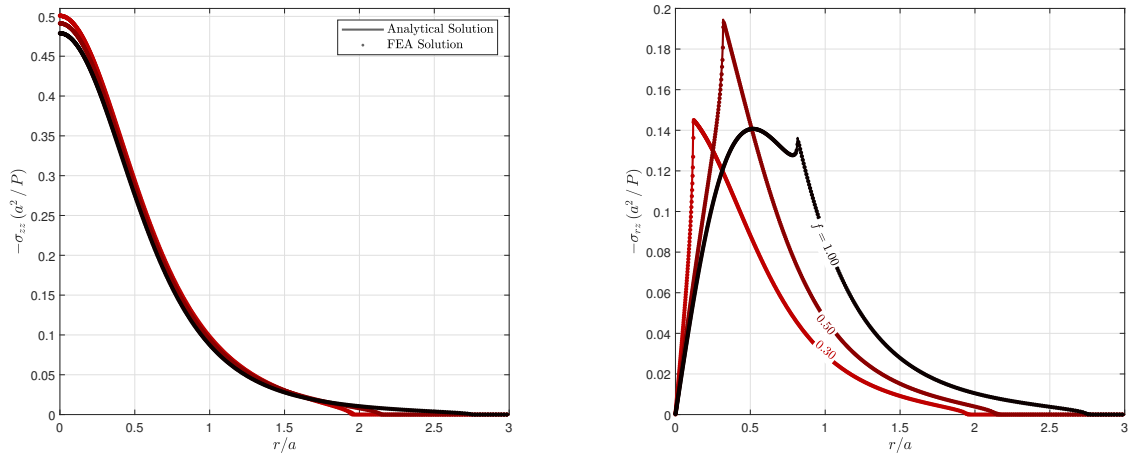

Figure C.7: Comparison between analytical and finite element solutions for layer pressed against half-space by point force.

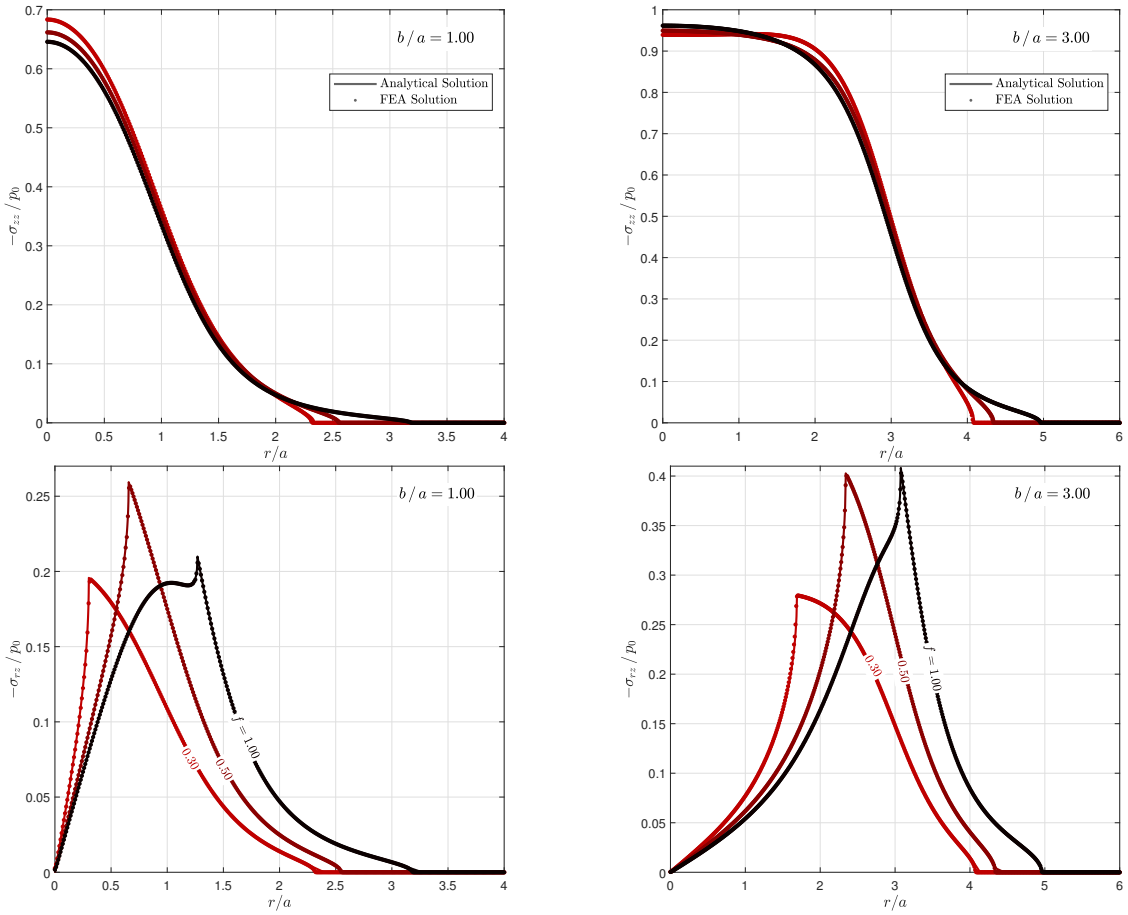

Figure C.8: Comparison between analytical and finite element solutions for layer pressed against half-space by pressure inside a disk.

D

Gauss-Laguerre Quadrature Tables

Table D.1: Gauss-Laguerre quadrature points and weights for $N = 1$.

$i,\ k$	u_i	X_i	v_k
1	1.5000000000000000e+00	8.8622692545275805e-01	3.5483389523526176e-01
2			3.8244030075698090e+00

Table D.2: Gauss-Laguerre quadrature points and weights for $N = 10$.

$i,\ k$	u_i	X_i	v_k
1	2.2987298051865621e-01	1.7547081504666026e-01	5.7391431494020533e-02
2	9.2448154698665741e-01	3.5522338880207205e-01	5.1837552227723793e-01
3	2.0994104627087982e+00	2.5268355967567796e-01	1.4504741047416962e+00
4	3.7828808737072901e+00	8.6356102695332629e-02	2.8752264781900334e+00
5	6.0199180277014612e+00	1.5109778034860811e-02	4.8285533636786759e+00
6	8.8803475979967086e+00	1.3282156283635641e-03	7.3665254394510198e+00
7	1.2474832404836205e+01	5.4187800211703440e-05	1.0576576140709943e+01
8	1.6990847293542554e+01	8.7374758691871452e-07	1.4601083292316480e+01
9	2.2791002894948946e+01	4.0196998869397951e-09	1.9694960301466008e+01
10	3.0806405917052722e+01	2.2922215302047090e-12	2.6409308817627146e+01
11			3.6674904936337754e+01

Table D.3: Gauss-Laguerre quadrature points and weights for $N = 20$.

$i,\ k$	u_i	X_i	v_k
1	1.1895908860796403e-01	7.2890472563476708e-02	2.9729115743119150e-02
2	4.7652106527261134e-01	2.0464756058744760e-01	2.6781813228000662e-01
3	1.0747619282656535e+00	2.5468502561168055e-01	7.4537102725297200e-01
4	1.9172162686228262e+00	1.9666755555059753e-01	1.4651816792008450e+00
5	3.0089953882055487e+00	1.0429708418429406e-01	2.4315547702917062e+00
6	4.3569660743407423e+00	3.9564676419709940e-02	3.6504526727952733e+00
7	5.9700059058394359e+00	1.0915967819206221e-02	5.1297100394536805e+00
8	7.8593597210710424e+00	2.1995244449111340e-03	6.8793359124967237e+00
9	1.0039135311274345e+01	3.2237602516737511e-04	8.9119339447328496e+00
10	1.2526997979116508e+01	3.4007746445557168e-05	1.1243288257674807e+01
11	1.5345159806815014e+01	2.5389053092581926e-06	1.3893190257771142e+01
12	1.8521823078408456e+01	1.3097453990576535e-07	1.6886629429221223e+01
13	2.2093354952633664e+01	4.5188859748141485e-09	2.0255557025464167e+01
14	2.6107701768389951e+01	9.9751438296765502e-11	2.4041595173456596e+01
15	3.0630040952691157e+01	1.3250477592223940e-12	2.8300396970554424e+01
16	3.5752805853034708e+01	9.7032223380562825e-15	3.3109099641695849e+01
17	4.1615202272985911e+01	3.4319296068706057e-17	3.8580122929105798e+01
18	4.8446589065314569e+01	4.7174749210545105e-20	4.4889689918464875e+01
19	5.6685019808011731e+01	1.6695481155796904e-23	5.2347216886354111e+01
20	6.7453383711098155e+01	5.3989144171417160e-28	6.1617090286686391e+01
21			7.5034073112988040e+01

Table D.4: Gauss-Laguerre quadrature points and weights for $N = 40$.

i, k	u_i	X_i	v_k
1	6.0556079496847867e-02	2.8055708450423118e-02	1.5137613789563461e-02
2	2.4231439945390584e-01	9.3658763141360221e-02	1.3627228163666411e-01
3	5.4554594294015102e-01	1.5585245457077301e-01	3.7872196470310493e-01
4	9.7070482530314739e-01	1.8150740139695029e-01	7.4284883873087726e-01
5	1.5184320613911118e+00	1.6446096273150190e-01	1.2291998992958559e+00
6	2.1895609453702050e+00	1.2146781246297257e-01	1.8385115237561054e+00
7	2.9851241535342448e+00	7.4926371635615260e-02	2.5717156964722188e+00
8	3.9063627190590040e+00	3.9138998066590373e-02	3.4299480263539883e+00
9	4.9547370720429882e+00	1.7457822896227847e-02	4.4145577270364162e+00
10	6.1319403903990413e+00	6.6824822337911323e-03	5.5271197780160293e+00
11	7.4399145697317222e+00	2.2013031987253846e-03	6.7694495421212419e+00
12	8.8808691964845501e+00	6.2486953448309061e-04	8.1436201835923328e+00
13	1.0457304002586541e+01	1.5287941224815336e-04	9.6519833154916306e+00
14	1.2172035397154005e+01	3.2214292582955626e-05	1.1297193409998151e+01
15	1.4028227819002220e+01	5.8377126104323602e-06	1.3082236636821170e+01
16	1.6029430842964775e+01	9.0778504475614353e-07	1.5010464962210119e+01
17	1.8179623217287791e+01	1.2079057915921143e-07	1.7085636555751517e+01
18	2.0483265328122386e+01	1.3704707146745409e-08	1.9311963830796138e+01
19	2.2945362007821824e+01	1.3203045787756135e-09	2.1694170810021355e+01
20	2.5571538165590827e+01	1.0747613458879108e-10	2.4237561993056012e+01
21	2.8368130478958264e+01	7.3502984741798143e-12	2.6948105555444773e+01
22	3.1342299426479435e+01	4.1955597676112370e-13	2.9832534596482187e+01
23	3.4502167391929746e+01	1.9836564034678418e-14	3.2898471380169354e+01
24	3.7856990620531676e+01	7.7006673080716012e-16	3.6154581234037813e+01
25	4.1417375758975119e+01	2.4298269862813704e-17	3.9610765224710896e+01
26	4.5195556043182862e+01	6.1588390186452082e-19	4.3278404295497772e+01
27	4.9205748697573419e+01	1.2368954134750845e-20	4.7170672842475305e+01
28	5.3464625103369485e+01	1.9366781913969396e-22	5.1302947739018137e+01
29	5.7991941090827197e+01	2.3191710054581008e-24	5.5693351337371126e+01
30	6.2811400481950265e+01	2.0755673449856517e-26	6.0363487068209523e+01
31	6.7951868610018522e+01	1.3497535054294870e-28	6.5339459616546478e+01
32	7.3449129492632835e+01	6.1594049634078483e-31	7.0653329244203903e+01
33	7.9348523110720592e+01	1.8871394756399462e-33	7.6345253934583340e+01
34	8.5709080557254978e+01	3.6651639387950678e-36	8.2466771797700588e+01
35	9.2610371480811409e+01	4.1765559663948417e-39	8.9086081687569759e+01
36	1.0016466698884538e+02	2.5043449651182829e-42	9.6297078399532410e+01
37	1.0854067117146624e+02	6.7128205034376117e-46	1.0423611113902135e+02
38	1.1801641862593260e+02	6.1562788880242915e-50	1.1311671031888666e+02
39	1.2912430268615788e+02	1.1623049545398330e-54	1.2331433534235896e+02
40	1.4323588304664480e+02	1.2454315853037260e-60	1.3563821189570945e+02
41			1.5295059369705189e+02

References

[1] J. Barber. *Contact Mechanics*. Solid Mechanics and Its Applications. Springer International Publishing, 2018.

[2] A. Thaitirarot, D. A. Hills, and D. Dini. “Contact mechanics of frictional lap joints”. In: *The Journal of Strain Analysis for Engineering Design* 48.5 (2013), pp. 321–329.

[3] L. Keer, J. Dundurs, and K. Tsai. “Problems involving a receding contact between a layer and a half space”. In: *Journal of Applied Mechanics* 39.4 (1972), pp. 1115–1120.

[4] K. Tsai, J. Dundurs, and L. Keer. “Contact Between an Elastic Layer with a Slightly Curved Bottom and a Substrate”. In: *Journal of Applied Mechanics, Transactions ASME* 39.3 (1972), pp. 821–823.

[5] S. El-Borgi, R. Abdelmoula, and L. Keer. “A receding contact plane problem between a functionally graded layer and a homogeneous substrate”. In: *International Journal of Solids and Structures* 43.3-4 (2006), pp. 658–674.

[6] M. Rhimi et al. “A receding contact axisymmetric problem between a functionally graded layer and a homogeneous substrate”. In: *International Journal of Solids and Structures* 46.20 (2009), pp. 3633–3642.

[7] J. Yan and X. Li. “Double receding contact plane problem between a functionally graded layer and an elastic layer”. In: *European Journal of Mechanics-A/Solids* 53 (2015), pp. 143–150.

[8] V. Kahya et al. “A receding contact problem for an anisotropic elastic medium consisting of a layer and a half plane”. In: *International Journal of Solids and Structures* 44.17 (2007), pp. 5695–5710.

[9] M. Ciavarella et al. “Reduced dependence on loading parameters in almost conforming contacts”. In: *International Journal of Mechanical Sciences* 48.9 (2006), pp. 917–925.

[10] Y. J. Ahn and J. Barber. “Response of frictional receding contact problems to cyclic loading”. In: *International Journal of Mechanical Sciences* 50.10-11 (2008), pp. 1519–1525.

[11] İ. Çömez. “Frictional contact problem for a rigid cylindrical stamp and an elastic layer resting on a half plane”. In: *International Journal of Solids and Structures* 47.7-8 (2010), pp. 1090–1097.

[12] S. El-Borgi, S. Usman, and M. A. Güler. “A frictional receding contact plane problem between a functionally graded layer and a homogeneous substrate”. In: *International Journal of Solids and Structures* 51.25-26 (2014), pp. 4462–4476.

[13] T. Chaise, R. Paynter, and D. Hills. “Contact analysis of a semi-infinite strip pressed onto a half plane by a line force”. In: *International Journal of Mechanical Sciences* 81 (2014), pp. 60–64.

[14] K. Parel and D. Hills. “Frictional receding contact analysis of a layer on a half-plane subjected to semi-infinite surface pressure”. In: *International Journal of Mechanical Sciences* 108 (2016), pp. 137–143.

[15] T. Chakherlou et al. “An experimental investigation of the bolt clamping force and friction effect on the fatigue behavior of aluminum alloy 2024-T3 double shear lap joint”. In: *Materials & Design* 32.8-9 (2011), pp. 4641–4649.

[16] J. Juoksukangas, A. Lehtovaara, and A. Mäntylä. “Experimental and numerical investigation of fretting fatigue behavior in bolted joints”. In: *Tribology International* 103 (2016), pp. 440–448.

[17] D. Hills et al. *Solution of crack problems: the distributed dislocation technique*. Vol. 44. Solid Mechanics and Its Applications. Dordrecht: Springer Netherlands, 2013.

[18] R. Paynter, D. Hills, and A. Sackfield. “The penny crack beneath the surface of a half-space: with application to the blister test”. In: *International journal of fracture* 142.1-2 (2006), pp. 173–182.

[19] R. Paynter, D. Hills, and J. Barber. “Features of the stress field at the surface of a flush shrink-fit shaft”. In: *Proceedings of the Institution of Mechanical Engineers, Part C: Journal of Mechanical Engineering Science* 223.10 (2009), pp. 2241–2247.

[20] R. D. Mindlin and D. H. Cheng. “Nuclei of strain in the semi-infinite solid”. In: *Journal of Applied Physics* 21.9 (1950), pp. 926–930.

[21] A. Korsunsky and D. Hills. “Solution of axisymmetric crack problems using distributed dislocation ring dipoles”. In: *The Journal of Strain Analysis for Engineering Design* 35.August 1999 (2005), pp. 373–382.

[22] F. Erdogan, G. D. Gupta, and T. Cook. “Numerical solution of singular integral equations”. In: *Methods of analysis and solutions of crack problems*. 1973, pp. 368–425.

[23] J. Lopes and D. Hills. “Ring cracks at the surface of a half-space”. In: *Engineering Fracture Mechanics* 194 (2018), pp. 105–116.

[24] J. Lopes, D. Hills, and R. Paynter. “The axisymmetric shrink fit problem subjected to axial force”. In: *European Journal of Mechanics-A/Solids* 70 (2018), pp. 172–180.

[25] J. Lopes and D. Hills. “The axisymmetric shrink fit problem subjected to torsion”. In: *International Journal of Engineering Science* 150 (2020), p. 103259.

[26] J. Lopes and D. Hills. “The axisymmetric frictional receding contact of a layer pressed against a half-space by pressure outside a disk”. In: *European Journal of Mechanics-A/Solids* 77 (2019), p. 103787.

[27] J. Lopes and D. Hills. “The axisymmetric frictional receding contact of a layer pressed against a half-space by a point force”. In: *International Journal of Solids and Structures* 171 (2019), pp. 47–53.

[28] J. Lopes and D. Hills. “An idealised description of the frictional receding contact behaviour of a bolted joint”. In: *European Journal of Mechanics-A/Solids* (2020), p. 104022.

[29] D. Hills and D. Nowell. *Mechanics of Fretting Fatigue*. London: Kluwer Academic Publishers, 1994, pp. 1–14.

[30] D. Hills, D. Nowell, and A. Sackfield. “Mechanics of elastic contacts”. In: *Butterworth-Heinemann, London* 21 (1993), pp. 235–237.

[31] J. Dundurs and M. Stippes. “Role of elastic constants in certain contact problems”. In: *Journal of Applied Mechanics* 37.4 (1970), pp. 965–970.

[32] J. Dundurs. “Properties of elastic bodies in contact”. In: *The Mechanics of the Contact between Deformable bodies* (1975), pp. 54–66.

[33] K. Tsai, J. Dundurs, and L. Keer. “Elastic layer pressed against a half space”. In: *Journal of Applied Mechanics* 41.3 (1974), pp. 703–707.

[34] A. E. Green and W. Zerna. *Theoretical elasticity*. Courier Corporation, 1992.

[35] J. Boussinesq. *Application des potentiels à l’étude de l’équilibre et du mouvement des solides élastiques*. Gauthier-Villars, Imprimeur-Libraire, 1885.

[36] S. Timoshenko and J. N. Goodier. *Theory of Elasticity*. Vol. 49. 1986, pp. 427–143.

[37] J. R. Barber. *Elasticity*. Springer, 1992.

[38] A. E. H. Love. “The stress produced in a semi-infinite solid by pressure on part of the boundary”. In: *Philosophical Transactions of the Royal Society of London. Series A, Containing Papers of a Mathematical or Physical Character* 228.659-669 (1929), pp. 377–420.

[39] K.-i. Terazawa. “On the elastic equilibrium of a semi-infinite solid under given boundary conditions”. In: *Journal of the College of Science* (1916), pp. 14–24.

[40] M. T. Hanson and I. W. Puja. “Love’s circular patch problem revisited: Closed form solutions for transverse isotropy and shear loading”. In: *Quarterly of applied mathematics* 54.2 (1996), pp. 359–384.

[41] K. L. Johnson. *Contact Mechanics*. Vol. 37. 22. 1985, pp. 1–17.

[42] K. Chowdhury. “Solution of the problem of a concentrated torque on a semi-space by similarity transformations”. In: *Journal of Elasticity* 13.1 (1983), pp. 87–90.

[43] C. Chow and F. Yang. “On the solution of a concentrated torque on an orthotropic half-space”. In: *International Journal of Engineering Science* 28.9 (1990), pp. 871–874.

[44] H. Hertz, D. E. Jones, and G. A. Schott. *Miscellaneous papers*. Macmillan and Company, 1896.

[45] G. Amontons. “De la resistance cause dans les machines”. In: *Memoires de L’Academie Royale* (1699), pp. 275–282.

[46] C. A. Coulomb. “The theory of simple machines”. In: *Mem. Math. Phys. Acad. Sci* 10.161-342 (1785), p. 4.

[47] R. Mindlin. “Compliance of elastic bodies in contact”. In: *J. Appl. Mech., ASME* 16 (1949), pp. 259–268.

[48] R. D. Mindlin. “Elastic spheres in contact under varying oblique forces”. In: *J. Applied Mech.* 20 (1953), pp. 327–344.

[49] R. Munisamy, D. Hills, and D. Nowell. “Contact of similar and dissimilar elastic spheres under tangential loading”. In: *Contact Mechanics, Int. Syrup* (1992), pp. 447–461.

[50] J. Dundurs and T. Mura. “Interaction between edge dislocation and circular inclusion”. In: *Journal of Mechanics and Physics of Solids* 12.3 (1964), pp. 177–189.

[51] R. E. Worden and L. M. Keer. “Green’s Functions for a Point Load and Dislocation in an Annular Region”. In: *Journal of Applied Mechanics* 58.4 (Dec. 1991), pp. 954–959.

[52] L. M. Keer, J. C. Lee, and T. Mura. “Stress Distributions for a Quarter Plane Containing an Arbitrarily Oriented Crack”. In: *Journal of Applied Mechanics* 50.1 (Mar. 1983), pp. 43–49.

[53] M. S. Lee and J. Dundurs. “Edge Dislocation in a Surface Layer”. In: *International Journal of Engineering Science* 11 (1973), pp. 87–94.

[54] H. Bueckner. “The propagation of cracks and the energy of elastic deformation”. In: *Transaction of the ASME, Series E* 80.6 (1958), pp. 1225–1230.

[55] D. J. Cartwright and D. Rooke. “Green’s functions in fracture mechanics”. In: *Fracture Mechanics*. Elsevier, 1979, pp. 91–123.

[56] R. Paynter and D. Hills. “The effect of path cut on Somigliana ring dislocations in a half-space”. In: *International Journal of Solids and Structures* 46.2 (2009), pp. 412–432.

[57] A. Sackfield et al. “A shrink-fit shaft subject to torsion”. In: *European Journal of Mechanics-A/Solids* 21.1 (2002), pp. 73–84.

[58] G. Eason, B. Noble, and I. N. Sneddon. “On certain integrals of Lipschitz-Hankel type involving products of Bessel functions”. In: *Philosophical Transactions of the Royal Society of London A: Mathematical, Physical and Engineering Sciences* 247.935 (1955), pp. 529–551.

[59] R. Paynter, D. Hills, and A. Korsunsky. “The effect of path cut on Somigliana ring dislocation elastic fields”. In: *International Journal of Solids and Structures* 44.2 (2007), pp. 6653–6677.

[60] N. I. Muskhelishvili. *Some Basic Problems of the Mathematical Theory of Elasticity*. 1977, p. 732.

[61] N. I. Muskhelishvili. *Singular integral equations*. Noordhoff, Groningen, 1953.

[62] R. Estrada and R. P. Kanwal. *Singular integral equations*. Springer Science & Business Media, 2012.

[63] A. Gerasoulis. “The use of piecewise quadratic polynomials for the solution of singular integral equations of Cauchy type”. In: *Computers & mathematics with applications* 8.1 (1982), pp. 15–22.

[64] P. Theocaris and N. Ioakimidis. “Numerical integration methods for the solution of singular integral equations”. In: *Quarterly of Applied Mathematics* 35.1 (1977), pp. 173–183.

[65] N. I. Ioakimidis. “Application of the gauss-Laguerre and radau-Laguerre quadrature rules to the numerical solution of Cauchy type singular integral equations”. In: *Computers & Structures* 14.1-2 (1981), pp. 63–70.

[66] M. Abramowitz, I. a. Stegun, and D. Miller. *Handbook of Mathematical Functions With Formulas, Graphs and Mathematical Tables (National Bureau of Standards Applied Mathematics Series No. 55)*. 1965.

[67] E. Gordeliy and E. Detournay. “Displacement discontinuity method for modeling axisymmetric cracks in an elastic half-space”. In: *International Journal of Solids and Structures* 48.19 (2011), pp. 2614–2629.

[68] Y. Murakami. “Analysis of stress intensity factors of modes I, II and III for inclined surface cracks of arbitrary shape”. In: *Engineering Fracfure Mechanics* 22.I (1985), pp. 101–114.

[69] M. Ciavarella and P. Decuzzi. “The state of stress induced by the plane frictionless cylindrical contact. I. The case of elastic similarity”. In: *International Journal of Solids and Structures* 38.26-27 (2001), pp. 4507–4523.

[70] M. Comninou, D. Schmueser, and J. Dundurs. “Frictional Slip Between a Layer and a Substrate Caused by a Normal Load”. In: *International Journal of Engineering Science* 18.9 (1980), pp. 131–137.

[71] H. Qiu et al. “Skew sliding of an elastic cylinder: An investigation of convection in contact”. In: *International Journal of Mechanical Sciences* 50.2 (2008), pp. 293–298.

[72] H. Qiu, D. Dini, and D. Hills. “Torsional contact of an elastic flat-ended cylinder”. In: *Journal of the Mechanics and Physics of Solids* 56.12 (2008), pp. 3352–3362.

[73] H. Qiu, D. Hills, and D. Dini. “An investigation of convection effects in complete and almost complete contact problems”. In: *European Journal of Mechanics-A/Solids* 28.4 (2009), pp. 680–687.

[74] R. Bentall and K. Johnson. “An elastic strip in plane rolling contact”. In: *International Journal of Mechanical Sciences* 10.8 (1968), pp. 637–663.